Annual Report Covering the Period October 1, 1985 to September 30, 1986

Princeton University
Plasma Physics Laboratory
Princeton, New Jersey 08543

PPPL-Q-44

PPPL-Q--44

DE88 007501

Edited by
Carol A. Phillips

DISCLAIMER

Unless otherwise designated, the work in this report is funded by the United States Department of Energy under Contract DE-AC02-76-CHO-3073.

Printed in the United States of America

Contents

Preface

During 1986, the Tokamak Fusion Test Reactor (TFTR) set world records for both the ion temperature and the Lawson parameter. Central ion temperatures of 20 keV were reached by injection of neutral-beam power in the 15-20 MW range. The discovery, in these experiments, of a new type of "enhanced confinement regime" led to the achievement of equivalent D-T Q-values above 0.2 at the 1-MA level of TFTR plasma current. The tokamak loop voltage required to drive this current was found to vanish—a result that supports the existence of the classically predicted "bootstrap effect," which could be of major importance for future tokamak reactors. In separate TFTR experiments, pellet injection into ohmically heated plasmas was used to reach a Lawson parameter $n\tau_E$ of 1.4×10^{14} cm^{-3} sec at a temperature of 1.4 keV.

For future TFTR operations, including D-T, the Engineering Department has developed a group of computer models that simulate the as-built configuration of the poloidal field coils, and can serve to set upper limits on all proposed operating scenarios. A substantial effort is now underway on TFTR tritium systems, in preparation for the demonstration of D-T breakeven in 1990.

A provisional conceptual design for the Compact Ignition Tokamak (CIT) was completed in June, 1986. The CIT is to be the next major step in the U.S. fusion program beyond TFTR. If authorized for construction in FY88, the CIT is scheduled to enter experimental operation at the TFTR site in 1993.

The Princeton Large Torus (PLT) has extended Ion Bernstein Wave Heating (IBWH) to the 0.5-MW level. Both the wave-coupling and plasma-confinement results were found to be promising for future high-powered applications of IBWH. Lower-hybrid current drive at 2.45 GHz was used to study the sawtooth-stabilization phenomenon at higher electron temperatures and densities. Preparations were made for PLT shutdown at the end of CY86.

The PBX (Princeton Beta Experiment) is being transformed into PBX-M, which will have stronger bean-shaping capabilities and various auxiliary stabilization techniques. The beta value is expected to rise from about 5% toward 10%, and it may be able to enter the theoretically predicted second stability regime.

The S-1 device was equipped with an improved flux core, and is investigating resistive-MHD dynamo mechanisms in 50-100 eV spheromak plasmas with beta value of 5-10%. The Current Drive Experiment (CDX) successfully demonstrated the generation of a closed tokamak configuration maintained in quasi-steady state by the injection of helicity from an electron gun.

The X-Ray Laser program achieved a 182-Å soft-X-ray beam with 500-fold enhancement above spontaneous emission and only 5 mrad divergence. Preparations are well underway for a 1-TW picosecond laser facility, which is to utilize multiphoton processes to extend X-ray lasers to shorter wavelengths. The Spacecraft Glow Experiment achieved significant initial results in both the areas of surface glow and erosion.

Extensive theoretical and computational studies were carried out in support of CIT and other experimental projects, particularly in the areas of MHD stabilization, alpha-particle physics, simulation of ignition conditions, and divertor design. The theory of tokamak MHD stability has been advanced by the discovery of an important new type of ballooning mode, by a comprehensive survey of resistive-kink-stable current profiles, and by the demonstration that stability is possible, under special conditions, for a central MHD safety factor well below unity.

PRINCIPAL PARAMETERS ACHIEVED IN EXPERIMENTAL DEVICES (Fiscal Year 1986)

Parameters	Tokamak Facilities				Alternate Concept Facilities	
	TFTR	PLT	PBX	PBX-M	S-1	CDX
R (m)	2.48	1.32	1.45	1.65	0.40	0.59
a (m)	0.83	0.42	0.3	0.3	0.25	0.1
I_p (MA)	2.5	0.7	0.6	0.8	0.35	—
B_T (T)	5.2	3.4	2.4	2.2	0.4	0.57
τ_{AUX} (sec)	1.0	0.5	0.3	0.5	—	dc
P_{AUX} (MW)						
NB	2.0 (100 keV)	—	7 (40 kV)	7 (40 kV)	—	—
ICRF	—	5.0 (30 MHz)	—	1.0 (30 MHz)	—	0.002
LH	—	1.0 (2.45 GHz)	—	2.0 (4.6 GHz)	—	—
ECRH	—	0.05 (60 GHz)	—	—	—	0.002
$n(0)$ (cm^{-3})*	4.0×10^{14}	0.8×10^{14}	1.5×10^{14}	—	3×10^{14}	3×10^{13}
$T_i(0)$ (keV)*	20	5.0	5.5	—	0.1	0.04
τ_E (msec)*	500	40	40	—	0.25	0.2

*These highest values of n, T, and τ were not achieved simultaneously.

TOKAMAK FUSION TEST REACTOR

SUMMARY

The main goal of the Tokamak Fusion Test Reactor (TFTR) is to carry out deutrium-tritium (D-T) break-even experiments in mid-1990, as indicated in the TFTR Research Plan (Fig. 1). TFTR has made significant progress toward this goal during calendar year 1986.

World-record ion temperatures of 20 keV were achieved by a combination of improved plasma handling techniques and high neutral-beam-heating power. The improved plasma handling—a reduction of deuterium recycling—was made possible by extensive conditioning of the large-area inner-wall bumper limiter. When low-density discharges at $I_p \sim 0.8$ MA were heated with near balanced injection, the plasma stored energy rose to 3 MJ with $n_e(0)\,\tau_E \sim 10^{13}$ cm^{-3} sec. This confinement is roughly three times the low-mode value projected from earlier experiments. These "supershots" also have record deuterium-deuterium (D-D) neutron yields of 1.2×10^{16} neutrons per second with 6×10^{15} neutrons per pulse. This neutron yield gave $Q_{DD} \sim 8.7 \times 10^{-4}$. If tritium were introduced with the same plasma (n_e, T_i, T_e, Z) and beam parameters, a $Q_{DT} \sim 0.2$ is projected. An improvement of almost two is expected when the high-species mix, ($n_{H0}/n_{tot} \sim 0.8$) 120-kV, long-pulse ion sources are used in 1987. A further improvement in $n\tau$ of 2 to 3 is required for the D-T break-even experiments. In the supershot regime, this will require that $n\tau$ improves with plasma current, and that techniques be developed to extend supershots from the present 1.0 MA to 2.5 MA.

TFTR is also exploring a high-density approach to D-T break-even experiments. Deutrium pellet injectors developed and constructed at the Oak Ridge National Laboratory (ORNL) have been used to create high-density (up to 4×10^{14} cm^{-3}) peaked-density profiles with world-record $n_E(0)\tau_E \sim 1.5 \times 10^{14}$ cm^{-3} sec in ohmically heated plasmas with $T_i(0) \sim T_e(0) \sim 1.3$ keV. Near-term experiments will concentrate on combining pellet injection with neutral-beam heating. Longer range experiments will utilize 6 MW of central ion-cyclotron radio-frequency (ICRF) heating to raise the ion temperature to multi-keV values.

In addition to producing world-record parameters, TFTR has made significant contributions to fundamental tokamak physics. The observation of a nonohmic plasma current which is in agreement with the theoretical prediction of the "bootstrap" current

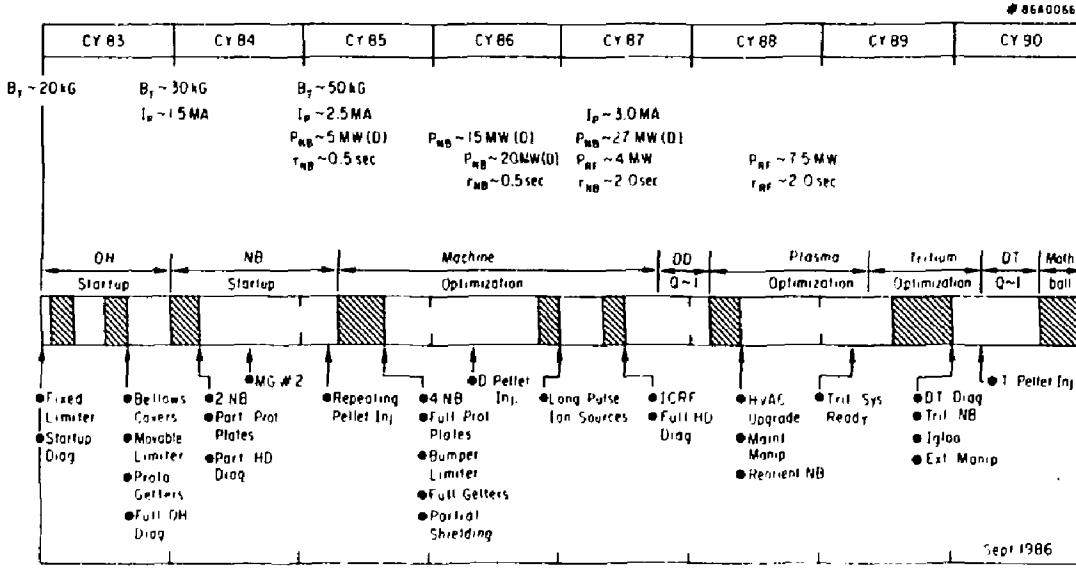

Fig 1 TFTR Research Plan

is very important for the development of high-gain steady-state tokamak reactors. Also, the extensive TFTR diagnostic set has allowed the study of the systematics of TFTR electron temperature profiles, which has led to an improved definition to the concept of "profile consistency." The TFTR equipment (diagnostics, power supplies, neutral beams) were all operated near full capability, with high reliability for a total of 5,200 high-power discharges and 50 gegabytes (GB) of data collected during 1986.

Activities related to D-T operation gained more visibility in 1986, as several technical reviews reaffirmed the 100-shot Q of 1 D-T program for TFTR. Specific D-T activities included commissioning of the tritium system, fabrication of an internal maintenance manipulator, and the initiation of designs for shielding upgrades.

Late in 1986, the TFTR project was reorganized and now has the following divisions: Physics Program, Diagnostics, Tokamak Operations, Heating Systems, and D-T Systems. The following description of 1986 TFTR accomplishments is presented in the new divisional structure.

PHYSICS PROGRAM

With the near tripling of the neutral-beam heating capability over FY85 levels, the FY86 experimental run proved very exciting and encouraging. Following the installation of the remaining two of four beamlines and the graphite inner toroidal limiter to handle the increased power load, neutral-beam-heating power was pushed steadily upwards during FY86 to 20 MW. Fortunately, one of the new beamlines had been chosen to inject tangentially in the "counter" direction (opposite to the plasma current) to supplement the three co-injection (same direction as the plasma current) beams without further increasing injected momentum. The availability of this counter-injecting beamline was crucial for the development of a regime of enhanced confinement and fusion reactivity in subsequent experiments. This regime is an extension of the "energetic ion" regime previously achieved in TFTR using low-density target plasmas. To obtain low densities, these experiments were conducted at low plasma currents. Further reduction of density was achieved by taking advantage of the fact that the graphite limiters act as very good pumps when degassed. The combination of low-density, low-current operation, reduced recycling with well-conditioned limiters, and a significant amount of counter-injected power resulted in the attainment of record tokamak parameters including $T_i(0) \simeq 20$ keV, $n_e(0)\tau_E T_i(0) \simeq 2.0 \times 10^{20}$ m^{-3} sec keV, and equivalent $Q_{DT} \sim 0.25$. This enhanced-confinement operation, locally dubbed the "supershot" regime, reveals a potential path toward approximate energy breakeven on TFTR, as shown in Fig. 2. The crosshatched regions represent progress made in FY86. The box shows the requirements for TFTR to achieve $Q \simeq 1$ with the beam energy and species mix available in the FY87 long-pulse ion source (LPIS) upgrade.

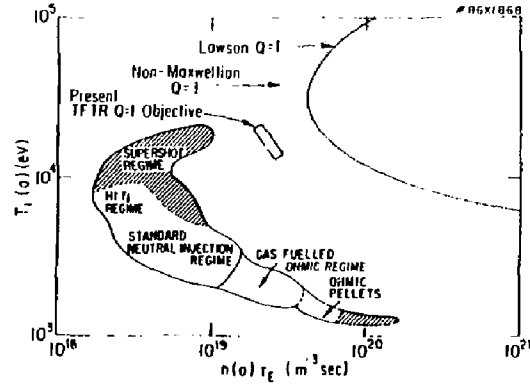

Fig. 2. The TFTR operating regimes on the Lawson diagram of central ion temperature versus the confinement parameter. The crosshatched region represents progress made in FY86. The left-hand boundary of the dotted region assumes 200 keV pure tritium beams injecting into a pure deuterium plasma.

As Fig. 2 indicates, encouraging results were also obtained in ohmically heated pellet-fueled experiments. Multiple pellets, injected by the ORNL pneumatic injectors resulted in highly peaked density profiles with $\tau_E \sim 0.5$ sec and $n_e(0)\tau_E T_i(0) \simeq 2.0 \times 10^{20}$ m^{-3} sec keV.

The details of the above highlights are given below. In addition, the following sections briefly describe the arduous initial conditioning of the new toroidal inner-wall limiter and the new results for confinement scaling in the standard L-mode neutral-beam-heating regimes. Subsidiary experiments including detached plasmas, gas modulation, and size scaling will also be discussed briefly. Finally, impurity behavior, MHD and stability, and the role of the electron profiles will be discussed as they relate to the FY86 runs.

Initial Conditioning of the Inner Wall Limiter

During the summer of 1985, a full toroidal inner-wall limiter consisting of 2,000 kg of graphite tiles was installed with a total surface area exposed to the plasma (20 m^2) ten times that of the previously installed graphite movable limiter. Much of the first three months of FY86 was spent learning how to condition this new first wall.[1] Initially the vessel was baked at 150°C for six weeks during which time 130 hours of glow-discharge cleaning (GDC) and 175 hours of pulse-discharge cleaning (PDC) were applied—similar to the procedure used for the smaller movable limiter. High-power operation then appeared satisfactory until the first major disruption at $I_p > 2.2$ MA, after which it was necessary to resume PDC, because subsequent attempts at normal discharges collapsed from radiative losses due to large impurity levels. The old procedure did not adequately condition the large inner-wall limiter, which liberated water vapor and hydrocarbons following disruptions.

A new technique, disruptive-discharge cleaning (DDC), was developed for controlled outgassing of the new limiter. This technique involved creating a sequence of discharges starting at low current (I_p = 0.6 MA) and increasing the current in 0.2-MA increments only after forced disruptions did not affect succeeding discharges. Surface temperature of 1,000-1,200°C were measured immediately after these disruptions. When recovery was immediate for 2.5-MA disruptions, the values for the radiated power fraction (<50%) and Z_{eff} ($\leq$1.5) in ohmic discharges were even lower than they had been following the old cleanup procedure on the movable limiter alone.

Gas-Fueled Ohmic-Heating Experiments

Gas puffing experiments using either periodic small gas puffs or a larger single puff utilized the MIRI (multichannel infrared interferometer) ten-channel laser interferometer to study particle transport by observing the details of the density profile evolution. The best match to this data was achieved with particle transport models which assumed central values of the particle diffusion coefficient D of 0.5 m^2/sec increasing to 2.0 m^2/sec at the edge and inward pinch velocities of near zero for $r/a < 0.25$ increasing to 0.4 m/sec at the edge.

Low-current TFTR plasmas could be reproducibly detached from the limiter by ramping down the current while maintaining the density with gas puffing. These discharges could be sustained for several seconds in this detached state at the lower-current level ($I_p \leq 1.2$ MA) radiating all of the ohmic input power.[2] The minor radius of the detached discharge defined by the strongly radiating boundary was found to scale as $a_{rad} \propto I_p^{0.64} n_e^{0.3}$ (Ref. 3). A crude explanation for the strong current dependence is that the plasma requires more surface area to radiate more input power, assuming roughly constant emissivity in the radiating boundary.

Fiscal year 1986 offered the first opportunity to conduct size scaling experiments on TFTR where discharges limited on the inner wall or the outer blade interacted with the same material. Studies were conducted in the low-density ohmic regime where the energy confinement depends strongly on density. Over a considerable range of size parameters (a = 0.41-0.83 m, R = 2.07-2.96 m) regression analysis resulted in $\tau_E \propto n_e^{0.8} q^{0.6} R^{1.8} a^{1.0}$, in reasonable agreement with previous ohmic scaling ($\tau_E \propto n_e^{1.0} q^{1.0} R^{2.0} a^{1.0}$) derived by comparing TFTR confinement results from full-sized plasmas with those of smaller machines.[4]

Pellet-Injection Results

From February-April 1986, experiments investigating fueling by multiple deuterium pellets were performed using the single-barreled, ORNL Repeating Pneumatic Injector. In June, a more flexible multiple-barrel, ORNL injector, the Deuterium Pellet Injector was installed. It is capable of injecting up to eight arbitrarily timed 3.4-mm-long pellets, ranging in diameter from 3.0 to 4.0 mm, at speeds up to 1,500 m/sec (Ref. 5).

One of the goals of the pellet-fueling experiments was to extend the density range in ohmic plasmas. With multiple pellet injection, successive pellets penetrate more deeply producing strongly peaked density profiles. Central densities up to 4.0×10^{20} m^{-3} have achieved with line-averaged densities up to 1.4×10^{20} m^{-2}, corresponding to a Murakami parameter of 6.5×10^{19} m^{-2} T^{-1}. This represents an increase of a factor of four in $n_e(0)$ and a factor fo two in the Murakami parameters compared to gas-fueled deuterium ohmic discharges.

Following pellet injection, the peaked density profiles decay on a 2 sec time scale, as shown in Fig. 3(a). Figure 3(b) compares the measured decay at four radial positions with modeling calculations

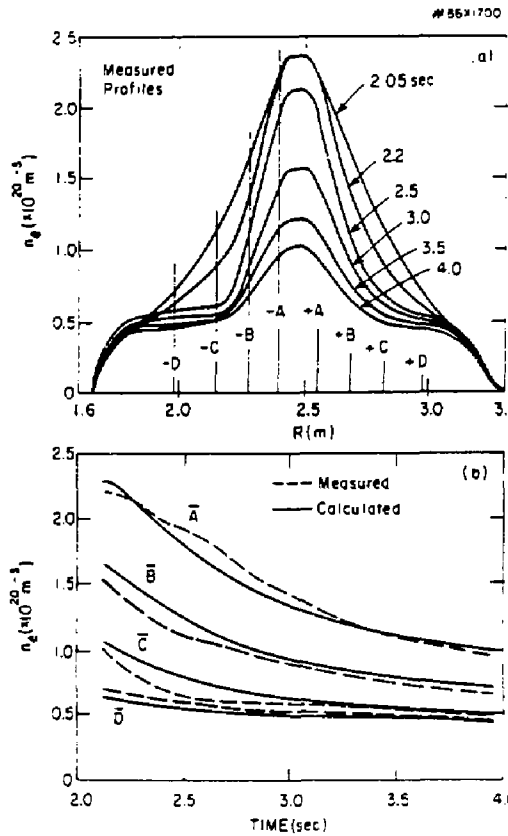

Fig. 3. (a) Electron-density profile evolution following pellet injection, obtained from Abel inversion of the far-infared (FIR) laser interferometer data (ten channels). (b) Measured and calculated decay of n_e at four radial positions r [= 0.08 m ($\bar{A}$), = 0.2 m ($\bar{B}$), = 0.3 m($\bar{C}$), and = 0.5 m ($\bar{D}$)] averaged about the plasma center.

which assume a fixed particle diffusion coefficient $D = 0.1\ m^2/sec$ inside a/2 [$D = 0.1+(r/a)^6\ m^2/sec$] and an inward pinch of <0.3 m/sec within this region. These same assumptions qualitatively model the observation that central concentrations of scandium, injected by laser blowoff following the last pellet, increase for 0.3-0.5 sec and then remain constant as the density decays.

A comparison of the confinement properties of pellet-fueled and gas-fueled discharges is shown in Fig. 4. The magnetically determined $\tau_E(a)$ includes measured corrections for dl_i/dt and dW/dt. As a function of time in a pellet-fueled discharge, the confinement time increases with the first few pellets and then is sustained with continued injection while the stored energy and density continue to rise. Values of $\tau_E > 0.5$ sec have been sustained for up to 0.7 sec. The best performance achieved was $n_e(0)\tau_E(a) = (1.4\pm0.3) \times 10^{20}\ m^{-3}$ sec with $T_e(0) = 1.4$ keV. The data are compard to Goldston[6] empirical scaling. The predictions assume a fixed $P_{tot} = 1.6$ MW and a deuterium plasma.

Neutral-beam heating with injection power up to 11 MW was apolied to high-density pellet-fueled target plasmas. As observed earlier at the 6 MW level,[7] the global confinement is similar to that in gas-fueled, beam-heated discharges although the heating profiles in these lower-density targets is peaked on axis; whereas, it is flat or even hollow for the pellet cases. More central heating will be available in the coming year with improved beam voltage and species mix and, in particular, with the addition of ion-cyclotron heating.

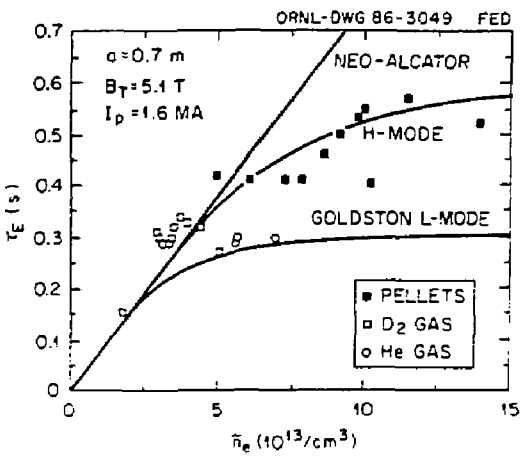

Fig. 4. Global energy confinement in deuterium and helium gas-fueled and deuterium pellet-fueled discharges. Plasma stored energy was obtained from diamagnetic measurements of β_p. (87X3009)

Confinement Scaling in the Standard Neutral-Beam Heating Regime

Previous experiments[8] at injection power $P_{inj} \leq 6.3$ MW showed that confinement degraded as a function of heating power at fixed current and scaled roughly linearly with current at fixed power, in rough agreement with Goldston L-mode scaling. In FY86, this data set was expanded systematically to $P_{inj} \leq 15$ MW over a wide range of current ($I_p = 1.0$-2.5 MA) and density ($n_e = 2.0$-$6.0 \times 10^{19}\ m^{-3}$). As shown in Fig. 5, the global confinement continues to degrade at the higher power levels, with values slightly higher than the L-mode predictions. For $P_{inj} \geq 4$ MW and roughly constant density at the end of injection, power law fits to this data indicate that $\tau_E \propto I_p^{0.9} P_{tot}^{-0.5}$ (Ref. 9). Figure 6 shows the stored energy from magnetic measurements as a function of P_{tot} and I_p. For constant power and density, the data is equally well described by an offset linear form $W_{tot} = \alpha + \beta P$, where the incremental confinement time $\tau_{inc} = dW/dP_{heat} \equiv \beta$ scales linearly with plasma current in this constrained density range. There is also an interesting density scaling, particularly at lower currents, which is illustrated in the figure. At high power, the stored energy is significantly higher in the lower-density 1.4-MA discharges. Since the electron stored energy in these two cases shows no significant density scaling, the improvement comes in the stored energy of the beam and thermal ions. This L-mode data will form a basis for comparison with the enhanced confinement regime in a later section.

By comparing the TFTR full-size inner-wall plasmas (R = 2.48 m, a = 0.82 m) described above with smaller aperture plasmas (a = 0.67 m) operated on both the inner wall and the outer movable limiter (R = 2.32, 2.85 m), preliminary size scaling results

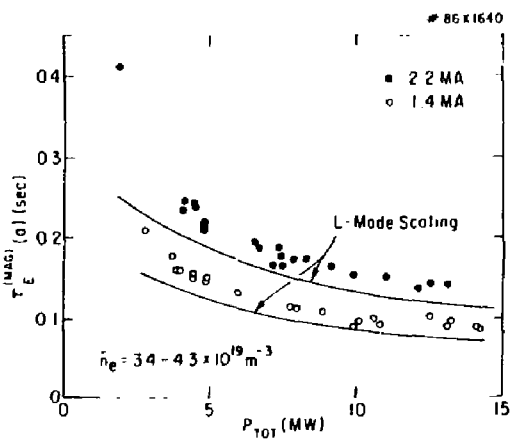

Fig. 5. Variation of the global confinement time for 1.4- and 2.2-MA power scans for a constrained density range and B_T 4.8 T, R 2.48 m, and a 0.82 m. Mrgnetic measurements are compared Goldston L-mode predictions.

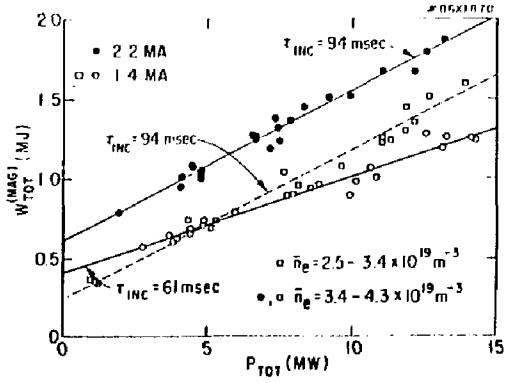

Fig. 6. Variation of the stored energy from magnetic measurements with total input power for the scans shown in Fig. 5. Also shown is data for a similar 1.4-MA power scan at lower density. The solid lines represent linear fits to the three data set.

for neutral-beam-heated TFTR plasmas were obtained. Power law fits to the combined L-mode data set resulted in $\tau_E \propto I_p^{0.6} P_{tot}^{-0.5} a^{0.8} R^{1.7}$, which has a significantly stronger size scaling and weaker current scaling than an empirical scaling based on data from smaller machines.[6,10]

Enhanced-Confinement Regimes

Because the FY85 L-mode confinement results did not extrapolate to the TFTR break-even goal, from the beginning of the FY86 run, the highest priority in the physics program was searching for enhanced confinement. The leading candidates for enhanced confinement were thought to be pellet-fueled discharges and discharges with more favorable profile shapes obtained, for example, by ramping the plasma current, modifying the heating profile, or controlling recycling. The energetic-ion (high T_i) regime was also studied, not on the basis of past confinement results but because of physics interest in high ion temperatures and high rotation velocities, and because of it's relevance to the two-component mode of operation for which TFTR was designed. It was indeed a pleasant surprise, therefore, that during energetic-ion experiments in June '86, enhanced-confinement operation was achieved along with record ion temperatures and Q values. In FY85, operation at low-plasma current yielded low densities giving central ion temperatures of $\leq$ 10 keV and toroidal rotation velocities of $\leq 6.5 \times 10^5$ m/sec (Mach number ~1) for co-injection with $P_{inj} \leq 6$ MW. In the beginning of the FY86 run, limiter degassing techniques were developed to reduce recycling in standard high-current TFTR discharges. In June, these techniques were applied to low-current target plasmas, while at the same time a significant amount of counter-injected power became available. This set the stage for the discovery of the "supershot" regime which thereafter dominated the FY86 physics program on TFTR.

Special Conditioning Necessary for the Enhanced-Confinement Regime

The graphite limiters on TFTR are capable of retaining deuterium, which can be desorbed from the surface layer and recycled back into the discharge. To degas the limiters and reduce recycling, a procedure was developed consisting of a large number (20-30) of low-current ohmic discharges which are not fueled following breakdown. Figure 7 shows the reduction in n_e and Dβ emission intensity during a 1.4-MA helium degassing sequence. A factor of 20 decrease in the deuterium influx indicates depletion of deuterium from the surface and near-surface regions of the limiter. Both deuterium and helium degassing shots have been used successfully, however, helium results in a lower density and a shorter density decay time τ_p^* following a brief diagnostic gas puff. The degassing is thought to involve deuterium desorption by carbon and helium ion bombardment. This is a separate process from the initial conditioning phase, in which water vapor and hydrocarbons are liberated. In addition to having a high-carbon density (Z_{eff} = 6-7), the low-density degassing discharges have a high edge temperature, which enhances the desorption rates. Once the machine is degassed in this fashion, it takes about five shots with significant gas puff fueling (50-100 Torr-liters total gas input) or 1-2 pellet-fueled shots

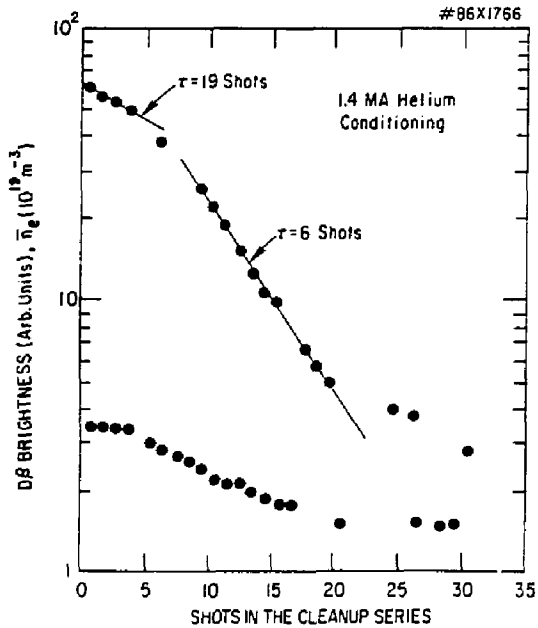

Fig. 7. Dβ emission intensity (upper points) and line-averaged electron density during a sequence of low-density 1.4-MA helium limiter-degassing discharges.

to refill the limiters. For a well-degassed inner limiter, values of τ_p^* as low as 0.15 sec have been observed, compared to 1.0 sec for gas-filled limiters and more than 10 sec for unconditioned limiters. Taken along with estimates of τ_p based on absolute Dβ intensity and Langmuir probe measurements, this means that the degassing reduced the recycling coefficient from about 1.0 to less than 0.5 and that the degassed limiters act as reasonably efficient pumps for deuterium.

Characteristics of Enhanced-Confinement Discharges

The change in performance in this regime is dramatic and is illustrated in Fig. 8, which compares an enhanced-confinement shot to a shot with similar discharge and beam parameters run with gas-filled walls. Although the density at the end of the beam pulse is the same, the prebeam density is quite different, as is the recycling rate indicated by the Dα intensity. A characteristic mark of a supershot is the continual rise in the stored energy and neutron emission through the 0.5-sec beam pulse. It is interesting to note that gas puffing with degassed walls to achieve the same prebeam density as the shot with gas-filled walls in Fig. 8 does not degrade the results, indicating that recycling is more important than average density in determining enhanced performance. Figure 9 shows the electron temperature and density profiles near the end of injection for the same two discharges. The central values are higher

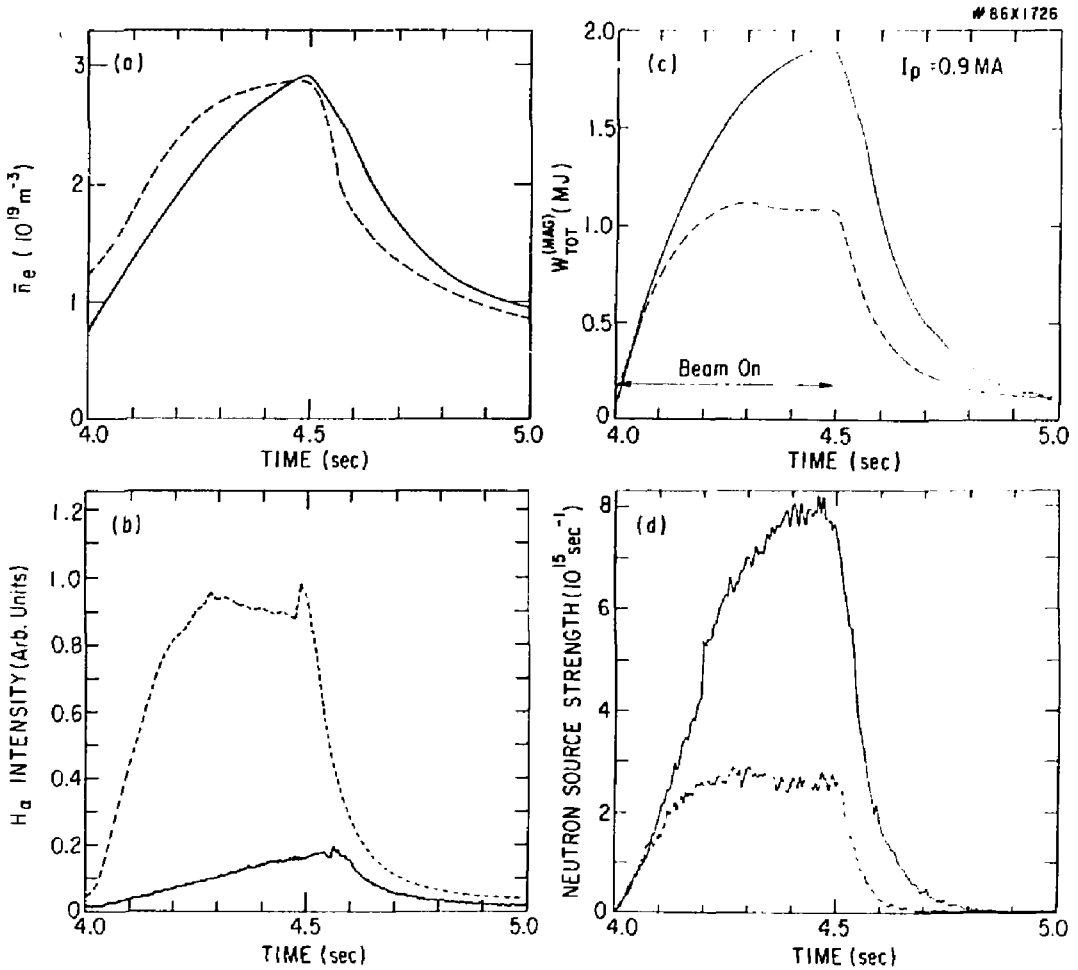

Fig. 8. Comparison of the evolution of line-averaged density, neutron source strength, Hα emission (which includes both Hα and Dβ emission), and stored energy for two discharges. The solid curves represent an enhanced-confinement discharge with degassed walls, and the dashed curves are for a similar discharge with gas-filled walls.

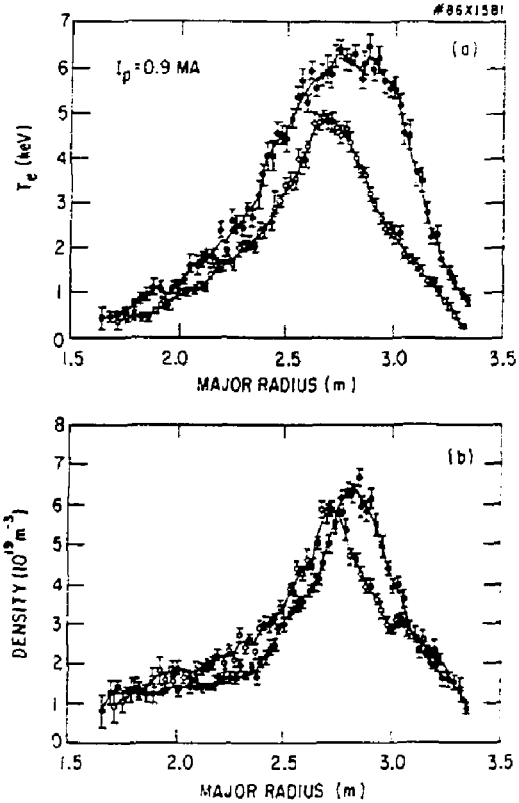

Fig. 9 Comparison of Thomson scattering measurements of the electron temperature and density profiles measured at 4.45 sec for the discharges shown in Fig. 4. The solid points are for the enhanced-confinement discharge.

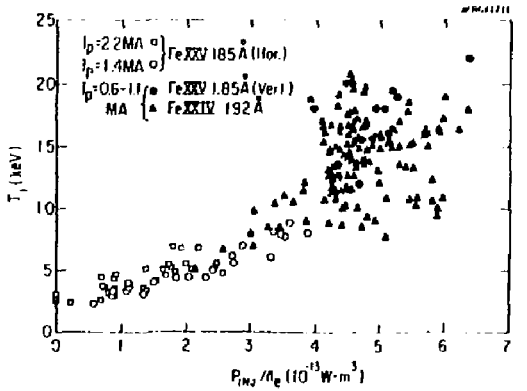

Fig. 10. Variation of ion temperature with normalized injected power. Closed symbols are for 4.8 < B_T < 5.2 T, 0.8 ≤ I_p ≤ 1.0 MA, R = 2.45 m, and a = 0.82 m. The open symbols are for the discharges shown in Fig. 5.

in the supershot, the temperature profile is broader, and the density profile is narrower. For these outward discharges $\beta_p \sim 2$, producing a large outward Shafranov shift of $\Delta R > 0.3$ m, and the vertical elongation κ changes from 1.05 to 0.90 during injection. One of the most striking features of this new regime is the high measured ion temperature. For the best shots, Doppler broadening of X-ray and vacuum ultraviolet (VUV) impurity Fe lines agree on a value $T_i \sim 20$ keV at a postion $r \sim 0.2$ m from the plasma magnetic axis. Figure 10 shows the ion temperature measured in the gas-fueled L-mode discharges along with those in the low-current, low-density regime.

Global Confinement Scaling in the Enhanced-Confinement Regime

From the time in June when it was discovered that an enhanced regime existing at low densities and currents, the neutral-beam-heating studies for the remainder of FY86 centered on understanding this mode of operation. A data base of magnetic measurements was assembled from about 600 discharges to study confinement scaling. Figure 11 shows how τ_E from the magnetics varies with I_p for injection powers of 10-15 MW. The open circles are from the standard L-mode regime described above with gas-filled limiters. The shaded region indicates the range of predictions of Goldston L-mode scaling. The best discharges in the range I_p = 0.8-0.9 MA show an enhancement of more than three times the L-mode confinement predictions. However, the I_p range for this optimum performance is narrow. The fall-off of τ_E at low I_p can be explained in terms of a β_p stability limit as discussed below. To remain within stable limits at high power, it will be necessary for TFTR to extend supershot operation to higher I_p. As indicated in Fig. 11, ramping up I_p during the heating pulse was a successful approach in this direction. Further extensions are expected with the

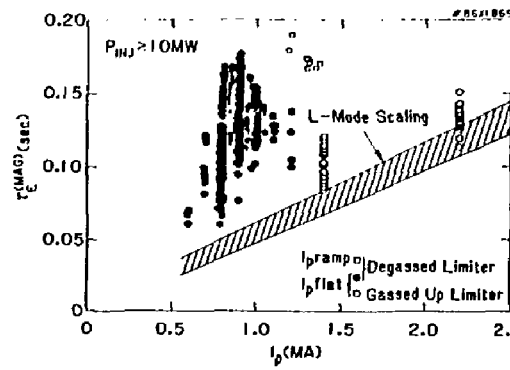

Fig. 11. Variation of total stored energy from magnetic measurements with plasma current for 10 ≤ P_{inj} ≤ 15 MW. Circled data points are for discharges with gas-filled walls. The crosshatched region indicates the predictions of Goldston L-mode scaling for this power range.

2.0-sec duration, high full energy species mix sources to be installed in FY87.

Unlike L-mode discharges, the confinement time in the enhanced-confinement regime did not degrade with heating power under optimized conditions as shown in Fig. 12. Note the importance of the co/counter fraction with optimum performance achieved using balanced injection. With unbalanced injection, rotation has several effects on the power deposition which might degrade confinement, as discussed in a later section. With one counter beamline in FY86, total injected power under balanced conditions was limited to about 12 MW. With $I_p = 0.9$ MA, using the full-power mix of $P_{co}/P_{ctr} \sim 0.7$, large-scale MHD activity or disruptions limited operation to $P_{inj} < 14$ MW. Operation at higher I_p or with I_p ramps allowed access to higher power. Installation of a second counter-injecting beamline

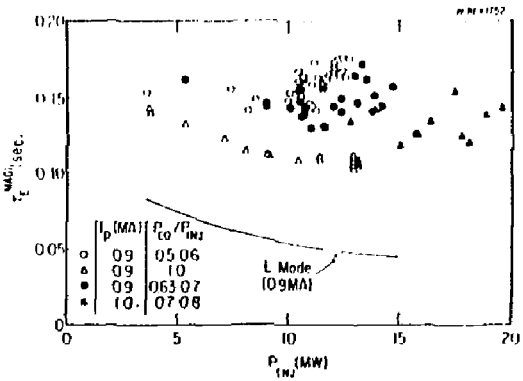

Fig. 12. Variation of global confinement with injected power for different values of fractional power in the co-direction. Data are for discharges with degassed walls and with no significant large-scale MHD activity. Magnetic measurements are compared to the L-mode predictions of Goldston.

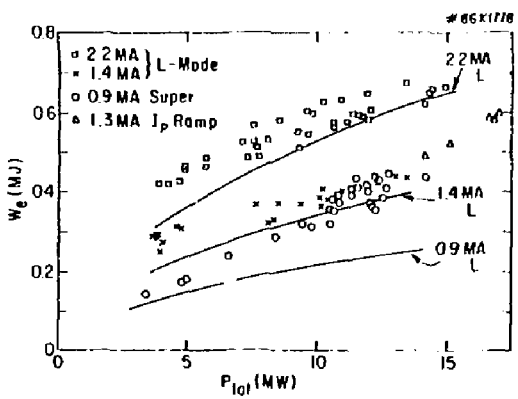

Fig. 13. Electron stored energy versus total heating power for 2.2-MA and 1.4-MA L-mode discharges and for 0.9-MA enhanced-confinement discharges. Also shown are enhanced confinement discharges at 1.3 MA, achieved by ramping the plasma current up from 0.9 MA during the injection pulse.

planned for FY87 will allow balanced injection to 27 MW.

In addition to an enhancement in the total stored energy, this new regime also exhibits improved electron stored energy as indicated in Fig. 13. The power scaling of electron stored energy for 0.9-MA discharges with degassed walls is compared to gas-filled L-mode discharges at 1.4 MA and 2.2 MA. The solid lines represent the predictions of Goldston L-mode scaling ($W_e^{pred} + 0.4W_{tot}^{pred}$).

Neutron Production and Q Values Achieved

The low-average densities with peaked density profiles and high temperatures have resulted in high-neutron source strengths for the enhanced confinement regime. A maximum neutron source strength S of 1.2×10^{16} n/sec and maximum yield of 6×10^{15} n/pulse were achieved with $P_{inj} \leq 19.6$ MW, beam voltage up to 98 kV (average full-energy component), and $P_{co}/P_{ctr} \sim 0.7$. S is proportional to $p_{inj}^{2.5\text{-}2.7}$, maximizes $I_p = 0.9\text{-}1.0$ MA, and increases strongly with $T_e(0)$. With more optimized balanced injection at $P_{inj} = 12$ MW and $I_p = 0.9$ MA, the best $Q_{DD} \sim 8.7 \times 10^{-4}$ was obtained, corresponding to $S = 8.9 \times 10^{15}$ n/sec.

The measurements of S generally agree well with the calculations of the SNAP time-independent radial profile code and with the TRANSP time-dependent transport analysis code with Monte Carlo beam ions. The discrepancy between the measured and predicted values is ±25%, which is within the experimental and modeling uncertainties. The simulations of the highest-Q case mentioned above show a breakdown at the end of the beam pulse of 17% beam-beam, 53% beam-target, and 30% thermonuclear reactions. With the same beam and plasma conditions (including $Z_{eff} = 3.3$) and with pure D^0 injection into pure T^+, this is equivalent to $Q_{DT} \sim 0.23$. Assuming a more realistic 50/50 D/T mix for the beams and the plasma gives $Q_{DT} \sim 0.18$. Substantial improvements in Q are expected from the better species mix and the higher voltage of the new FY87 sources. Further improvements should result from the addition of a second counter-injecting beamline and from a reduction in plasma impurity-ion content.

Driven Currents in the Enhanced-Confinement Regime

The surface voltage in these discharges is observed to drop during injection, sometimes to $V_{SUR} \sim -0.5$ V, which is consistent with the existence of the predicted bootstrap current.[11] The TRANSP simulation, which uses a 1½-dimensional magnetic diffusion calculation based on measurements of the time evolution of the temperature profile, Z_{eff}, and the magnetic boundary, indicates that much of this drop is expected due to changes in the plasma conductivity β_p and shape. Monte Carlo calculations show that beam-driven currents[12] further contribute to the drop,

even for balanced injection. To account for the observed negative V_{SUR} for near-balanced enhanced-confinement discharges, the model requires the inclusion of additional driven current and is consistent with the bootstrap current, as shown in Fig. 14. Verification of these driven currents would increase the prospects of a future steady-state tokamak.

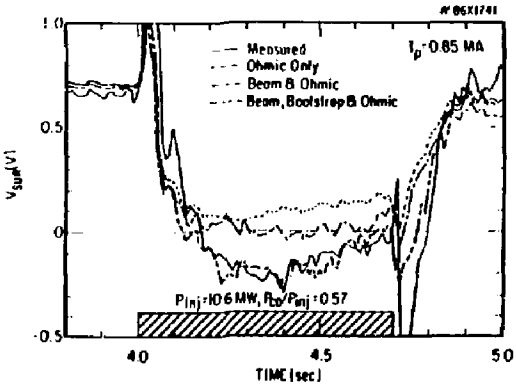

Fig. 14. Comparison of the measured surface voltage of an enhanced-confinement discharge with the calculated surface voltage under different assumptions for the role of nonohmically driven currents.

Impurity Behavior

For ohmic discharges on either the toroidal or movable limiter the dominant impurities are carbon and oxygen ranging (for I_p = 2.2 MA) from 10% of the electron density at the low-density limit to 1% at the high-density limit.[13] The ratio of carbon to oxygen varied from 10 to 1 between these limits, resulting in Z_{eff} values of 5-6 to 1.2, respectively, with a negligible contribution due to metals.

In the neutral-beam-heated phase of standard L-mode discharges on either limiter, Z_{eff} was found to increase with beam power for constant I_p and n_e.[1] Because of significant beam fueling, however, to hold n_e constant at the end of the beam pulse, the low-power discharges had higher density, cleaner target plasmas. X-ray measurements of impurity concentrations at the end of the beam pulse were found to correlate less strongly with the beam power or density at that time than with the target density as shown by the Z_{eff} trend in Fig. 15. The trend is similar to the Z_{eff} trend before injection except for a reduction due to impurity dilution by beam fueling. Carbon was again the dominant impurity, with significant metallic contributions to Z_{eff} only at very low density. The radiated power fraction was typically 20% for $P_{inj} >$ 10 MW.

The low-density enhanced-confinement target plasmas were again carbon dominated with total Z_{eff} = 6-7, a metallic (Cr, Fe, Ni) Z_{eff} contribution of 0.3-1.5, and a radiated power fraction of 60-70%. The target

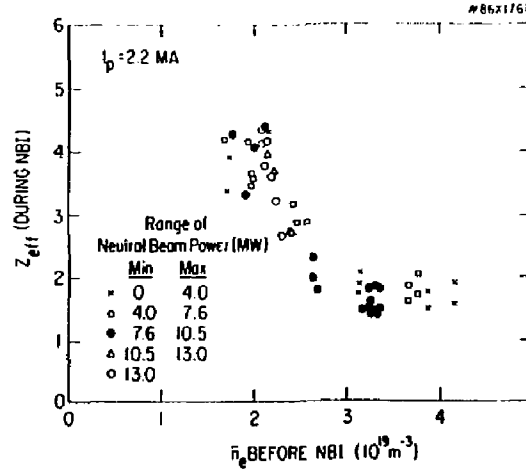

Fig. 15. Z_{eff} during neutral-beam injection as a function of electron density before injection, sorted by ranges of neutral-beam power. The values are near the prebeam values, but somewhat reduced due to neutral-beam fueling.

deuteron density was estimated at only 10-20% based on the increase in neutron emission following a deuterium gas puff. During neutral-beam heating, Z_{eff} dropped to 2-4, the deuteron fraction increased to 50-75%, and the radiated power fraction fell to 30% for $P_{inj} >$ 10 MW. The impurity confinement time for germanium introduced by laser ablation was about 0.25 sec for both phases. The time evolution of several germanium impurity lines was modeled for both cases by the MIST code using an assumption of a radially independent diffusion coefficient D = 0.65-0.75 m^2/sec and convective velocity at the limiter radius v = 0.0-0.2 m/sec (Ref. 14).

Metal levels increased by a factor of ten in the five run weeks following the initial supershot results. Presumably, the metals originated from Inconel slats near the toroidal limiter and were subsequently deposited on the graphite surface. Even though metals eventually contributed up to 1.5 to the total Z_{eff} at the end of the heating pulse, the central radiated power was insignificant in the overall core power balance. However, to maximize Q in the future, it will be very important to minimize ion depletion by reducing carbon and metallic impurities.

MHD Activity, Stability, and Fluctuations

The most obvious MHD phenomenon in ohmic and standard L-mode discharges are the sawtooth oscillations which limit the central temperature and may dominate the central energy transport. Characterizations of several types of TFTR sawteeth were made, and these were not well correlated with the usual global quantities.[15] This suggests a strong sensitivity to local parameters. Work continued in an effort to understand the fast time scale of the sawtooth

crash τ_{cr} = 40 μsec – 5.0 msec, which can be much faster than the resistive time scale of the Kadomtsev model. The crash duration was well correlated with growth time of an m = 1 mode during the crash. One of the interesting features of the enhanced-confinement regime, which could relate to the observed I_p scaling, was the lack of sawteeth for discharges with $q_{cyl} > 5$. For lower-q_{cyl} discharges in this regime produced by lowering B_T, there were infrequent minor sawtooth-like events which were believed to be insignificant.

Large-scale MHD activity was, however, a problem in the enhanced-confinement regime, particularly as β_p approached two by going to lower I_p or higher P_{inj}. Figure 16 compares two discharges with the same operational parameters and limiter histories. There is a clear correlation between the onset of the MHD activity and the degradation of confinement. This coherent MHD activity is typically characterized by m/n = 2/1 or m/n = 3/2. In some cases, disruptions result in a loss of thermal energy in less than 100 μsec and a slower 50-msec collapse of the current. The β_T values achieved are compared in Fig. 17 to the Troyon predictions of optimized ideal-MHD kink stability theory.[16] The experimental limit of $\beta_n \leq 2.2$-2.5 observed primarily for $q < 4$ on other machines does not appear to be the governing limit for TFTR high-q enhanced-confinement plasmas. Rather, there appears to be a $\beta_p \leq 2.2$ ($\epsilon\,\beta_p \leq 0.7$) limit, as illustrated in Fig. 17. High-β_p pressure profiles (with calculated ion components) are found to be marginally unstable to $n \rightarrow \infty$ ideal ballooning modes,[17] although high-n modes were not always observed before high-β_p disruptions.

Broadband turbulence (10-200 kHz) has been measured by Langmuir probes in the plasma scrape-off region with fluctuation levels $\Delta n/n \sim 0.3$-0.5 and $\Phi/T_e \sim 0.1$. Similar frequencies are seen in the imaging of Dα light from the inner wall (see Fig. 36 in the Diagnostics Section) with λ_{pol} = 0.03-0.07 m and $\lambda_{tor} > 1.0$ m. Magnetic fluctuations at 100 kHz measured 0.11 m from the plasma increase with injection power for both L-mode and supershot discharges. However, the fluctuation levels do not appear to be correlated with global confinement, since they are very sensitive to small gas puffs which

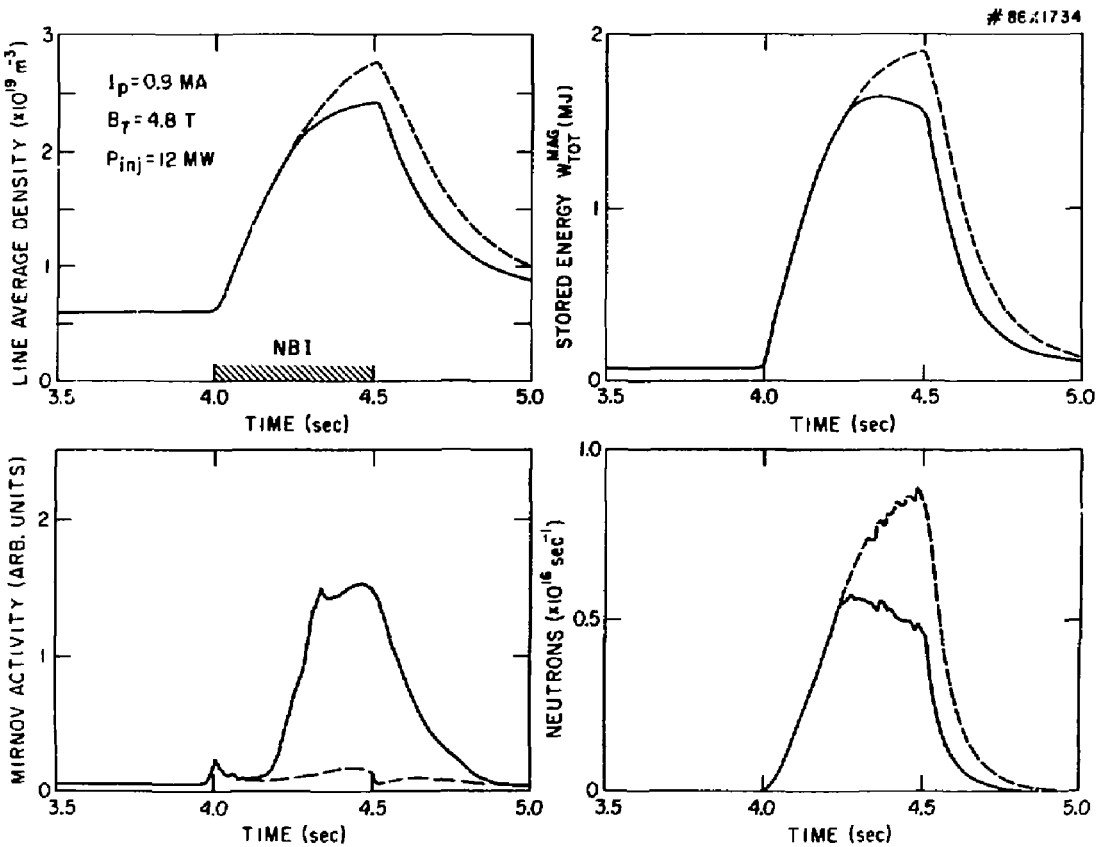

Fig. 16. MHD activity, as indicated by the Mirnov signal, can have a large effect on performance in the enhanced-confinement regime.

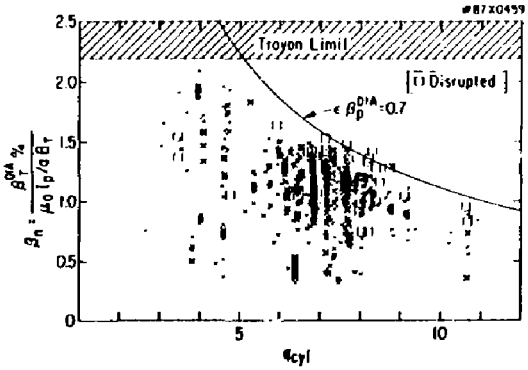

Fig. 17. Beta values normalized according to $\beta_n = \beta/\beta_c$ ($\beta_c = \mu_0 I_p/aB_T$) for TFTR enhanced-confinement regime plotted as a function of q_{cyl}. The square symbols show discharges that disrupted during the neutral-beam pulse. The curve represents $\epsilon\beta_t = 0.7$.

strongly affect the local edge conditions but not the global parameters.

The Role of Electron Temperature and Density Profiles

In the last several years, it has been found that the shape of the electron temperature profile is insensitive to a variety of conditioons. This observation has been termed "profile consistency." Since the profiles of $T_e(r)$ and J(r) are related through Ohm's law, one expects to find in normal ohmic and L-mode discharges that the parameter $T_e(0)/\langle T_e\rangle$ is a well-defined increasing function of q(a) for a wide range of densities and heating powers. This observed relationship, together with the constraints imposed by sawteeth on the current profile J(r) and a thermal diffusivity profile $\chi_e(r)$ that is peaked at the edge, provides a substantial profile-control mechanism.[6,18] Another formulation of profile consistency argues that sawtooth oscillations dominate the profiles within the inversion radius and, therefore, the consistency of profiles normalized, for example, to T_e at a/2 is more relevant as an indicator of microscopic transport mechanisms. To transiently decouple $T_e(r)$ and J(r), a fast current ramp (up to 3 MA/sec) was applied to a TFTR discharge in equilibrium. Calculated J(r) profiles, which were in agreement with global magnetic measurements, showed large perturbations. $T_e(r)$ profiles normalized at a/2 were unchanged during the transient, indicating that the shapes based on normalized profiles are not tightly coupled to J(r) or q(r).[19] In another experiment, $T_e(r)$ was unchanged when the same amount of power was used to heat the plasma first with sources aimed at the edge and then at the center.[20] This confirmed earlier experiments on the invariance of the temperature profile shape to heating profile. These experiments had been based on comparisons of the shapes for ohmic versus neutral-beam-heated dischages and for neutral-beam-heated discharges with and without pellets.[9]

The 0.9-MA TFTR enhanced-confinement $T_e(r)$ profile clearly violates profile consistency based on $T_e(0)/\langle T_e\rangle = f[q(a)]$, since it is significantly broader than a 1.4-MA L-mode profile under the same conditions. Figure 18 shows flux-surface-mapped profile shapes normalized at a/2 for the data shown in Fig. 13. Outside a/3, the shapes are very similar for a wide variety of conditions. In the absence of sawteeth, which depress the central region of the L-mode discharges, one mechanism for the depression in the enhanced confinement shapes is convection loss due to the cold electrons introduced by the beams. With the constraint of profile consistency, it has been argued[21] that energy confinement is significantly determined by edge conditions. For enhanced-confinement discharges, the edge is characterized by higher temperature and temperature gradients, lower density, and low recycling than in L-mode discharges.

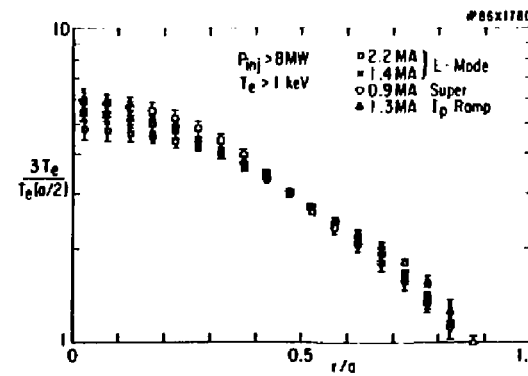

Fig. 18. Electron-temperature profile shape normalized at r = a/2 for the data sets of Fig. 13. The factor of three applied to center the mid-radius on a single decade scale. Error bars represent root mean square variation of data.

Profile consistency arguments would also predict a gain in confinement for given transport coefficients if the density profile were centrally peaked, since edge heat outflow would then be minimized.[21] The peaking in the case of enhanced-confinement discharges may well be caused by a beam build-up instability, which for low currents is intensified by low-edge density and the Shafranov shift. Experimentally, it is observed that at constant power the peaking is maximum for balanced injection and falls off toward either an all-co or all-counter mix. Classical effects would predict this behavior, to some degree, due to rotation for unbalanced injection. The rotation speed has been measured to be as high as 8×10^5 m/sec for co-only injection at 13.5 MW. The reduced beam-ion velocity in the plasma frame could cause a broadened deposition profile as well as more charge-exchange loss. In addition, the power invested in rotation (up to 40% in extreme cases) is likely to be dissipated by viscous damping in the edge regions and may

not be efficiently converted to plasma heating. The broadened deposition and possible loss in heating may contribute to the confinement dependence on co/counter fraction.

Near the end of the run, an experiment was performed in an effort to capitalize on the advantages of peaked density profiles using free expansion target plasmas. It had been noted previously[22] that the density profiles for discharges which were compressed away from the outer limiter, and then allowed to expand back into limiter contact, could be quite peaked during the expansion stage. Preliminary results using these peaked target profiles indicated slight improvements in stored energy and neutron emission over the best performance of the normal target plasma at the same plasma current (0.73 MA). This is at least partially due to the fact that the free expansion target was able to absorb more injected power without disrupting.

HEATING SYSTEMS

Neutral-Beam Heating

Injection with four beamlines and eleven ion sources began in January 1986 and continued throughout the fiscal year. The twelfth power system was left with the test stand to allow pre-tokamak operation of long-pulse ion sources. During the course of the year, the power injected into TFTR gradually increased as a result of source conditioning and improvements to hardware and operating techniques. By the end of this operating period (late October 1986) a maximum of 20 MW at energies up to 110 keV had been injected. During the last day of operation, the pulse length was extended, with 17 MW being injected for 0.8 sec and 15 MW for 1.0 sec.

Neutral-Beam Operations

The fall shutdown of the neutral-beam systems, in early FY86, ended with the completion of the upgrades of the modulator/regulators (mod/regs) and the total system dummy load test of eleven neutral-beam power systems. Ion sources were mounted in the TFTR Test Cell and eleven ion-source operation began in January 1986. Much emphasis was put on training the neutral-beam operators and improving system reliability while supporting TFTR operations.

The end of FY86 saw the remote manual control of ion sources through central instrumentation, control, and data acquisition (CICADA) from the TFTR control room. A maximum of 20 MW was injected into TFTR at beam energies up to 110 keV.

Neutral-Beam Control Systems

Toward the end of this year the neutral-beam and CICADA groups achieved their goal of complete computer control of the eleven plasma heating beams and the single beam test stand. The scope of this complex task has required more than 80 electronic-equipment racks, 95 satellite input/output (I/O) stations, and approximately 1,500 input/output modules. During each beam-pulse cycle, this equipment scans over 8,000 signals and generates 1.5 million data words input to the host computer system. Most of the data represent transient phenomena that are processed and displayed in the control room as 300 diagnostic waveforms. The goal of presenting all this information to the beam operators in a time consistent with a beam-pulse cycle, or approximately 2 minutes, is near. In addition to the technical features of the system, the controls and displays of the operating station have been arranged and organized to allow an operator simultaneous control and monitoring of three ion sources. Formerly, under local control, each of the 12 ion sources required a dedicated operator. The reduced requirement has allowed beam operations with all sources to extend into two shift runs with no increase in support staff level.

The remote computer-control functions are augmented by a number of real-time control systems designed to protect and interlock the beams from equipment damage and illicit modes. The most complex is the vacuum- and cryogenic-control system that manages the sequencing, monitoring, and fault logic of the valves, pumps, ion gauges, and level indicators on all beamlines. The heart of this system is an Allen Bradley programmable logic controller (PLC) that scan over 2,000 signals every 100 msec. During this fiscal year, all control subsystems have been integrated into the beam system or are in the final stages of checkout.

Neutral-Beam Diagnostics

Diagnostic activities in support of TFTR heating operations were pursued in parallel with continued installation and integration of diagnostic hardware and software systems. Emphasis was given to integration and enhancement of the calorimetery system, improved optical measurements of species,[23] beam-line dynamic-gas response measurements, transition-duct reionization loss and outgassing measurements, pyrometer-interlock[24] integration, and off-line VAX cluster data-base analysis.

Figure 19 shows a correlation of ion-source N4C accel current in amperes versus the accel voltage in volts to the 3/2 power obtained using the off-line neutral-beam data-base on the VAX cluster. This data shows the ion-source behavior as accel grid conditioning was attempted from 70 kV to 100 kV at constant perveance (perv). The line through the data is the result of a least-squares-fit showing the average operating perveance was 1.65 micropervs. Similar correlations between beam electrical, gas, cryogenic, and physical variables can, if desired, be performed daily to optimize operations.

Five diagnostic systems were used for initial species measurements during TFTR neutral-beam

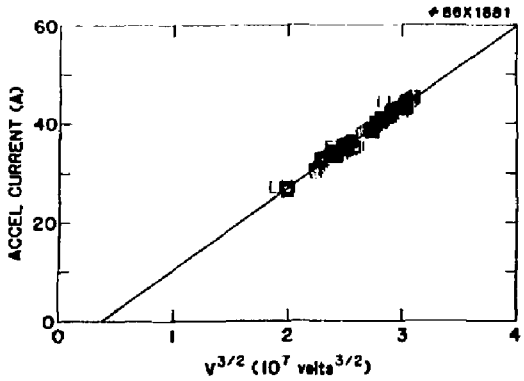

Fig. 19. Accel current in amps versus accel voltage in volts to the 3/2 power for ion source N4C. Shown is the accel grid conditioning history from 70 kV to 100 kV at constant perveance and the result of a least-squares-fit that yielded an average operating perveance of 1.65 micropervs.

test-stand operations involving four different 500-msec ion sources and a variety of configurations and operating conditions. Measurements were made using an optical multichannel analyzer (OMA), charge-exchange spectrometer, Rutherford backscatter spectrometer, beam implantation/secondary-ion mass spectroscopy (SIMS), and a D-D reaction product analyzer. Using these diagnostic systems, initial results were obtained for total neutral-species fractions at the beam-line input and the beam-line output, differential radial profiles of species fractions, angular divergencies of species components, species radial power-density profiles, and beam impurity component for various conditions.[25]

After completion of 500-msec pulse operations, the TFTR neutral-beam test stand was upgraded in preparation for testing 2-sec long-pulse ion sources (LPIS) at full power. The diagnostic modifications involved placement of additional thermocouples to monitor prototype upgraded LPIS scrapers, installation of high transmission fiber optics from the LPIS and transition duct regions to spectrometers located at the 138-ft level diagnostic area for improved OMA species measurements, remote control of the Rutherford backscatter spectrometer viewing angle to allow species radial-profile scanning, a neutron-He^3 coincidence experiment for species measurements in the neutralizer region, enhancements to the charge-exchange analyzer system to allow improved beam energy profile measurements and the detection of low intensity beam components, placement of an annular surface-barrier particle detector in the gas stripper cell of the charge-exchange analyzer for in-situ D-D reaction species measurements, and modification of the automated beam implanation/SIMS sample changer to permit insertion of implantation targets at the entrance to the gas-stripper cell of the charge-exchange analyzer.

Cryogenics

The 1070-watt helium refrigerator was operated and maintained by CVI, Incorporated of Columbus, Ohio under subcontract to PPPL. The operations crew was supplemented with PPPL personnel. This refrigerator supplied liquid helium at 4.5°K to cool the helium cryogenic-pumping panels in the neutral beams in the Test Cell and test stand. During FY86, the refrigerator was operated for a total time of 5,621 hours.

Power System Upgrade

The upgrade of the mod/regs by RPC Industries was completed in December 1985, and all mod/regs were tested to full voltage (120 kV) on the dummy load and certified as passing acceptance tests. Except for minor thermal problems and documentation inconsistencies, the RPC upgrade appears to be successful.

Last year's report stated that operation was limited to 95 kV and below because of the lack of arc-modulator units. However, it has been found that operation was greatly improved by eliminating a leading-edge transient. This was done by reversing the accel and gradient-grid triax connections and adding appropriate voltage-compensating capacitors at the input to the transmission line beween the mod/regs and the high-voltage enclosure (HVE). This has improved operation to the extent that the arc modulators are not presently used.

Mechanical Systems

The primary emphasis during this year's activities was on maintaining operational readiness of all four neutral-beam lines and improving reliability.

Significant downtime was attributable to an inadequate fatigue lifetime of the bellows in the calorimeter assemblies. These bellows provide the primary vacuum boundary for the mechanism that raises and lowers the calorimeters between source-conditioning pulses and injection into the torus. These bellows only survived 1,000 to 2,000 cycles before developing leaks necessitating a beam-line warm-up and opening to atmosphere. The resultant downtime of that beamline was five run days. Design was completed for a new bellows with an anticipated fatigue lifetime in excess of 20,000 cycles. Fabrication of the new bellows was started with delivery expected during December 1986-January 1987.

A major effort was the maintenance of ion sources whose filament lifetime was limited to approximately 8,000 pulses, i.e., four to eight weeks of operations. Therefore, the eleven operational sources had to be replaced with refilamented units on a regular basis. This was accomplished by maintaining an adequate number of spare assemblies. Three ion-source assemblies were completed within their source housing and five spare arc chamber assemblies were completely tested in preparation for installation during maintenance downtimes.

During the previous TFTR operational period, five arc-chamber assemblies suffered significant mechanical damage due to electrical shorts developing. The arc chambers contain 204 filaments of 0.020-inch diameter tungsten, each carrying a current of about 23 A. Shorts developed as filaments wore out, allowing a substantial portion of the 5,000-A filament current to flow at a single location and resulting in major hardware damage. Various ceramic and mica insulators were installed so that multiple shorts were required to permit a total arc-power discharge. Operations with eleven sources resulted in no damage to any arc chambers, even though electrical shorts developed in several.

Long-Pulse Ion-Source Upgrade

The two prototype long-pulse ion sources produced by the industrial subcontractor (RCA) were tested at the Lawrence Berkeley Laboratory (LBL) on the Neutral-Beam Engineering Test Facility (NBETF). One hundred consecutive two-second pulses were achieved at 120 kV utilizing deuterium gas with good performance characteristics. The extraction area of the new sources is 12 cm by 43 cm in comparison with the 10 cm by 40 cm aperture of the existing one-half second sources. The full energy component of the ion beam is between 80% to 90%. RCA delivered eight production long-pulse sources to PPPL (see Fig. 20) and the prototype units were returned to RCA for refurbishment.

Detailed design and analysis of the various components requiring upgrading was completed with the exception of the ion-dump/bending-magnet system. Hardware was fabricated and installed in the neutral-beam test cell (NBTC).

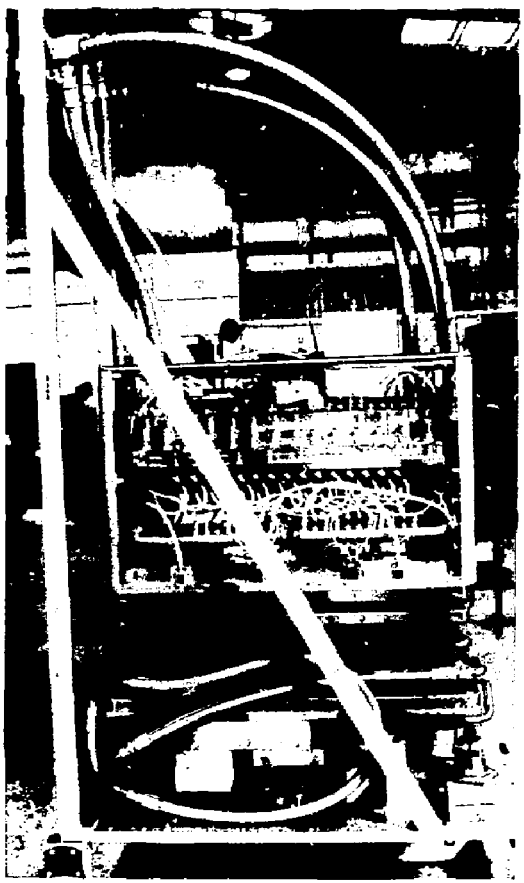

Fig. 20. TFTR long-pulse ion source (LPIS) mocked up for installation. (86E0955)

Long-Pulse Ion-Source Operation

In November and December 1986 the present LBL short-pulse ion sources (with a nominal pulse-length capability of 500 msec) will be replaced with LBL long-pulse sources. The accelerator structure is actively cooled, with water flowing through each of the molybdenum grid rails. In addition, the plasma chamber has been deepened, and it is surrounded by samarium-cobalt permanent magnets that create a multiple-line cusp field to improve plasma confinement and enhance the atomic-ion fraction of the plasma. Finally, the filaments are less numerous and of a different design, and they must be run well into the emission-limited regime to avoid mode flipping. Running with the filaments strongly emission limited means that the arc conditions are very sensitive to the filament temperature, which is in turn determined by the sum of the directly applied filament heating current and the arc current flowing through the filaments.

The "first article" long-pulse ion source was run during spring 1986. This source differed from most of the production sources in that it had a stainless steel flange on the cusp-confinement section of the arc chamber. Although considerably more difficulty was encountered in conditioning this source than has been experienced with the short-pulses sources, it did eventually reach 96 kV for one second (although with interrupts). When this source was opened it was found to have nine melted areas on the stainless steel flange.

In September, a production long-pulse source was mounted on the test stand, equipped with 44 double-hairpin filaments which were subsequently replaced with 32 filaments of a new design in which the lengths and shapes are varied to place the emitting tips in relatively similar magnetic fields. Operations have since resumed, with the source conditioning upwards in voltage. The goal of these operations is to develop techniques and procedures for long-pulse source operation on TFTR, and to test the limits of the ion source, power supplies, and beamline components.

Ion Cyclotron Radio-Frequency Heating

A proposal to apply heating in the ion-cyclotron range of frequencies (ICRF) to TFTR was submitted to the Department of Energy (DOE) in September 1985, reviewed in December 1985, and officially approved in March 1986. Subsequently, in April 1986, the schedule was modified in accordance with the DOE TFTR Program Review Panel recommendation that high-power experiments begin on TFTR as soon as possible.

The goal of the TFTR ICRF project is to provide an ICRF system with 9-10 MW of source power that is to be used to heat the core of relatively high-density plasmas in TFTR and thereby optimize the Q value. Under the present schedule, 6 MW of source power will be applied through two antennas, one of which is to be supplied by ORNL in summer 1987. An additional 3-4 MW of source power is to be added in the spring 1988.

The project will utilize radio-frequency (rf) generators that are already installed on the Princeton Large Torus (PLT) device. They will remain in place at C-Site, but their operating frequencies will be changed and their output power increased. The power will be transmitted to TFTR at D-Site via a low-loss transmission line system, and a rf enclosure containing safety switching and impedance matching will be erected in the mock-up area adjacent to the Test Cell. Appropriate ports on the torus were selected which satisfy the coupling requirements for the rf and which incur a minimum disruption of the machine configuration by movement of devices already connected. The limiter configuration will be changed; the removal of the limiters at Bay M and the installation of new "rf limiters" permit the use of large port at Bay M and a medium port at Bay L for the antennas (Fig. 21). Two antenna elements will be installed in each of these ports.

An accelerated schedule was developed that requires two 3-MW radio-frequency generators to be available to operate at 47 MHz, the transmission system to be in place, and two antennas to be installed at a machine opening in May 1987. At this time, the new rf limiters will also be installed on TFTR. The second two rf generators to operate at 1.5-2 MW, each at a variable frequency between 40 MHz and 80 MHz, are to be completed to maintain the schedule for full 9-10 MW operations by April 1988.

In order to design, fabricate, test, and install the antennas in the planned May 1987 shutdown, a cooperative agreement with Oak Ridge National Laboratory (ORNL), Fusion Energy Research Division, has been made, whereby ONRL will design and fabricate the launcher assembly for installation in Bay L in May 1987 (Fig. 22). The ORNL antenna will be capable of tuning from 40-80 MHz, whereas the PPPL antenna will operate at fixed frequency. The designs will be reviewed on a combined basis, and component testing will be carried out at Oak Ridge using the Radio-Frequency Test Facility (RFTF). This

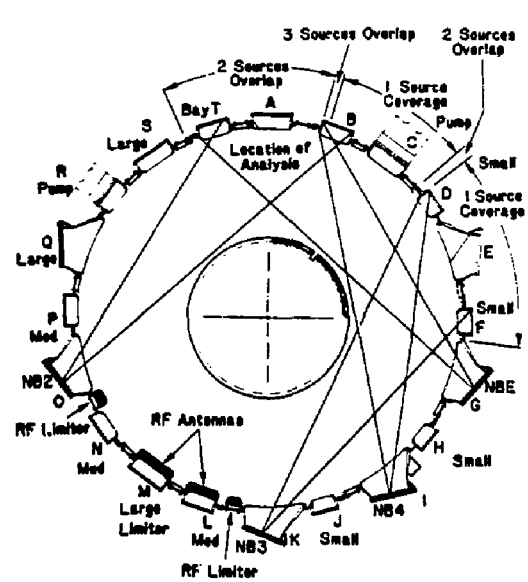

Fig. 21. Radio-frequency antennae and radio-frequency limiter locations.

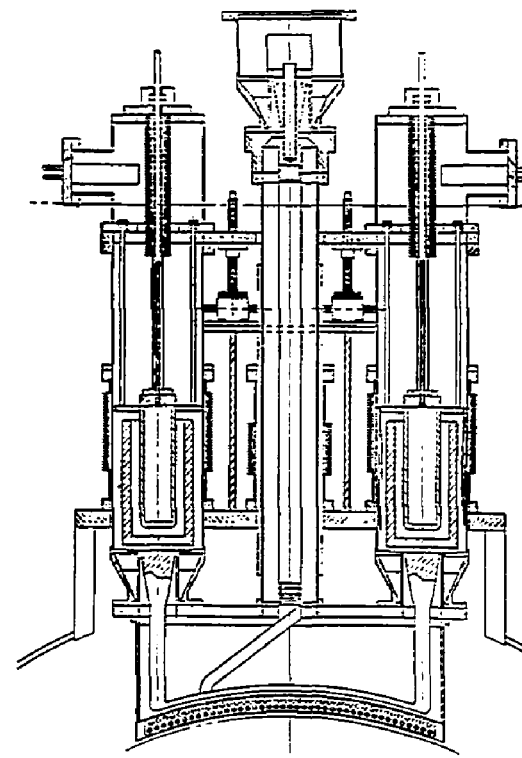

Fig. 22. Oak Ridge National Laboratory antenna design. (86X3357)

facility will be powered by an upgraded rf source presently being modified by Continental Electronics Manufacturing Company (CEMC) in Dallas, Texas. This source is almost identical to the two sources that will be upgraded at PPPL to provide the additional 3-4 MW by April 1988.

Power Systems

In July 1986 a restructuring of the TFTR organization led to the creation of the Heating Systems Division and, within that division, the Power Systems Branch. With the creation of the Power Systems Branch, consisting of the Energy-Conversion System (ECS) and Motor-Generator (MG) Section, it is recognized that these systems have technical commonality and have matured sufficiently so that a single group of engineers and technicians can most effectively operate, maintain, and improve the equipment.

The ECS and MG systems have reached and now routinely operate at levels corresponding to their original design ratings so that the focus for 1986, that will continue in 1987, has been toward reliability, maintenance, upgrades, and cross-training for efficient operation.

Motor-Generator System

The MG sets are now routinely operating at their full pulsed power rating and have achieved availability levels exceeding 95%.

With mechanical balance problems resolved and well understood, problems in the area of cycloconverter-control circuitry remained as the last impediment against the realization of the high reliability expected for this type of equipment. Improvements in the controls have now virtually eliminated the spurious cycloconverter suppressions and fuse blowing that had previously caused considerable downtime.

Maintenance work is performed on a subcontract basis by the equipment manufacturer, General Electric (GE), which ensures continuing reliable operation.

In order to provide the higher levels of pulsed power and energy associated with the upgrading underway in the ECS, and in anticipation of the Compact Ignition Tokamak (CIT) demands, a program has been underway to determine the maximum performance that can be safely obtained from the MG equipment. Preparations have been made and await testing for the extension of the lower limit of output frequency from 60 Hz down to 50 Hz. An extra 610 MJ per set becomes available with this improvement, raising the energy available during a TFTR pulse from 4.5 to 5.72 GJ. Additionally, in cooperation with GE via subcontract, studies are underway to determine the maximum peak power available from the MG sets. Measurements of stator end winding forces and deflections were made to verify computer modeling being used to quantify stress levels and margins against safe limits. Additional studies will be required to quantify the limitations imposed by the exciter and field response. Preliminary expectations are for an increase in rating on the order of 15% to 20%.

In anticipation of the remote control necessitated by TFTR D-T operation and in an effort to tailor power demand so as to minimize operating expenses, efforts toward the full automation of MG control via CICADA (excepting the start-up and shutdown sequences) will continue and should lead to full functionality during the next year.

Energy Conversion System

All ECS equipment has now been fully commissioned and all subsystems have been operated at or above their original design ratings. The parallel capacitor bank discharge awaits test time for full-energy demonstration, however, since this mode has been successfully tested only up to 2/3 rated voltage.

Availability levels exceeding 95% have been achieved. This accomplishment is attributable to many factors, including the control hardware improvements introduced via the efforts of the PPPL Engineering Division, the utilization of a more or less fixed configuration (now that the commissioning phase is complete), an expanded preventive-maintenance program, a complete spare parts inventory, and a stable and experienced operations team.

The primary technical accomplishments for the year included the commissioning of the equilibrium-field paralleling mode, the bidirectional horizontal-field mode, and the parallel capacitor bank operation. The two former accomplishments were achieved in cooperation with the PPPL Power Engineering Branch of the Engineering Division, while the latter was done in cooperation with an engineer on temporary assignment at PPPL from the University of Braunschweig in Germany.

During the year, the section has continued to concentrate on the elimination of remaining reliability weaknesses and the realization of the ultimate capabilities of the equipment, both for TFTR upgrades and in anticipation of CIT. The latter effort involves some hardware upgrading, but it primarily entails the identification and precise statement of limits and the implementation of a higher level of protection sophistication so as to take full advantage of all existing capability. The outcome of this work will lead to greater capability in all systems, but in particular will permit the ohmic-heating upgrade from ± 24 kA existing to ± 30 kA future.

Finally, a determined effort was undertaken to procedurize the accessing of equipment enclosures to enhance the safety of the operation. Besides a general reduction in accident probability, the procedurization reduces the daily operation's dependence on the presence of key individuals. This effort is nearly complete and will lead to a formal training and certification program in the near future.

DIAGNOSTICS

Fiscal year 1986 was a period of vigorous operation of the TFTR machine. The majority of the effort of the Diagnostic Division was expanded on acquiring and analyzing data and preparing presentations. There was scant access to the machine for upgrade and installation during the few open periods between September 1985 and October 1986. In addition, the large number of weeks of two-shift operation made maintenance of the existing diagnostic set, listed in Table I, more difficult. Nevertheless, TFTR diagnostics operated with high reliability to produce the data required for the physics program of the past year. The data is interesting from the diagnostician's point of view, but space limitation does not permit presentation here. Readers seeking details of the experimental techniques will find an excellent collection of articles in *Review of Scientific Instruments*, Vol. 57, (August 1986).

In spite of the limited access to TFTR during the year a large number of upgrades and additions were made to diagnostics (Table II). These new features are highlighted in this section.

The division gave high priority to improvements in the measurement of ion temperatures. To provide additional spatially resovled ion-temperature profiles a diagnostic neutral beam (DNB), improved charge-exchange neutral analyzer (CENA), and a system to do charge-exchange recombination spectroscopy (CHERS) were installed.

Diagnostic Neutral Beam

Figure 23 shows a layout diagram of the DNB and its relationship to the other ion-temperature diagnostics.[26] The device operated up to 70 hours per week with more than 95% reliability for H^0 injection into D^+ plasmas, achieving fluxes of 13 A at 63 kV. This is short of its maximum rated capability of 80 kV, 22 A, but is more than adequate for the accurate measurement of ion-temperature profiles during ohmically heated plasmas, giving a factor of 3-9 increase in charge-exchange flux. The current is not yet sufficient to determine profiles during high-power neutral-beam heating.

The DNB has operated with single pulses of 20-200 msec duration thus far. In the coming year it is planned to increase the pulse length to 500 msec and to modulate the beam for some experiments. There was only one day of DNB operation to produce D beams, and the injector achieved 54 kV at 9 A (max rating in D is 80 kV, 17 A). There does not appear to be any fundamental impediment to increasing the current and voltage to their maximal ratings.

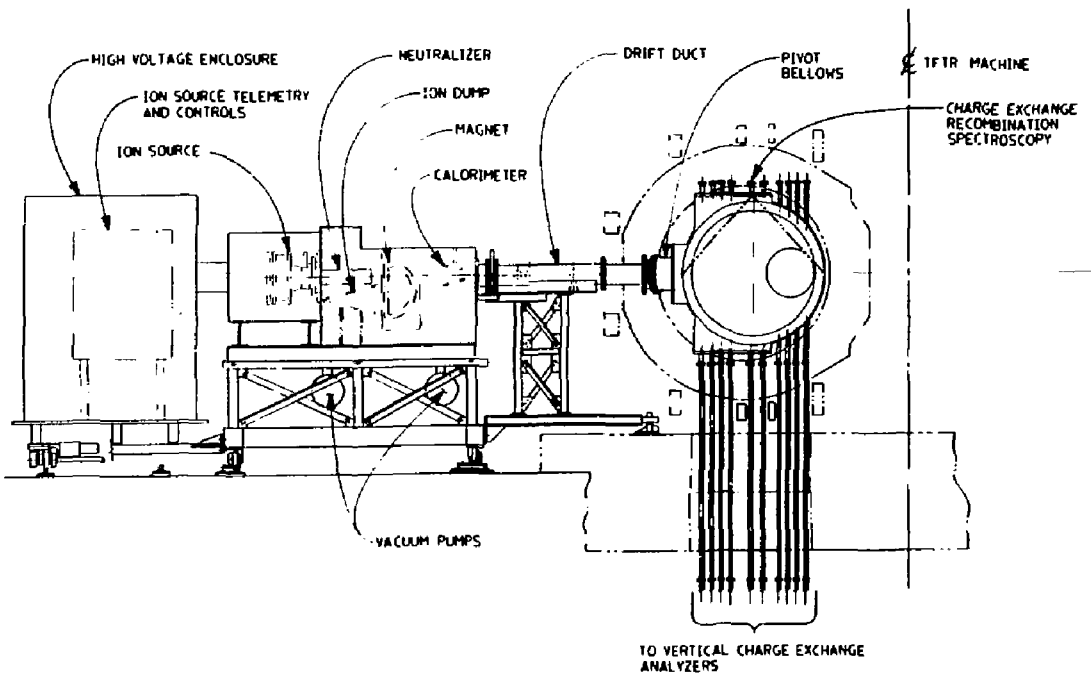

Fig. 23. Schematic of the diagnostic neutral beam showing its relationship to charge-exchange neutral analyzer (CENA) and charge-exchange recombination spectroscopy diagnostics.

Table I. Diagnostics Operational at Start of FY86.

Electron Density	
1-mm Microwave Interferometer	Horizontal Midplane
Multichannel FIR Interferometer	5 Vertical Chords
Electron Temperature	
TV Thomson Scattering	Radial Profile at two times during pulse
ECE Heterodyne Radiometer (75-210 GHz)	Radial Profile
X-Ray Pulse-Height Analyzer	Horizontal Midplane
ECE Fourier Transform Spectrometer	Radial Profile
Ion Temperature	
Charge-Exchange	2 Horizontal Chords
X-Ray Crystal Spectrometer	Horizontal Midplane
Multichannel Visible Spectrometer	2 Horizontal Midplane
Impurity Concentration	
Interference Filter Array (HAIFA)	18 Chord Array, 4 Toroidal Locations
UV Survey Spectrometer	Horizontal Midplane
Radiated Power	
Bolometer Arrays	19 Horizontal, 19 Vertical Chords
Wide-Angle Bolometers	6 Toroidal Locations
Magnetic Properties	
Rogowski Loops	2 Toroidal Locations
Voltage Loops	6 Poloidal Locations + Saddle
B_θ/B_ρ Loops	2 Sets of 26 Pairs, External
Diagmagnetic Loops	2 Toroidal Locations
Wave Activity	
Internal Mirnov Loops	19 Coils
X-Ray Imaging System	64 Horizontal Array
Fusion Products	
Epithermal Neutrons	4 Toroidal Locations
Proton Detectors	4 Vertical Locations
Neutron Activation System	2 Toroidal Locations
Two-Channel Collimator	1 Toroidal Location
Neutron Fluctuation Detector	1 Location
Plasma Edge/Wall	
Plasma TV/IR TV	Periscopes at 3 Toroidal Locations
Neutral Beam Pyrometer	2 Toroidal Locations
Probes	2 Horizontal, 1 Vertical
Miscellaneous	
Hard X-Ray Monitors	5 Wall Locations
Torus Pressure Gauges	2 Toroidal Locations
Residual Gas Analyzers	2 Toroidal Locations
Vacuum Vessel Illumination	3 Toroidal Locations
Laser Impurity Injector	1 Toroidal Location
Glow-Discharge Probes	2 Mechanisms

Table II. Diagnostic Additions and Upgrades in FY86.

Electron Density	
Multichannel Interferometer	Added five channels. Prototype Faraday Rotation. Vertical.
Electron Temperature	
X-Ray Pulse-Height Analyzer	Relocated horizontal system; added two vertical channels.
Ion Temperature	
Charge-Exchange	Added third horizontal chord, first vertical chord.
Diagnostic Neutral Beam	Installed. Horizontal at Bay A.
Charge-Exchange Recombination Spectroscopy	Prototype instrument installed. Poloidal array.
Spatial Scan Spectrometer	Radial profiles (near UV). Horizontal.
X-Ray Crystal Spectrometer	Installed third chord vertical system.
Fusion Products	
Neutrons	Instrumented one channel of collimator (movable onto ten vertical sight lines); installed activation counting system.
Plasma Edge/Wall	
NB Pyrometer Interlocks	Enhanced for additional four beamlines.
Plasma TV/IR TV	Added data handling. Horizontal.
Edge Probes	Horizontal fast probe installed.
Thomson Scattering	Vertical edge TVTS installed.

Horizontal Charge-Exchanger Analyzer

A third analyzer was added to the horizontal charge-exchange array.[24-27] This analyzer includes extensive gamma and neutron shielding. The shield, shown in Fig. 24 consists of a 10-cm thick lead box nested in a 30-cm thick shell of 1% borated polyethylene. The entire assembly is encapsulated in modular stainless-steel sections to facilitate maintenance. An improvement of a factor of 125 in signal-to-noise has been achieved. This shielding provides a prototype for the extensive shielding thought to be necessary for some diagnostics in the Q ~ 1 D-T phase of the TFTR operation in 1990. The horizontal array permits the spectrum of fast neutrals to be resolved along several tangential views, as shown in Fig. 25. The full and half-energy components of the heating beam are clearly visible at the outer tangency radius. Because of the improved signal-to-noise it is now possible to deduce ion temperature from the charge-exchange spectrum of residual hydrogen, which constitutes only a few percent of the plasma. Figure 26 shows a comparison between the horizontal CENA and X-ray diagnostics at moderate beam power (10 MW) where the ion temperature exceed 15 keV. The agreement is good.

The first vertical viewing CENA arm was installed and operated this year. Figure 27 shows the time history of a 0.9-MA D^+ discharge with 3.6 MW of deuterium neutral-beam injection. In this discharge, a 5 Torr-liter puff of hydrogen and a pulse from the DNB were used to facilitate charge-exchange measurement. The local ion temperature deduced from the active charge-exchange spectrum is in good agreement with the X-ray crystal spectrometer. The passive deuterium measurement seriously overestimates the temperature during beam injection, due to the contribution of non-Maxwellian beam ions at low-plasma densities. Preliminary Fokker-Planck calculations suggest that the deuterium spectrum may give a more reliable estimate when the central ion temperature exceeds 10 keV.

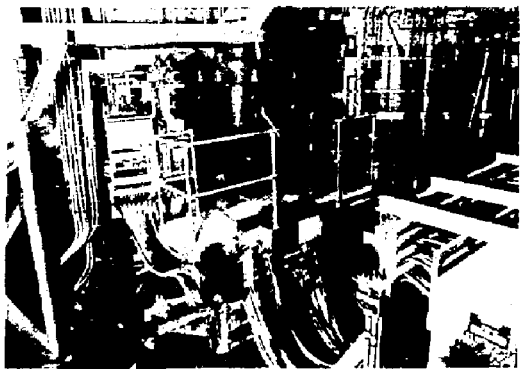

Fig. 24. Photograph of the CENA shielding box installed on the diagnostic platform. (86E0936)

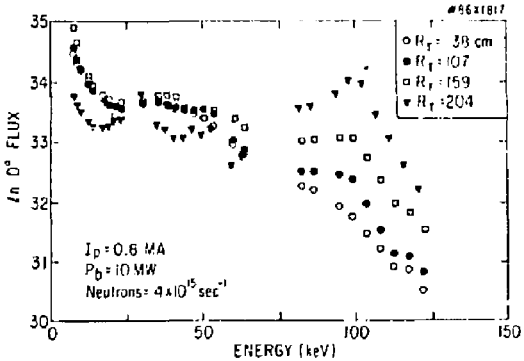

Fig. 25. Charge-exchange spectra of D^0 for 10 MW $D^0 \rightarrow D^+$ at four different tangency radii.

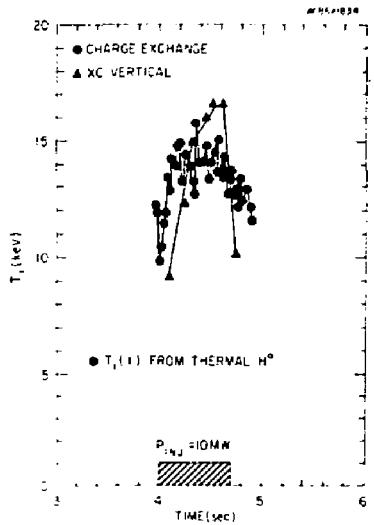

Fig. 26. Comparison of ion temperatures from CENA (•) and X-ray crystal spectrometer (Δ). Residual differences can be accounted for by differences in the sight lines of the diagnostics.

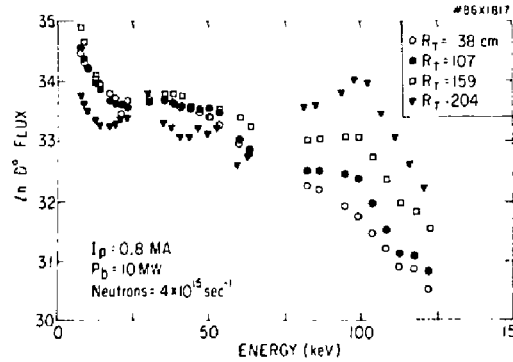

Fig. 27. Comparison of active and passive CENA T_i to X-ray measurement. The time of the gas puff and diagnostic neutral beam pulse are indicated.

CHERS

The charge-exchange recombination spectroscopy (CHERS) system was installed to provide radial profiles of plasma ion temperature and rotation velocity during a single TFTR pulse. Light is emitted in the visible and near-ultraviolet from hydrogen-like ions (e.g., C^{5+}, He^{+}, Ne^{9+}, Al^{12+}, etc.) created by charge-exchange reaction of the fully-stripped species with neutral hydrogen or neutral deuterium from the DNB or heating beams. This light is collected along various viewing lines normal to the beam giving spatial resolution of approximately 3.5 cm (when the DNB is used). The light from each view is spectrally dispersed to provide Doppler shift measurement of rotation and Doppler broadening measurement of ion temperature. The present system consists of 70 sight lines distributed around the machine to enable views of the DNB, the heating beams, toroidal rotation, or mercury calibration lamps. Between shots up to 12 views can be selected for acquisition and analysis. The software system[28] resides in a stand-alone micro-VAX computer which interacts with a fast image array processor under the control of the CHERS operator. Figure 28(a) shows CHERS data taken viewing a 40-msec DNB pulse in 5292-Å C VI light. The increasing width toward the plasma center indicates progressively higher ion temperature. Figures 28(b) and 28(c) show the profile of C VI 3434-Å light taken viewing a heating beam. A nongaussian profile results from viewing a wide (FWHM = 60 cm) source that samples a large range of ion temperature. The tail of the distribution may be used to estimate the ion temperature in the central region of the discharge. This method verifies that the carbon ion temperature in the center of TFTR has reached 15 to 20 keV, in agreement with measurements of higher-Z elements made by X-ray crystal and soft X-ray monochromators.

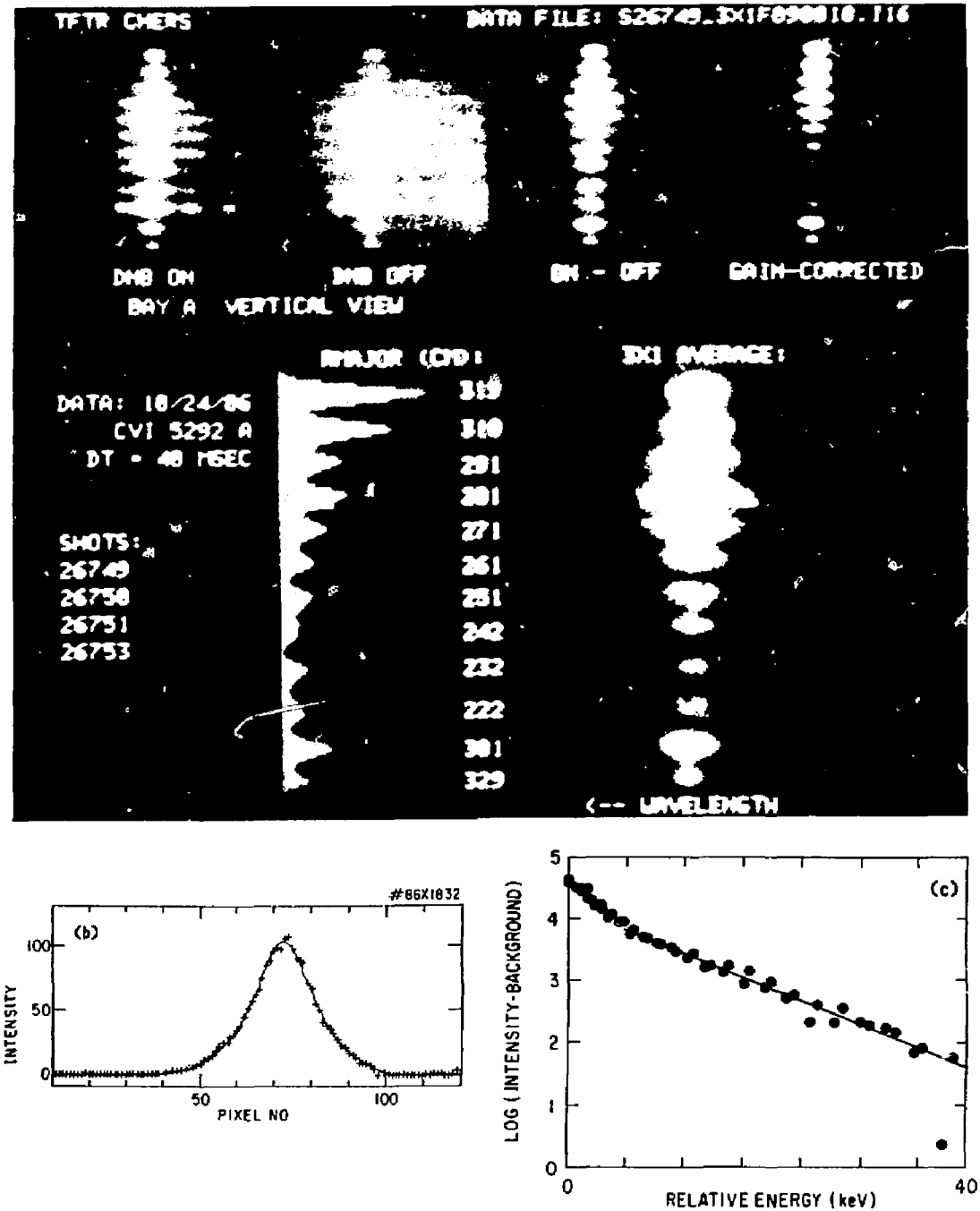

Fig. 28. (a) Data from CHERS diagnostic. The various dispersed spectra (lower right) are broader in the center channels indicating higher central T_i. (b) A two-gaussian fit to CHERS data for T_i determination. (c) Fit to spectrum viewing heating beam. The form is assumed to be Maxwellian in wings of the distribution. Central T_i is estimated from such fits.

X-Ray Spectrometers

A new three-arm X-ray crystal spectrometer system was installed in the diagnostic basement to measure radial profiles of the ion temperature and toroidal and poloidal rotation velocities.[29] The spectrometer presently has lines-of-sight for Doppler shifts and widths of Fe XXV and Ni XXVII at R = 2.34, 2.49, and 2.95 m, with a radial resolution of 2-3 cm. The energy resolution E/dE = 10,000 allows ion-temperature measurement down to 1 keV. The spectrometer spectral range permits observation of dielectronic satellite lines to study ionization equilibria and impurity transport from line intensity ratios. For rotation studies the instrument has sensitivities of 7×10^6 cm/sec toroidally and 5×10^5 cm/sec poloidally.

Figure 29 shows the observed Ni XXVII spectrum for a low-density discharge ($n_e = 8 \times 10^{12}$ cm^{-3}) where

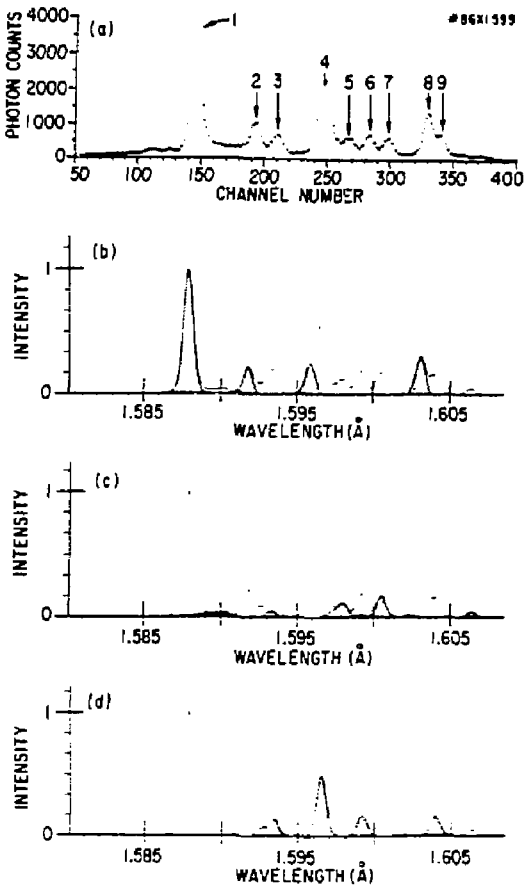

Fig. 29. (a) Data from X-ray crystal spectrometer and (b-d) fits (crosshatched regions) to subsets of the spectral lines.

electron-ion coupling is low. For comparison, a synthetic spectrum computed from the theory of Safranova[30] including contributions from helium-like ions and dielectronic lithium-like satellites is shown. In recent discharges with enhanced confinement at heating powers of 15-20 MW, this diagnostic shows ion temperatures of 20 keV.

The soft X-ray monochromator (SOXMOS) was used extensively this year to provide central ion temperature from measurement of Doppler broadening of Fe XXIV at 192 Å. Analysis with the MIST code indicates that emission from this line peaked on axis. This temperature measurement was routinely performed on every shot since high neutron levels have not disabled SOXMOS as they did the horizontal X-ray crystal system. Where data were available for comparison, the agreement between the systems was quite good.

Interferometry

Measurements of the profiles of electron temperature and density[31] have been substantially improved. The multichannel infrared interferometer (MIRI), operating at 119 μm, was expanded from five channels to ten channels. This diagnostic gives time-dependent radial profiles of electron density. Though large and complicated, MIRI has achieved such high reliability that it is used for density feedback control. We have tried to determine whether the MIRI system can provide measurements of plasma Faraday rotation[32] to measure current density profiles. This measurement is made by comparison of the polarization of a beam transmitted through the plasma to that of a reference oscillation. The MIRI geometry is not optimal for such measurements; spurious paths result from the numerous beam splitters in the system. It remains to be seen whether the problems can be identified and corrected.

Thomson Scattering

The multipoint Thomson scattering system installed last year is now fully operational. This dual system is comprised of two independent subsystems capable of providing 76-point radial profiles of electron density and temperature at two arbitrary times during a discharge. Improvements in the relay optics of the spectrometer have given better signal-to-noise and higher spatial resolution. The improved spatial resolution was important in determining the optimal alignment of the laser. The ability to measure profiles at two times is most useful during pellet experiments, as shown in Fig. 30. Problems in the gating circuit of the second system have made it unavailable for some important experiments, but this difficulty will be rectified in FY87. Efforts are underway to determine the feasibility of using this system to measure poloidal-field profiles.[33]

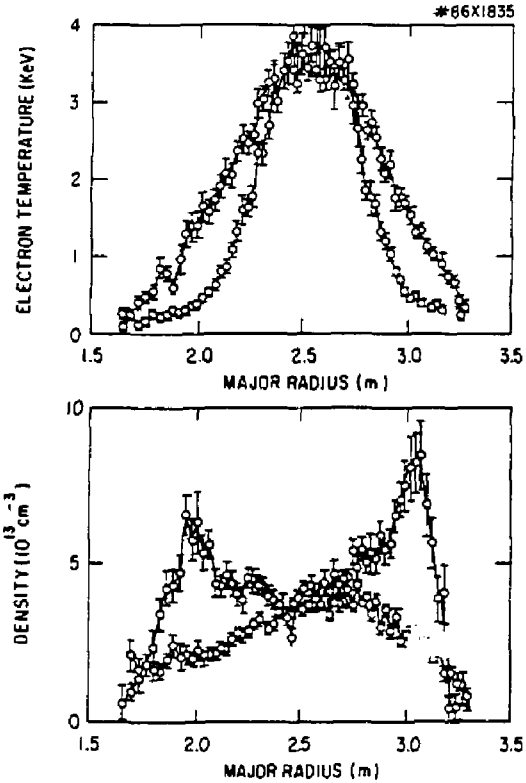

Fig. 30. Top: TVTS profiles of electron temperature before (outer) and after (inner, peaked) pellet injection on TFTR. Bottom: TVTS profiles of electron density before (lower) and after (higher, hollow) pellet injection.

Cyclotron Radiation

An Ebert-Fastie grating monochromator designed to disperse electron-cyclotron emission (ECE) over the wavelength range 1 mm – 25 mm is now complete.[34] The instrument, shown in Fig. 31, follows the time evolution of an electron-temperature profile. Twenty sight lines provide spatial resolution of 3 cm and temporal resolution of approximately 1 μsec. The fast response results from the use of liquid helium-cooled indium antimonide bolometers and matched, cooled preamplifiers for the detection of the emitted light. This fast response will be useful in upcoming studies of fluctuations on TFTR at high background radiation levels.

The high level of redundancy (see Table I) in temperature measurements on TFTR is desirable as $Q \sim 1$ is approached. The agreement between the various electron temperature measurements is quite good in general, although the Michelson interferometer gives a reading 10-20% higher than the others at high temperature. This discrepancy, not previously observed at low temperatures, does not appear to be fundamental and should be resolved in the near future.

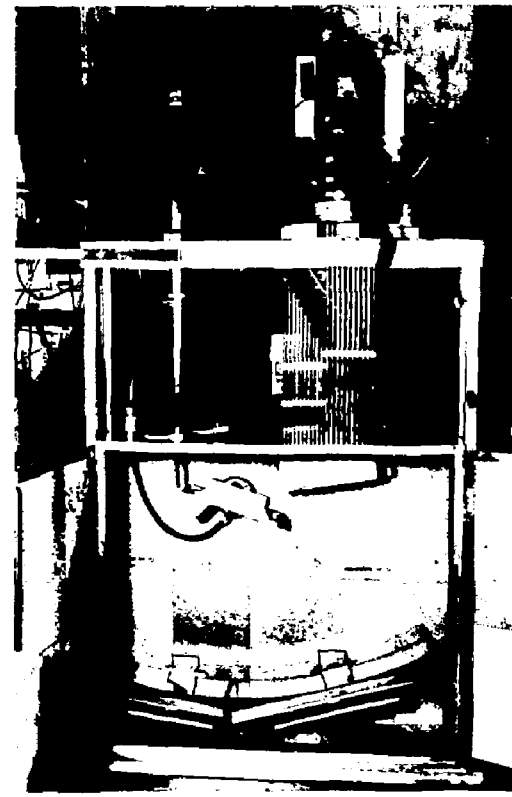

Fig. 31. Photograph of the grating polychromator spectrograph. (86X3301)

Diagnostic Loops

TFTR now has a reliable, accurate diamagnetic measure of stored energy to complement the above kinetic measurements. Improvements were made in the hardware compensation of the vacuum toroidal flux linked by the loop. These improvements, coupled with the development of new analysis software, has led to an uncertainty of less than 70 kJ (~5%) in the transverse component of stored energy at full toroidal field. The time evolution of β_p is now shown as a waveform after every TFTR shot and, along with neutron source strength, is of primary interest in the study of enhanced-confinement discharges. Such discharges have significant ellipticity which has required the development of a code designed to model the resulting noncircular cross section. The plasma is treated as a set of six coupled filamentary currents adjusted to give agreement with data taken by flux loops, poloidal-field moment arrays, and the Rogowski loop. The code allows an accurate determination of the plasma boundary from which the

asymmetry parameter can be calculated. This boundary data is also fed to the TRANSP code where noncircular effects are now included in the transport analysis.

Bolometry

Another important diagnostic for the analysis of the energy balance in TFTR is the bolometric measurement of total radiated power. During the past year a pair of bolometers viewing tangentially were installed, one viewing parallel to the plasma current direction, the other (toroidally 90° away) antiparallel. Figure 32(a) shows the response of these bolometers during a co-only neutral-beam pulse. The larger antiparallel signal during beams is caused by fast-ion charge-exchange. The equal transients at 5.3 sec from impurity injection of iron, serve as a check on the relative sensitivity of the two channels. Another important improvement is a better algorithm for the reconstruction of highly asymmetric radiation profiles.[35] An example is shown in Fig. 32(b), taken during an edge thermal instability known as a MARFE, which causes a cold dense plasma to form on the inside edge.

Another subset of intense development this year has been fusion product diagnostics.[36-41] A new radiation counting laboratory was completed and the neutron activation diagnostics were moved from their temporary location in the mock-up area. The necessary pneumatic handling hardware and software for the activation sample transfer system is fully functional. This diagnostic measured the triton burn-up during the last run period and will be used extensively during the D-D runs in the coming year.[42]

The epithermal fission-detector system hardware has been modified to accommodate higher neutron source fluxes associated with the enhanced-confinement discharges. The Campbell-mode amplifiers (mean-square-voltage detection during high-flux operation) have been completely calibrated and are now routinely operated.[43] This extends the utility of the one-gram ^{235}U detectors from 2×10^{14} n/sec, where they saturate in the count rate mode, to 10^{18} n/sec in the Campbell mode. The 50-gram ^{238}U detectors can function in the count rate mode up to 10^{16} n/sec, allowing comparison of the Campbell and count rate measurements. The agreement between measured neutron source strength and calculations based on the SNAP and TRANSP codes is quite good.

The multichannel neutron collimator will be capable of measuring neutron emission profiles and absolute source strengths required to test models of ion-temperature profile and beam deposition. This requires the installation and calibration of ten vertically viewing channels. During the last run period, preliminary data was obtained with a single ZnS detector moved between shots from sight line to sight line via remote control. Figure 33 compares the measured chord-integrated 2.5-MeV D-D emission profile with that calculated by the SNAP analysis code. The results are encouraging, and significant improvements to both the diagnostic and the code simulations can be expected in the coming year.

The neutron fluxes on the TFTR are approaching the levels needed for significant nuclear pumping of gas mixtures by fast ions produced by reaction of the (moderated) neutrons with He^3 or other substances. Analysis show[44] that the neutron fluxes expected in full D-T operation of the TFTR will be sufficient to pump He-Ne and He-Xe lasers. A moderator and gas cell system has been designed that, if installed next to the TFTR vacuum vessel, will permit investigation of gain in gas mixtures containing He^3 (Ref. 44).

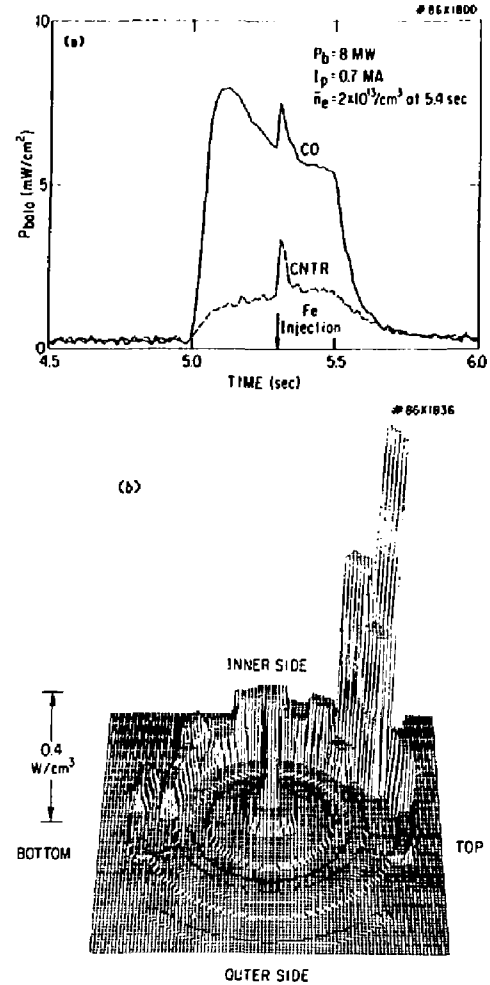

Fig. 32. (a) Parallel (lower) and antiparallel viewing bolometer signals for NBI heated discharges having Fe impurity injection at 5.35 sec. The anistropy is due to fast ion charge-exchange. (b) Reconstruction of MARFE radiation profile.

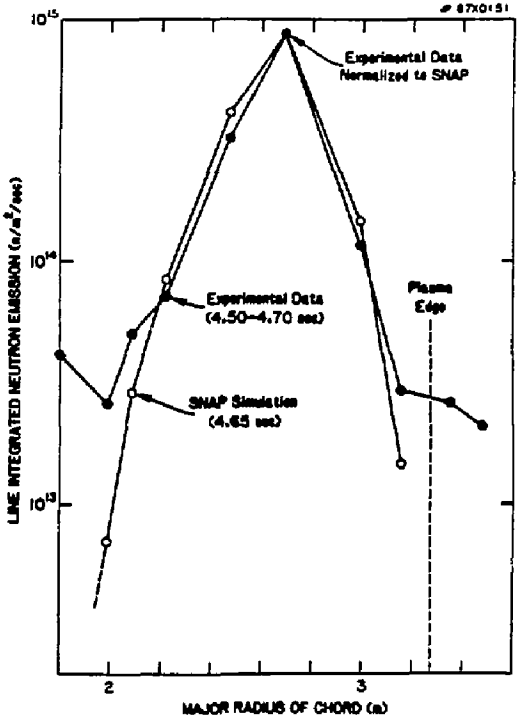

Fig. 33. Line-integrated neutral emission profile for a TFTR "supershot" (10-MW neutral-beam power) measured by the multichannel neutron collimator, compared with simulated data from the SNAP analysis code. This constitutes the first effective determination of the neutron emission profile from a tokamak.

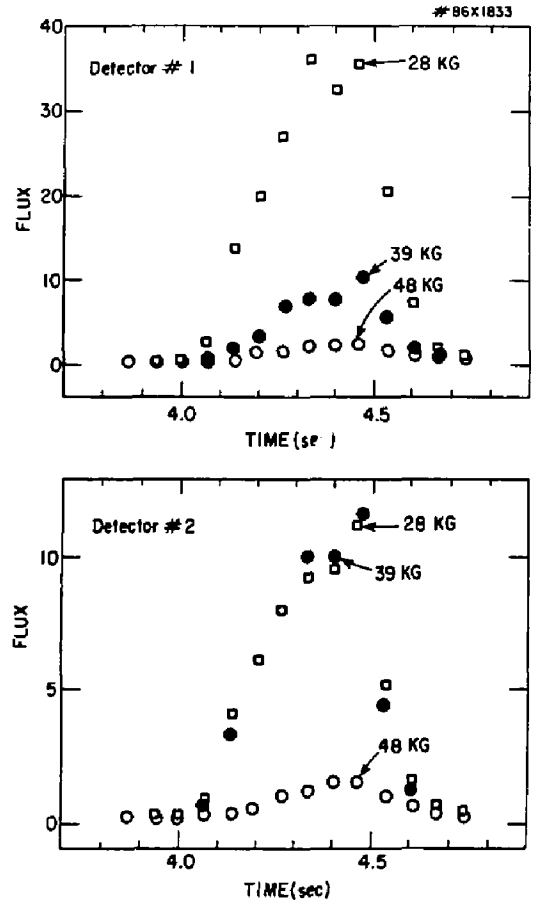

Fig. 34. Two channels of escaping triton detector probe at three different values of toroidal field. Note the cut-off of signals as B_T increases.

Charged-Fusion Products

The prototype escaping triton/alpha scintillation detector operated successfully this year.[45,46] Signal-to-noise is determined by comparing shots having different toroidal fields; at certain field levels tritons are geometrically excluded from the detector. Figure 34 shows such a comparison. The time dependence, absolute flux levels, and plasma current dependence of the triton signals are in rough agreement with the expected prompt losses. In the next year, this diagnostic will be improved to provide both pitch-angle and gyroradius of the escaping tritons or alphas.

Edge Plasma Diagnostics

The enhanced-confinement mode in TFTR is thought to be predominantly the consequence of phenomena at the edge, such as changes in limiter recycling.[47] The mechanisms by which these effects produce such a mode are unclear but there have been suggestions that the suppression of microinstabilities may play a role. In the past year, numerous modifications and additions were made to diagnostics particularly suited to investigate properties of the edge plasma and fluctuations both at the edge and in the core.

A new Thomson scattering spectrometer/detector system for the edge plasma was assembled and installed.[48] Predispersed signals from any three adjacent channels of the 76 channels are diverted from the main profile system. These are analyzed with a higher dispersion spectrometer and more sensitive detector. Despite operational schedule demands on manpower, the diagnostic was refined nearly to completion. The system will provide radial profiles of edge density and temperature to be compared to those from probes.

Impurity injection has been used extensively for spectroscopic studies are impurity transport.[29] Most of the scenarios of TFTR operation appear to have

the same impurity transport, in particular, neutral-beam-heated plasma have the same impurity transport as ohmic-heated plasmas. The MIST code was modified to run on the VAX using SNAP code output making it possible to determine absolute impurity densities between shots. Analysis shows that the target plasma for enhanced confinement is almost pure carbon. Preliminarily, C-C sputtering seems to be the main contributor to this level. Better edge temperature profiles from TVTS (TV Thomson scattering) and fast-probe studies are needed for further clarification.

The vertical long probe has been used extensively in the past year.[49] This multipurpose system has been employed to provide time-resolved studies of impurity generation with probe heads for sample-exposure collection. Using Langmuir elements, it has characterized electron density and temperature profiles, ion fluxes, and power deposition for various operating scenarios. Such studies have been important in the determination of particle-confinement time in TFTR.[50] The probe has been made very robust; during ohmic heating the probe can be used as far inward radially as the last closed flux surface (LCFS).[51] A new fast probe, shown in Fig. 35, has been recently installed at the midplane. This probe uses a powerful ac motor to move ±30 cm at speeds up to 30 cm/sec during the discharge. The probe can be set to move in at an arbitrary time during a shot, dwell for adjustable periods (including no dwell), and move out. This permits sampling of beam-heated discharges to very near the LCFS, and this will permit radial profiles of the scrape-off to be determined in a single shot, overlapping edge TVTS profiles.

A major effort this year has been to characterize the fluctuation levels within the plasma. Orthogonal Mirnov coils have been used in the long probe head to record magnetic fluctuations. These are compared to fluctuations observed in electrostatic collectors on the same probe head and to magnetic fluctuations recorded by the stationary Mirnov poloidal-coil array. The radial profile of the fluctuation amplitude inferred from the array agrees well with that from the movable probe, as do the frequency spectra.[52] To facilitate these studies, the coil array[53] has been equipped with a custom Comb filter comprised of 16 narrow-band filters to cover the range 0.2 to 350 kHz at widths of 5, 10, or 50 kHz. Very high-frequency fluctuations can now be studied using a 2-MHz digitizer added this year. A mode analysis instrument now uses the array data to produce a time waveform of the MHD activity amplitude during TFTR discharges and to indicate the presence or absence of an X-point in the vessel.

A new diagnostic used to examine fluctuations is the rapidly gated intensified video camera which views the inner wall in D-alpha light and contributes to a comprehensive picture of turbulent effects in

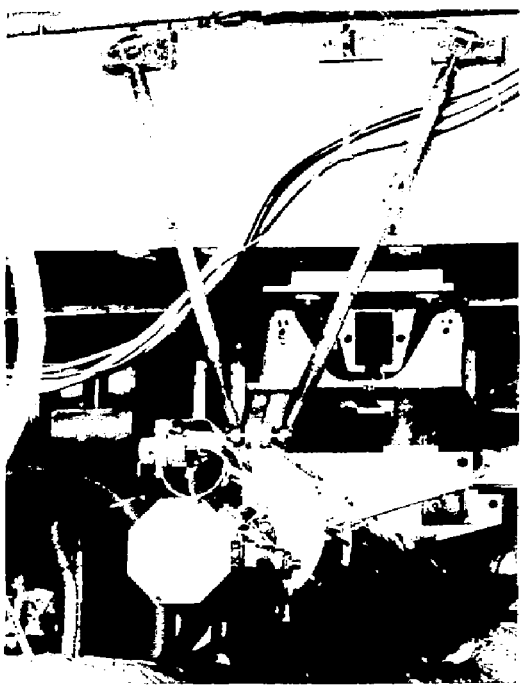

Fig. 35. Photograph of the fast probe. The ac motor is visible at the back. (86E0763)

Fig. 36. Bands of D_α light due to edge density fluctuations viewed by fast scanning camera. (86X3189)

TFTR.[54] Figure 36 shows the resulting filamentary structure of the plasma against the inner wall. If the intensity modulations are attributed to fluctuations in edge density, these filaments have characteristics similar to the turbulence detected with the Langmuir probes.

A fast-infrared thermometer was installed on TFTR for the purpose of determining the energy deposition on the inner bumper limiter during disruption. The system has a time response of 10 μsec. Figure 37 shows a representative time-temperature response during a 2.2-MA disruption. A rapid heat pulse is seen at the onset of current decay, attributable to a fast loss of stored energy. This system will be useful in determining the actual time scale of energy deposition during the high-energy-content discharges anticipated in FY87.

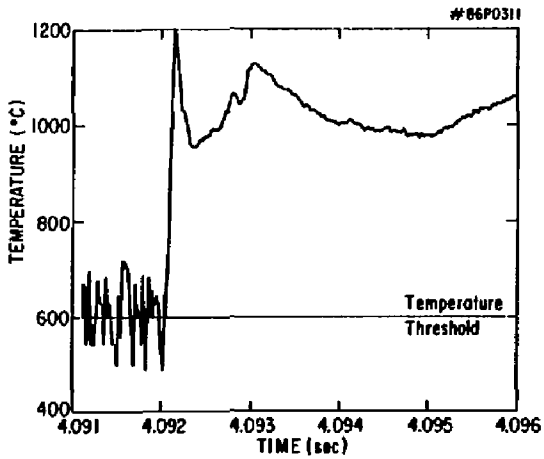

Fig. 37. Fast infrared thermometer measurement of bumper limiter surface temperature during a disruption.

D-T SYSTEMS

As a result of the TFTR reorganization in the summer of 1986, the Technical Systems Division was renamed the D-T Systems Divison. The purpose of the new division is to provide a focus within the TFTR project for the deuterium-tritium (D-T) phase of TFTR operation. In addition, the division has the responsibility to provide the tritium systems, shielding, and manipulators required for tritium operation.

The TFTR program plan includes D-T operations as an important final part of the effort. Due to changing programmatic and budgetary pressures, many of the D-T preparations have been delayed until now. The present plan was proposed in 1985 as a minimum effort necessary to provide interesting D-T physics and useful engineering data in 1990. It is presently planned to produce approximately 10^{21} D-T neutrons in TFTR in 1990 and then to shut down operation so that the Compact Ignition Tokamak (CIT) can be constructed as soon as possible in the same facility.

Tritium Systems Branch

The Tritium Systems Branch is responsible for managing the modifications to the tritium systems and tritium-related systems (installed in 1984) that will provide full tritium-handling and radiation-monitoring capability for TFTR. A complete project schedule is in place. It includes the design changes, implementation of the changes, commissioning, and operation which leads to the 100 D-T shot scenario in 1990.

In 1985, the Burns and Roe Company was selected as the subcontractor to modify the design of the process systems for tritium storage, tritium cleanup, radwaste, monitoring, and HVAC (heating, ventilating, and air conditioning). This design work started in September 1985 and continued throughout FY86. Design modifications concentrated on the tritium-process systems and, by the end of the year, the tritium-storage and tritium-delivery systems' modifications were largely ready for implementation in FY87. Figure 38 shows the tritium-storage and delivery system in the tritium vault.

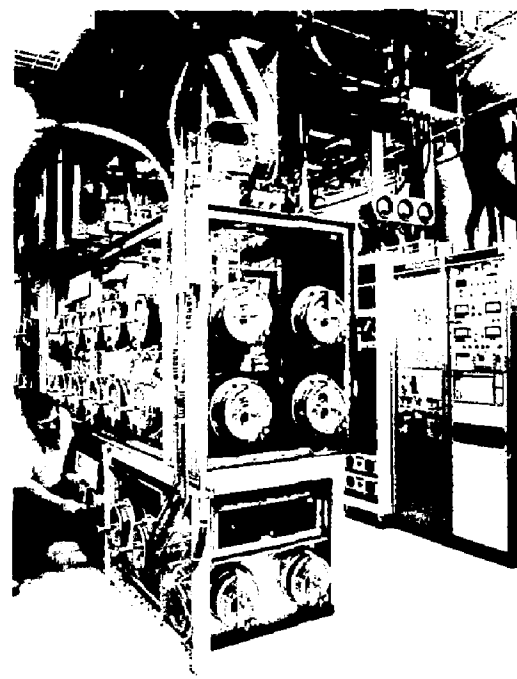

Fig. 38. Tritium storage and delivery system in the tritium vault. (86E1074)

The tritium systems are almost ready for a hydrogen-test run in which the system as a whole, as well as the individual components, will be tested. These tests will start in the first quarter of FY87.

The design of the piezoelectric gas-injection valves was completed and two valves will be ordered in early FY87.

The PPPL Computer Division completed a study that established the requirements for the tritium remote-control and monitoring system (TRECAMS) that will remotely control and monitor the above mentioned systems. Detailed design work will be initiated in early FY87.

Manipulator and Shielding Branch

The Manipulator and Shielding Branch was formed toward the end of FY86 from the Nuclear Engineering Branch. The intent of the reorganization is to focus more clearly on specific needs of the TFTR 100-Shot D-T Program, namely:

- Provide the required radiation shielding.
- Provide a maintenance manipulator to perform designated tasks inside the TFTR vacuum torus and thus limit human exposure to radiation.
- Provide an external manipulator to perform limited, but critical, inspection and maintenance tasks on the tokamak, diagnostics, and heating devices.

Radiation Shielding

Following the September reorganization, the branch formulated plans to provide the required radiation shielding by the fall of 1989. This task requires close coordination with TFTR Operations, Diagnostics, and Heating Systems Divisions to ensure compatibility with the configuration the machine will be in at that time. Therefore, the design group, consisting primarily of engineers from the Mechanical Engineering and Engineering Analysis Divisions, formed a working committee with representatives from the TFTR divisions. The first major milestone was to select a shielding configuration by February 1987. The shielding is scheduled for installation during a six-month shutdown, commencing in June 1989.

Manipulators:

Maintenance Manipulator

In the fall of 1985, Kernforschungszentrum Karlsruhe (KfK), a West German nuclear research facility, assumed responsibility for the design and fabrication of the TFTR maintenance manipulator. A formal cost-sharing agreement was signed in July 1986. Under this agreement, KfK will provide the required design engineering and support services and PPPL will provide funds for the fabrication of the manipulator and its associated control system and for the development and integration of tooling for an existing master-slave manipulator. The maintenance tasks the manipulator will perform include visual inspection, in-vessel leak detection, and replacement of protective carbon tiles.

Following discussions with engineers at the Japan Atomic Energy Research Institute (JAERI) JT-60 device, PPPL placed an order for an in-vacuum, high-sensitivity ion-gauge-type leak detector with Seiko. This device was developed by Seiko with JAERI's support. Delivery is expected in January 1987 and PPPL will then integrate this device into the manipulator.

The vision and lighting system for the manipulator will be supplied, under a cost-sharing agreement, by Commissariat a l'Energie Atomique (CEA), the French nuclear research organization. (CEA participated in conceptual design of the device.) As of the end of FY86, the framework of the agreement and statement of work was decided and formal signing was imminent.

PPPL is providing overall program coordination, the vacuum antechamber in which the device is stored, the control room, and installation. A successful Final Design Review was held in July 1986 for the manipulator and antechamber. The manipulator is shown in Fig. 39.

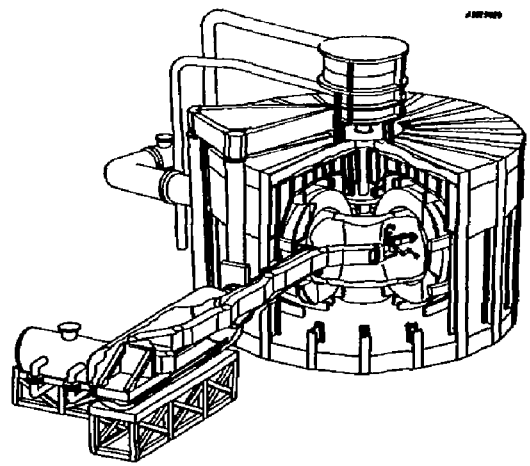

Fig. 39. TFTR maintenance manipulator.

External Manipulator

A study is planned to determine the requirements of an external manipulator. The presently envisioned concept would provide a telescoping boom from the crane bridge. The boom would provide a remotely controlled vision and lighting system for general machine inspection and would have provision for mounting an existing master-slave manipulator. Such a system could be adopted to predefined critical machine maintenance operations. A concept selection in the first quarter of CY87 is expected, followed by detailed design and fabrication in CY88 and CY89.

Pellet Injector

Fabrication of the deuterium pellet injector (DPI) continued during the first quarter of FY86. The

approach made use of designs and drawings that were applicable to the DPI from both the repeating pellet injector (RPI) and the tritium pellet injector (TPI) Conceptual Design Review of 1984. The schedule was accelerated to install the DPI during a mini-shutdown in May 1986.

The gunbox and gunline system was fabricated, assembled, and then subjected to limited testing at the Oak Ridge National Laboratory (ORNL). It was then disassembled to the minimum extent and shipped to PPPL where it was preassembled prior to installation in TFTR.

PPPL designed the DPI control system in conjunction with ORNL. The radiation-sensitive electronics were assembled into racks and enclosures at PPPL and moved to the newly installed mezzanine platform located in the basement of TFTR. A new support scheme was developed by PPPL for the DPI.

The DPI required a new gas manifold, a control system, alignment into TFTR, supports, and gas tubing. However, the existing RPI support structure, vacuum system, vacuum-vessel interface items, and liquid-helium-delivery system were utilized.

The DPI is capable of injecting from one to eight pellets ranging in size from 3.0 to 4.0 mm diameter at variable speeds up to 2,000 m/sec. The pellets are propelled by hydrogen gas through guide tubes, located approximately 5.5 meters from the gunbox, to the vacuum-vessel inlet. The hydrogen propellant gas entering TFTR is negligible (2000:1 reduction) due to the conductance-limiting design that uses fast solenoid valves, variable diameter guide tubes, and two vacuum systems. The first pellet was injected into TFTR on July 2, 1986. Figure 40 shows the DPI installed on TFTR.

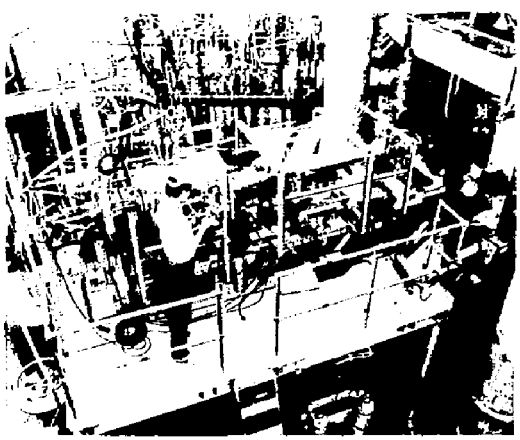

Fig. 40. The deuterium pellet injector (DPI) installed into Bay T of TFTR. The DPI is now operational. (86X3228)

Radio-Frequency Limiters

A project was established to design, fabricate, and install two 240° poloidal limiters to shield the future rf antennas. The limiters will be located outboard of the antennas (Bays M and L) and will cover the bellows protective plates and getter panels at Bays M/O and K/L.

The present design is focused on using carbon-carbon composite, thereby permitting radiation cooling and, via slots cut into the limiter, permitting pumping by the getter panels. Design efforts are being aided by a subcontractor firm with expertise in the design and analysis of carbon-carbon composite materials.

In FY87, it is planned to have a Phase I study with selected subcontractors and a Phase II fabrication by the successful firm. Installation of the limiters is scheduled for August 1987, at which time the rf antennas will be installed and the movable limiter (Bay M) will be removed.

Lithium Blanket Module Program

An experimental program of neutron transport studies with the lithium blanket module (LBM) was carried out using the LOTUS point-source neutron facility at E'cole Polytechnique Fédéral Lausanne (EPFL), Switzerland.[55] The D-T neutron source was placed approximately 20 cm from the LBM front face in order to provide a nearly uniform current over the central region of about 15-cm diameter. Neutron flux was determined by activation analyses of dosimetry foils located within the LBM fuel rods. Both the thermal extraction and dissolution methods were used to assay tritium bred in Li_2O diagnostic wafers and LBM pellets.

TOKAMAK OPERATIONS

Productive time on TFTR greatly increased in FY86, as shown in Table III. Increases in the ratio of productive to nonproductive times, as compared to FY85, resulted in a factor of 2.5 increase in plasma pulses. The ability to rapidly and efficiently explore operating parameter space contributed to the discovery of the "supershot" regime.

Machine availability increased from an average of 61 percent in FY85 to 66.5 percent in FY86, while operating near maximum levels of the toroidal-field and ohmic-heating systems. This increasing trend in machine availability, illustrated in Fig. 41, was the

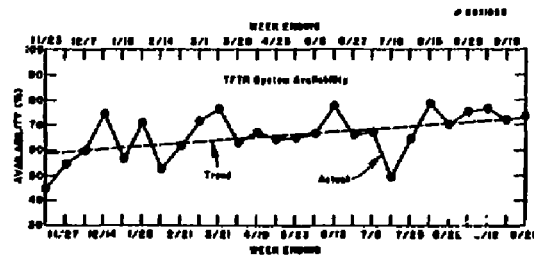

Fig. 41. The Tokamak Fusion Test Reactor system availability.

Table III. Summary of TFTR Operational Time.

	FY86	FY85
Total productive time (minutes)	79,885	36,720
Total nonproductive time (minutes)	40,290	21,414
Ratio: Productive time/Nonproductive time	2.0	1.7
Productive time per plasma discharge* (minutes)	15	18
Nonproductive time per plasma discharge** (minutes)	8	11

*Theoretical Minimum 5 minutes
**Theoretical Minimum 0 minutes

result of administrative, hardware, and software improvements. In particular, the maturing of reliability efforts in Central Instrumentation, Control, and Data Acquisition (CICADA) and field coil power conversion systems was evident; the weekly availabilities averaged 95 percent and 97 percent, respectively, at the end of the run period. Other improvements include: streamlining operational procedures to make daily start-ups more time efficient; addition of a third shift to accommodate daily maintenance greatly enhancing diagnostic reliability and facilitating recovery from vacuum leaks encountered; extension of the preventive-maintenance program instituted last year to include field coil bus connections; and the addition of remote, automatic controls to the cooling-water valves and pumps in the motor generator, cooling tower, and pump room circuits thus establishing central control of the integrated cooling water-system and thereby reducing manpower requirements and improving reliability.

The advent of supershots with attendant large increases in neutron yield, resulted in appreciable machine activation. Appropriate procedures were invoked, and additional personnel were trained in radiation safety; the transition to higher radiation levels was accomplished without incident and with little impact on operating efficiency.

A total of 5,198 successful experimental plasma discharges resulted from 6,296 attempts. During vessel conditioning operations, 334,178 discharge-cleaning shots were made. More detailed statistics are listed in Table IV.

The Operations System Engineering Support (OSES) study performed by the Engineering Analysis Division, under the direction of Tokamak Operations Division, was completed. The study produced detailed thermal and electromagnetic models of the poloidal-field coil systems that yield structural stresses and deflections. The computer models are being used to determine simplified expressions for the critical elements in the poloidal-field system and to support efforts to extend poloidal-field systems performance.

Preparations to increase the ohmic-heating system volt-second capability continued, with planned increases in maximum ohmic-heating current and in the number of ohmic-heating coil turns. The ac line breakers with higher rating and the current limiting reactors with lower voltage drop were ordered for five feeder lines. They will replace the present three ohmic-heating feeders. A design was proposed for reinforcing existing ohmic-heating coil supports in order to accommodate the increased loads imposed by the "Mode D" configuration. In Mode D, the horizontal-field and vertical-curvature coils are

Table IV. Fiscal Year 1986 Shot Statistics for TFTR.

Attempts		6,296
No Plasma Discharges		1,098
Plasma Discharges		5,198
Ohmic Heating (Ohmic Heating with Pellet Injection—107)	3,348	
Neutral-Beam Heating (Pellet Injection—49)	1,850	
Discharge Cleaning		334,178

included in the ohmic-heating circuit to give a 10 percent increase in volt-seconds for the same current swing.

A summary of TFTR operations during FY86 is shown in time-line fashion in Fig. 42.

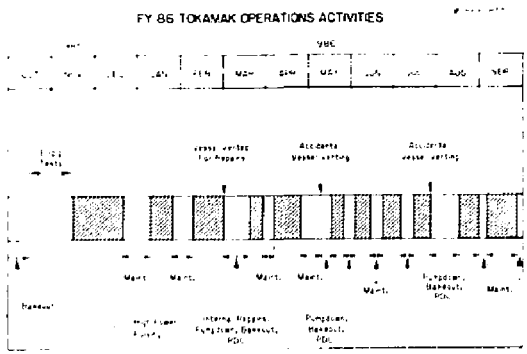

Fig. 42. The FY86 Tokamak Fusion Test Reactor device operations activities.

SAFETY AND ENVIRONMENT

With increased emphasis by DOE on the environment, the TFTR Project supported a program for off-site environmental monitoring to complement its present on-site programs. In anticipation of tritium use, baselines are being established to document the present status of surface waters, ground water, air, soil, and vegetation. Off-site soil and vegetation samples were collected and analyzed in FY86. Preferred off-site air-sampling locations were identified and negotiations are under way to obtain access to these locations. The U.S. Geological Service (USGS) ground water program was nearing completion at the end of the fiscal year. A final report, due out in FY87, is expected to provide most of the data required for the proposed CIT project, in addition to meeting all the requirements for TFTR. Split samples were taken by the USGS and supplied to the PPPL Health Physics Group and the University of Miami, Florida for tritium analysis. The results from these two independent analyses were within counting statistics of each other and indicated a present level of approximately 2.6 Bq per liter (70 pCi per liter) in the wells located on the TFTR site. It is felt that the Health Physics Group now has one of the best capabilities in the U.S. in the detection of low levels of tritium in the environment. Also, the second full year of meteorological data was collected and analyzed, providing the required baseline for future operation.[56]

With the increased neutron production, especially after "supershots," elevated activation levels of the TFTR machine have been measured. The activation has been characterized and found to be predominantly ^{56}Mn following high-powered pulsing. Other radioisotopes identified include ^{58}Co, ^{60}Co, ^{54}Mn, and ^{82}Br. The activation decayed quickly to approximately 2.5 μSv/h (0.25 mrem/h) after several days (see Fig. 43).[57] Tritium contamination in pump oils from D-D reaction remained low [less than 3.7 Bq/ml (100 pCi/ml)]. No TFTR-related radioactive particulates were found in the TFTR air-filtration system. However, natural radon daughters have been detected. Even with the increased neutron production, because of the extra shielding and labyrinths added in 1985, the radiation-monitoring system detectors at the Test Cell walls and perimeter fence indicated insigificant levels at these locations.

Access to the Test Cell was tightened. A written access procedure made personal dosimetry mandatory and allows only radiation-trained individuals for a specified condition. Access procedures, mainly for electrical safety, were written for the energy-conversion system. Written procedures, in general, continue to be an important feature for all component installations, integrated systems testing, operational testing, and lifting activities. These are being reviewed and approved by the Project and Operational Safety Office prior to implementation. Material Safety Data Sheet (MSDS) awareness was initiated, and employee safety awareness for all types of hazards has increased in the past year. The Area Safety Coordinator Program was given credit as an important element in keeping the Laboratory accident-performance indices very low.[58]

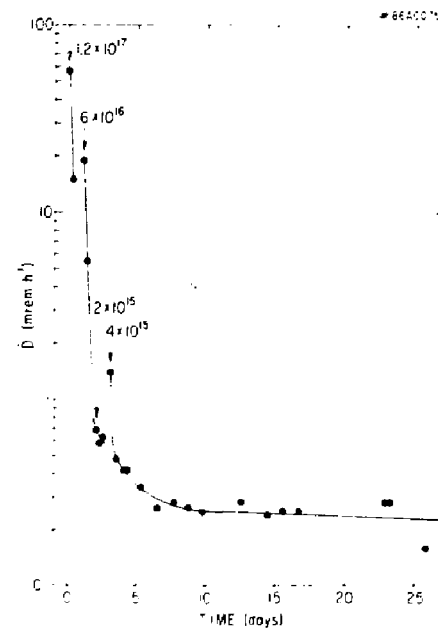

Fig. 43. Average dose rate at contact with the TFTR vacuum-vessel midplane just prior to and during a maintenance period. Each arrow points to the initial radiation survey data point immediately following a day of operations. Numbers are neutrons produced during the preceding 16 hours of operation.

References

[1]H.F. Dylla, M.G. Bell, W.R. Blanchard, *et al.*, "Plasma-Material Interactions in TFTR," J. Nucl. Mater. *145-147* (1987) 48-60.

[2]J.D. Strachan, F.P. Boody, C.E. Bush, *et al.*, "Formation of Detached Plasmas in TFTR," in *Controlled Fusion and Plasma Physics* (Proc. 12th Europ. Conf., Budapest, Hungary, 1985) L. Pocs and A. Montvai editors, Contributed Papers Vol *I* (European Physical Society, 1985) 339.

[3]J.D. Strachan, F.P. Boody, C.E. Bush, *et al.*, "Experimental Results from Detached Plasmas in TFTR," J. Nucl. Mater. *145-147* (1987) 186-190.

[4]P.C. Efthimion, N. Bretz, M. Bell, *et al.*, "Confinement Studies of Ohmically Heated Plasmas in TFTR," in *Plasma Physics and Controlled Fusion Research 1984* (Proc. 10th Int. Conf., London, 1984), Vol. *I* (IAEA, Vienna, 1985) 29.

[5]S.K. Combs and S.L. Milora, "Pneumatic Pellet Injectors for TFTR and JET," in *Fusion Technology* (Proc. 11th Symp., Avignon, 1986) to be published.

[6]R.J. Goldston, "Energy Confinement Scaling in Tokamaks," Plasma Phys. and Contr. Fusion *26* (1984) 87.

[7]S.L. Milora, G.L. Schmidt, V. Arunasalam, *et al.*, "Confinement of High Density Pellet Fueled Discharges in TFTR," Plasma Phys. and Contr. Fusion *28* (1986) 1435.

[8]M. Murakami, V. Arunasalam, J.D. Bell, *et al.*, "Confinement Studies of Neutral Beam Discharges in TFTR," Plasma Phys. and Contr. Fusion *28* (1986) 27.

[9]M.G. Bell, V. Arunasalam, M. Bitter, *et al.*, "TFTR Confinement Results," Plasma Phys. and Contr. Fusion *28* (1986) 1329.

[10]S.M. Kaye and R.J. Goldston, "Global Energy Confinement Scaling for Neutral-Beam-Heated Tokamaks," Nucl. Fusion *25* (1985) 65.

[11]A.A. Galeev and R.Z. Sagdeev, "Transport Phenomena in a Collisionless Plasma in a Toroidal Magnetic System," Zh. Eksp. Teor. Fiz. *53* (1967) 348 [Sov. Phys.-JETP *26* (1968) 223].

[12]S.P. Hirschman and D.J. Sigmar, "Neoclassical Transport of Impurities in Tokamak Plasmas," Nucl. Fusion *21* (1981) 1079.

[13]B.C. Stratton, A.T. Ramsey, F.P. Boody, *et al.*, "A Spectroscopic Study of Impurity Behavior in Neutral Beam and Ohmically Heated TFTR Discharges," submitted to Nuclear Fusion.

[14]B.C. Stratton, S.A. Cohen, F.P. Boody, *et al.*, "Impurity Transport in Ohmic- and Neutral-Beam-Heated TFTR Discharges," J. Nucl. Mater. *145-147* (1987) 587-591.

[15]K. McGuire, J.D. Callen, R.J. Colchin, *et al.*, "Compound Sawteeth and Heat Pulse Propagation in TFTR," in *Controlled Fusion and Plasma Physics* (Proc. 12th Europ. Conf., Budapest, Hungary, 1985) L. Pocs and A. Montvai editors, Contributed Papers Vol. *I* (European Physical Society, 1985) 134.

[16]F. Troyon, R. Gruber, H. Sauermann, *et al.*, "MHD Limits to Plasma Confinement," Plasma Phys. and Contr. Fusion *26* (1984) 209.

[17]W.H. Choe and J.P. Freidberg, "Finite Shift Stabilization of Ballooning Modes in a High-Beta Tokamak," Phys. of Fluids *29* (1986) 1766.

[18]R.E. Waltz, "Comments on Profile Consistency," GA Technologies, Inc. Report GAT A18365 (1986).

[19]E. Fredrickson, K. McGuire, R.J. Goldston, *et al.*, "Profile Consistency on TFTR," in *Controlled Fusion and Plasma Physics* (Proc. 13th Europ. Conf., Schliersee, FRG, 1986) S. Methfessel and G. Thomas, editors, Contributed Papers Vol. *I* (European Physical Society, 1956) 148.

[20]R.J. Goldston, E. Fredrickson, K. McGuire, *et al.*, "Heating Profile Experiments on TFTR," in *Controlled Fusion and Plasma Physics* (Proc. 13th Europ. Conf., Schliersee, FRG, 1986) S. Methfessel and G. Thomas, editors, Contributed Papers Vol. *I* (European Physical Society, 1986) 41.

[21]H.P. Furth, "Enhancement of Confinement in Tokamaks," Plasma Phys. and Contr. Fusion *28* (1986) 1305.

[22]G. Tait, J. Bell, M.G. Bell, *et al.*, "Adiabatic Toroidal Compression and Free-Expansion Experiments in TFTR," in *Plasma Physics and Controlled Nuclear Fusion Research 1984* (Proc. 10th Int. Conf., London, 1984), Vol. *I* (IAEA, Vienna, 1985) 141.

[23]J. Kamperschroer, H.W. Kugel, M.A. Reale, *et al.*, "A Multiple Track Doppler-Shift Spectroscopy System for TFTR Neutral Beams Injectors," Princeton University Plasma Physics Laboratory Report PPPL-2381 (1986) 28 pp; submitted to Rev. Sci. Instrum.

[24]S.S. Medley, H.W. Kugel, T.A. Kugel, *et al.*, "Neutral Beam Interlock System on TFTR Using Infrared Pyrometry," Rev. Sci. Instrum. *57* (1986) 2063.

[25]H.W. Kugel, H.P. Eubank, G. Gammel, *et al.*, "Diagnostics for TFTR Neutral Beam Species Measurement," Rev. Sci. Instrum. *57* (1986) 2066.

[26]G. Schilling, T.A. Kozub, S.S. Medley, and K.M. Young, "TFTR Diagnostic Neutral Beam," Rev. Sci. Instrum. *57* (1986) 2060.

[27]A.L. Roquemore and S.S. Medley, "Design Concepts for Compact Mass/Energy Charge Exchange Analyzers," Rev. Sci. Instrum. *57* (1986) 1797.

[28]L. Lagin, U. Schneider, N. Arnold, *et al.*, "CHERS Software System—A MicroVAX-Based Diagnostic," Rev. Sci. Instrum. *57* (1986) 1889.

[29]M. Bitter, K.W. Hill, S. Cohen, *et al.*, "Vertical High-Resolution Bragg X-ray Spectrometer for the Tokamak Fusion Test Reactor," Rev. Sci. Instrum. *57* (1986) 2145.

[30]U.I. Safranova, A.M. Urnov, and L.A. Vainshtein, "Dielectronic Satellites for Highly Charged Ion Resonance Lines," Proc. of the Academy of Sciences of the USSR, Work of the P.N. Lebedev Physics Institute, Vol. *119* (1980) 13.

[31]D. Johnson, N. Bretz, D. Dimock, *et al.*, "Multichannel Thomson Scattering Systems with High Spatial Resolution (invited)," Rev. Sci. Instrum. *57* (1986) 1856.

[32]C.H. Ma, D.P. Hutchinson, K.L. Vander Sluis, *et al.*, "Measurements of Faraday Rotation in TFTR Plasmas," Rev. Sci. Instrum. *57* (1986) 1994.

[33]A. Brizard, B. Grek, B. LeBlanc, and D. Johnson, "Feasibility Study of Using the TFTR Thomson Scattering System for q Profile Measurements," Rev. Sci. Instrum. *57* (1986) 1813.

[34]A. Cavallo, M.P. McCarthy, and R.C. Cutler, "A Twenty Channel Grating Polychromater for Millimeter Wave Plasma Emission Measurements," in *Infrared and Millimeter Waves* (Proc. 11th Int. Conf., Tirrenia-PISA, Italy, 1986) to be published.

[35]J. Schivell and C.E. Bush, "Analysis of Highly Asymmetric Radiation Loss Profiles in TFTR," Rev. Sci. Instrum. *57* (1986) 2081.

[36]A.E. Proctor and E.B. Nieschmidt, "Neutron Calorimeter as a Fusion Diagnostic," Rev. Sci. Instrum. *57* (1986) 1760.

[37]T. Elevant, H.W. Hendel, E.B. Nieschmidt, and L.E. Samuelson, "Silicon Surface Barrier Detector for Fusion Neutron Spectroscopy," Rev. Sci. Instrum. *57* (1986) 1763.

[38]T.J. Murphy, W.W. Heidbrink, and J.D. Strachan, "Application of Coincidence Techniques to Fusion Product Measurements," Rev. Sci. Instrum. *57* (1986) 1766.

[39]W.W. Heidbrink, "Neutron Fluctuation Measurements on TFTR," Rev. Sci. Instrum. *57* (1986) 1769.

[40]J.D. Strachan, "Detector Array for the Measurement of the 14.7-MeV Proton Emission from TFTR," Rev. Sci. Instrum. *57* (1986) 1771.

[41]F.E. Cecil, S.S. Medley, E.B. Nieschmidt, and S.J. Zweben, "Nuclear Reaction Diagnostics of Fast Confined and Escaping Alpha Particles," Rev. Sci. Instrum. *57* (1986) 1777.

[42]E.B. Nieschmidt, "Analysis Programs and Standardization of the Neutron Activation System at TFTR," Rev. Sci. Instrum. *57* (1986) 1757.

[43]A.C. England, H.W. Hendel, and E.B. Nieschmidt, "Neutron Diagnostics on TFTR Utilizing the Campbelling Technique," Rev. Sci. Instrum. *57* (1986) 1754.

[44]D.L. Jassby, "Feasibility of Laser Pumping with Neutron Fluxes from Present-Day Large Tokamak," Princeton University Plasma Physics Laboratory Report PPPL-2377 (1986) 12 pp.

[45]S.J. Zweben, "Aproaches to the Diagnostics of Alpha Particles in Tokamaks (invited)," Rev. Sci. Instrum. *57* (1986) 23.

[46]S.J. Zweben, "Scintillation Detector for Escaping Alphas and Tritons in TFTR," Rev. Sci. Instrum. *57* (1986) 1774.

[47]J.D. Strachan, M. Bitter, A.T. Ramsey, *et al.*, "High Temperature Plasmas in the Tokamak Fusion Test Reactor," *accepted for publication in Rev. Lett.*

[48]D. Johnson, B. Grek, D. Dimock, R. Palladino, and E. Tolnas, "TFTR Edge Thomson Scattering System," Rev. Sci. Instrum. *57* (1986) 1810.

[49]D.M. Manos, R.V. Budny, S. Kilpatrick, P. Stangeby, and S. Zweben, "Probes for Edge Plasma Studies of TFTR (invited)," Rev. Sci. Instrum. *57* (1986) 2107.

[50]R.V. Budny, D.B. Heifetz, S. Kilpatrick, *et al.*, "Evolution of TFTR Scrape-Off Plasmas with Neutral Beam Injection," J. Nucl. Mater. *145-147* (1987) 245-249.

[51]S. Kilpatrick, D. Manos, P. Stangeby, and R. Ritter, "Use of Graphite in Langmuir-Calorimeter Probe Heads," Rev. Sci. Instrum. *57* (1986) 2075.

[52]K. McGuire, V. Arunasalam, M.G. Bell *et al.*, "Coherent and Turbulent Fluctuations in TFTR," in *Plasma Physics and Controlled Nuclear Fusion Research 1986* (Proc. 11th Int. Conf., Kyoto, Japan, 1986) to be published by IAEA.

[53]E. Fredrickson, R. Colchin, K. McGuire, W. Morris, and N. Sauthoff, "TFTR Mirnov Loop System," Rev. Sci. Instrum. *57* (1986) 2084.

[54]S.J. Zweben, D. Manos, R.V. Budny, *et al.*, "Edge Turbulence Measurement in TFTR," J. Nucl. Mater. *145-147* (1987) 250-254.

[55]See Fusion Technol. *10* (1986) 925-982 for an overview of the Lithium Blanket Module Program.

[56]J. Kolibal, L.P. Ku and S.L. Liew, "Meteorological Data Summaries for the TFTR from January 1984 to December 1985," Princeton University Plasma Physics Laboratory Report PPPL-2369 (1986) 73 pp.

[57]J.D. Gilbert, J.R. Stencel, J.G. Couch, and J.J. Fennimore, "Activation Measurements on the Tokamak Fusion Test Reactor (TFTR)," in *Health Physics of Radiation-Generating Machines* (Proc. Health Physics Society's 20th Midyear Topical Symp., Reno, Nevada, Feb. 1987) 365-369.

[58]J.R. Stencel and G. Rappé, "Management and Line Responsibility Provide Team Safety," National Safety and Health News, Vol. *II* (1986) 35.

PRINCETON LARGE TORUS

The FY86 research program on the Princeton Large Torus (PLT) focused on advanced applications of radio-frequency (rf) to tokamak plasmas. The experimental time was divided roughly between ion-Bernstein-wave heating (IBWH) and current-drive experiments. Fast-wave ion-cyclotron radio-frequency (ICRF) heating was reduced from a major activity to a supporting role, providing a benchmark for IBWH.

Due to their relatively short wavelength, ion-Bernstein waves can directly heat the main bulk component of the fusion ions, even at high harmonics of the ion-cyclotron frequency. Hence, they have two attractive features: no hot ion tail formation and the possible use of waveguide launching.

Lower-hybrid current-drive (LHCD) experiments emphasized the study of MHD mode stabilization and consequent electron heating; a central electron temperature of 6 keV was obtained. In turn, current drive was studied by launching the fast-wave current-drive (FWCD) mode.

Modest power experiments using electron-cyclotron heating (ECH) showed damping at frequencies downshifted from the cyclotron frequency, a principle which would allow the use of available rf sources on present-day tokamaks.

In addition to the radio-frequency program, spectroscopic studies were carried out, especially in the X-ray region, to take advantage of the high electron temperature obtained with LHCD.

In technology, the study of coupling of the fast mode in the ion-cyclotron range of frequencies was successful, using a ridged waveguide loaded with a very high dielectric constant material. Also to be mentioned is the successful operation of the new PPPL-fabricated, sixteen-waveguide grill for LHCD.

The PLT machine ran very reliably during all FY86 using the full complement of diagnostics; its operation was extended one and a half months in FY87 to complete the fast-wave current-drive studies. Then, after approximately a month of operation dedicated to X-ray line identification, PLT ceased operation on December 23, 1986. PLT had been in operation for eleven years.

ICRF HEATING EXPERIMENTS

Several areas of concern for future experiments on fast-wave ion-cyclotron range of frequencies were explored. Previous antennas used for ICRF had a ceramic insulator placed between the Faraday screen and the radiating element. The purpose of this ceramic was to ensure that the plasma did not penetrate the antenna structure. The presence of ceramic is not viewed as viable for future experiments in an environment with a high neutron fluence. To investigate the properties of antennas without the ceramic, it was removed from a pair of antennas. The results proved very encouraging. The antenna operated up to comparable power levels to those previously obtained. In addition, the conditioning of the antenna after a vacuum opening was found to be faster without the ceramic.

A waveguide for use at ICRF heating frequencies was constructed as a prototype of future ICRF launchers. In order to operate at the low frequencies and small dimensions suitable for PLT, the waveguide was of the ridged-waveguide design and, in addition, dielectrically loaded. Low power coupling experiments were performed to demonstrate that good plasma coupling could be achieved. The design of the waveguide is such that a match between the plasma and the transmission line can be achieved without tuning elements.

ION-BERNSTEIN-WAVE HEATING EXPERIMENTS

In FY86, PLT ion-Bernstein-wave heating experiments investigated the higher power regime ($P_{rf} > P_{OH}$). Of particular interest was the confinement properties arising from bulk ion heating[1-3] as opposed to those from high-energy ion-based heating, such as fast-wave ICRF or neutral-beam heating. In order to preferentially excite the ion-Bernstein wave, a B_θ-E_z type loop coupler was used. The rf current for this antenna flows in the toroidal direction, whereas the fast-wave antenna has its current flowing in the poloidal direction. Two high power IBWH antennas were installed on PLT: up to 500 kW of rf power could be applied to each antenna. The plasma loading for such antennas is 2-4 Ω, resulting in 80-90% coupling of the applied rf power to the plasma.

Ion-Bernstein-wave heating at high power levels was performed in the ^{3}He and $(3/2)\Omega_D$ regimes utilizing the existing PLT ion-cyclotron radio-frequency 30-MHz transmitter. Figure (1)a shows a typical heating result: ion temperature increases a factor of three with 500 kW of power for the $(3/2)\Omega_D$ mode. Three ion-temperature diagnostic techniques, Doppler broadening (Ti XXI), charge-exchange (Cx),

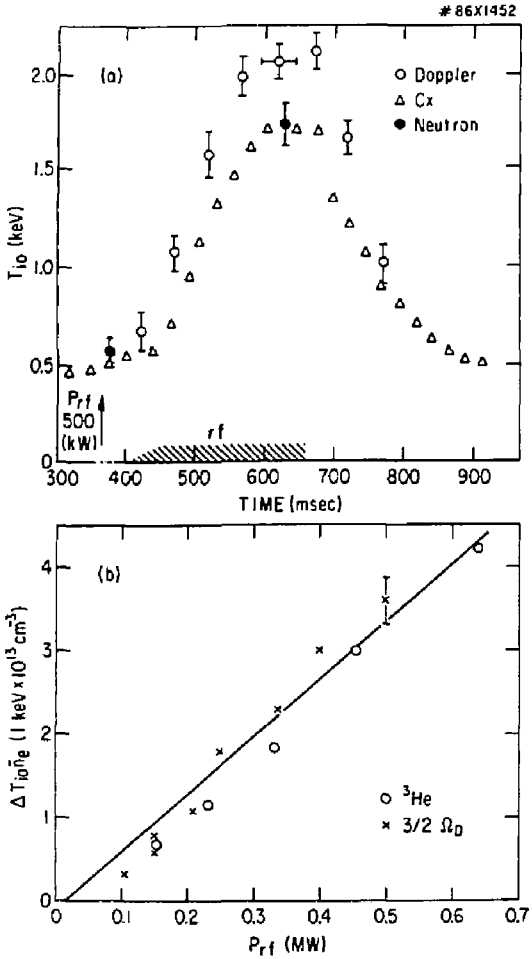

Fig. 1. (a) A typical time evolution of ion temperature. P_{rf} = 500 kW, F = 30 MHz, B_o = 29 kG, (3/2)Ω_D, and n_e = 3.0 x 10^{13} cm^{-3}. Other parameters are shown in Fig. 2(a)-(c). (b) Ion heating efficiency versus radio-frequency power.

and neutron emissions, were in good general agreement. The charge-exchange velocity distribution is Maxwellian without any high energy tail ions up to the highest power level. The ion temperature profile as measured by the Doppler broadening of various ion lines is similar to the ohmic profile. The ion heating efficiency, as shown in Fig. 1(b), is nearly linear up to the 650-kW level with the heating quality factor of $\Delta T_i n_e / P_{rf}$ = 6-7 x 10^{13} eV cm^{-3} per kW. It is interesting to note that both ^{3}He and (3/2)Ω_D heating have similar heating efficiencies. The toroidal magnetic field for (3/2)Ω_D heating is about 10% lower than the ^{3}He case, and the (3/2)Ω_D regime, of course, requires no ^{3}He injection. In the 500-600 kW range, the central Doppler ion temperature reaches approximately 2 keV, which exceeds the central TV Thomson scattering (TVTS) electron temperature. The time evolution of the plasma density is shown in Fig. 2(a). The density and electron temperature TVTS profiles at t = 600 msec are shown in Figs. 2(c) and 2(d). The dashed curves are for an ohmic case where the gas feed is programmed to yield similar density evolution. As can be seen from the figures, the density and electron temperature profiles are very similar for the two cases.

During IBWH, particle confinement shows a significant improvement. The plasma density increases by more than a factor of three without increased particle fueling, as seen from a drop in the H-alpha emission [Fig. 2(b)]. From the impurity behavior and fusion neutron yields, the density rise can be attributed mainly to hydrogenic species which, therefore, is an indication of improved ion-particle confinement.

Associated with this improvement in the particle confinement, a number of interesting phenomena were observed. During IBWH, the outward flux level

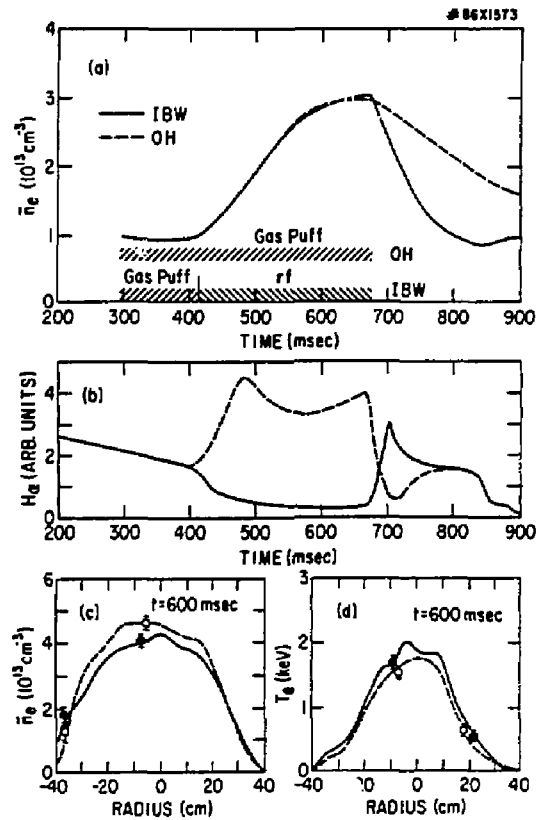

Fig. 2. (a) Density time evolution for the IBWH case (solid curve) shown in Fig. 1(a) and the ohmic case (dashed curve) in which gas puffing was used to simulate the density rise of the IBWH case. (b) Time evolution of H-alpha emission for IBWH and simulated ohmic cases taken near the antenna-limiter region. (c) Density profiles at t = 600 msec for the IBWH and simulated ohmic case shown in Fig. 2(a). (d) Corresponding electron temperature profiles.

of low energy neutrals (at energies less than 1 keV) decreases significantly. This drop may be related to the drop in the H-alpha emission and the neutral density level. In order to further understand the particle transport processes during IBWH, a laser blow-off impurity injector was used to inject a very small amount of selenium (Se), which can be monitored through spectroscopy. As shown in Fig. 3(a), the decay time of the Se XXV radiation (the central selenium confinement time) increases by a factor of two from the ohmic level (from 50 msec to 100 msec). Similar behavior was observed with a helium gas puff. When a given amount of helium is injected with a preprogrammed fast gas valve, the net density rise during IBWH is at least twice the level of the no rf case, again showing an improvement in the particle confinement time. The high ionization states of carbon (C V, C VI), however, show no rise (or even a drop) during IBWH, representing an exceptional case.[2]

Another striking effect of IBWH is in the change of the low-frequency turbulence activity in the plasma. A microwave scattering system was used to investigate the turbulence in the half-radius region between the q = 1 and q = 3 surfaces (r = 25±10 cm). In Fig. 3(b), the time evolution of the scattering signals at 100 kHz for both IBWH and simulated ohmic cases is shown. In this case, the scattered wave number is 6-8 cm^{-1}. A significant drop in the turbulence level during IBWH can be seen, as compared to the simulated ohmic case. In the insert, the frequency spectrum for each case is shown immediately after the rf pulse (t = 710 msec). A frequency shift along with an amplitude reduction occurs during IBWH.

From the frequency shift, a net increase of the poloidal rotational velocity of approximately 5 × 10^4 cm per sec in the electron diamagnetic drift direction can be inferred. The net result is a near doubling of the electron diamagnetic drift velocity. This drift velocity would correspond to an electric field of 15 volt per cm in the radially inward direction. Measurements with an rf-shielded Langmuir probe in the plasma edge have shown the development, during IBWH, of a large floating potential which is negative with respect to the chamber wall [Fig. 3(c)]. This observation is correlated with the appearance of the frequency shift in the turbulence spectrum.

During IBWH, an increase in the influx of metallic impurities (predominately iron) was observed. This high-Z impurity influx, together with the longer particle confinement, can result in nonnegligible central radiation losses during high power (high density) IBWH. Therefore, it is quite important for a sucessful high power IBWH experiment to reduce the iron influx level as much as possible. In order to understand the source of the iron impurity, the outer Faraday shields of one of the antennas were coated with a 20-μm thick carbon film. This antenna was compared with the noncoated antenna. For the same rf power level, the carbon-coated antenna produced half as much iron influx (and half as much central bolometric radiation) as the uncoated antenna, demonstrating

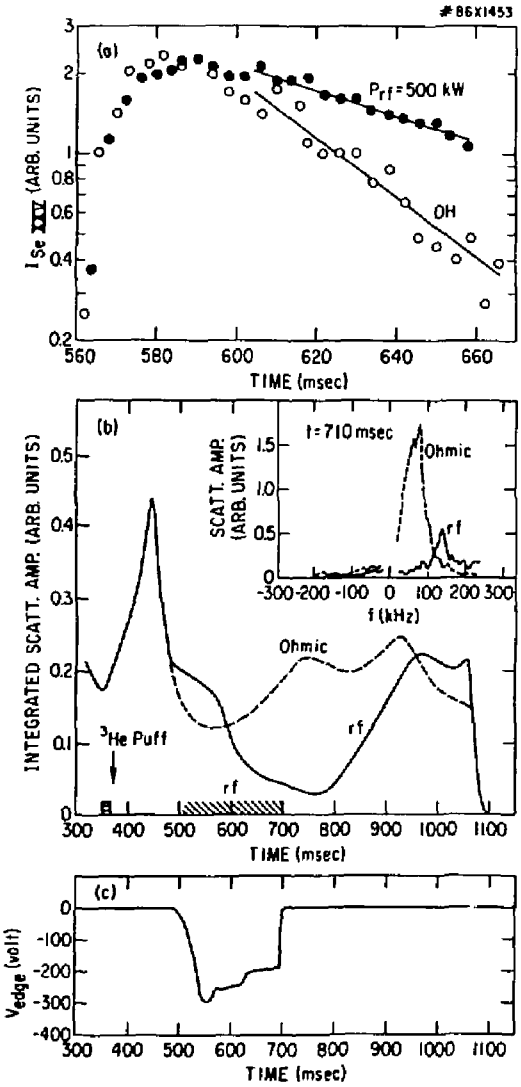

Fig. 3. (a) Time evolution of the selenium XXV resonance line intensity for IBWH and simulated ohmic cases. The selenium was injected at t ~ 550 msec. (b) Time evolution of low-frequency turbulence level at 100 kHz for the two cases. k(scatt) = 6-8 cm^{-1} at r = 25± 10 cm. Insert: frequency spectrum at t = 710 msec for the two cases. (c) Floating potential at plasma edge.

that the metallic impurity level during IBWH can be controlled. The ion heating efficiency and the density rise, however, remained similar for both antennae.

Plasma confinement during IBWH is of interest due to its bulk ion heating properties.[3] To investigate the scaling of energy confinement with plasma current, the current was varied from 200 kA (q_{edge} = 10) to 630 kA (q_{edge} 3) with a constant rf power level of

250 kW. For a given rf power, the ion temperature increase remains constant down to the lowest current of 200 kA. The normalized energy confinement time τ_E/n_e also remains constant. This may be due to the bulk ion heating characteristic of IBWH such that fast ion losses are negligible, even for the low current case. For a given current, I_p = 500 kA, the power scaling shows a gradual degradation of confinement time with increasing rf power, as shown in Fig. 4. At 650 kW, the confinement time is about 40 msec at 4.5 × 10^{13} cm^{-3}, which is significantly below the ohmic value of 50-55 msec but appears to be higher than the L-mode scaling time of approximately 33 msec. This drop in the global confinement time can be attributed to an increase in the electron loss channel. However, in view of increased radiation losses during IBWH, the electron thermal diffusivity still appears to be ohmic-like.

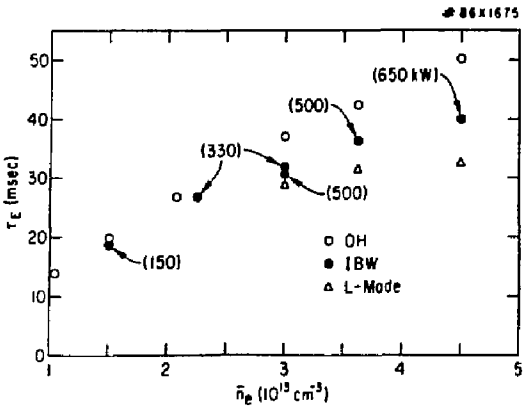

Fig. 4. Global confinement time versus the line-averaged plasma density. Open circles are that of ohmic plasma, solid dots are that of IBWH (the applied IBWH power is shown in parentheses), and triangles are from the L-mode scaling with comparable applied power.

LOWER-HYBRID CURRENT-DRIVE EXPERIMENTS

Recent experience on large tokamaks has brought out the importance of MHD stabilization and profile control to the attainment of high Q in tokamak discharges. The FY86 lower-hybrid program on PLT was therefore tailored to study MHD stabilization and modification of the electron temperature profile using the PLT 1-MW 2.45-GHz lower-hybrid system.[4,5] For this purpose, a newly designed optimum lower-hybrid coupler was installed, consisting of a sixteen-element waveguide array on the outside of the torus in place of the former eight-element array. This grill, which launched a narrow spectrum of moderately fast (v_{ph}/c ~ 0.8) lower-hybrid waves, was used in combination with an eight-element array at the top of the torus.

A useful test of the effectiveness of a coupler is to measure the rf power required to maintain the plasma current in the absence of any ohmic current drive. Expressed in terms of the standard figure of merit $In_{13}R/P$, the effectiveness of the new grill is compared to the eight-element 2.45-GHz and 800-MHz grills in Fig. 5. As shown, the new grill is about 40-50% more effective than the grills used formerly. This improvement is attributed to a better compromise between accessibility (requiring slow waves) and current-drive effectiveness (requiring faster waves). This result, demonstrating the superiority of multiarrays, should strongly affect the design of high-power lower-hybrid experiments on large tokamaks. It is important to emphasize continued improvement in coupler design, because the inherent current-drive phenomena just discovered in high temperature tokamak plasmas may reduce the requirements for rf current drive well below the pessimistic estimates of several years ago. In other experiments with combined rf and ohmic-heating current drive, it has been determined that the density limit for current drive at 2.45 GHz was greater than 4 × 10^{13} cm^{-3}, at least six times the limit found at 0.8 GHz.

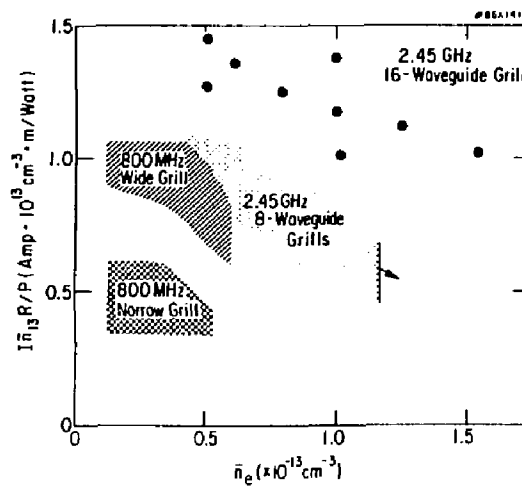

Fig. 5. Current drive figure of merit $I\bar{n}_{13}R/P$(kA · 10^{13} cm^{-3} · m per kW) versus electron density for 800-MHz, six-element wide and narrow grills, and 2.45-GHz, eight- and sixteen-element grills.

If the current-drive efficiency is high, lower-hybrid power can also strongly affect the MHD stability of a tokamak discharge. Monitoring of the stability was accomplished with a microwave polychrometer tuned near the second harmonic of the electron-cyclotron resonance and with Mirnov loops. The cyclotron radiation measurements showed that above a certain power threshold, depending on the plasma density, the rf waves suppress sawteeth activity near the center of the plasma, as shown in Fig. 6. The effective power threshold is about one-third of that needed for current drive by rf power alone, so that the power

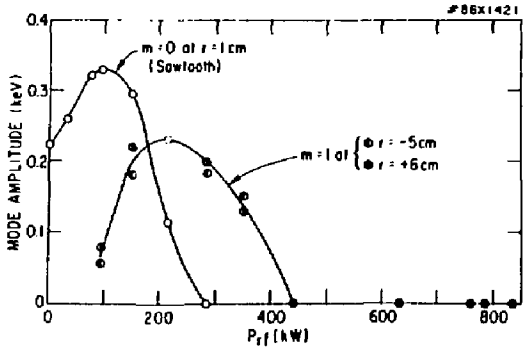

Fig. 6. Mode amplitude of m=0 (sawtooth) at r = 0 and m = 1 at r = -5 and 6 cm as a function of lower-hybrid power as determined from $2\Omega_{ce}$ emission. $\bar{n}_e \approx 10^{13}$ cm^{-3}, B = 29 kG, and I ≈ 500 kA.

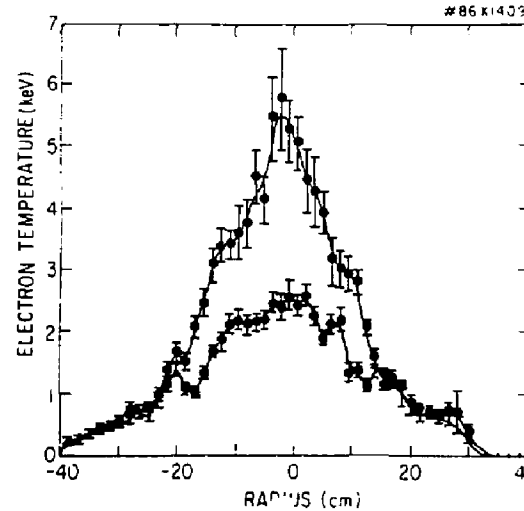

Fig. 7. Temperature profiles during ohmic (lower curve) and lower-hybrid discharges measured by laser Thomson scattering. B = 30 kG, I ≈ 500 kA, and $\bar{n}_e \approx 10^{13}$ cm^{-3}. (The T_e profiles are measured along a fixed vertical chord which cannot follow any outward shift of the axis.)

requirements for sawtooth suppression in world-class reactors are not impossibly large. On JET (Joint European Torus), for example, serious consideration is being given to a 10-MW lower-hybrid system for this purpose.

Suppression of the m=0 instability (sawteeth) tends to drive up the amplitude of the m=1 mode, as shown in Fig. 6. A further doubling of rf power is required to stabilize the m=1 mode. The most likely reasons for the MHD stabilization are a reduction in the plasma resistivity and a change in the current distribution near the plasma center. The Garching group, on the basis of direct measurements of the poloidal field, believe that the sawtooth suppression results from an increase in the central q value above 1. Our measurements, although inconclusive, are consistent with their claim. The hard X-ray profile tends to broaden somewhat with rf power and the internal inductance drops by about 10% during rf current drive, as would be expected from current broadening. On the other hand, the m=1 inversion point does not appear to shift outward, but this point is rather far removed from the plasma center and, thus, is insensitive to the central q.

The MHD stabilization is accompanied by a sharp rise in the central electron temperature and a peaking of the temperature profile in spite of the broadening of the current profile. The data of Fig. 7 show a rise in central electron temperature for approximately 2.2 keV during ohmic heating to approximately 5 keV during rf heating. The temperature profile has apparently been decoupled from the current profile. The temperature continues to rise up to about 500 kW, the approximate level of ohmic heating, and then appears to saturate. The stored energy in the electrons continues to increase with power, but at a rate less than that expected from ohmic discharges, so that the confinement time begins to drop. The temperature increase becomes smaller as the plasma density rises. Above $n_e \approx 3 \times 10^{13}$ cm^{-3}, the available rf power is insufficient to eliminate the sawteeth oscillations. The electron energy confinement time rises initially with rf power and then slowly decreases to the ohmic level. The electron energy confinement time, which is proportional to the density in ohmic discharges for which $n_e < 3 \times 10^{13}$ cm^{-3}, rises more slowly with density when rf power is applied.

With $q > 2.5$ it is possible to suppress the m=0 and m=1 modes without driving up the m=2 mode or causing a disruption. As q is reduced below 2.5, the m=2 mode tends to grow in millisecond bursts during the rf pulse, leading to small dips in the plasma current, as shown in Fig. 8. Although the MHD activity affects the plasma current only slightly, it usually leads

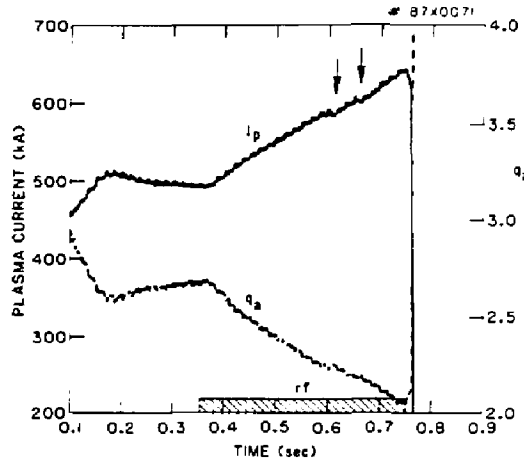

Fig. 8. Rise in plasma current following application of rf power during low-q discharges. Note current hesitation at times of m = 2 activity — noted by arrows.

to a 30-40% drop in X-ray production by the tail electrons and a similar drop in electron temperature.

Large amplitude sawteeth invariably accompany high power ICRH heating of tokamak plasmas. In large tokamaks the sawteeth involve ions as well as electrons and appear to limit the maximum Q. Several studies using combined ICRF and lower-hybrid heating were carried out on PLT during the year. It was found that the heating effects with combined excitation were additive, i.e., the lower-hybrid heating was unaffected by the ICRH and vice versa. Sawtooth suppression was possible in the density range between 1 and 3 × 10^{13} cm^{-3} (see Fig. 9). The lower-hybrid power required to stabilize the sawteeth did not vary significantly from 700 kW as the ICRF power ranged up to 800 kW. This scaling rule would have favorable implications on plans for sawteeth suppression in ICRF-heated large tokamak plasmas.

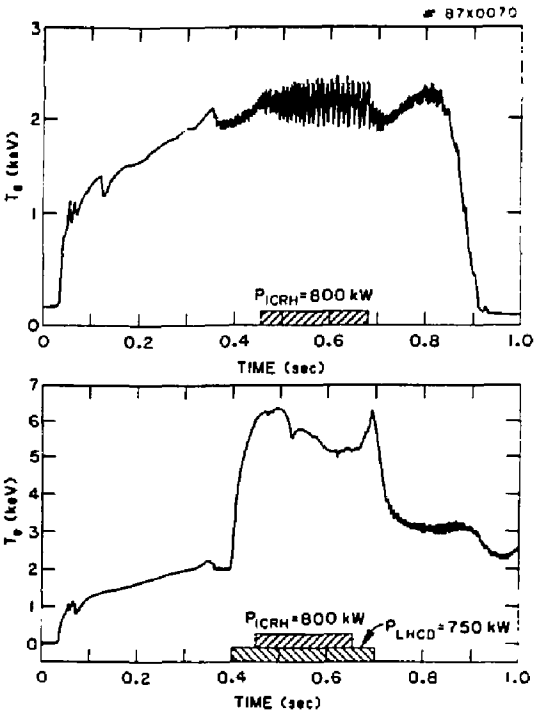

Fig. 9. Suppression of sawteeth activity during combined ICRH and lower-hybrid heating in PLT. $\bar{n}_e$ = 2.5 × 10^{13} cm^{-3}.

FAST-WAVE CURRENT-DRIVE EXPERIMENTS

During FY86, experiments were carried out on PLT to ascertain the feasibility of driving plasma current with rf waves above the density limit which has been observed with conventional slow-wave lower-hybrid current-drive experiments, with the hope that the overall efficiency of the current-drive process could be improved. Investigations were conducted in two frequency ranges where power sources in the range of several hundred kilowatts were available and in conjunction with higher frequency slow-wave lower-hybrid current drive. A number of potential current-drive schemes were studied using the flexible operating regimes of PLT. A series of antennas comprised of multiple element arrays to direct the wave momentum into a particular toroidal direction were used. The results of this work did not yield the hoped for higher efficiency current-drive mechanism; however, information from these experiments helped to clarify the nature of the wave propagation and current-drive limit itself.

In the low-frequency regime (30 MHz), 100-200 kW of power was applied to a 6-element array of half-turn loop antennas identical to those used in the highly successful fast-wave-heating experiments of previous years. In this case, proposed current-drive schemes were based on either heating of resonant ion species or nonresonant Landau damping on fast electrons. In the resonant ion scheme, ^3He ions heated resonantly by a wave propagating predominently in one toroidal direction would yield a net plasma current by reducing the drag on electrons traveling in that direction. In the nonresonant scenario, a weak but finite direct damping of the low frequency on a hot electron population could lead to current drive, provided competing ion-damping mechanisms were removed from the plasma cross section. Attempts to drive currents in either regime were precluded by a large density rise, which has been observed usually in conjunction with intense fast-wave heating on PLT. Such high densities would normally prevent the formation of fast electron tails due to strong collisional drag and, hence, reduce the effectiveness of direct electron acceleration. In addition, under these circumstances the presence of high ion harmonic damping could dominate any electron-wave interaction. As a result, no manifestations of wave-driven currents or fast electrons were observed in this frequency range.

Higher frequency experiments were also carried out with an 800-MHz system using a 1 × 6 array of resonant loops (Fig. 10) and a 3 × 4 array of dielectrically loaded waveguides (Fig. 11). In the former case, up to 180 kW was applied to the array of resonant loops using stub tuners to match the antennas to the transmission line. Current drive was observed using this coupler, but it had the same density limit as that observed with the slow-wave 800-MHz launcher. To determine whether the loop coupler might have been launching predominantly the slow wave (rather than the fast wave) and to increase the coupled power levels, a dielectrically loaded waveguide array was fabricated by the Grumman Corporation using a novel construction technique. This launcher was intrinsically nonresonant but under optimal plasma conditions was capable of coupling about 80% of the incident power into plasma waves. A comparison of the reflection coefficient measurements from this array with theoretical predictions indicated that fast waves were indeed being launched

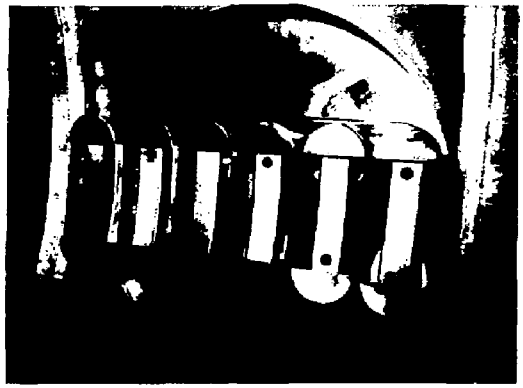

Fig. 10. Loop array for fast-wave current drive.

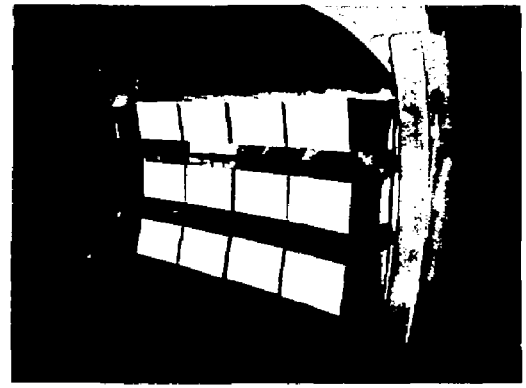

Fig. 11. Waveguide array for fast-wave current drive.

from this array with near predicted spectral properties. However, the current drive from this array also displayed the same density limitation associated with the slow wave, indicating that the wave propagation effects in the plasma may play a key role in determining the effectiveness of wave penetration and current drive. Further studies combining the 2.45-GHz slow-wave current-drive system and this array above density limit suggested that the launched fast waves did not interact with core electrons, but remained on the surface of the plasma.

While these studies did not lead to the establishment of an efficient current-drive scheme at high density, they underscore the importance of understanding the wave propagation in the plasma in determining the viability of these current-drive methods. It is likely that further progress in this area will require careful study on toroidal devices where detailed measurements of the wave propagation can be carried out.

ELECTRON-CYCLOTRON-WAVE ABSORPTION AT DOWNSHIFTED FREQUENCIES

The damping of electron-cyclotron waves with the extraordinary mode and an oblique angle of propagation was investigated in the PLT tokamak.[6] This is of interest because it allows the use of existing wave sources in present-day large tokamaks at values of toroidal field close to their maximum. For instance, in JET at B 35 kG and f = 70 GHz or in TFTR at B 50 kG and f = 100 GHz.

The output of a 60-GHz gyrotron was launched into the PLT plasma from a port located on top of the vacuum vessel with an initial direction of 30° with respect to the local toroidal magnetic field. Owing to a very lossy transmission line, the rf power was limited to a maximum of about 50 kW. At a plasma density of 1.3×10^{13} cm^{-3}, the injection of rf power produces a large increase of the hard X-ray and electron-cyclotron emission (ECE) signals, indicating the formation of an energetic electron population. The X-ray profile suggests that the energetic electrons are located in a central plasma core with a minor radius of approximately 10 cm, while the ECE frequency range indicates that their energy distribution extends up to 400 keV.

The production of energetic electrons peaks in a very well defined and narrow range of magnetic field (see Fig. 12) where the wave frequency is much smaller than the electron-cyclotron frequency. These observations are in agreement with the relativistic theory of electron-cyclotron damping, which predicts that the extraordinary mode with oblique propagation can be strongly absorbed by energetic electrons. This process can be used for both current drive and plasma heating. Existing rf sources make this a viable method for the present generation of large tokamaks.

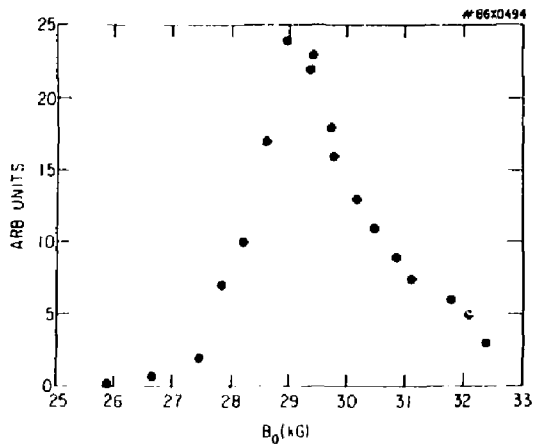

Fig. 12. Electron cyclotron emission signal as a function of B_0 at the end of the rf pulse.

SPECTROSCOPY STUDIES

Ultraviolet and Soft X-Ray Spectroscopy

The extensive spectrometic instrumentation on PLT continued to serve studies of impurity line emission, both in terms of computations of the line intensities and wavelengths.

In the vacuum ultraviolet (VUV) region, many spectra were taken under various discharge conditions with the normal-incidence McPherson spectrometer equipped with a multichannel detector. With this sensitive instrument observing weak lines in a region without many strong resonance lines, a number of phenomena worthy of investigation could be observed, especially during various rf heating modes.[7] These included recombination radiation, charge-exchange with neutrals, and existence of doubly excited states. Additional population of levels by proton excitation was observed as a line intensity ratio change due to deuteron heating during high power ICRF heating on PLT.

In the soft X-ray region, the high-resolution, interferometrically adjusted grazing-incidence spectrometer "SOXMOS" (adapted on PLT with multichannel detectors for use on tokamaks and other high temperature plasmas[8]) was also extensively used for line identification studies. Many spectra were taken during injection of impurities (from nickel to krypton) with various combinations of slit, grating, and detector to show the weak 3→3 transitions in the neonlike sequence (these lines have importance in X-ray laser research). At the same time, lines of very high states of ionization for these injected impurities were observed, and can only be explained by the very high electron temperatures reached in lower-hybrid-heated discharges.

All these observations fostered interest in line identification research, and the PLT tokamak became a unique spectroscopic source for the study of highly ionized, moderate-to-high atomic number elements. To help in these studies, a composite spectrum and list of all the intrinsic impurity lines (as they usually appear before the injection of elements by the laser blow-off technique) were compiled and published.[9] A compilation of spectra of injected impurities is planned, comprising the elements from iron (Z = 26) to krypton (Z = 36) or higher. This kind of data has already been shown to be useful in the study of 3 3 transitions by helping elucidate the Al I sequence,[10] and considerable effort is being provided to expand these data to higher-Z elements and higher temperature, as studies on Zr, Mo, and Ag[11,12] have demonstrated.

X-Ray Spectroscopy

During FY86, X-ray spectroscopy on PLT continued to focus on the investigation of neonlike ions. The major effort was directed towards understanding the atomic physics processes involved in the production of neonlike spectra and towards opening up neonlike spectroscopy for use in plasma diagnostics. Interest in neonlike systems also exists in the area of X-ray laser research. This common interest has resulted in a collaboration with the Lawrence Livermore National Laboratory.

The X-ray line radiation in neonlike ions involves transitions between the n = 3 and the n = 2 shell. Using the PLT high-resolution, helium-filled Bragg crystal spectrometer, these transitions were measured for silver in the wavelength region between 3.3-4.1 Å (Ref. 13). (See Fig. 13.) The measurements provided the first tokamak observation of the forbidden electric quadrupole (E2) lines of interest in X-ray lasing schemes. Seven different spectra of hydrogen-like and helium-like ions fall in the same wavelength region in first or second order and have been measured concurrently. These spectra provided a

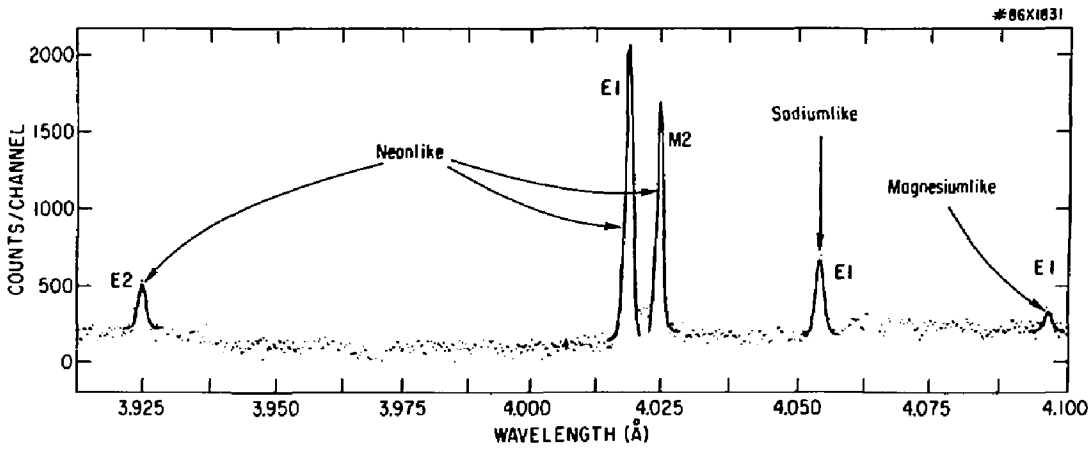

Fig. 13. Typical X-ray spectrum obtained with the PLT helium-filled crystal spectrometer showing n 3 to 2 transitions in various charged states of silver.

coherent set of wavelength reference data which was used to determine the transition energies of the silver lines with an unprecedented accuracy of one part in 20,000.

The attainment of very high electron temperatures in PLT with lower-hybrid heating has spurred investigation of highly charged ions with atomic charge higher than silver (Z = 47). Neonlike 3→2 transitions were measured in xenon (Z = 54) and lanthanum (Z = 57). The precision measurements of the X-ray transition energies promise to yield valuable information on quantum electrodynamical effects in multielectron systems.

In order to measure spectra of medium-Z ions in the soft X-ray region (5-25 Å), a new high-resolution vacuum Bragg crystal spectrometer was developed. It allows measurement of the intensity ratios of the neonlike lines as a function of plasma radius with 5 cm spatial and 4 msec temporal resolution.[14] Complete 3→2 spectra of neonlike selenium were obtained, and a first examination of the data indicates significant deviations from the intensities predicted by radiative-collisional models.

PLT RIDGED-WAVEGUIDE EXPERIMENT

The use of waveguides to couple power to a plasma in the ion-cyclotron range of frequencies is a potentially attractive alternative to conventional loop antennas.[15] A prototype ridged-waveguide coupler was recently installed in a radially-movable port on PLT, and the coupling characteristics of the guide were studied. In order to propagate waves in the frequency range of interest for PLT, given the available port dimensions, it was necessary to load the waveguide with a material of high dielectric constant.[15] Solid titanium dioxide ($\epsilon \approx 80$) was chosen, resulting in a cutoff frequency of approximately 50 MHz. A picture of the waveguide installed in PLT is shown in Fig. 14.

The complex impedance at a point in the transmission feedline was measured from which the equivalent series resonant resistance was calculated. Experiments were carried out at low power (0.05-10 W) with typical plasma parameters $n_e = 1\text{–}3 \times 10^{13}$ cm^{-3}, $B_o = 30$ kG, $I_p = 500$ kA for various radial positions of the coupler. The vacuum loading is approximately 8 Ω, while the plasma loading increases from approximately 20 Ω to approximately 100 Ω as the coupler approaches the plasma. These results indicate that efficient power transfer to the plasma is possible using this coupler. Further experiments show that the loading increases with line-averaged plasma density, and rf magnetic probes at various locations around PLT show evidence of eigenmodes similar to those observed during conventional ICRF heating.

It is of considerable interest that the observed plasma loading can be made equal to 50 Ω for a particular radial position of the coupler. At this position the waveguide presents a perfect match to the generator without the usual impedance-matching devices required with conventional ICRF loop antennas. This would be a desirable characteristic for future reactor ICRF couplers.

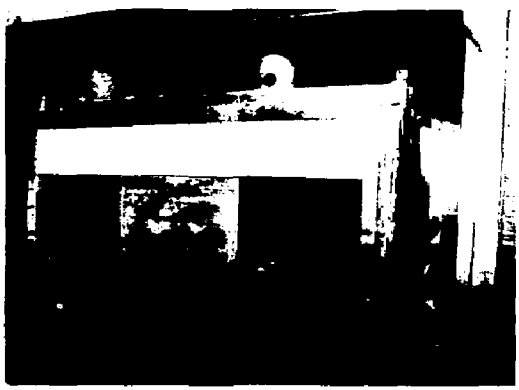

Fig. 14. The PLT ridged-waveguide coupler.

References

[1]J.C. Hosea, J.R. Wilson, W. Hooke, *et al.*, "RF Experiments on PLT," Plasma Physics and Controlled Fusion *28* (1986) 1241.

[2]J.R. Wilson, R. Bell, A. Cavallo, *et al.*, "The Evolution of Plasma Parameters as Governed by Edge Phenomena During Ion Bernstein Wave (IBWH) Heating," J. Nucl. Mater. *145-147* (1987) 616.

[3]M. Ono, R. Bell, S. Bernabei, *et al.*, "Ion Bernstein Wave Heating Experiments on PLT," *in Plasma Physics and Controlled Nuclear Fusion Research 1986* (Proc. 11th Int. Conf., Kyoto, Japan, 1986), paper IAEA-CN-47/F-1-3 (IAEA, Vienna, 1987), to be published.

[4]T.K. Chu, R. Bell, S. Bernabei, *et al.*, "Suppression of Internal Disruptions in Inductively Driven Tokamak Discharges by Lower Hybrid Wave Current Drive," Nucl. Fusion *26* (1986) 666.

[5]S. Bernabei, R. Bell, A. Cavallo, *et al.*, "Electron Temperature and MHD Modes During Lower Hybrid Current Drive and Preliminary Results of Fast Wave Current Drive on PLT," in *Plasma Physics and Controlled Nuclear Fusion Research 1986* (Proc. 11th Int. Conf., Kyoto, Japan, 1986), paper IAEA-CN-47/F-II-1 (IAEA, Vienna, 1987), to be published.

[6]E. Mazzucato, I. Fidone, A. Cavallo, S. von Goeler, and H. Hsuan, "Experimental Investigation on Electron Cyclotron Absorption at Down-Shifted Frequency in the PLT Tokamak," Nucl. Fusion *26* (1986) 1165.

[7]K. Sato, S. Suckewer, and A. Wouters, "Effect of Deuteron Temperature on Iron Forbidden Line Intensities in RF-Heated Tokamak Plasmas," Princeton University Plasma Physics Laboratory Report PPPL-2449 (in press); submitted to Phys. Rev. A.

[8]J.K. Schwob, A. Wouters, and S. Suckewer, "High-Resolution Duo-Multichannel Soft X-Ray Spectrometer for Tokamak Plasma Diagnostic," Princeton University Plasma Physics Laboratory Report PPPL-2419 (1987) 58 pp; submitted to Rev. Sci. Instrum.

[9]J.H. Dave, U. Feldman, J.F. Seely, A. Wouters, S. Suckewer, E. Hinnov, and J.L. Schwob, "Time-resolved Spectra in the 80-340 Å Wavelength Region from PLT Tokamak Plasmas, J. Opt. Soc. Am. *B*, to be published 1987.

[10]E. Hinnov, F. Boody, S. Cohen, U. Feldman, J. Hosea, K. Sato, J.L. Schwob, S. Suckewer, and A. Wouters, "Spectrum Lines of Highly Ionized Zinc, Germanium, Selenium, Zirconium, Molybdenum, and Silver Injected into Princeton Large Torus and Tokamak Fusion Test Reactor Tokamak Discharges," J. Opt. Soc. Am. *B* (1986) 1288.

[11]M. Finkenthal, B.C. Stratton, H.W. Moos, W.L. Hodge, S. Suckewer, S. Cohen, P. Mandelbaum, and M. Klapish, "Spectra of Highly Ionized Zirconium and Molybdenum in the 60-150 Å Range from PLT Tokamak Plasmas," J. Phys. B *18* (1985) 4393.

[12]J.L. Schwob, A. Wouters, S. Suckewer, S. Cohen, and M. Finkenthal, "Emission in the 50-80 Å Region from Highly Ionized Silver in Princeton Large Torus Tokamak Plasmas," J. Opt. Soc. Am. *B* (1986) 68.

[13]P. Beiersdorfer, M. Bitter, S. von Goeler, *et al.*, "High Resolution n=3 to n=2 Spectra of Neonlike Silver," Phys. Rev. A *34* (1986) 1297.

[14]K. Hill, P. Beiersdorfer, M. Bitter, *et al.*, "Tokamak X-Ray Diagnostic Instrumentation," Princeton University Plasma Physics Laboratory Report PPPL-2403 (1986) 54 pp.

[15]C.M. Fortgang and D.Q. Hwang, "ICRF Technology Development on the Princeton RF Test Facility, in *Radiofrequency Plasma Heating 1985* (American Institute of Physics, NY, 1985) 61.

PRINCETON BETA EXPERIMENT

As reported earlier,[1] plasma betas above 5% have been successfully achieved in the Princeton Beta Experiment (PBX) device with bean-shaped plasmas idented by 20% and heated by over 5 MW of neutral-beam power. These beta values, the highest yet achieved in tokamaks of comparable size,[2] were obtained in discharges for which the Troyon-Gruber parameter β_c was greater than 2 and β_t = 2-2.5β_c. Here $\beta_c = \mu_o I_p / a_{mid} B_t$, with a_{mid} the plasma half-width on the midplane. However, these discharges all terminated in a hard disruption.[3] At medium and low β_c, beta saturation and/or beta collapse took place and limited the maximum achievable beta to $\beta_t < 3\beta_c$. Thus, for all values of β_c, β_t did not exceed (2-3)β_c, consistent with the limit obtained by Troyon, Gruber, *et al.* for optimized plasma equilibria, where a n=1 kink was the most unstable mode.[4] The high-beta, high-β_c disruptions were indeed found to have a magnetic signature in approximate agreement with that calculated for a n=1 kink, but the situation at lower β_c was less clear.

In the final period of PBX operation (October 1985 - December 1985), extensive efforts were made to document the MHD instabilities near the Troyon-Gruber beta limit with medium and low β_c, where beta saturation and beta collapse were dominant phenomena. Another experimental emphasis during the period was to evaluate the effect of the neutral beam injection angle on MHD stability by using two perpendicular and/or two parallel beams. The main conclusion of this work is that, independent of the beam orientation, the internal n=1 fishbone mode is more unstable in less indented and high-q plasmas, in reasonable agreement with MHD theory. Finally, ion thermal diffusivities in H-mode discharges were evaluated by using the observed ion-temperature profiles and a generalized transport code, TRANSP.

Experimental studies were completed by the end of CY85 and modification of the PBX device started as a second phase of the Princeton Beta Experiment (PBX-M). The purpose of the modification is to stabilize the high-β_c MHD activities near the Troyon-Gruber β_t limit with a nearly complete conducting shell and to explore the regime beyond the first ballooning limit. The present modification requires the construction of five new poloidal-field coils and installation of six additional power supplies to gain better control over the plasma shape.

MHD STABILITY NEAR THE TROYON-GRUBER β_t LIMIT

Ideal-MHD Beta Limits

A complication of the PBX is that the main experimental parameters, such as indentation i_n, q_{edge}, β_c, and the achievable β_t, are not independently variable, but are strongly coupled to each other near the Troyon-Gruber β_t limit. Figure 1 shows these experimental parameters versus β_c for $\beta_t > 1.5\beta_c$. Indentations of 18 to 22% were attainable in high-β_c discharges with q_{edge} as low as 2.5-3.5. However, at lower β_c, the highest achievable indentations were

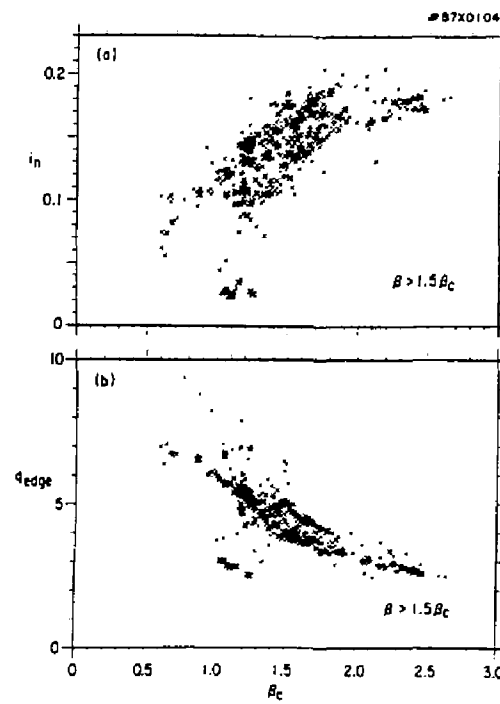

Fig. 1. (a) Indentation i_n versus β_c and (b) q_{edge} versus β_c where $\beta_c = \mu_o I_p / a_{mid} B_t$ and $\beta_t > 1.5\beta_c$.

limited to 5-10% and the q_{edge} values were increased to 6-7. The configurations corresponding to β_c = 2.0 and 1.0 are illustrated in Fig. 2. The profiles of density and electron temperature are also different in these cases: the electron temperature profile was peaked at high β_c and broadened at lower β_c, and the gradient of the density at the periphery was sharp at high β_c and became smoother at lower β_c.[13]

In order to clarify the significance of the changes in these parameters for the onset of ideal-MHD instabilities, the stability conditions were evaluated numerically for experimentally determined equilibria.

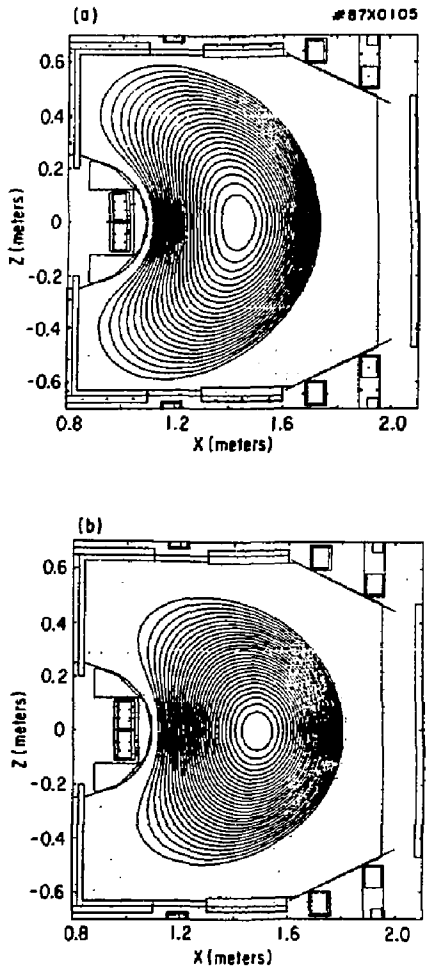

Fig. 2. Equilibrium configurations for (a) i_n 20%, I_p 570 kA, β_t 5.3%, B_t 0.9 T and (b) i_n 10%, I_p 360 kA, β_t 2.8%, B_t 1.1 T. Note the appearance of a separatrix in (b).

Three representative cases were chosen with β_c = 2.5, 1.5, and 1.0. The calculations were focused on three instabilities: the internal kink (n=1), external kink (n=1), and ballooning modes. Some cases were calculated for n=2,3 in order to study the possibility of higher-n modes.

As Fig. 3 shows, at high β_c and hence high indentation with low q_{edge}, the internal kink mode is completely stable under the experimental conditions, and the marginal β_t for ballooning modes is 8-9%. However, without a conducting shell the external kink becomes unstable at β_t = 3.5%; but with a conducting shell located at one plasma midplane half-width, b_w/a_{mid} = 2, the marginal β_t for the stability is increased to 4.5-5%, close to the observed value.

At the intermediate β_c value of 1.5 (β_t = 3.1%, i_n = 17%, q_{edge} = 4.2), the relative stability of the three modes is similar to that at high β_c. At the lowest β_c with a lower indentation (β_t = 2.7%, i_n = 10%, q_{edge} = 4.5), the internal kink is unstable around the obtained β_t. This indicates that the experimental pressure profile at low β_c belongs to the strongly peaked cases discussed in Ref. 5. With these pressure and q profiles, the external kink and ballooning modes can be destabilized at the relatively low values of β_t = 1.5 to 2.5%. Note that in all three cases ideal-MHD theory has the n=1 external kink as the most unstable mode, and, in fact, the experimental beta values are higher than what might be expected. What stabilizing effects are responsible is not known; conducting wall, scrape-off plasma, or a more favorable current distribution than inferred from the temperature profile may all have a part.

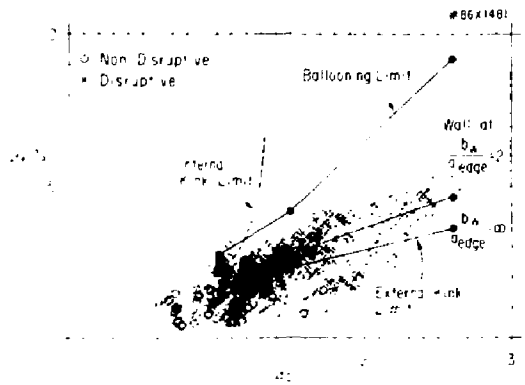

Fig. 3. Plot of β_t versus β_c showing highest attainable beta values. Below $\beta_c \simeq 1.4$, discharges survive but show beta saturation or collapse; above $\beta_c \simeq 1.9$, discharges end in a hard disruption. The ballooning and internal kink limits are calculated for experimental conditions with fixed plasma boundary; the external kink is calculated with the wall at infinity and at one plasma radius away.

Observed Instabilities

MHD Instabilities at β_t Saturation and Collapse

At high β_c, the dominant β_t-limiting instability has a MHD signature generally consistent with the external kink, as discussed in Ref. 3. At lower β_c, the dominant activity is related to a strong m/n = 1/1 mode coupled to higher-m modes. The detailed manifestations of the mode, as well as how it interacts with either perpendicular or parallel fast ions, depend on the plasma condition, particularly plasma density and the internal plasma snape. The mode which does not fall in either of the above categories is the ERP (edge relaxation phenomenon, known as an edge localized mode or ELM in ASDEX).

Here, MHD activities at low β_c are summarized with a typical shot which exhibited β_t saturation and subsequent β_t collapse. In this shot, the plasma current was kept steady near I_p = 370 kA with B_t = 1.2 T, $\beta_t = 2.4\beta_c$, β_c = 1.0, and β_p = 1.4 before β_t collapse was initiated. A total power of 5.2 MW was injected with two perpendicular neutral beams from t = 450 msec and two parallel neutral beams from t = 500 msec. Figure 4 shows the various measurements used to monitor the MHD behavior at the center and plasma edge. Figures 5(a), (b), and (c) show the same data in 20-msec segments. The

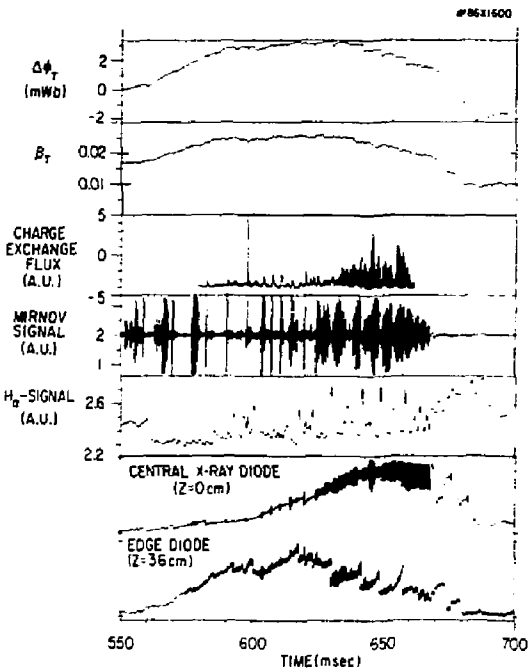

Fig. 4. MHD activity during β_t saturation and collapse in relation to diamagnetic flux, β_t, etc. A drop in H_α at t = 560 msec marks transition to the H mode.

energy losses associated with the MHD activities were measured with a fast (50 μsec) and accurate (0.1-0.2% of total stored energy) diamagnetic loop installed inside the vacuum vessel. The major activities were fishbones (e.g., at 604 msec, 607 msec, 611 msec, 615 msec), internal m/n = 1/1 sawtooth-like precursors with their crashes (583 msec, 590 msec, 598 msec), and the edge relaxation phenomenon (586 msec, 593 msec, 597 msec, 600 msec, 618 msec). The sudden drop of the H_α signal at t = 560 msec indicates the transition to an H mode. After β_t saturated at $\beta_t = 2\beta_c$ (600-630 msec), it decreased—"collapsed"—down to $\beta_t = 1.5\beta_c$ around 650 msec. The MHD activities were ERP's, e.g., at 640 msec, 648 msec and 658 msec, and continuous m/n = 1/1, as shown by Fig. 5(c).

The internal m/n = 1/1 precursors and their crashes are different from typical sawteeth in several respects. A crash produces a finite loss of stored energy up to 8% according to the diamagnetic loop measurement. This amount is higher than the upper limit of the hot ion loss estimated by the neutron signal, indicating the substantial loss of thermal plasma energy. The inversion radius at the crash is sometimes considerably beyond the radius of the maximum amplitude of the precursor signal (presumably, the location of the q = 1 surface), as observed with the soft X-ray wave detector array.[6]

In Fig. 6(a), the mode structure of the precursor of the internal sawtooth-like m/n = 1/1 mode observed by the soft X-ray radial array is compared with the theoretical prediction derived from the ideal-MHD mode, assuming the soft X-ray emissivity is proportional to the square of the plasma pressure and the measured detector signal is the integral of the perturbed pressure along the line of sight.[7] For comparison, the measured amplitude and phase shift of a typical sawtooth (as functions of distance from the midplane) in the same shot are shown in Fig. 6(b). The phase shift of the internal m/n = 1/1 mode takes place gradually, in contrast to the case for the typical sawtooth which shows a sudden 180° jump around the z = 0 plane. This result indicates that higher-m components are excited simultaneously with the internal m/n = 1/1 mode, causing the more gradual phase shift. The radial mode structure of the continuous modes measured by the soft X-ray array showed the same gradual phase shift and peaked amplitude around the half-plasma radius as the internal sawtooth-like m/n = 1/1 mode, also indicating a strong coupling to higher-m modes. No indication of higher-n modes was observed. This implies that the β_t collapse may take place without the excitation of higher-n modes, in spite of the fact the numerical study showed the plasma to be only marginally stable to the ballooning mode. However, at much lower β_c (0.5-0.6), corresponding to $\beta_p > 2.2$, there is some indication that n=2,3 modes are excited simultaneously with the continuous m/n = 1/1 mode, but no strong correlation has so far been seen between the onset of the n=2,3 modes and the initiation of collapse.

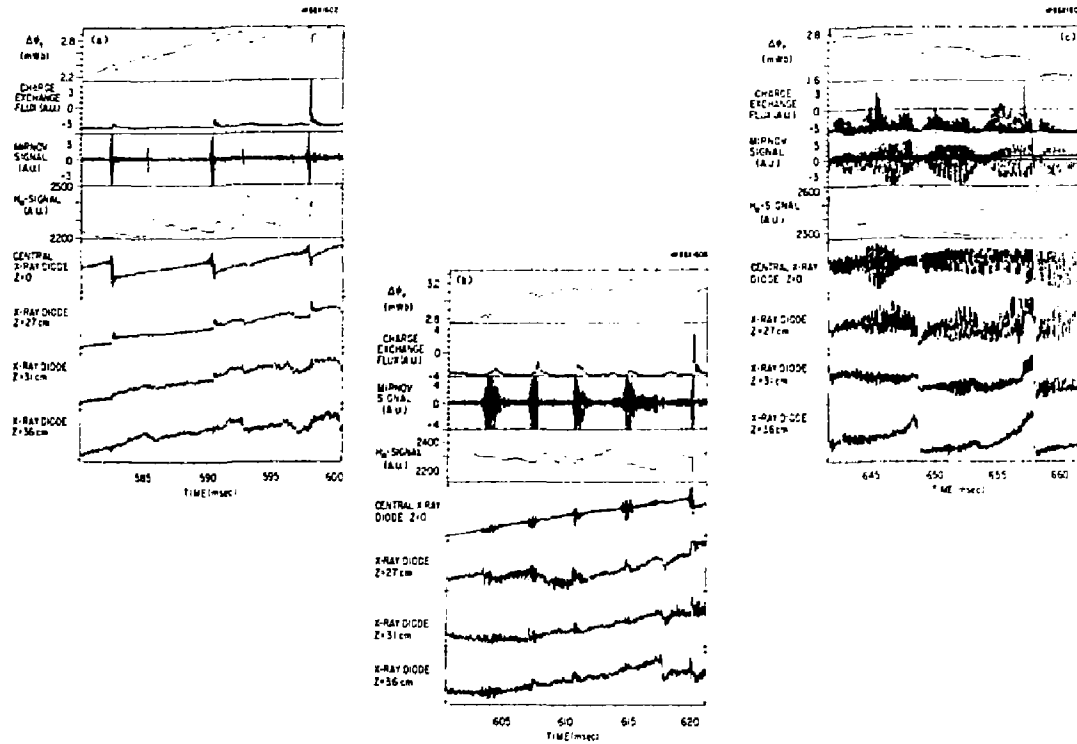

Fig. 5. Same as Fig. 4 but with expanded scale: (a) t = 580-600.5 msec (β_t rise); (b) t = 600-621 msec (β_t saturation); (c) t = 641.5-662 msec (β_t collapse).

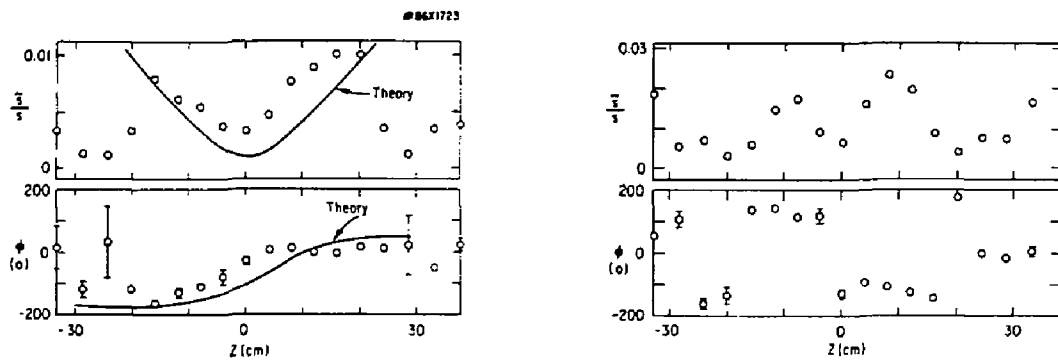

Fig. 6. (a) Comparison of measured amplitude and radial phase shift with theoretical prediction for internal sawtooth-like m/n = 1/1 mode (at t = 598 msec in Fig. 5). (b) Experimental observation for typical sawtooth. Note the characteristically abrupt phase change at z = 0.

Energy Loss Due to MHD Activities

During β_t saturation [cf. Fig. 5(b)], there are strong correlations between the MHD activities and the reduction of stored energy. Drops in β_p of 1.2-1.5% at each crash of the internal mode and the repetitive loss of the energy every 7-9 msec give an equivalent average loss rate of 0.2-0.3 MW. In addition, ERPs cause an average loss rate of 0.2-0.4 MW. Although the effective loss rates are much smaller than the energy input of 5.2 MW, the β_t rise was already very slow, with stored energy increasing at a rate of only 0.8-0.9 MW even in intervals without MHD activities, such as observed around t = 595 msec. After 600 msec, with increasingly frequent fishbone bursts, the stored energy saturated completely. During this period the toroidal β_t was reduced by about 1.5% with each fishbone burst, causing an effective average loss rate of 0.6 MW for a burst repetition rate of 3-4 msec. This small increase of the average loss rate from 0.25 MW during the internal sawtooth-like m/n = 1/1 period to 0.6 MW in the fishbone period, in addition to the ERPs, eventually reduced the effective heating rate to zero. This result indicates that the heating input of 5.2 MW was predominantly lost through a mechanism unassociated with the observed MHD activities. The confinement time corresponding to this underlying loss rate is approximately 25 msec, a poor H-mode confinement time (the L-mode confinement time is about 20 msec).

During β_t collapse, two types of MHD activity are excited. One is ERP and the other is the continuous mode between two ERPs (for example, 649-657 msec). The effective power loss due to ERPs is increased to 0.5 MW. The decrease in stored energy between the two ERPs, where the continuous mode is dominant, is 0.7-0.9% over 5-10 msec with an average loss rate of 0.25 MW. However, if this loss rate is compared with the rate of energy increase in a quiescent interval just before the saturation [cf. Fig. 5(a)], such as the 0.85-MW rate at 595 msec, it could be concluded that these MHD activities cause an effective average loss rate of 1.1 MW (0.85 MW + 0.25 MW). No direct confirmation was made that the continuous mode is responsible for the energy loss. However, the observation of a monotonical increase of the loss rate with increase of amplitude, along with the gradual radial extension of the m/n = 1/1 activities, as observed in the relative oscillation amplitude and the phase shift, tend to support this hypothesis.

Thus, it may be reasonable to assume that ERPs and the continuous mode, which at 1.6 MW (0.5 MW + 1.1 MW) may together cause the loss of a third of the input power, are responsible for the β_t collapse, without invoking the excitation of the ballooning mode.

PARALLEL INSTABILITIES AT LOW PLASMA DENSITY

The dependence of plasma instabilities on neutral-beam-injection angle was studied by utilizing the perpendicular and parallel injectors.[8,9] The results at low density operation ($n_e < 1.5 \times 10^{13}$ cm^{-3}) are summarized in Fig. 7. With parallel injection, periodic drops of the neutron signal are accompanied by increases in the loss rate of fast neutrals, as measured by charge-exchange analyzers. These losses of beam ions are similar to those observed when the fishbone instability is excited with perpendicular injection. This

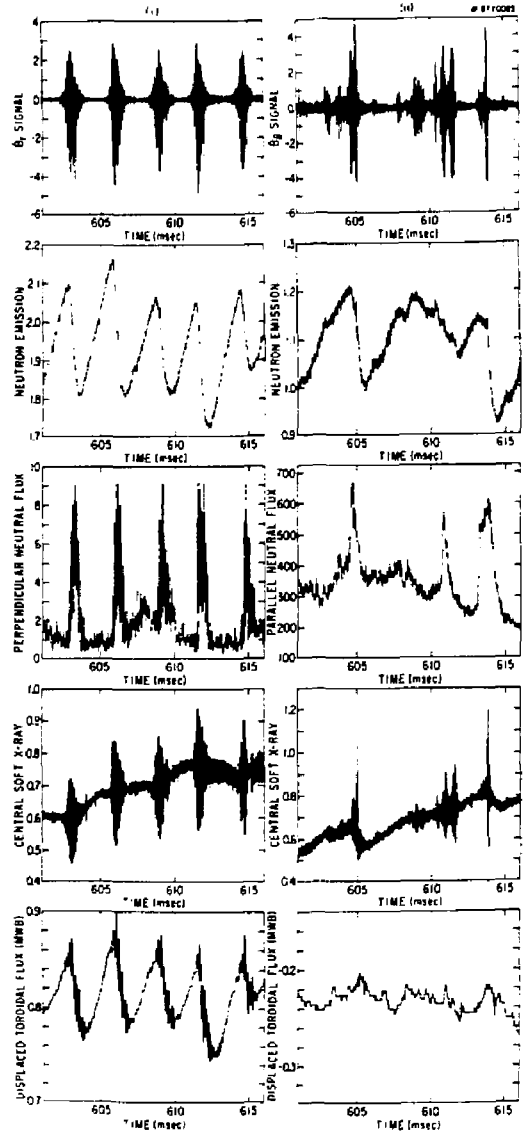

Fig. 7. Comparison of the MHD behavior with the instability driven by (i) perpendicular and (ii) parallel injection. Note that the neutrons are affected about equally but that more energy is lost from plasma in (i).

result indicates that with this parallel instability fast ions are redistributed from the center to the outer regions of the plasma at each event. The dominant frequency of the mode, also m/n = 1/1, is in the range of 10-15 kHz, close to the plasma toroidal-rotation frequency. The soft X-ray array signals showed the mode to have a broad phase shift in the radial direction, like that of the internal sawtooth-like m/n = 1/1 mode discussed earlier.

In addition to the low-frequency activity, oscillations with high frequency in the range 100-150 kHz were present between occurrences of the low-frequency internal m/n = 1/1 modes and were also correlated with decreases in the neutron production rate and increases in the fast ion loss rate. Although these higher frequencies are near the toroidal transit time frequency of the fast ions, it is not clear at present whether a mode-particle interaction, as considered for the fishbone instability,[10] is responsible for the fast ion energy loss.

The onset condition for fast ion loss by the parallel instability is plotted in Fig. 8 on a β_t, β_p diagram, along with that for the perpendicular instability. The onset conditions are more or less independent of the injection angle, indicating that at least a part of the onset mechanism is related to the total plasma pressure. It is also obvious that the ratio of beam density to plasma density plays a significant role, since low plasma density is the key factor for exciting these unstabilities for both injection angles.

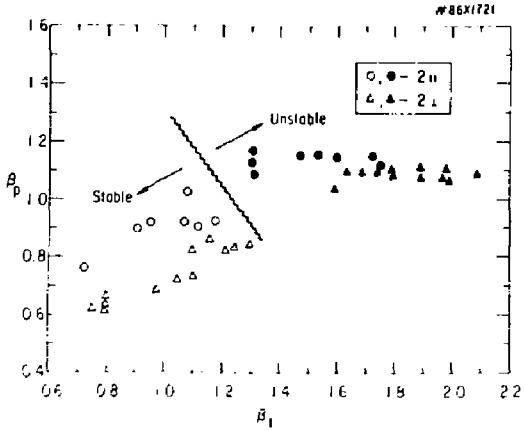

Fig. 8. Comparison of onset condition for fast ion-driven instabilities with perpendicular (triangles) and parallel (circles) injection plotted on a (β_t, β_p) diagram.

MEASUREMENT OF THE INTERNAL PLASMA SHAPE

The geometrical shape of the magnetic surfaces around q = 1 is one of the important factors for determining the local and global MHD stability of a high-β_t plasma. If a sharp gradient of plasma pressure appears in the interior area, for example, the energy source of the instability must be delicately balanced by magnetic shear and triangularity to maintain stability.

In PBX, a prototype soft X-ray pinhole camera diagnostic was developed to measure the shape of internal flux surfaces by measuring the soft X-ray emissivity contours.[11] The X-ray emission, observed tangentially, is converted to visible light with a microchannel plate image intensifier, and the resulting image is sent through an optical fiber system to be measured by a CCD TV camera located outside the vacuum vessel. The X-ray intensity depends strongly on the electron temperature and, since the electron isotherms should closely coincide with the magnetic surfaces, a mapping of the magnetic surfaces can be obtained, assuming no strong density asymmetries. The measured intensity contours are numerically converted to a two-dimensional poloidal emissivity distribution through an inversion technique that minimizes the propagation of noise-generated numerical errors. This diagnostic system was applied to the study of the dependence of fishbone activity at low plasma density on the interior flux-surface shape. Two plasma conditions were chosen: one with a fast current ramp[3] and the other with constant plasma current. With a 1.5 MA per sec current ramp, the fishbone instability is reduced substantially (Fig. 9), although the bursts did not disappear completely, as can be seen in the charge-exchange efflux signals in Fig. 9.

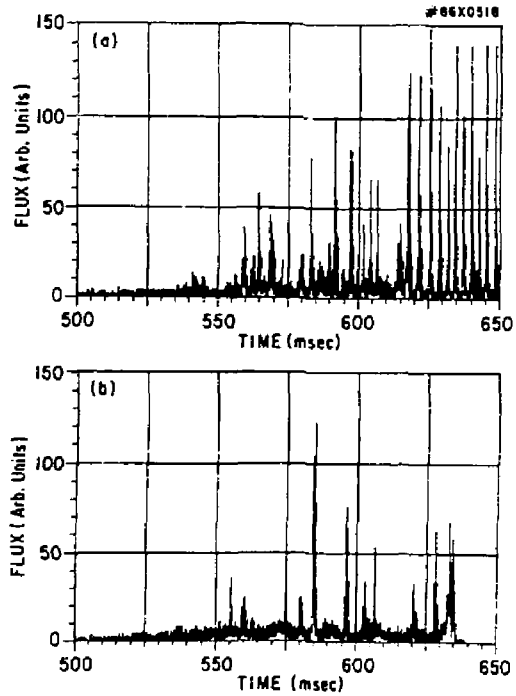

Fig. 9. Charge-exchange signals of fast neutrals (35 keV) with (a) weak indentation and (b) stronger indentation produced by fast plasma current ramp.

Figure 10 shows (a) the observed intensity contours for these two cases and (b) the emissivity contours after inversion. Evidently, a fast plasma current ramp can increase both elongation and triangularity around the half-radius area. The change in the internal shape is more or less consistent with the magnetic surfaces calculated for these parameters and shown in Fig. 10(c), and this qualitative agreement is acceptable given the calibration uncertainties in this prototype system and the possibility of density asymmetries in the plasma cross section. These results support the hypothesis that triangularity can stabilize the internal MHD activities, reducing the frequency of the fishbone bursts. Based on the promising results of these initial tests, a redesigned soft X-ray pinhole camera diagnostic will be implemented on PBX-M to provide routine measurements of the internal plasma shape.

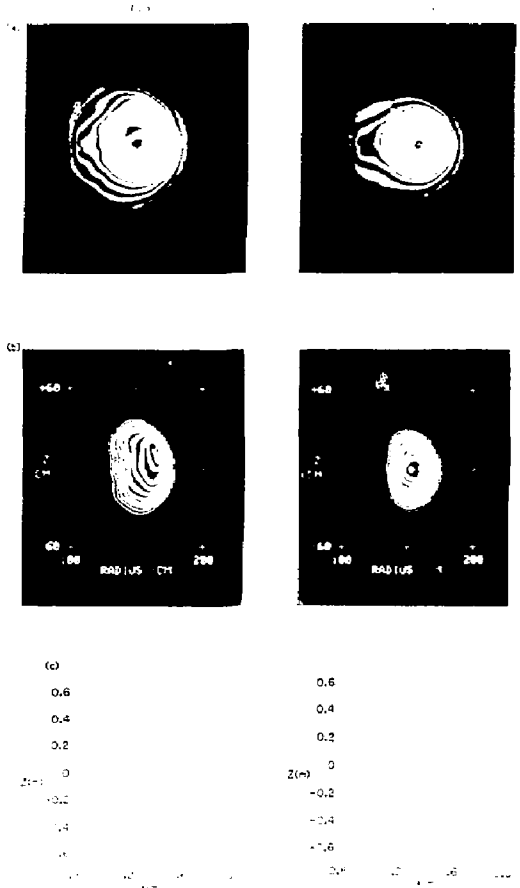

Fig. 10. The results (i) with large plasma current ramp and (ii) without current ramp. The X-ray emissivity contours (a) observed along the line of sight; (b) after inversion; and (c) the calculated equilibrium flux surfaces.

Related plasma imaging techniques can be used to determine the shape of the outermost flux surfaces, especially near the separatrix, by using filtered cameras sensitive to visible radiation emitted from the cool plasma edge regions. Figure 11 shows a series of views of the hydrogen-alpha radiation emitted from the cool divertor plasma region. The sharp increase in electron temperature at the separatrix produces strong gradients in the H_α emission at the separatrix, where the hydrogen gas is ionized and hence can no longer radiated line emissions. Edge sharpening techniques are applied to the H_α image to enhance the detection of gradients in the picture and, consequently, reveal the location of the separatrix, which is in good agreement with the magnetically determined position.

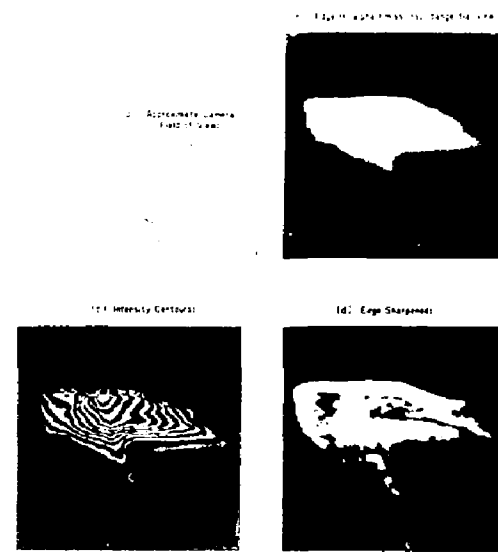

Fig. 11. H-alpha images of the plasma divertor region. (a) Calculated equilibrium flux surfaces in the camera field of view; (b) raw signal; (c) intensity contours to show the localization of recycling in the divertor region; and (d) edge enhanced to show the location of the separatrix.

TRANSPORT PROPERTIES OF HIGH-CONFINEMENT REGIME (H MODE)

In PBX, H-mode discharges can be produced by locating the magnetic separatrix just inside the passive stabilizer plates. The transport properties of these H-mode plasmas were investigated with the TRANSP code, using radial profiles of the ion temperature as measured with the charge-exchange

recombination light[12] of O^{8}. Figure 12(a) shows a measured T_i profile in an H-mode discharge obtained from several reproducible shots, chosen to avoid impurity accumulation in H-mode plasmas.[13] Figure 12(a) also shows a model profile obtained by scaling the neoclassical ion-thermal diffusivity with a constant factor, alpha, to match the centrally measured $T_i(0)$. In this case α = 0.5, and the corresponding diffusivity is shown in Fig. 12(b). The diffusivity was also derived directly from the measured T_i profile, and the shaded area in Fig. 12(b) reflects the allowed range of χ_i, given uncertainties arising from the modeling procedures and in the measured profiles. Because of sensitivity to errors in the T_i and T_e profiles, the results inside 5 cm and beyond 20 cm are ignored. The results indicate that the ion thermal diffusivity is comparable to the electron thermal diffusivity over the central plasma region, but is also comparable to the neoclassical values within the uncertainties of the theoretical and measured values for χ_i. It should be noted that the ion thermal loss was not dominant in these discharges and was responsible for, at most, 30% of the total loss.

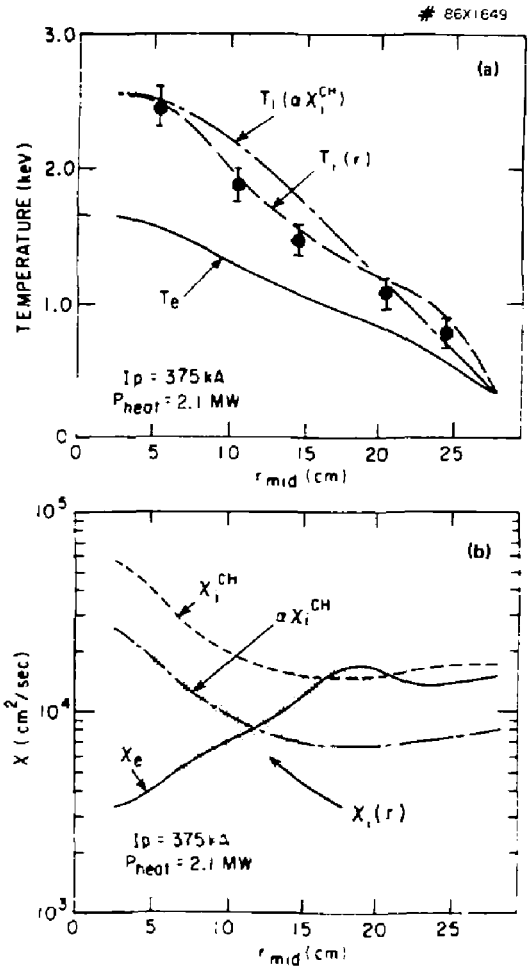

Fig. 12. Transport analysis for (a) ion and electron temperature profiles: T_e and $T_i(r)$ are measured; second T_i curve assumes neoclassical diffusivity scaled by α = 0.5 for best fit at r = 0. (b) Scaled neoclassical diffusivity χ^{CH} and results for χ_i and χ_e based on measured temperature profiles analyzed with the TRANSP code.

MODIFICATION TO PBX-M

The PBX was shut down in January 1986 to begin modification to PBX-M. As shown in Fig. 13, this modification calls for an increase in plasma major radius from 1.45 m to 1.65 m, allowing room for a divertor; for the construction of five new coils inside the vacuum vessel, consisting of a new pusher or indentation coil on the midplane and two pairs to shape the separatrix in the construction of five new coils inside the vacuum vessel, consisting of a new pusher or indentation coil on the midplane and two pairs to shape the separatrix in the divertor region; and, most importantly, for a (segmented) conducting shell that nearly surrounds the plasma and which is expected to stabilize the surface modes that evidently limited β_t in PBX. The shell also provides greater stability against axisymmetric modes than the more rudimentary one in PBX, and hence permits greater indentation.

An important early issue of great consequence for project cost and schedule was the choice of fabrication method for the new coils. Three fabrication methods were considered: (1) prefabrication of the complete coil system for installation in a dismantled machine, the costliest and most time consuming, but the surest option; (2) prefabrication of jointed coils for subsequent encasement and potting inside the vacuum vessel; (3) fabrication of the coils out of soft copper *in situ*, subsequently brazing the leads to the coils and encasing and potting the windings as the last step. After a successful trial of the winding procedure, the third method was chosen (cf. Figs. 18 and 19, Engineering Department Section). At the end of the period covered by this report, all five coils had been wound and encased in 0.060-inch stainless steel cans without encountering any difficulty. Only electrical leads and power feedthroughs remained to be installed.

The passive "coils" comprising the new, extended conducting shell are not only the heart of PBX-M from a physics perspective, but, because of their size, offer an even greater technical challenge than the active coils. By the end of the reporting period, one-inch-thick aluminum plates had been break-formed into conical elements and were being trimmed to size. It is expected that the maximum deviation of the actual

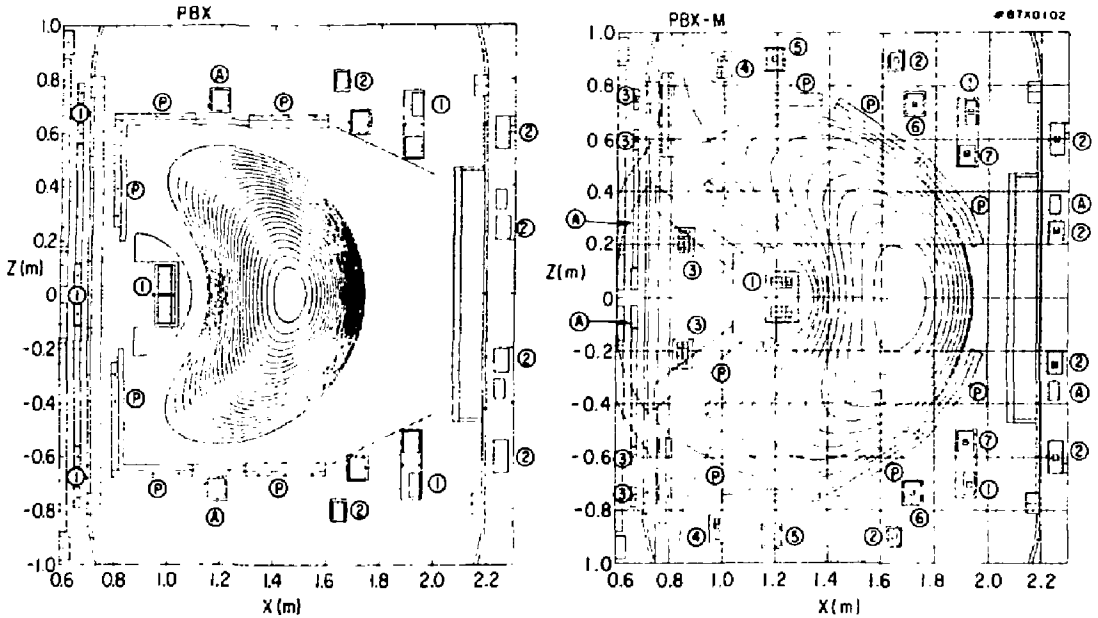

Fig. 13. Comparison of PBX and PBX-M. (a) PBX: (1) indentation field coils; (2) equilibrium-field dipole field; (P) passive stabilizer plates; (A) active feedback coil for vertical position control. (b) PBX-M: (1) indentation field coils; (2) equilibrium-field dipole field; (3) divertor field coils; (4)-(7) trimming coils; (P) passive stabilizer plates; (A) active feedback coil for vertical position control.

surfaces from the ideal ones can be kept to 0.5 cm, an acceptable tolerance. Since aluminum has a high sputtering coefficient, one-eighth-inch stainless steel was explosively bonded to the plasma-facing side of the plates as the first step of fabrication. The last step will be assembling complete conical annuli inside the vacuum vessel and mounting them on supports paralleling the ones for the active coils. This task will pace the completion of the modification.

Auxiliary heating of the plasma by neutral beams as well as various diagnostic requirements dictate the 40-cm gap in the outboard midplane section of the shell that is shown in Fig. 13. Although it weakens the stabilizing effect of the shell, the gap can be compensated for by a relatively small reduction in the plasma-shell separation, as shown by the calculations summarized in Fig. 14. Ten vertical jumpers bridging the gap also mitigate its effect.

A cost- and schedule-driven feature of the original PDX/PBX conversion was that all shaping-field coils were powered in series by a single current source, i.e., one source of current. In PBX-M, this single current source is replaced by six thyristor power supplies, thus vastly increasing both the flexibility and the complexity of the system. Including the ohmic heating and equilibrium field (the equilibrium field is a more or less uniform vertical field), the control of the plasma shape and position now require eight coupled power supplies. (A ninth supply, for the mean vertical position of the plasma is sufficiently decoupled from the rest so as not to pose a problem.) The number of supplies and the necessity for keeping the plasma within a tightly defined envelope have made design of a practical control system a major challenge. The control scheme that appears most promising, and which will probably be implemented, first resolves measured deviations of the plasma boundary from the desired shape into a few pseudoharmonics. To each such pseudoharmonic there corresponds a combination of power supplies which will most nearly affect only that shape component. Contributions arising from each pseudoharmonic are then summed to obtain the input signals to the power supplies. Three harmonics, corresponding more or less to the first three cylindrical harmonics (dipole, quadrapole, and hexapole), appear sufficient to define the shape with adequate precision.

Strictly speaking, the power supply combination which best matches a given pseudoharmonic depends on the details of the plasma equilibrium, and the question is whether such variations can be safely ignored. Results, so far, indicate that with coefficients optimized for a β_t 5% plasma, a range of β_t 0-10% can be covered. This means the transformation of the magnetic signals (from which the shape is determined) into power supply signals is a simple linear one over that range and is amenable to analog implementation. A PPPL-owned EAI-2000 analog computer will be used for this purpose. If subsequent study shows that at much higher beta values (10%) the problem becomes nonlinear (i.e., the coefficients depend markedly on the magnetic signal interpretation), then a digital system may have to be implemented

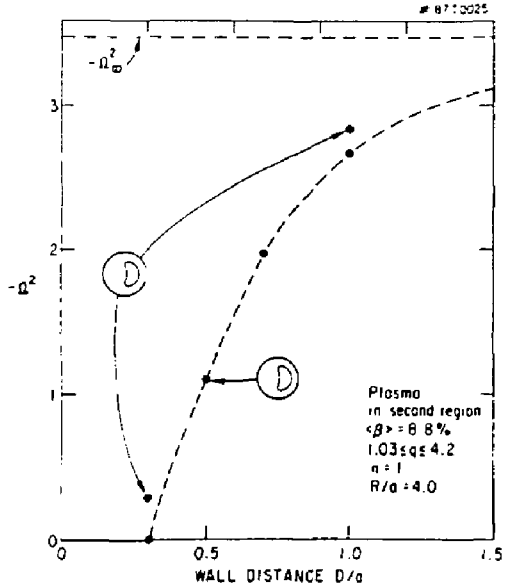

Fig. 14. Wall stabilization of the external kink. Dotted curve gives the growth rate as function of the distance D of the closed shell from the plasma on the outboard side. The gap in the shell is destabilizing, as indicated, but can be compensated for by reducing D/a to 0.25 from 0.3. The PBX-M design has D/a 0.17.

CONCLUSION

Detailed MHD studies have revealed the excitation of various modes near the Troyon-Gruber β_t limit. In the high-β_c regime, the poloidal structure of the mode and the onset condition of the plasma-terminating hard disruption are consistent with the external kink mode. At medium and low β_c in weakly indented plasmas, a m/n 1/1 mode structure underlies all the observed high-β_t instability phenomena except ERPs. These include an internal sawtooth-like *m/n 1/1 mode*, fishbones, a continuous mode, and a fishbone analog observed with parallel injection that has been named the parallel instability.

More deeply indented plasmas, with more highly triangular internal flux surfaces (as shown by shape studies with a two-dimensional soft X-ray imaging system) exhibit the occurrence of only a much weakened fishbone instability. These results are consistent with the theoretical analysis of the underlying 1/1 mode is basically an internal kink, though necessarily modified in various degrees by resistive and kinetic effects. Thus, there is a reasonable basis for anticipating that the stronger triangularity of PBX-M will stabilize all 1/1 mode activity specifically associated with high beta, and that with the conducting shell to raise the external kink threshold it will become possible to realize a stable high-beta-plasma regime.

References

[1]Princeton University Plasma Physics Laboratory Annual Report PPPL-Q-42 (October 1, 1983 - September 30, 1984) and Princeton University Plasma Physics Laboratory Annual Report PPPL-Q-43 (October 1, 1984 - September 30, 1985).

[2]K. McGuire, P. Beiersdorfer, M. Bell, *et al.*, "Divertor and Scoop Limiter Experiments on PDX," in *Plasma Physics and Controlled Nuclear Fusion Research 1984* (Proc. 10th Int. Conf., London, 1984), Vol. *I* (IAEA, Vienna, 1985) 117; M. Keilhacker, G. Fussmann, G. von Gierke, *et al.*, "Confinement and Beta-Limit Studies in ASDEX H-Mode Discharges," *ibid.*, Vol. *I*, 71; M. Murakami, P.H. Edmonds, G.A. Hallock, *et al.*, "Confinement of Beam-Heated Plasmas in ISX-B," *ibid.*, Vol. *I*, 87; R.D. Stambaugh, R.W. Moore, L.C. Bernard *et al.*, "Tests of Beta Limits as a Function of Plasma Shape in Doublet III," *ibid.*, Vol. *I*, 217.

[3]K. Bol, D. Buchenauer, M. Chance, *et al.*, "High β-Plasmas in the PBX Tokamak," Phys. Rev. Lett. 57 (1986) 1891.

[4]F. Troyon, R. Gruber, H. Sauremann, *et al.*, "MHD Limits to Plasma Confinement," Plasma Physics and Controlled Fusion *26* (1984) 209.

[5]J. Manickam, R. Grimm, and M. Okabayashi, "Stability of n 1 Kink Modes in Beam-Shaped Tokamaks," Phys. Rev. Lett. *51* (1983) 1959.

[6]H. Takahashi, W. Morris, S. Sesnic, *et al.*, "Loss of Confinement Following a Sawtooth Internal Disruption in PBX Tokamak," Princeton University Plasma Physics Laboratory Report PPPL-2391 (1986) 11 pp.

[7]M. Okabayashi, K. Bol, M. Chance, *et al.*, "Stability and Confinement Studies in the Princeton Beta Experiment (PBX)," in *Plasma Physics and Controlled Nuclear Fusion Research 1986* (Proc. 11th Int. Conf., Kyoto, Japan, 1986), paper IAEA-CN-47/A-V-2, to be published.

[8]R. Kaita, K. Bol, P. Couture, *et al.*, "Effects of Plasma Indentation and Neutral Beam Injection Orientation on MHD Instabilities in PBX," Plasma Physics and Controlled Fusion *28* (1986) 1319.

[9]W. Heidbrink, K. Bol, D. Buchenauer, *et al.*, "Tangential Neutral-Beam-Driven Instabilities in the Princeton Beta Experiment," Phys. Rev. Lett. 57 (1986) 835; Princeton University Plasma Physics Laboratory Report PPPL-2405 (1986) 42 pp.

[10]L. Chen, R. White, and M. Rosenbluth, "Excitation of Internal Kink Modes by Trapped Energetic Beam Ions," Phys. Rev. Lett. *52* (1984) 1122.

[11]R. Fonck, M. Reusch, K. Jaehnig, R. Hulse, and P. Roney, "Soft X-ray Imaging System for Measurement of Noncircular Tokamak Plasmas," in *Proceedings of SPIE—the International Society for Optical Engineering*, Vol. 691, (SPIE, Washington, D.C., 1986), 111.

[12]G. Gammel, R. Kaita, R. Fonck, K. Jaehnig, and E. Powell, "High Time Resolution Ion Temperature Profile Measurements on PBX," Rev. Sci. Instrum. 57 (1986) 1800; K.P. Jaehnig, R.J. Fonck, K. Ida, *et al.*, "Charge Exchange Recombination Spectroscopy Measurements of Ion Temperature and Plasma Rotation in PBX," Rev. Sci. Instrum. *56* (1985) 865.

[13]K. Ida, R.J. Fonck, S. Sesnic, *et al.*, "Observation of Neoclassical-like Impurity Transport in the q = 1 Region of the PBX Tokamak," Princeton University Plasma Physics Laboratory Report PPPL-2313 (1986) 14 pp.

S-1 SPHEROMAK

A spheromak is a toroidal magnetic confinement configuration for plasmas of the "compact toroid" type.[1] The toroidal field in the plasma is sustained entirely by poloidal plasma currents, eliminating the need for coils that link the plasma. This topology allows for a simply connected first wall and blanket and also allows for translation so that the plasma can be created in one place and then moved to a separate burn region. In addition, adiabatic compression can be conveniently applied to the spheromak. The very low aspect ratio of the spheromak permits a small volume for a given characteristic confinement scale length, which makes possible a small-sized reactor core. The objectives of the S-1 experiment[2-6] are to investigate the formation, equilibrium, stability, confinement characteristics of hot plasmas, scaling of confinement quality with various parameters, and the physics of sustainment of spheromak plasmas. Spheromak plasmas produced in the S-1 device have major radii in the range 0.4 to 0.65 m and minor radii of 0.25 to 0.45 m.

The main features distinguishing S-1 from other spheromak schemes are (1) the plasma formation technique, which is based on an inductive transfer of toroidal and poloidal magnetic flux from a toroidal "flux core" to the plasma, and (2) the stabilization of the plasma against dangerous rigid-body tilt and shift instabilities by use of loose-fitting conductors and coils.

SUMMARY

Operation of the S-1 Spheromak device was resumed in August 1986 after a one-year period in which efforts and funds were devoted to a program upgrading the plasma current capability. This program focused on the design, fabrication, and installation of a new flux core (Fig. 1). Because of technical problems which developed after thousands of discharge pulses, the original flux core was no longer capable of operation at its design values and could not take advantage of the full stored energy available from the energy storage (capacitor bank) systems. The new core is not only more reliable than the original one, but it can operate at 50% higher coil currents than the original.

Although the upgraded S-1 device has been operated for only a few months, much progress has been made. Magnetic results from earlier operation periods (typical plasma currents I_{pl} of 250 kA and with figure-8 coils)[2,6] were quickly reproduced. Recently, relatively detached and stable plasmas with toroidal currents greater than 0.5 MA (580 kA) were obtained (Figs. 2 and 3)—a milestone in the S-1 research program. The linear trend of I_{pl} with capacitor bank voltage (Fig. 2) extrapolates to currents of 650 kA at maximum voltages. (Design values 600 kA.) High-current operation increases the strength of the toroidal and poloidal fields in the plasma to greater than 3 kG.

The approximately linear scaling[3] of T_e with j^2 (with n_e const) was reconfirmed up to an I_{pl} of 250 kA. This scaling is consistent with the commonly quoted reversed-field pinch (RFP) scaling where beta is constant. It is this scaling which motivates the study of higher-current spheromak plasmas. At plasma currents of 250 kA or less, peak plasma electron densities n_e range from 2×10^{13} to 1×10^{14} cm^{-3} for hydrogen discharges; shot-averaged electron temperatures T_e range from 25 to 70 eV with measured temperatures ranging from 10 to 100 eV; the volume-averaged beta is 5-10%. In the near future, temperature measurements will be made at high current (I_{pl} · 0.5 MA).

All diagnostics which were initially planned for are now installed and operable, including a new multipoint Thomson scattering (TVTS) system to replace the previous single-spatial-point system. The improved data analysis capabilities from the multipoint system together with the upgraded flux core constitute the elements needed to begin an intensive study of temperature scaling, confinement, and transport at high currents and high current densities in spheromak plasmas.

The simultaneous use of the full array of diagnostics enabled a more detailed study to be made of relaxation phenomena during plasma formation and decay. A significant effort was made to compare the detailed experimental observations of relaxation phenomena with predictions from various simulations using ideal and resistive magnetohydrodynamic (MHD) computer codes. Impressive agreement was observed.

Another large effort this past year was the design of a poloidal-flux transformer which would provide additional inductive current drive.[7-11] This transformer would enable attainment of over 1-MA toroidal plasma current in a spheromak configuration. Operation with this transformer would constitute a large-scale test of the plasma's tendency to relax toward the Taylor state and would allow further study of the physics of (inductive) sustainment of spheromak plasmas.

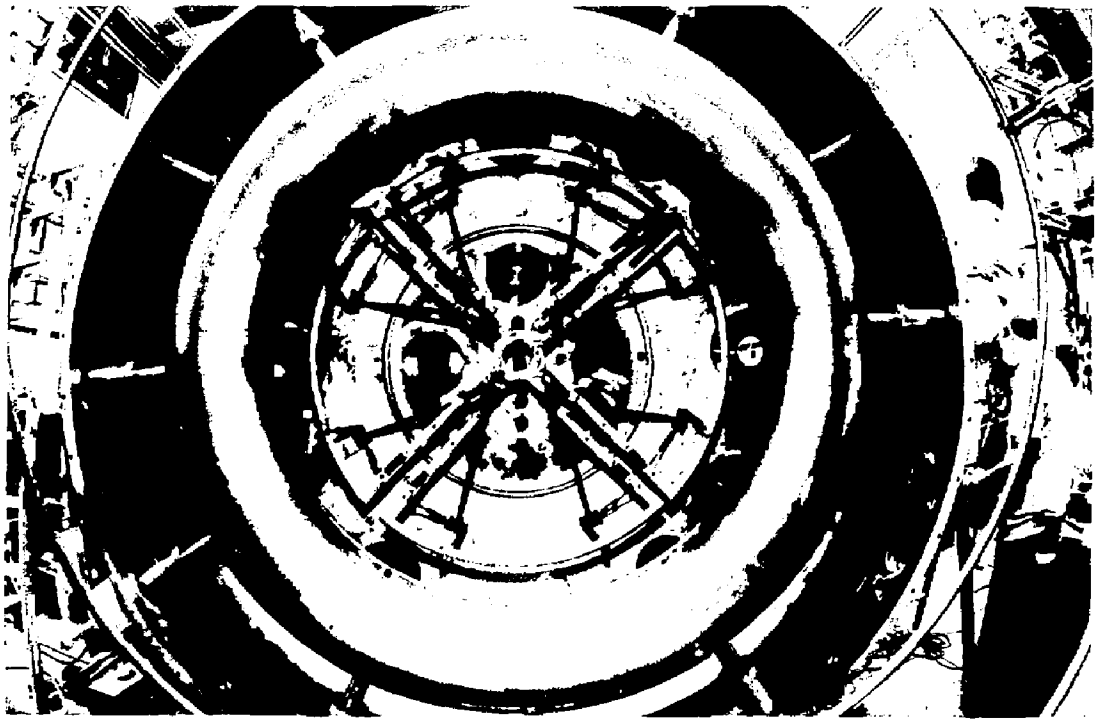

Fig. 1. New flux core installed in S-1. One dome of the vacuum vessel was removed allowing this view. Also visible is one (of two) pair of the figure-8 coils. (86X3225)

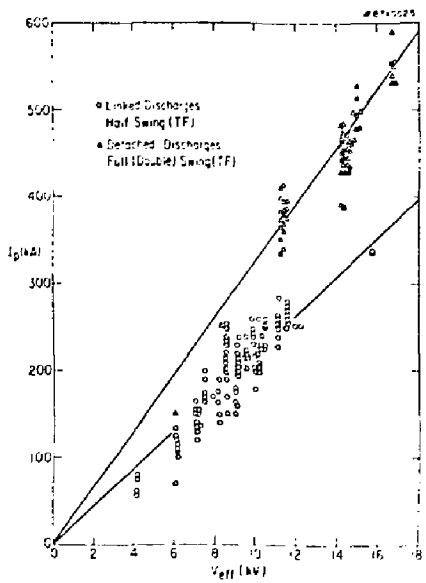

Fig. 2. Linear scaling of toroidal plasma current I_{pl} with "normalized" bank voltage. Currents over 0.5 MA were achieved with relatively stable and detached plasmas. This scaling extrapolates to 650 kA at maximum bank voltages.

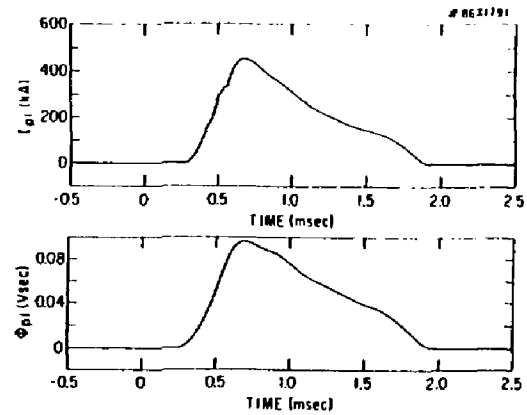

Fig. 3. Toroidal plasma current I_{pl} and toroidal magnetic flux Φ_{pl} in the plasma versus time for a relatively high-current long-lived discharge.

FLUX CORE UPGRADE

The purpose of the flux core upgrade was to create a flux core (Fig. 1) with greater vacuum wall reliability; with greater mechanical strength of its coils, power feedthrus, and bus work; and with the capability to operate at higher coil currents. The major changes

incorporated into the new core were: (1) An improved liner, which was manufactured by explosion-forming (to eliminate nonuniformities in thickness due to the old spinning process) and a closely controlled annealing process (to avoid excessive grain growth). Chemical milling was still needed to reduce the liner thickness to 0.015 inch, although the operation was much simpler due to the explosion-forming technique. To further reduce stresses and to increase fatigue life, the liner was reinforced with 0.100 inches of epoxy glass. (These same techniques were used successfully on a replacement liner installed in 1984). (2) Extruded solid copper conductors (with channel for water cooling) to replace the flexible-stranded "ATC" cables used for the poloidal-field and toroidal-field windings in the flux core. These conductors permit 50% higher coil current capability and will help void downtime caused by cable failure. (3) Redesign of the vacuum feedthrus that carry the pulsed power to improve the mechanical strength, the vacuum integrity, and to simplify leak checking and replacement of bellows and/or electrical breaks. Pump ports were also added to permit the core liner and current feeds to be evacuated if leaks should develop. These improvements essentially double the nominal toroidal plasma current achievable. The spatial dimensions of the core remained the same.

The S-1 device passed all engineering tests and has produced over 1,000 plasma discharges with $I_{pl} > 250$ kA, many with $I_{pl} > 500$ kA. The first successful use of double-swinging of the current in the toroidal-field coils has allowed increased injection of toroidal flux, while decreasing the impulse to the bus work. Vacuum condition is now better than that achieved with the old flux core, with base pressures as low as 2×10^{-8} mTorr.

CONFINEMENT STUDIES

A method to measure the local perpendicular particle diffusion coefficient in S-1 was developed using Proto S-1C.[12] A localized carbon discharge is created on the midplane using a pair of small electrodes, and the temporal evolution of the injected impurity density is observed spectroscopically at different radial locations. The arrival time of the impurity pulse is determined by the perpendicular diffusion coefficient. The two major results are: (1) During the spheromak decay phase, diffusion of carbon can be explained classically, with $D \sim 10^5$ cm^2 per sec, and (2) diffusion during the formation (relaxation) phase is approximately three times larger than during the decay phase. This method is now being tried on S-1.

RELAXATION PHENOMENA

Of fundamental importance to understanding the physics of spheromak plasmas is the concept of the Taylor minimum-energy state. Taylor proposed that a plasma in which the resistivity is small but finite will relax with the aid of some type of turbulence to a minimum-energy state through reconnection of magnetic field lines. He further suggested that the only important constraint for determining the final state was the conservation of global magnetic helicity defined as $\int dV\, \vec{A} \cdot \vec{B}$, where the integration is over the whole plasma volume. (Helicity can be thought of as the linkage of magnetic flux tubes.) The Taylor principle predicts the final state to be the force-free equilibrium $\vec{j} = (\mu/\mu_0)\vec{B}$ for which μ is a constant in space (μ_0 is the permittivity of free space, j is current density, and B is magnetic field strength).

A very important experimental result from S-1 (and other recent spheromak reseach) is the observation that the plasma tends to relax toward a stable spheromak plasma configuration by itself.[13-16]

Formation Phase

It has been experimentally verified that the final state of the plasma, after formation, is near the Taylor state, regardless of the initial conditions or the details of the formation process.[13,14] Large amplitude, low-n number, m=1 modes are observed to coincide with the flux conversion and relaxation processes during formation.[15,16] Recently, it was observed that, under certain conditions, a reversal of the toroidal field occurs at the edge of the magnetic configuration during the formation phase (Fig. 4). This reversal,

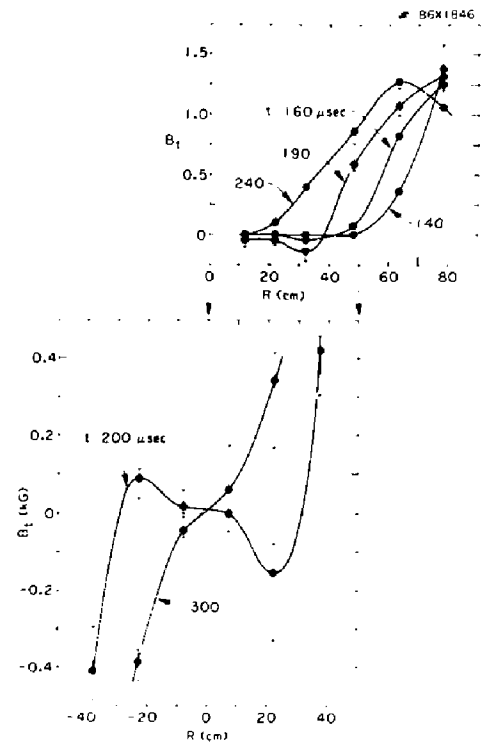

Fig. 4. Radial (midplane) profiles of toroidal field B_t inside the plasma, showing field reversal at the edge of the spheromak during formation.

which is typically ≤10% of the peak toroidal field, occurs during the relaxation period when low-n mode activity is high. Field reversal is most evident in the region of the symmetry axis. Magnetic-field measurements were made with a one-dimensional array of magnetic probes, extending along a major radius line, which could be moved between shots along the direction of the symmetry axis.

These observations are interesting since recent numerical simulations[17] of the relaxation process in low-q spheromak plasmas predict a field reversal as a consequence of the magnetic-field-line reconnection associated with the relaxation of the magnetic configuration. Further experiments are needed, since it is too early to say what the toroidal distribution of the reversal is and whether the reversal is a consequence of relaxation or is an artifact of large, low-n number kinking of the axisymmetric fields.

Decay Phase

As more discharges are fired and the plasma becomes cleaner, magnetic activity during the decay phase increases. Previously reported[13] relaxation oscillations observed during the decay phase appeared again. With several diagnostics operating simultaneously, it was observed that the sudden relaxation events were preceded by n=2 modes, which grew to 30% of the axisymmetric field strength before relaxation was triggered (Fig. 5). The n=2 mode decays after relaxation. The role of $n \geq 3$ modes is uncertain at this time. In addition, it appears that the current profiles [$B_z(R)$, $B_t(R)$] peak before relaxation and broaden as a result of the relaxation event. After the relaxation event, I_{pl} and Φ_{pl} decay much more rapidly, suggesting increased transport due to the relaxation event.

Numerical simulation of the evolution of a decaying spheromak by colleagues[18] in this field has provided impressive agreement with these, and other, experimental observations in S-1. According to theory, for a plasma with moderately high magnetic Reynolds' number S, a spheromak initially in a minimum-energy state will resistively diffuse until it becomes unstable to an n=2 mode (due to the decrease of q to below 1/2). After the mode saturates, the three-dimensional equilibrium resistively evolves until it reaches another unstable configuration, after which it relaxes back to the axisymmetric minimum-energy state. This evolutionary cycle can start again, in principle, unless the cycle time becomes comparable to the configuration decay time. One consequence of plasma relaxation back to the minimum-energy state is that the magnetic axis and hot plasma near it approaches the wall, and a new magnetic axis is formed, causing increased transport.

Experimentally, S is high enough to expect these relaxations, and the cycle time is less than or near the configuration lifetime, so that one or more cycles may be expected, as is the case. Also, the experimentally observed n=2 predecessor and the increased decay rate (increased resistivity) after a relaxation are both consistent with the results of the simulations.

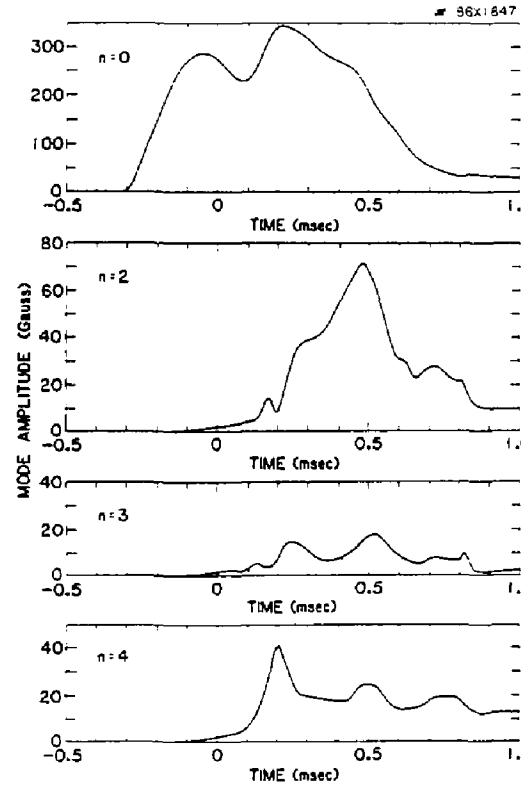

Fig. 5. Mode analysis of a discharge with one relaxation event near t = 0.5 msec. Amplitude of the n = 2 mode increases during formation, then grows until $B_{n=2}/B_{n=0}$ = 30%, at which time relaxation occurs. Therefore, the plasma decays very quickly.

OPERATION WITH POLOIDAL-FLUX TRANSFORMER AT 1 MA

The tendency of spheromak plasmas to reach or maintain the stable minimum-energy state can be exploited to further increase or maintain the toroidal and poloidal fields of a spheromak. One scheme for inductive current drive is the use of a poloidal-flux transformer along the major axis.[7-11] The transformer is similar in design and function to the ohmic-heating transformer in a tokamak, but it is inserted from only one end of the device. This technique maintains two important advantages of the spheromak configuration: translation and compression.

A prototype S-1 device was used to test this technique. The experiment was successful in demonstrating that not only the toroidal plasma

current but also the toroidal magnetic flux in the plasma could be increased and prolonged while maintaining a spheromak configuration. It can be shown that the linear increase of I_{pl} with flux swing can be explained by conservation of helicity arguments alone, assuming either instantaneous relaxation of the plasma or relaxation after a delay if $\Delta\Psi_{transformer} \leq \Psi_{pl(initial)}$.

Operation of a poloidal-flux transformer in S-1 was simulated[8,9] using a two-dimensional computer code model having a term in the mean-field Ohms law that describes the three-dimensional relaxation effects and flux conversion. This simulation demonstrated that the toroidal current can be increased from 0.5 MA to 1.0 MA (Fig. 6), while maintaining a relaxed spheromak plasma configuration for a poloidal-flux swing of approximately 1.0 Vsec. It is planned to use this technique on S-1.

The design of the poloidal-flux transformer for S-1 is nearly complete and some fabrication has begun. Installation is scheduled for mid-to-late 1987. This scheme requires two pulsed equilibrium-field coils with associated power supplies and controls, in addition to the main transformer. The liner, or cover, of the transformer is the most challenging component. The temperature rise can be excessive for thin, high-resistance, metallic materials, and nonconducting surfaces are either fragile or have undesirable plasma interactions. A temporary solution, using a glass bell jar, will be used until a better liner is designed.

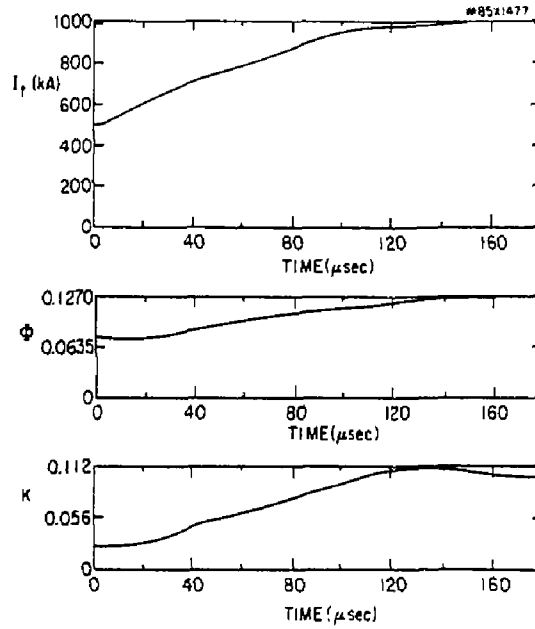

Fig. 6. Simulation of current drive with the poloidal-flux transformer, showing how I_{pl} is increased from an initial 0.5-MA level to over 1.0 MA.

References

[1]M. Yamada, "Review of Experimental Spheromak Research and Future Prospects," Fusion Tech. 9 (1986) 38.

[2]M. Yamada, R. Ellis, Jr., H.P. Furth, *et al.*, "Initial Results From S-1 Spheromak," in *Plasma Physics and Controlled Nuclear Fusion Research 1984* (Proc. 10th Int. Conf., London, UK, 1984), Vol. II (IAEA, Vienna, 1985) 535.

[3]R.A. Ellis, Jr., G.W. Hart, A. Janos, *et al.*, "Recent Progress of S-1 Experiments," in *Seventh Compact Toroid Research Symposium (Santa Fe, NM, 1985)*, Los Alamos National Laboratory, Los Alamos, NM (1986) 1.

[4]A.C. Janos, *et al.*, "Recent Progress of S-1 Spheromak Experiments (Magnetics)" in *Seventh U.S.-Japan Workshop on Compact Toroids* (Bellevue, WA, 1985), L.C. Steinhauer Editor, Spectra Technology, Bellevue, WA (1986) 37.

[5]M. Yamada, "S-1 Spheromak," Nucl. Fusion 25 (1985) 1327-1330.

[6]A.C. Janos *et al.*, "Recent Advances in S-1 Experiments," in *Eighth U.S.-Japan Workshop Compact Toroids* (Osaka, Japan, 1986), K. Watanabe and S. Goto editors, Osaka University, Osaka, Japan (1986) 1.

[7]A.C. Janos, "Steady-State Operation of Spheromaks by Inductive Techniques," Princeton University Plasma Physics Laboratory Report PPPL-2095 (1984) 21 pp; A.C. Janos and M. Yamada, "Inductive Sustainment of Spheromaks," Fus. Technol. 9 (1986) 58.

[8]S.C. Jardin *et al.*, "Amplification of S-1 Spheromak Current by an Inductive Current Transformer," in *Seventh U.S.-Japan Workshop on Compact Toroids* (Bellevue, WA, 1985), L.C. Steinhauer Editor, Spectra Technology, Bellevue, WA (1986) 13.

[9]S.C. Jardin, A. Janos, and M. Yamada, "The Effect of a Column Inductive Transformer on the S-1 Spheromak," Princeton University Plasma Physics Laboratory Report PPPL-2279 (1985) 25 pp; Nucl. Fusion 26 (1986) 647.

[10]R.A. Ellis, Jr. *et al.*, "Current Transformer for the S-1 Spheromak," in *Conference Record—Abstracts of the 1986 IEEE International Conference on Plasma Science* (Saskatoon, Canada, 1986), published by IEEE, New York, NY (1986) 76.

[11]M. Yamada *et al.*, "Injection of Magnetic Fluxes into Spheromak Plasma Through an Inductive Transformer," in *Conference Record—Abstracts of the 1986 IEEE International Conference on Plasma Science* (Saskatoon, Canada, 1986), published by IEEE, New York, NY (1986) 76-77.

[12]D.D. Meyerhofer *et al.*, "Measurements of Particle Diffusion in the Proto S-1C Spheromak," in *Conference Record—Abstracts of the 1986 IEEE International Conference on Plasma Science* (Saskatoon, Canada, 1986), published by IEEE, New York, NY (1986) 77.

[13]A.C. Janos, "Magnetic Flux Conversion and Relaxation Toward a Minimum-Energy State in Spheromak Plasmas," Princeton University Plasma Physics Laboratory Report PPPL-2066 (1985) 55 pp; Phys. Fluids *29* (1986) 3342.

[14]G.W. Hart, A. Janos, D.D. Meyerhofer, and M. Yamada, "Verification of the Taylor (Minimum Energy) State in the S-1 Spheromak," Princeton University Plasma Physics Laboratory Report PPPL-2257 (1986) 11 pp; Phys. Fluids *29* (1986) 1994.

[15]A.C. Janos, G. Hart, C.H. Nam, and M. Yamada, "Global Magnetic Fluctuations in S-1 Spheromak Plasmas and Relaxation Toward a Minimum-Energy State," Princeton University Plasma Physics Laboratory Report PPPL-2214 (1985) 31 pp; Phys. Fluids *28* (1985) 3667-3675.

[16]A.C. Janos, G.W. Hart, and M. Yamada, "Relaxation of Spheromak Plasmas Toward a Minimum-Energy State and Global Magnetic Fluctuations," Princeton University Plasma Physics Laboratory Report PPPL-2231 (1985) 15 pp; Phys. Rev. Lett. *55* (1985) 2868.

[17]K. Katayama and M. Katsurai, "Three-dimensional Numerical Simulations of the Relaxation Process in Spheromak Plasmas," Phys. Fluids *29* (1986) 1939.

[18]S.G. Sgro *et al.*, "The Evolution of a Decaying Spheromak," accepted for publication by Phys. Fluids.

[19]S.F. Paul, R.A. Ellis, Jr., G.W. Hart, *et al.*, "Initial Power Balance Studies in S-1" in *Seventh U.S.-Japan Workshop on Compact Toroids* (Bellevue, WA, 1985), L.C. Steinhauer Editor, Spectra Technology, Bellevue, WA (1986) 71.

[20]D.D. Meyerhofer, R.A. Hulse, and E.G. Zweibel, "Zero-Dimensional Study of the Compression of Low Temperature *Spheromaks*," *Nucl. Fusion* *26* (1986) 235.

CURRENT-DRIVE EXPERIMENT

The Current-Drive Experiment (CDX) was initiated in FY86 to test new ideas of nonclassical radial-current diffusion, ideas that may lead to more efficient methods for current drive and for current profile control, both crucial for economic tokamak reactors.[1] One approach, called dc helicity injection, utilizes steady-state injection of an electron beam at the plasma edge and subsequent radial penetration of the current to maintain the plasma current. A complementary approach, that of ac helicity injection, utilizes periodic modulation of several fields to yield a time-averaged steady-state plasma current. A third approach, referred to as "viscous" current drive, relies on the asymmetric character of an instability-driven radial-current penetration mechanism.[2]

The CDX experimental facility is the former Advanced Concepts Torus-I (ACT-I), a steady-state, 5-kG toroidal device with minor and major radii of 10 cm and 59 cm, respectively. During 1985, internal coils and powerful electron-beam injectors were added to the ACT-I facility to prepare for CDX. A schematic drawing of the ACT-I experimental setup is shown in Fig. 1(a).

The main research effort in the CDX program during FY86 was channeled into the dc helicity injection concept. That effort yielded a tokamak-like discharge, the first ever initiated and maintained by this technique.

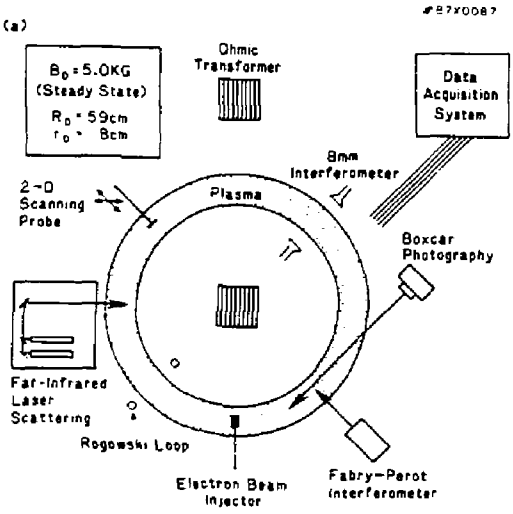

Fig. 1(a). Schematic of the experimental setup of the ACT-I experimental facility.

HELICITY INJECTION CONCEPTS FOR CURRENT DRIVE

In order to drive plasma current, it is necessary to inject "helicity" into the plasma (helicity is a quantity closely related to the amount of current in the plasma). Inductive ohmic drive and radio-frequency current drive are the two main methods now employed for helicity injection into tokamak plasmas. However, the former method is inherently *not* steady-state and the efficiency of the latter may not be high enough for reactor application.

Recently, other types of helicity injection have been proposed that are generally called "dc" and "ac" helicity injection. In CDX, the dc helicity injection utilizes a nonrelativisitic electron beam to introduce helicity into the plasma. In the second approach, ac helicity injection, currents in a pusher coil and in an ohmic-heating transformer coil are modulated in proper phase and the resulting steady-state electromotive force drives current in the outer region of the plasma.

For both dc and ac helicity injection, the current is generated near the plasma edge and diffuses into the inner region of the plasma to offset the resistive current decay. This process requires a nonclassical mechanism for current diffusion such as a current-profile-dependent instability. For example, a strong edge current triggers the double-tearing instability only if its direction of flow is parallel to that of the interior current. Magnetic turbulence associated with the instability then facilitates the rapid radial penetration of the edge current. In fact, the strongly asymmetric character of the current penetration condition gives rise to an interesting current-drive concept called "viscous current drive" (VCD).[2] One implementation of this concept calls for repeated pulsing of the primary circuit of the ohmic-heating transformer. Due to the unidirectional nature of the current diffusion, the plasma itself rectifies the transformer-induced alternating current resulting in a net steady-state current.

Experiments for ac helicity injection and "viscous" current drive are scheduled to start in FY87.

DC HELICITY INJECTION EXPERIMENT

Figure 1(b) shows a poloidal cross-sectional view of the dc helicity injection experimental setup: the electron beam is injected into the main plasma region from a LaB_6 (lanthanum-hexaboride) cathode which is located in a diverted region. The injected beam (lightly shaded area) circulates around the main plasma (densely shaded area) while the beam's helicity is being transferred to it.

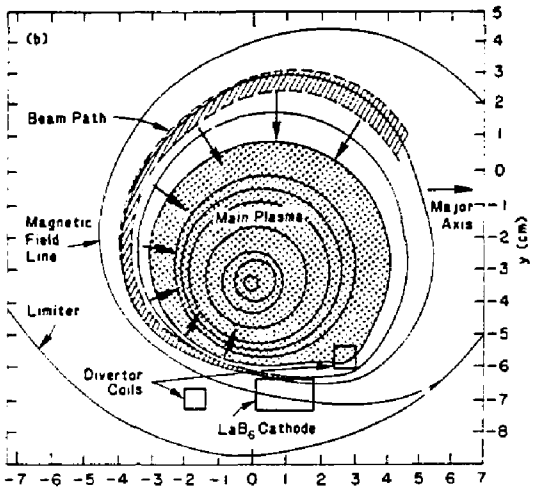

Fig. 1(b). Poloidal view of the dc helicity injection experiment.

In order to model the dc helicity injection experiment, a two-dimensional (2-D) simulation code was developed. In Figs. 2(a)-(c), three representative simulation cases are shown. The first one is a discharge where the current is still low ($B_{beam} << B_{vac}$) so that the vacuum fields (the vertical and divertor fields) determine the electron-beam path. As the injected current is increased, as shown in Fig. 2(b), the self-generated magnetic fields start to affect the beam trajectory. When the plasma current has increased sufficiently so that the self-generated fields dominate the beam trajectory, a considerable change in the magnetic field structure takes place. As can be seen in Fig. 2(c)—it is now in a diverted-tokamak configuration.

For comparison, time-resolved images of the poloidal cross-sectional view of the CDX plasma were obtained with a technique dubbed "boxcar photography" that makes use of an electronically controlled solid-state shutter. Figures 2(d)-(f) show pictures taken for three representative discharges similar to the series shown in Figs. 2(a)-(c), i.e., the first picture is a low current case, the second picture is a medium current case, and the third picture is a high current case.

As in the simulations, one can indeed see the formation and maintenance of a tokamak-like circular discharge. The resulting edge q, the safety factor at the plasma edge, lies between 4 and 10, and it is in the range of safety factors for a tokamak plasma. The ion temperature, measured by Doppler broadening of the He II 4686-Å line, shows a dramatic increase from 1 eV to about 15 eV in the high current discharge. The corresponding line-averaged plasma density increases to the tokamak-like 2×10^{13} cm^{-3} range. A preliminary estimate of the observed dc helicity injection efficiency in the experiment is about 50%. Comparison of the experimental observation with the simulation suggests the presence of a very strong inward current diffusion.

In FY86, many of the CDX diagnostics were completed and introduced into the dc helicity injection experiment. Boxcar photography produced time-resolved images of the plasma, as shown in Fig. 2, and a Fabry-Perot interferometer was employed to measure the helium ion temperature and other spectroscopic line emissions. The CDX data acquisition system was completed and was used to take the density fluctuation data. In addition, the CDX far-infrared laser diagnostic system was assembled and operation was demonstrated in all its modes. In its heterodyne interferometer mode, this laser system showed excellent agreement with the existing 8-mm microwave interferometer, confirming a high-current-discharge density of approximately 2×10^{13} cm^{-3} homodyne mode, density fluctuations were made in both low and high current discharges at wavelengths of a few millimeters up to several tens of centimeters and at frequencies of 5 kHz up to 1 MHz. These fluctuation measurements revealed the presence of coherent, long wavelength waves in the edge region, tentatively identified as drift waves.

In the future, the far-infrared laser system will be applied to a more detailed study of the waves and fluctuations present in the CDX plasmas. Preparations for the two-dimensional scanning probe system, which will map out the magnetic field and plasma potential structure, are now under way.

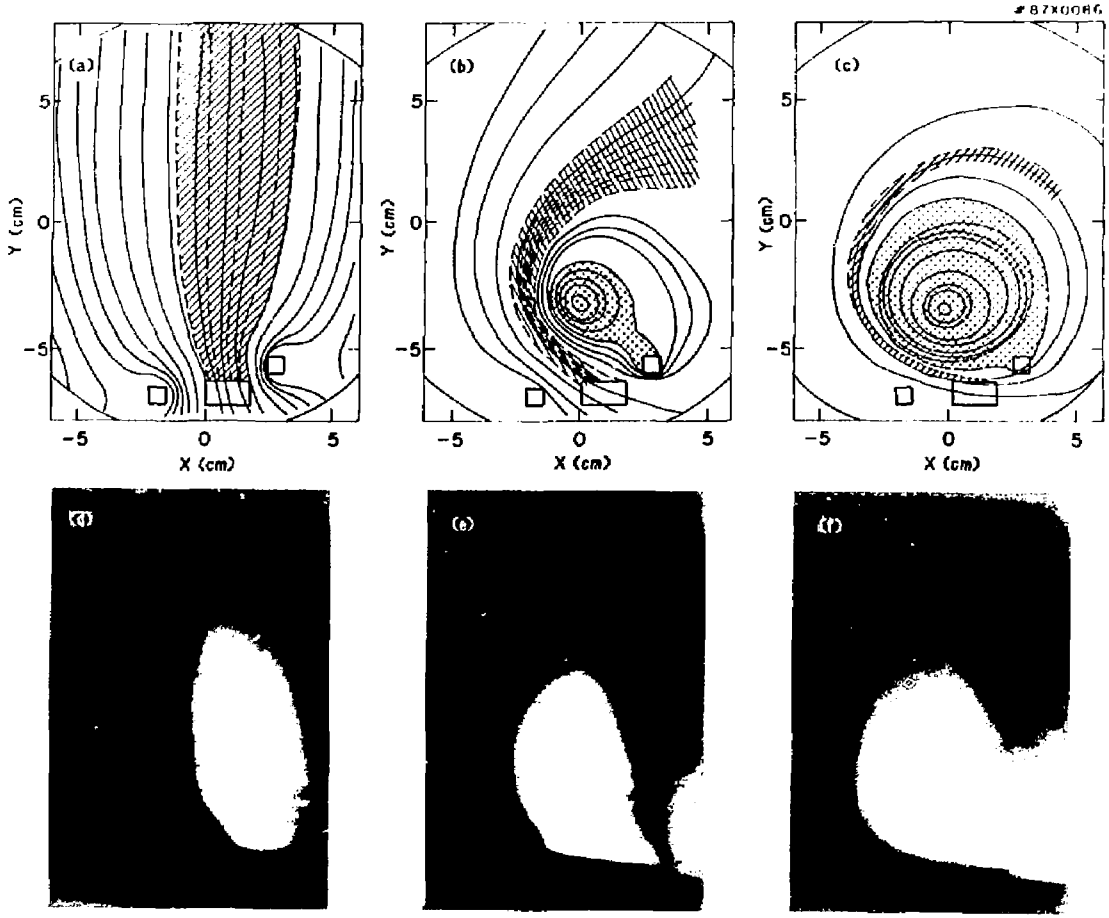

Fig. 2. Poloidal cross sections of plasmas produced by dc helicity injection. (a)-(c) Magnetic field contours computed by a 2-D numerical simulation code. The lightly shaded area shows the electron-beam path and the darker shaded area indicates a region of closed magnetic field lines. (a) Low current case where $B_{beam} << B_{vac}$, (b) medium current case where $B_{beam} \simeq B_{vac}$, and (c) high current case where $B_{beam} >> B_{vac}$. (d)-(f) Poloidal view of the discharge. (d), (e), and (f) correspond to the cases shown in (a), (b), and (c), respectively.

References

[1]*Current Drive Experiment (CDX) Proposal*, submitted for the "Tokamak Improvement Initiative" of the Department of Energy (September 1985).

[2]T.H. Stix and M. Ono, "Viscous Current Drive," Princeton University Plasma Physics Laboratory Report PPPL-2211 (1985) 10 pp; submitted to Phys. Rev. Lett.

[3]M. Ono, G.J. Greene, D. Darrow, H. Park, R. Armstrong, and T.H. Stix, "DC Helicity Injection in the Current Drive Experiment (CDX)," Advanced Current Drive Concepts Workshop, Kyoto, Japan (1986).

X-RAY LASER STUDIES

In FY86, X-Ray Laser Research at the Princeton Plasma Physics Laboratory continued to advance on several fronts. In the recombining approach to X-ray laser development (Experiment 1), significant progress was made resulting in a factor of five increase in stimulated emission at 182 Å in carbon plasmas[1] and in the demonstration of gain in magnesium and aluminum at wavelengths of 187 Å and 154 Å, respectively. In this approach, a CO_2 laser of energy approximately 1 kJ creates a plasma in a magnetic field of up to 90 kG. Radiation losses cause rapid recombination and gain is generated in the soft X-ray region. In previous years' annual reports,[2] stimulated emission from carbon targets at a wavelength of 182 Å at intensities 100 times brighter than spontaneous emission (enhancement $E \approx 100$) was discussed. In FY86, investigation of the divergence of this soft X-ray beam resulted in measurement of an enhancement of $E \approx 500$ with a remarkably low divergence of 5 mrad.[1] The soft X-ray beam intensity was 100 kW with a pulse length of 10-30 nsec. In addition, stimulated emission at 187 Å and 154 Å from magnesium and aluminum targets was observed; this progression to shorter wavelengths is particularly important for applications of X-ray lasers.

Significant progress was also made in an alternative approach (Experiment 2) to X-ray laser development.[3] This two laser approach involves creating a plasma of highly ionized ions with a carbon dioxide (CO_2 or neodymium (Nd) laser and then producing a population inversion and gain by multiphoton excitation with a powerful picosecond laser (PP-laser). The region around 40 Å (the so-called water window) is particularly important for biological applications of X-ray lasers, however, laser action in this region has not so far been achieved due to the tremendous power required from the pump source (the power required scales approximately as the inverse third to fourth power of the wavelength). The present approach to generating gain and laser action at wavelengths below 100 Å has several advantages: first, the task of generating and exciting the lasing medium is split between two lasers; second, the PP-laser offers a convenient way to produce extremely high powers without investing in a large laser facility; and third, the duration of the PP-laser pulse is a good match to the transition rates involved. The construction of this experiment is presently nearing completion, a significant milestone being the achievement of a power output of 2×10^{10} W from the PP-laser system before installation of the final amplifier.

A small-scale supporting experiment (Supporting Experiment), set up to investigate the interaction of CO_2 laser and Xenon Chloride (XeCl) laser pulses on high-Z targets, showed that the combination of two laser pulses has a stronger interaction with the target than the sum of the results from each laser by itself.

Several advances were made in theory and modeling in FY86. The laser/atom interaction at the intensity levels generated by the PP-laser cannot be treated by established perturbative methods since the laser field is comparable to the Coulomb field between the electrons and nucleus. However, an asymptotic analysis was successful in obtaining transition rates, resonance conditions, and resonance widths for a simple two-level system strongly coupled to the laser field. Modeling of a carbon/selenium plasma[4] and radiative cooling studies[5,6] were also completed in FY86.

The success of the soft X-ray laser experiments at Princeton achieved widespread recognition in ten invited talks and a number of conference proceedings.[7-12]

RECOMBINATION APPROACH—EXPERIMENT 1

In this section, the recombination approach (Experiment 1), one of two approaches to X-ray laser development under intensive investigation at Princeton, is discussed. As already reported,[1] this approach has been successful in demonstrating lasing action gains of $G = k \times \ell = 8$ (enhancement $E \approx 500$) at 182 Å. A brief description of the experimental set-up is provided here, for further details the reader is referred to previous annual reports.[2]

A plasma is created in a strong (up to 90 kG) magnetic field by the interaction of a CO_2-laser beam with a carbon, magnesium, or aluminum target assembly. The maximum power density on target is approximately 2×10^{13} W cm^{-2}. A slot in the target disc, offset from the central plasma axis, transmits the stimulated emission which is predominately generated in the low-temperature/high-density off-axis region of the plasma. The enhancement, that is the ratio of stimulated to spontaneous emission, is measured by soft X-ray spectrometers equipped with microchannel plates that observe the emission in the axial and transverse directions. Amplification of

stimulated emission has also been demonstrated by the use of multilayer soft X-ray mirrors.[13]

One of the key parameters characterizing the soft X-ray laser beam is the divergence, and a device for a precise spatial scan of the axial spectrometer across the soft X-ray beam was installed. The axial emissions are normally imaged by a grazing-incidence mirror onto the entrance slit of the axial spectrometer. The mirror is constructed by the bending of a glass strip, and, consequently, the optical quality of the system is not ideal. Hence, a transverse scan of the axial spectrometer gives information of the relative divergence of the lasing-line radiation in comparison to nonlasing lines.

Initial measurements of the divergence of the CVI 182 Å soft X-ray beam relative to nonlasing lines showed an intense peak in the 182 Å beam pattern, whereas the CV 186 Å and OVI 173 Å nonlasing lines remained weak with flat spatial profiles. The optical alignment of the spectrometer is normally established with a helium-neon (He-Ne) laser beam. However, the 182 Å emission peaked at a position 200 μm from that indicated by the He-Ne and used for all earlier measurements. The peak intensity of the 182 Å emission was measured to be approximately a factor of five larger than that presented earlier.[1]

To obtain information about the absolute divergence of the soft X-ray laser beam, the grazing-incidence mirror was removed. Figures 1 and 2 show the results of a shot-by-shot transverse scan of the axial soft X-ray spectrometer. The angular resolution given by the ratio of the spectrometer entrance-slit width to the plasma-to-spectrometer distance was 20 μrad. The principle of the experiment is presented schematically on the right-hand side of Fig. 1, and on the left-hand side is shown the intensity distribution of the CVI 182 Å (3→2), CV 186 Å (4d→2p), and OVI 173 Å(3d→2p) lines for a magnetic field B = 20 kG. For every shot, the intensities of all three lines were recorded simultaneously on the multichannel detector of the axial soft X-ray spectrometer. It is shown that the lasing line CVI 182 Å is strongly peaked on axis with FWHM ≈ 2.7 cm at a distance of 304 cm from the plasma (target), which corresponds to a horizontal divergence of the beam of approximately 9 mrad. At the same time, the intensities of the nonlasing lines OVI 173 Å and CV 186 Å are quite constant over the 3-cm scan region.

With increasing magnetic field (B = 35 and 50 kG), further narrowing of the soft X-ray laser beam down to approximately 5 mrad (Fig. 2) is observed. This indicates that with higher magnetic field maximum gain is created in a more narrow plasma region (less than 50 μm transversely). Also observed is a slight shift of the peak intensity of the 182-Å radiation at higher magnetic field, which may be caused by a small tilt of the magnet at high currents. In order to decrease the effect of shot-to-shot line-intensity fluctuations, the 182-Å radiation was normalized to the OVI 173-Å line intensity in Fig. 2 (the 173-Å line intensity was quite uniform across the scan as was shown in Fig. 1). Knowledge of the divergence allowed the

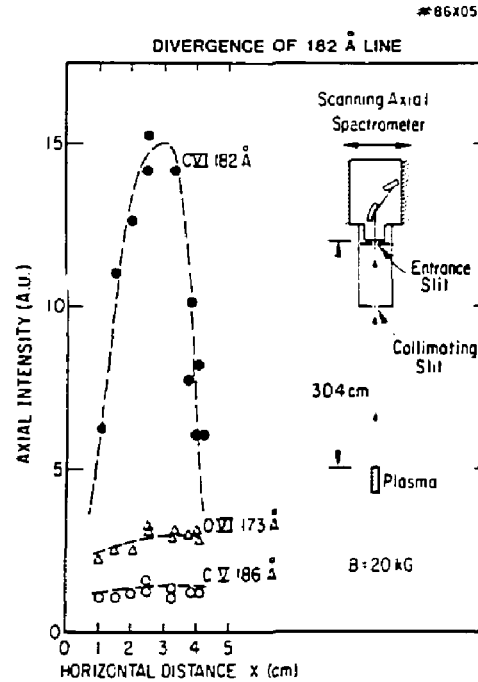

Fig. 1. Absolute divergence measurements (approximately 9 mrad) of the 182 Å lasing radiation for a magnetic field B = 20 kG. The intensities of nonlasing lines OVI 173 Å and CV 186 Å, recorded simultaneously with the 182 Å line, are shown for comparison.

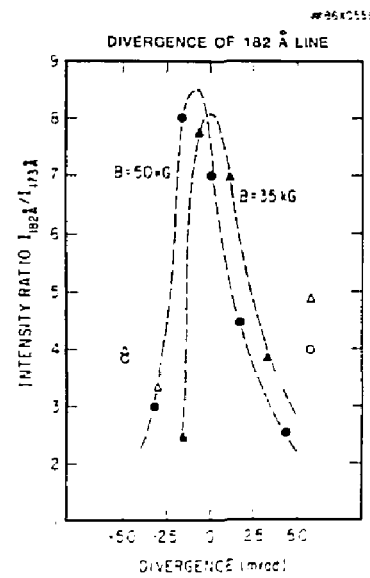

Fig. 2. Divergence measurements (approximately 5 mrad) of the 182 Å radiation (relative to the OVI 173 Å line) for B 35 and 50 kG.

estimation of the total power of the soft X-ray beam, approximately 100 kW, from measurements (using absolute-intensity-calibrated spectrometers) of the total intensity of the 182-Å radiation (4×10^8 W sr^{-1}) and pulse duration (≈10-30 nsec). This corresponds to a pulse energy of 1-3 mJ.

Magnesium and aluminum target assemblies were investigated, and stimulated emission was observed in lithium-like MgX at 187 Å and AlXI at 154 Å. The AlXI result at 154 Å is significant as a step toward the wavelength region below 100 Å, important in application of X-ray lasers. Since the plasma electron density is limited to approximately 10^{19} cm^{-3} by the wavelength of the CO_2 laser, the ion density of AlXI in such a plasma is necessarily lower than that of CVI, and, hence, it is more difficult to achieve high gain.

Figure 3 shows a typical target assembly used in these experiments. A plasma column is created by the CO_2 laser focused onto an aluminum disc. A composite blade, made from aluminum and stainless steel, is attached normal to the target surface to improve the laser/target interaction, the stainless steel providing additional radiation cooling. An off-axis vertical slot in the target disc transmits the stimulated and spontaneous emission to the axial spectrometer, while the spontaneous emission is recorded by the transverse spectrometer.

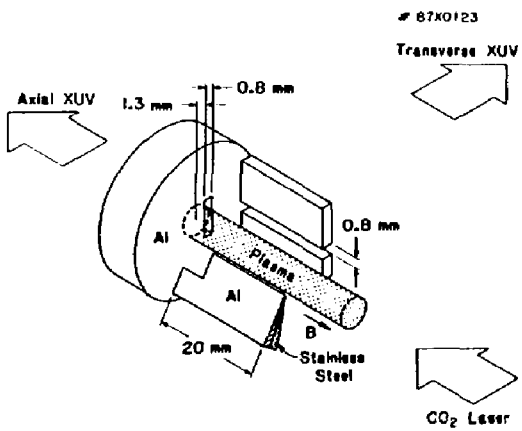

Fig. 3. An aluminum disc target with a 0.8 mm × 4 mm vertical slot and with an aluminum/stainless steel composite blade attached normal to the target surface.

Typical spectra obtained are shown in Fig. 4. The AlXI 154-Å (4f→3d) and 150-Å (4d→3p) lines in the on-axis spectrum are intense compared to the AlXI 141-Å (4p→3s) and OVI 150-Å lines. The latter two do not exhibit gain, and their isotropic spontaneous emission intensities are used as a relative intensity calibration in order to measure gain. The ratio of the AlXI 154-Å line to AlXI 141-Å line intensity is three times higher in the on-axis spectrum, Fig. 4(a), than in the off-axis spectrum recorded with the same instrument, Fig. 4(b). Further off-axis (Fig. 5) the ratio is higher with a corresponding on-axis gain, G ≈ 3. The AlXI 154-Å line in the transverse spectrum, Fig. 4(c), is blended with FeVII lines, however, the AlXI 52.46 Å doublet is seen in third order with the components in a 2:1 intensity ratio, indicating that the plasma is optically thin. This is important as it permits the AlXI 52.46-Å transition to efficiently depopulate the 3p level and generate a population inversion. Future plans include work with higher-Z elements, e.g., silicon, with potential lasing transitions at shorter wavelengths.

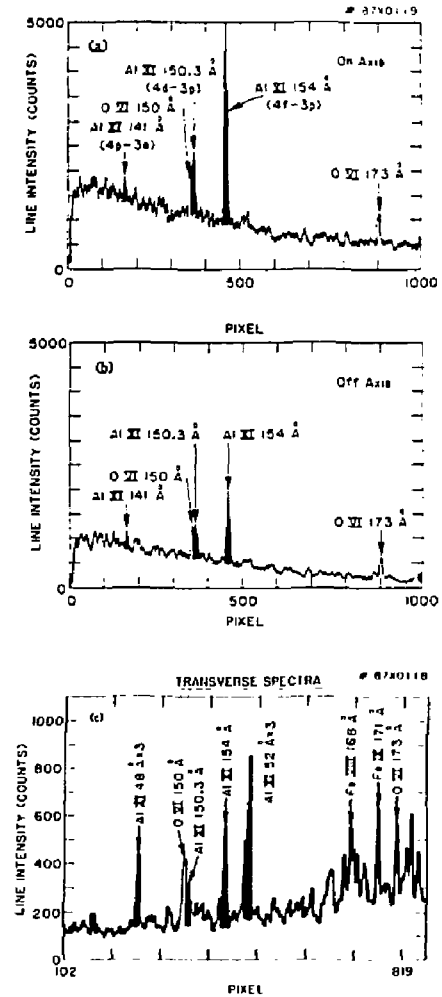

Fig. 4. Emission from the aluminum target assembly. Figure 4(a) and (b) show the axial emission recorded with the grazing-incidence mirror installed. Figure 4(a) is the on-axis emission and shows strong stimulated emission on the AlXI 154 Å line. In Figure 4(b), the axial instrument was moved transversely 200 μm to record the off-axis emission. Figure 4(c) shows the transverse emission spectrum for comparison.

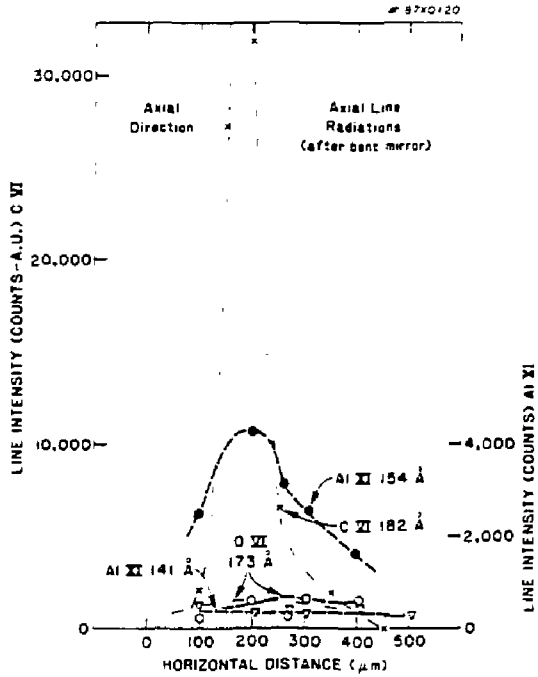

Fig. 5. Relative divergence of the AlXI 154 Å stimulated emission recorded with the grazing-incidence mirror installed. The spectral line intensities of the AlXI 154 Å, 141 Å and OVI 173 Å lines are shown as a function of the transverse position of the axial spectrometer. For comparison, the previous relative divergence measurements of the CVI 182 Å stimulated emission compared to the OVI 173 Å emission is shown (light dots).

APPROACH TO X-RAY LASING USING MULTIPHOTON PROCESSES—EXPERIMENT 2

The two-laser approach to X-ray development (Experiment 2) is primarily designed to provide X-ray lasing action at wavelengths below 100 Å.[3] The energy and, in particular, power requirements of the pump laser rapidly increase as the wavelength of the X-ray laser decreases. The two-laser approach separates these aspects and, among other things, keeps the system on a small laboratory-scale size. As with the recombination method, a high energy laser pulse is used to produce the lasing medium (a highly ionized, high-Z plasma), which is confined by a strong magnetic field. A second laser, the powerful picosecond laser (PP-laser), is then used to provide the high power level required to populate excited states through multiphoton processes. The experiment consists of a number of subsystems including the PP-laser, the magnet and its support structure, the vacuum and target systems, and the diagnostics and data acquisition systems.

In the past year, an intensive effort was directed toward the development of the PP-laser system.[4] With the completion of the final stage, it will be capable of delivering a 1-J, 1-psec, 248-nm laser pulse corresponding to terawatt power levels and focused power densities in excess of 10^{18} W per cm^2. The layout of the PP-laser system is shown in Fig. 6.

The master oscillator in the system is a cavity dumped, tunable dye laser. This unit (both actively and passively mode locked) produces approximately 1-psec pulses with energy levels of approximately 10 nJ. The dye oscillator is pumped with the frequency-doubled output of a mode-locked YAG laser. The output of the dye laser oscillator is then amplified by a three-stage dye amplifier in order to provide enough power to efficiently shift the wavelength into the ultraviolet. This amplifier is pumped with amplified-YAG pulses, which originate from the same source as those used to pump the dye oscillator. This synchronous pumping procedure relaxes the timing requirements of the system. The output pulse energy from the dye amplifier is approximately 100 μJ. The amplified 648-nm pulses are frequency doubled and then mixed with 1060-nm YAG pulses to produce pulses with a wavelength of 248 nm. Three KrF* amplifiers are then used to amplify this ultraviolet pulse.

In CY86, the first stage of the PP-laser fabrication was completed. The autocorrelation trace (Fig. 7) of the output pulse from the oscillator has a width of approximately 1.3 psec, which corresponds to an actual pulse width of $\lesssim 1$ psec. An output energy of approximately 25 mJ was extracted from the KrF* amplifiers. The output power at this stage is, then, P ~ 25 GW (assuming no temporal broadening through the conversion and amplification processes). The system can be operated at a repetition rate of 10 Hz. Work is presently directed toward obtaining a detailed characterization of the output beam and performing some initial experiments with laser-produced plasmas.

The final stage of fabrication of the PP-laser system consists of the construction of a large (5 × 10 cm) cross section, one meter long, KrF* amplifier. This unit, being built at PPPL in cooperation with the University of Maryland, will bring the power of laser pulse into the terawatt regime, comparable with the power of the largest laser facilities. Fabrication of this final amplifier is expected to be completed in a few months, and the power supplies and gas handling system are presently being constructed.

Much effort was also directed to the construction of the experimental chamber for Experiment 2. Construction of the magnet, the support assembly, the capacitor bank, and the high-voltage cabling was completed. Work is now progressing on the control logic, and the entire magnet system should be ready for initial testing in early CY87. Major elements of the vacuum system are now in place. The extreme ultraviolet spectrometers which are the primary diagnostics of the system are presently being prepared, and a software package to control the system is being developed. Initial results from Experiment 2 are expected in the summer of 1987.

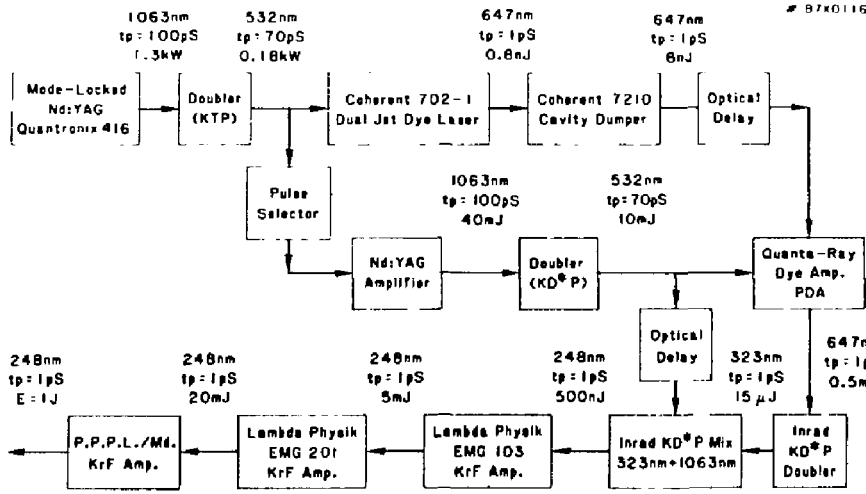

Fig. 6. Layout of the powerful picosecond laser (PP-Laser).

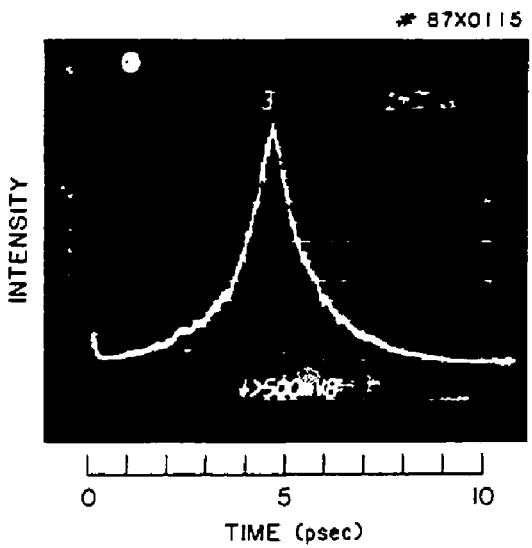

Fig. 7. Autocorrelation trace of the dye oscillator output showing a pulse duration of $\tau \approx 1$ psec (FWHM).

THEORY AND NUMERICAL MODELING

Theoretical investigation of multiphoton processes, those in which many quanta are simultaneously absorbed or emitted during a transition, have initially centered on the simplest possible model: one with two quantum levels coupled by an imposed periodic electromagnetic field. In this model, the multiphoton nature of the interaction is evidenced by the requirement that the resonant excitation condition $n\hbar\nu \approx E_2 - E_1$, which relates the energy difference between the levels $E_2 - E_1$ to the absorbed photon energy $n\hbar\nu$, is satisfied for only a large (integral) number of n photons each of energy $h\nu$. The analysis of the model is based on an asymptotic procedure that relies on large (integer) n and that becomes increasingly accurate as n increases. Results are obtained for transition rates and nonlinear shifts in the excitation energy as functions of electromagnetic field intensity and frequency. In the weak external field limit, the results of perturbative analyses are recovered. There the transition rate between states, and the resonance width, are both proportional to the n^{th} power of the external field intensity while the shift in resonance condition varies linearly with intensity:

$$n\hbar\nu \approx E_2 - E_1 + [2\pi D^2F^2/h(E_2 - E_1)].$$

Here D is the transition dipole moment and F is the electromagnetic field in cgs (centimeter gram second) units. For the case of large fields [$DF \gg \pi(E_2 - E_1)/h$] we have:

$$n\hbar\nu \approx 4DF/\pi.$$

The model has been applied to ions with allowed transitions in the 100-Å spectral region and suggests that if the external field intensity is maintained at a value sufficiently high to achieve resonant excitation rates comparable to the spontaneous radiative decay rates, then nonlinear frequency shifts will become a significant fraction of the unperturbed frequency separation. For a high-order multiphoton process, this means that the resonant harmonic number n will change substantially during the laser pulse. The

narrowness of these high-order resonances and their relatively strong dependence on intensity suggest that experimental observation of any single high-order resonance may be difficult in short-pulse experiments. Efforts are under way to extend the analysis to more complicated systems.

Fiscal year 1986 also saw the publication of computational modeling studies of a carbon/selenium plasma[4] and work on radiative cooling.[5,6]

SUPPORTING EXPERIMENTAL STUDIES

During FY86, the Supporting Experiment was directed to the preparation of instruments, obtaining spectroscopic data necessary for Experiments 1 and 2, and investigations into plasmas generated by the use of two lasers. The preparation of the instruments included the installation and the calibration of the multichannel extreme ultraviolet (XUV) spectrometer and the development of computer software for data acquisition and analysis. Soft X-ray spectra of some high-Z elements (Ag, Mo, Zn, Pd, Cd) was obtained by focusing a 10-J CO_2-laser beam on a target installed inside a vacuum chamber. A XeCl laser (energy 1 J) was used together with the CO_2 laser to investigate the interaction of two lasers with carbon targets. These lasers were fired simultaneously or in sequence with short-time intervals of approximately 50 nsec between pulses. The spectra obtained were compared with those produced by firing each laser separately. The XeCl laser beam could be focused to a much smaller spot, and it produced a much denser plasma than the CO_2 laser. With flat targets, it was observed that the dense plasmas produced by the XeCl laser showed evidence of self-absorption in the soft X-ray emission lines, however, by using blade targets of thickness 300 μm, this absorption was significantly reduced. The emission produced by the combination of the two lasers on the target was significantly more intense than sum of emission produced by each laser separately, and a quantitative study of this effect is planned when a more precise triggering system for the lasers becomes available. Future plans also include using a multichannel detector to obtain line profiles in the air wavelength region to further investigate self-absorption effects.

In FY86, several components of the large-scale CO_2 laser HELIOS were transferred to PPPL from the Los Alamos National Laboratory, and the master oscillator and preamplifier systems are currently being adapted for use in the soft X-ray laser experiment. The original Lumonics CO_2 laser at PPPL generates a gain switched pulse with an approximately 50 nsec fall time, which is nonideal for producing a strongly recombining plasma. The HELIOS system on the other hand was designed to generate a pulse $\leq$1 nsec, too short for our application. A plasma shutter device was installed on the HELIOS master oscillator which then generated the required 10-20 nsec pulses with an approximate 1-nsec fall time. these pulses were then amplified to 500 J with the Lumonics laser units, however, the extremely high gain in the combined system caused self-oscillation which was difficult to control. A system of saturable absorber cells is presently being installed to overcome this problem.

The extensive spectroscopic data available from the well-diagnosed Princeton Large Torus (PLT) stimulated studies of line intensities and wavelengths relevant to the X-ray laser experiment. In the vacuum ultraviolet (VUV) and extreme ultraviolet (XUV) regions, many spectra were taken under various discharge conditions with a normal-incidence McPherson spectrometer and grazing-incidence spectrometer "SOXMOS,"[15] both equipped with *multichannel detectors. These will be used in studies* of excitation rates, recombination radiation, charge-exchange with neutrals, and phenomena populating doubly excited states. These observations at relatively low density complement laser-produced plasma studies at higher densities. The PLT tokamak has become a unique spectroscopic source for the study of highly ionized, medium- to high-Z elements which are of fundamental importance to X-ray laser schemes.

GRADUATE STUDIES

The X-ray laser program continues to provide an experimental environment that is well suited to graduate education. In FY86, Christopher Keane completed his doctorate[16] and accepted a position in the X-ray laser group at the Lawrence Livermore National Laboratory. Chang Hee Nam made significant contributions to the PP-laser system. Dong Eon Kim was engaged in Experiment 1, including computational modeling of the results. Young Joo Chung was involved with the supporting two-laser experiment, in preparation for Experiment 2. Kevin Ilcisin joined the group in FY86 and began work on an imaging system for laser-beam diagnostics.

References

[1]S. Suckewer, C.H. Skinner, D. Kim, D. Voorhees, and A. Wouters, "Divergence Measurements of Soft-X-Ray Beam," Phys. Rev. Lett. 57 (1986) 1004.

[2]Princeton University Plasma Physics Laboratory Annual Report PPPL-Q-42 (October 1, 1984 to September 30, 1984) 58; Princeton University Plasma Physics Annual Report *PPPL-Q-43* (October 1, 1984 to September 30, 1985) 61.

[3]C.W. Clark, M.G. Littman, R. Miles, T.J. McIlrath, C.H. Skinner, S. Suckewer, and E. Valeo, "Possibilities for Achieving X-Ray Lasing Action by use of High-Order Multiphoton Processes," J. Opt. Soc. Am. B 3 (1986) 371.

[4]C.H. Nam, E. Valeo, S. Suckewer, and U. Feldman, "Radiation Cooling and Gain Calculation for CVI 182 Å Line in C/Se Plasma," J. Opt. Soc. Am. B 3 (1986) 1199.

[5]C. Keane and C.H. Skinner, "Radiative Power and Electron Cooling Rates for Oxygen in Steady State and Transient Plasmas at Densities Beyond the Coronal Limit," Phys. Rev. A 33 (1986) 4179

[6]C.H. Skinner and C. Keane, "Model for Electron Cooling by Radiation Losses in Plasmas: Application to Development of X-Ray Lasers," Appl. Phys. Lett. *48* (1986) 1334.

[7]S. Suckewer, C.H. Skinner, D. Kim, E. Valeo, D. Voorhees, and A. Wouters, "Recent Progress in Soft X-Ray Laser Development at Princeton," invited talk in proceedings of the *Optical Society of America Conference Meeting on Short Wavelength Coherent Radiation: Generation and Applications* (AIP Conf. Proc., New York, 1986) *147*, 123.

[8]S. Suckewer, C.H. Skinner, C. Keane, D. Kim, J.L. Schwob, E. Valeo, D. Voorhees, and A. Wouters, "Stimulated Soft X-Ray Emission in a Confined Plasma Column," invited talk in proceedings of the *First International Laser Science Conference Advances in Laser Science-1* (AIP Conf. Proc., New York, 1986) *146*, 81.

[9]S. Suckewer, C.H. Skinner, C. Keane, D. Kim, J.L. Schwob, E. Valeo, D. Voorhees, and A. Wouters, "Stimulated Soft X-Ray Emission in a Confined Plasma Column," invited talk in proceedings of the *International Conference on Lasers '85* (STP Press, McLean, Va., 1986) 15.

[10]S. Suckewer, C.H. Skinner, D. Kim, E. Valeo, D. Voorhees, and A. Wouters, "Recent Progress in Soft X-Ray Laser Development at Princeton," invited talk in proceedings of the *International Colloquium on X-Ray Lasers* (Journal de Physique; Colloque C6, Supplement au No. 10, Tome *47*, Octobre 1986) C6-23.

[11]C.H. Skinner, C. Keane, H. Milchberg, and S. Suckewer, "Measurements of Population Inversion and Gain in Carbon Fiber Plasmas; Theoretical Calculations of Radiation Cooling," in proceedings of the *International Colloquium on X-Ray Lasers* (Journal de Physique; Colloque C6, Supplement au No. 10, Tome *47*, Octobre 1986) C6-239.

[12]C.H. Skinner, "Recent Progress in Soft X-Ray Laser Development at Princeton," invited talk in proceedings of the *8th International Conference on Spectral Line Shapes* (de Gruyter, Berlin-New York, 1987).

[13]C. Keane, C.H. Nam, L. Meixler, H. Milchberg, C.H. Skinner, S. Suckewer, and D. Voorhees, "Measurement of Multilayer Mirror Reflectivity and Stimulated Emission in the XUV Spectral Region," Rev. Sci. Instrum. *57* (1986) 1296.

[14]W. Tighe, "Soft X-ray Lasers: Present and Future Plans at Princeton," invited talk in proceedings of the *International Conference on Lasers '86* (STP Press, McLean, Va., 1987).

[15]J.L. Schwob, A. Wouters, and S. Suckewer, "High-Resolution Duo-Multichannel Soft X-Ray Spectrometer for Tokamak Plasma Diagnostics," Princeton University Plasma Physics Laboratory Report PPPL-2419 (1987) 58 pp; to be published in Rev. Sci. Instrum.

[16]C. Keane, "Studies of Population Inversions in the Soft X-ray Spectral Region in Laser Produced Plasmas," Ph.D. Thesis, Princeton University, 1986.

THEORETICAL DIVISION

The main activities of the theory group are (1) the investigation of instabilities in a magnetically confined static plasma and the effect on its confinement and equilibrium, and (2) the elucidation of the equilibrium, heating, and classical transport in stable plasmas based on presently understood physics. In addition, some effort is devoted to general plasma physics problems and to other areas of plasma physics, such as space physics and astrophysics, that share common techniques with fusion plasma physics. The investigations are carried out by primarily numerical techniques, but some analytical approaches are also of value. The goal is to develop sufficient understanding of plasma behavior observed in present-day tokamaks so that ways can be found to improve the confinement properties of these plasmas and to alleviate the more serious threats to fusion, such as disruption. For this reason there is close cooperation between theorists and experimentalists.

A significant accomplishment of the theoretical group during the past year was the successful numerical simulation of the Compact Ignition Tokamak (CIT) plasma evolution. It was shown that the magnetic-field design can be chosen in such a way so as to achieve ignition. This simulation depends on a particular choice for transport rates. Such transport rates are provided by a plausible nonlinear theory which is able to show under the assumption of profile consistency that the transport can be produced by the electron trapped-particle mode. This agrees with present measurements and gives a theoretical basis for the empirically accepted rates. On this basis, reliable extrapolation to the CIT plasma regime is possible. The stability of the CIT plasma has not yet been calculated.

Important new results on various plasma instabilities also emerged. It was demonstrated that a plasma can be stable to the kink and tearing modes with q on axis as low as 0.6, provided the correct current profile is chosen. Further, it was shown that sufficient heating of the island in an internal kink can lead to a nonlinear saturation of the internal disruption that slows down its evolution. New results on ballooning modes also appeared. For example, it was found that for low-shear systems the worst ballooning modes occur for finite toroidal mode numbers n rather than infinite ones, as has been generally assumed. These low-n modes have been designated as "infernal" modes. Another correction to ballooning mode theories was the realization that in the second stability region the maximum amplitude for the ballooning mode does not occur on the tokamak equator but rather, because of large local shear on the equator, it is shifted off the equator by a large poloidal angle. This raises the beta at which second stability is achieved to values greater than what was previously accepted as the lower limit for second stability.

Another important result uncovered this past year was that for certain assumptions about transport the CIT plasma may be susceptible to fishbone oscillations which could expel as much as a quarter of the alpha particles. This result could have an important bearing on the chance of ignition in the CIT.

Because of the importance of the various anomalous transport mechanisms for the future of the fusion program, it is important to provide more reliable estimates for the nonlinear behavior of the responsible modes. These estimates can best be supplied by the gyrokinetic particle simulation code. Originally it was felt that these calculations might be too expensive because of the large number of particles required. However, it has been shown that when the code is made electromagnetic, smaller noise is produced then for the same number of particles in the electrostatic case. This opens the possibility for the achievement of rather high accuracy transport rates from this code.

MODELING OF THE CIT AND ANOMALOUS TRANSPORT

The PPPL Theoretical Division is coordinating the national effort in the magnetic design and MHD analysis of the proposed Compact Ignition Tokamak (CIT). Shown in Fig. 1 are the poloidal magnetic flux surfaces at selected times during the 12-sec period corresponding to a single CIT shot. These were generated by the PPPL Tokamak Simulation Code (TSC),[1] which models the continuous evolution of the axisymmetric magnetics and plasma profiles during the current ramp-up, flattop, and current ramp-down phases.

Plasma equilibrium generated by TSC for CIT are passed to the PEST code, where they are analyzed for nonaxisymmetric stability. The TSC code is also used for axisymmetric stability and shape control studies. To study the effects of a plasma disruption, the standard evolution computed by TSC can be modified to include a disruptive event by causing a sudden decrease in the plasma beta (thermal quench). The TSC then models the response of the plasma (current quench) and calculates the induced currents

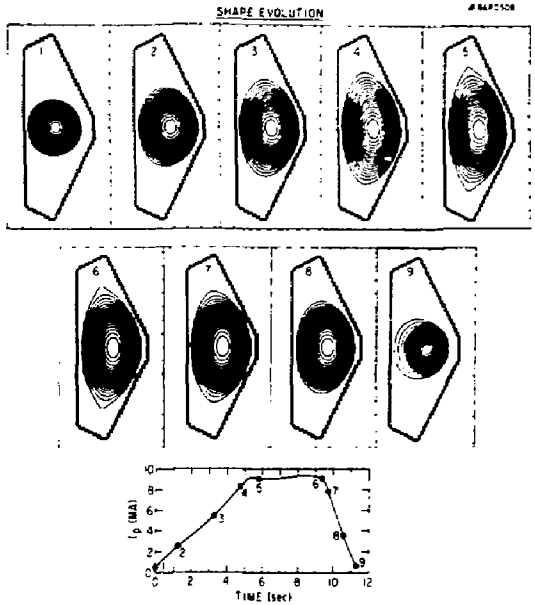

Fig. 1. The TSC simulation of CIT start-up showing current ramp-up (1-4), flattop (5-6), and current ramp-down (7-9).

and forces in the vacuum vessel and other conducting structures. These codes are being verified by performing many comparisons of similar evolutions of the Princeton Beta Experiment (PBX), Tokamak Fusion Test Reactor (TFTR), and D-III-DEE tokamak plasmas with those observed evolutions.

Identification of the primary physical processes responsible for the anomalous thermal transport properties currently observed in tokamak plasmas is vitally important, not only for the development of methods to improve performance in existing devices but also for the proper planning of future ignition experiments such as CIT. Recent work has demonstrated that if realistic profile constraints are invoked, then most of the significant confinement trends in present-day tokamaks can be explained by electrostatic transport due to drift-type microinstabilities (trapped-electron modes and toroidal ion temperature gradient modes). Theoretical transport models (for the electron and ion thermal diffusivities) based on the associated physics have yielded predictions in very favorable agreement with respect to both the scaling and the magnitude of the energy confinement time (τ_E) and the central electron temperature (T_{eo}).[3,3] These profile-constrained microinstability models have been used in the BALDUR transport code for the purpose of interpreting experimental results from TFTR, including ohmic heating, neutral-beam heating (NBI), and pellet fueling. Results from the simulation of nearly two dozen TFTR plasmas covering a wide range of experimental conditions yielded excellent agreement. These results are illustrated for an ohmic plasma in Fig. 2 and for NBI-heated plasmas in Table I. The last entry of Table I represents a typical "supershot" case.

The agreement of these anomalous transport studies with confinement show that[4] they can be used to extend the consequences of drift-type instabilities to future ignition devices such as CIT. Under steady-state conditions, the simplest form of the basic homogeneous (zero-dimensional) thermal energy balance equation is given by

$$P_h = P_{Le} + P_{Li} + P_R - P_\alpha,$$

where P_h is the external heating power density, P_{Le} and P_{Li} represent the losses due to electron and ion thermal conductivity, respectively, P_R represents radiation losses, and P_α is the α-particle heating term. In earlier calculations[5] it was shown that the familiar Murakami density limit represents a balance between radiation losses (P_R) and ohmic-heating input power (P_h). However, since the fusion power (P_α) will offset P_R at temperatures characteristic of ignition conditions ($T_o > 6$ keV), this limit should not be relevant. Instead, attention needs to be focused on the influence of enhanced forms of P_{Le} and P_{Li} caused by the presence of microinstabilities. Relatively simple estimates of P_{Le} and P_{Li} indicate that in order to achieve an optimal ignition margin, in light of the adverse temperature scaling of anomalous losses, it is best to operate the CIT at the maximum allowable density while holding the temperature close to the minimum value required for ignition.[6]

Although the primary loss mechanism is probably microinstabilities, these are forced to operate on a temperature profile determined by MHD instabilities, "profile consistency." The extent to which this is true was investigated.[7]

The total range of MHD-stable j(r) profiles in a pressureless straight cylinder of length $2\pi R$ subject

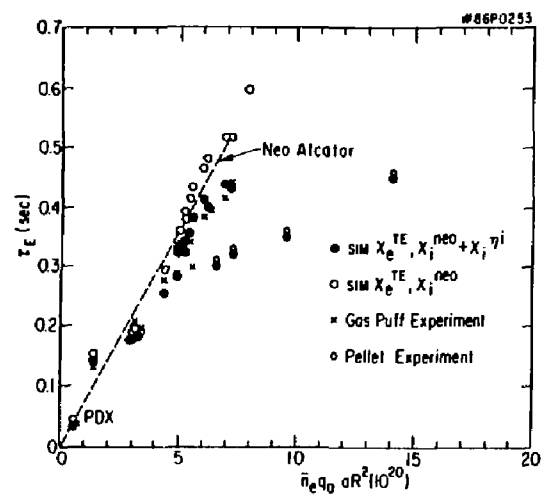

Fig. 2. Comparison of simulated and experimental electron confinement times for ohmic-heating discharges.

Table I. Parameters of Simulated Neutral-Beam-Heated TFTR Shots.

Shot (MA)	I_p (T)	B_Z (m)	R (m)	A	$\bar{n}_e$ ($10^{19}m^3$)	P_{inj} (MW)	Z_{eff}	q_a	T_e^{exp} (keV)	T_e^{Sim}	τ_E^{exp} (sec)	τ_E^{Sim}	ℓ_{ie}(q 1.5)
14727	2.2	4.8	2.56	0.82	4.8	5.3	2.6	2.8	4.0	3.6	0.20	0.18	0.19
14773	2.2	4.7	2.57	0.82	3.0(7.0[a])	5.7	1.9	2.8	2.4	2.8	0.14	0.19	0.29
19965	2.2	4.8	2.49	0.83	4.2	6.8	3.2	3.0	3.8	3.7	0.11	0.11	0.25
22014	0.8	4.6	2.55	0.82	3.2	11.3	2.5	7.6	5.8	6.2[b]	0.12	0.14[b]	0.13

[a]After pellet injection.

[b]Collisionless model.

to the constraints that $j(r) \geq 0$ and $dj/dr \leq 0$ where j is the axial current density was determined. For q(0) > 1, stable profiles can be obtained only when q(a) > 2, where q(0) and q(a) are the safety factors on axis and at the plasma edge, respectively. For 0.5 < q(0) < 1, j(r) profiles can be found that are unstable only to m = n = 1 modes.[7] To indicate the degree of latitude of the j(r) profiles, the boundaries for permissible ℓ_i and $\langle T_e(r)\rangle/T_e(0)$ were determined as functions of q(a) for q(0) = 1.01, where ℓ_i is the internal induction of the plasma and $\langle T_e(r)\rangle$ is the volume-averaged temperature. A value of ℓ_i or $\langle T_e(r)\rangle/T_e(0)$ is considered permissible if some stable j(r) profile exists that corresponds to it. No values outside the permissible region should be observed in experiments since, within the accuracy of the assumptions, any j(r) profile corresponding to such a point should be unstable. The $\langle T_e(r)\rangle/T_e(0)$ is found from the j(r) profile and the relation $j(r) \sim T_e^{3/2}(r)$, which is valid in steady-state if neoclassical corrections are ignored.

Figure 3 is the permissible region for $\ell_i/2$ as a function of q(a) for q(0) = 1.01. The lower boundary has a jigsaw shape. This boundary corresponds to broader j(r) profiles, and its shape is determined mainly by ideal external kink modes. The upper boundary corresponds to narrower j(r) profiles, and it is determined by low-order resistive kinks, mainly m/n = 2/1 and 3/2. If a conducting wall is introduced in the stability calculation, the lower boundary is relaxed but the upper boundary is only slightly affected. Data from nondisrupted TFTR discharges are found to give points that fall inside the permissible region only. However, for disrupted discharges the points move into the upper unstable region as the plasma disrupts. Two time traces of disrupting discharges are shown in Fig. 3. The open circles represent the beginning and the solid circles the end of the discharges. A similar plot for $\langle T_e(r)\rangle/T(0)$ is given in Fig. 4.

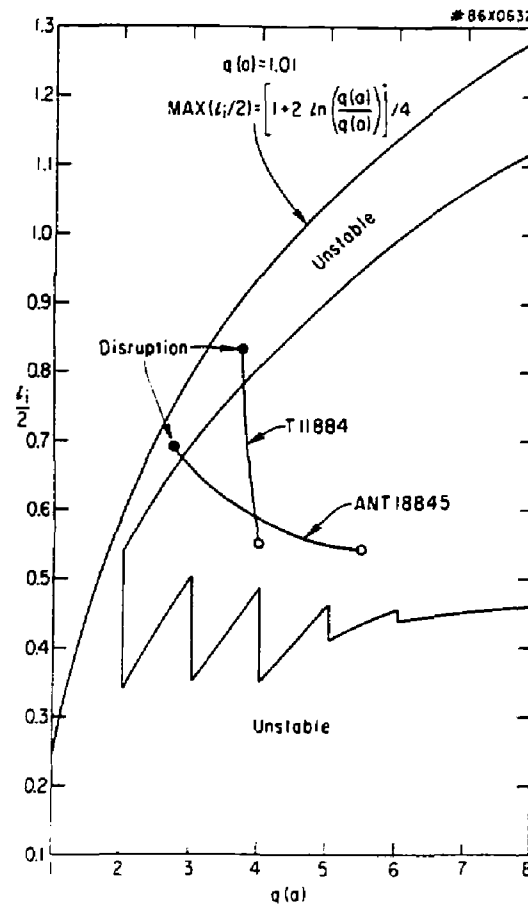

Fig. 3. Permissible region for stable operation in ℓ_i, q(a) space.

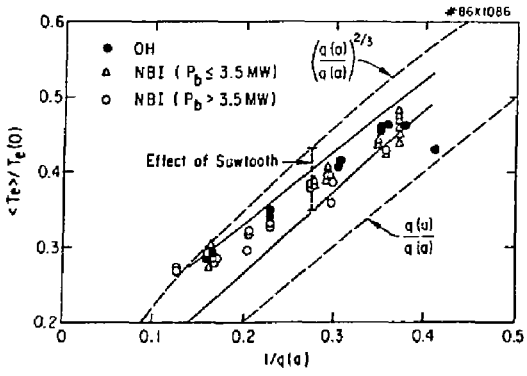

Fig. 4. The permissible region for stable operation in $\langle T_e \rangle / T_e(0)$, $1/q(a)$ space is bounded by the solid curves.

The proper determination of stable $j(r)$ profiles is important. First it gives better estimates for temperature profiles employed under the "profiles consistency" hypothesis employed in the study of anomalous transport by microinstabilities. Second, it demonstrates quantitatively the extent to which the discharge is controlled by MHD instabilities of the kink and tearing type.

KINK AND TEARING INSTABILITIES

An essential feature of tokamak operations is the appearance of sawtooth oscillations during most plasma discharges. The general understanding of these oscillations involves the resistive m=1, n=1 instability (the 1/1 mode). Theoretical analysis of this instability, based on a cylindrical model, shows it to be always unstable when the q = 1 surface is present anywhere in the plasma. However, recent measurements of the q profile in the TEXTOR tokamak show sawtooth-free operations even when the q = 1 surface is present in the plasma. These experiments[8] are among the first to accurately measure the safety-factor profile in a hot tokamak plasma and to show that the q on axis can be as low as 0.6. This contradiction with previous results was resolved with the aid of the recently revived resistive version of the PEST code (PEST-3), which solves for Δ' using an extended form of the marginal Euler-Lagrange equations in full toroidal geometry. Analysis with the PEST-3 code indicates that toroidal effects coupled with a flattening of the q profile in the vicinity of the q = 1 surface can effectively stabilize the 1/1 mode. The code was next used to analyze the low-q sawtooth-free profile measured by the TEXTOR group. This best-determined profile was found to be slightly unstable, but a very small change in this q profile produced stability to all the resistive as well as ideal instabilities. The modified profile lies well within the experimental error. The two profiles are shown in Fig. 5. These results were reported at the 1986 International Atomic Energy Agency (IAEA) Conference in Kyoto, Japan.[9] Further studies to understand the details of the stabilization of the 1/1 mode are under way. It is not yet understood why this stable profile is not more generally seen.

Investigations with the nonlinear compressible MHD code MH2D, has led to the discovery of a method to stabilize sawtooth oscillations.[10] The basic nonlinear stabilizing effect is related to increased pressure of the island formed in the instability. When the pressure inside the magnetic island is higher than that in the original core plasma, a saturated nonlinear equilibrium state as shown in Fig. 6 is obtained. This increase can be produced by local heating by radio-frequency (rf) heating. The saturation condition is of the form

$$\Delta\beta_p \geq 8\epsilon^{-1}(\Delta q)^2,$$

where $\Delta\beta_p$ measures the excess island pressure and $\Delta q = 1 - q_0$ the degree of the required stabilization. This saturation effect can be used to actively stabilize sawteeth by heating or raising the density in the island. In the proposed scheme the saturation condition must be satisfied continuously. This is not difficult because $\Delta\beta_p$ only need be increased as Δq increases, and the increase is on a slow resistive time scale. The stabilizing effect mentioned here, together with a stabilizing toroidal effect, could be the explanation of the saturation of sawteeth observed in recent lower-hybrid wave-driven experiments in PLT, where the experimental electron-cyclotron emission (ECE) signals showed that the island was heated effectively at the time when the saturation was observed. The present stabilizing effect can also explain the "snake" phenomenon seen in the Joint European Torus (JET)

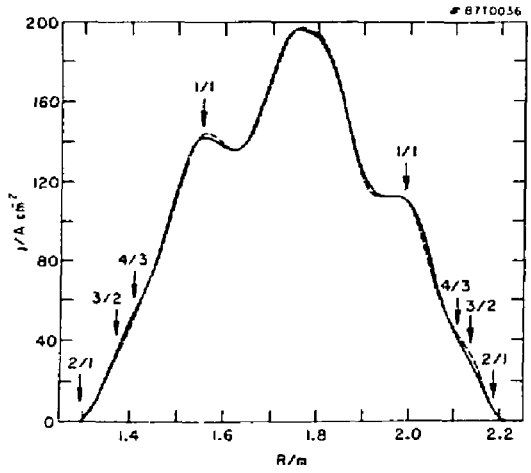

Fig. 5. Full line—best determined experimental current density profile on TEXTOR with $q(0) \lesssim 1$. Dotted line—theoretical current profile which is stable to tearing modes. The positions of various rational surfaces are indicated.

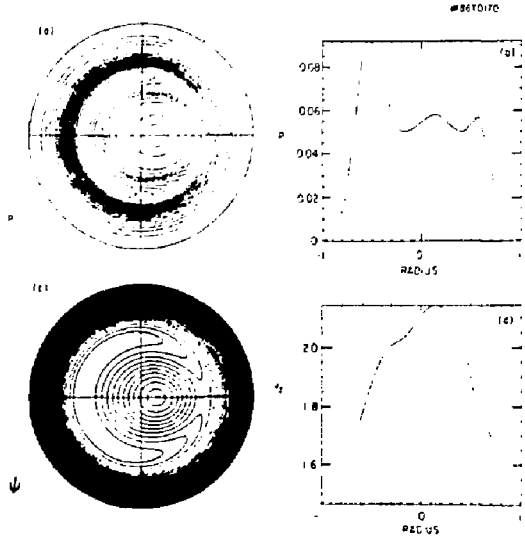

Fig. 6. A saturated nonlinear state for m/n = 1/1. The p and ψ profiles are given.

experiments, which have a helical high pressure structure lasting for seconds. The confinement of this high pressure region suggests that this region is a magnetic island and that a saturated equilibrium has been reached.

Another mechanism suggested for the saturation of the m=1 internal kink mode is based on the observation that in toroidal geometry the perturbed magnetic field lacks symmetry. This should lead to stochasticity of the magnetic field lines. The resultant transport associated with the stochasticity leads to enhanced transport that might stabilize the mode. However, numerical simulation employing three-dimensional reduced-MHD equations has shown that the amount of stochasticity developed by the modes is insufficient to saturate it.[11]

BALLOONING INSTABILITIES

The role of shear in determining stability of current-driven kink instabilities is reasonably well known. However, its role in pressure-driven modes is imperfectly understood. In an effort to clarify this, a systematic study of low-shear pressure-driven modes was undertaken. This study revealed the inadequacy of the high-n ballooning theory to predict the stability of low-n modes in low-shear systems. Here it must be noted that the low shear refers to a region of the plasma and does not refer to the total shear from axis to the plasma edge. It is observed that when such low-shear regions exist and if the pressure gradient in these regions is sufficiently large, then a new class of internal modes are driven unstable even before the high-n ballooning mode is destabilized. These are termed "infernal modes," and appear as sharp resonances in $\omega^2(n)$, where ω is the growth rate and n is the toroidal mode number which is treated as a continuous parameter, see Fig. 7. These modes can drastically reduce the β threshold for instability, Fig. 8, and may play a significant role in tokamak operation, especially in the reactor regime.[12]

The model ballooning equation of Connor, Hastie, and Taylor for large-aspect-ratio circular tokamaks is studied both analytically and numerically in the limit of large pressure gradients. This complements the previous, seminumerical results for the general geometry case,[13] and it provides more insight into the behavior of these modes. The dependence of the stability upon the local shear, curvature, and the field-line bending are more clearly elucidated. Expressions for the first and second stability boundaries are derived. For $\theta_k = 0$, where θ_k is the poloidal location of the ballooning mode, these are given by the expressions[13]

$$\alpha_{01} \quad [S + 1.4 - (8S+9)^{1/2}]/2.$$

and

$$\alpha_{02} = [S + 0.5 + (8S+9)^{1/2}]/2,$$

where $S \quad (r/q_{cyl})dq_{cyl}/dr$ and $\alpha - 8\pi R^2 q_{cyl}^2 (dP/dr)/B_\phi^2$.

Nonzero θ_k is stabilizing to the first boundary but destabilizing to the second. Because of the periodic nature of the equilibrium, as the pressure is increased there can exist potential wells which are localized away from $\theta_k = 0$. Unstable modes feeding on the same mechanisms as above can appear there and generate an infinite sequence of unstable bands that merge asymptotically when one minimizes over the wave number: the ensuing high-beta stability boundary is given by $S = 0.3\alpha^{4/5}$. This behavior could lead to interesting implications for the radial behavior of the modes.

Stability of anisotropic plasma to ballooning modes was investigated using a generalized ballooning mode formulation.[14] However, a fraction of the

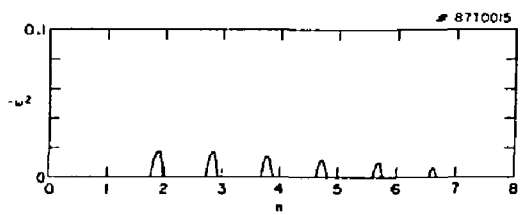

Fig. 7. Growth rate - ω^2 versus n, the toroidal mode number for a plasma with aspect ratio four and a circular cross section. The q profile has a ψ^6 dependence, which implies very low shear near the axis. The pressure profile has its maximum gradient in the region of low shear and is adjusted to make β 1%. This equilibrium is stable to high-n ballooning modes.

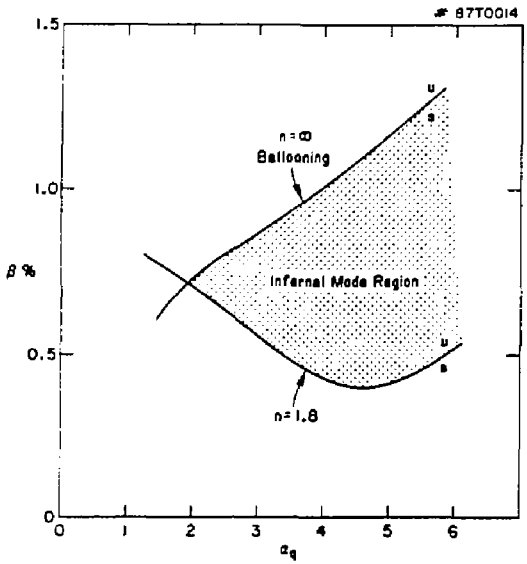

Fig. 8. The β thresholds for onset of instability as a function of the q-profile shear parameter, e.g., $\alpha_q = 1$ implies a linear and $\alpha_q = 2$ a quadratic profile. The thresholds are shown for the $n = \infty$ ballooning and a low-n mode. The shaded region indicates the region of parameter space, where the high-n theory is inadequate and low-n "infernal" modes are observed.

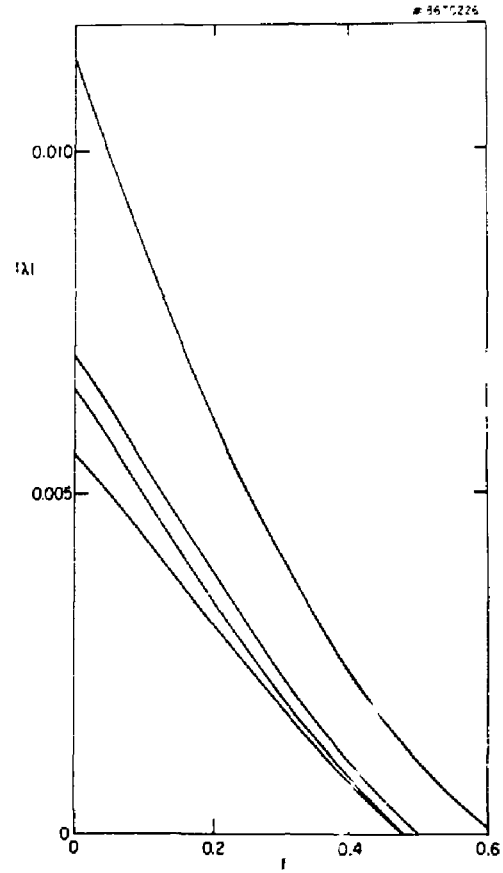

Fig. 9. Most unstable eigenvalue λ I of the ballooning-mode equation is a function of f ne fraction of hot ions that are treated as highly energ .c and nonresonant) for injection into a nearly circu r anisotropic pressure equilibrium with a broad pressure profile, with β = 4.5% and β_{beam} = 3.0%. The uppermost curve is for an equilibrium constructed with a beam-injection angle that provides a significantly larger perpendicular pressure component than parallel, the next lower one is for an artificial isotropic case, the third is for an intermediate-injection case where the two components are near balanced halfway out in the plasma, and the bottom c rve is for an equilibrium where the parallel pressure com ponent dominates.

energetic particles f may be precessing so fast that they do not interact with the mode. To take this into account, terms in the ballooning mode equation were correspondingly reduced and the results on the growth rate were derived.[15] These results are illustrated in Fig. 9 where the eigenvalue of the ballooning mode equation is plotted as a function of f. For the case considered, stability is achieved when about half of the hot ions are thus decoupled.

The potential benefits of tokamak operation at values of q(0) well below unity are being explored. As an example, a DEE-shaped equilibrium was chosen with the q profile given by the expression $q(\psi) = 0.6 + 1.2(\psi/\psi_0)^3$. The pressure profile is optimized such that it is just below the threshold for ballooning instability; because of the absence of the magnetic well, the pressure profile is very flat near the magnetic axis. The averaged beta of 10% exceeds the Troyon limit by about 30%.

However, application of the PEST code for kink modes[16] shows instability for n=1, 2 and 3. These modes can be stabilized by partially surrounding the plasma with a conducting wall (of angular extent 2α) and bringing it within a distance D. Figure 10 displays the squared growth rates of the lowest n=1 modes, Ω_1^2 and Ω_2^2, and the lowest n=0 mode, Ω_0^2, versus α and for $\alpha = 180°$ (closed wall) versus D/a. Also displayed is the squared growth rate for the n=2 kink, $\Omega_{m=2}^2$ versus D/a. As can be seen from this figure, a sufficiently nearby, sufficiently closed shell can stabilize these modes. The necessity for such a close proximity of the shell can be attributed to the low value of q(a) and the presence of a finite current at the plasma edge. More careful tailoring of the current profile could make stabilization of the kink instabilities easier.

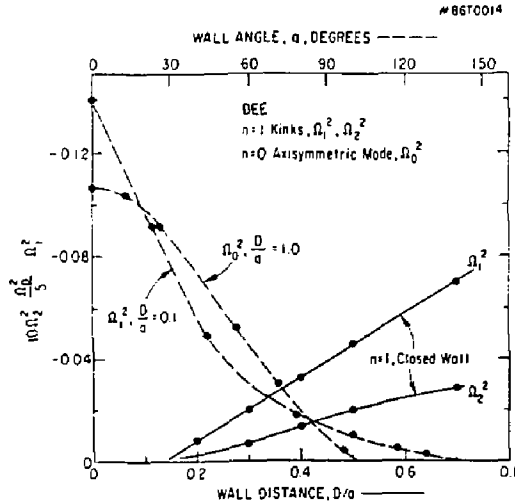

Fig. 10. Lowest growth rate Ω^2 versus relative wall distance D/a and versus angle α subtended by a partially closed conducting shell.

RESULTS OF TRANSPORT CALCULATIONS

The results of Ref. 1 on the possible ignition of the Compact Ignition Tokamak (CIT) did not specifically consider losses of the alpha-particle population due to fishbones. There is a significant possibility for alpha-particle-induced fishbone oscillations[17] to be excited in ignition devices. Such oscillations would result in the loss of about one-fourth of the fusion product alpha particles in a short time compared to their slowing-down time, and this would significantly affect the onset of ignition.

The expected alpha-particle beta during an ignition experiment depends on scaling assumptions. The critical beta for fishbone destabilization is

$$\beta_{\alpha c} = \frac{1}{4}\frac{\omega_d}{\omega_A}$$

where ω_A is the Alfvén frequency and ω_d is the toroidal precession frequency. Ohmic scaling gives $\beta_\alpha/\beta \sim 0.2$ and Kaye-Goldston scaling gives $\beta_\alpha/\beta \sim 0.1$ at peak, i.e., several seconds into the discharge. The CIT design appears to be susceptible to fishbone oscillations if ohmic scaling is assumed. More detailed analyses are being made, as well as investigations of ways to avoid this mode.

It has been shown that energetic particles trapped in the bad-curvature region of a tokamak plasma can resonantly excite ideal as well as resistive interchange-ballooning modes.[18] Such modes with frequencies comparable to the hot-particle precessional frequencies may be candidates for the high-n, high-frequency "precursor" oscillations to the "fishbone" events. In the ideal limit, the instability threshold conditions are too demanding to allow instability due to the strong field-line bending stabilization. However, finite resistivity significantly reduces this stabilizing mechanism, and thus the threshold conditions, to values more consistent with experimental conditions.

Injection of a fast neutral beam into a tokamak plasma has proven to be an effective means for heating a laboratory plasma to thermonuclear temperatures. With the increase of the injection power, however, deterioration of plasma confinement has been detected. In order to study one effect of neutral injection on plasma confinement, two-dimensional numerical simulations have been carried out in a uniform magnetic field. Neutral-beam particles injected across magnetic field are assumed to be ionized along the beam line via various ionization processes, as in the geometry sketched in Fig. 11. As the neutral particles become ionized and trapped by the magnetic field, an electric field is generated across the plasma which convects both the beam and the ambient particles (by $\tilde{E}\times\tilde{B}$ drift) in the direction of the beam injection. Such a macroscopic plasma convection is dissipated by anomalous viscosity that mixes the beam and the ambient plasma more or less uniformly, leading to anomalous diffusion in the x direction.

Results of numerical simulations using a two-dimensional slab model clearly indicate a presence of such turbulence and substantial anomalous diffusion. Theoretical investigation reveals that the scaling of the beam-driven diffusion with plasma density, temperature, and magnetic field is similar to the diffusion due to normal thermal convection. However, the magnitude is much larger, and the diffusion increases with the injection power.[19]

It is tempting to apply the model presented here to a toroidal geometry in order to explain the deterioration of confinement in a neutral-beam-injected tokamak plasma. Preliminary results from simulations using a tokamak geometry indicate a generation of dc electrostatic potential contours which are not concentric with magnetic surfaces because of the presence of injected ions. The

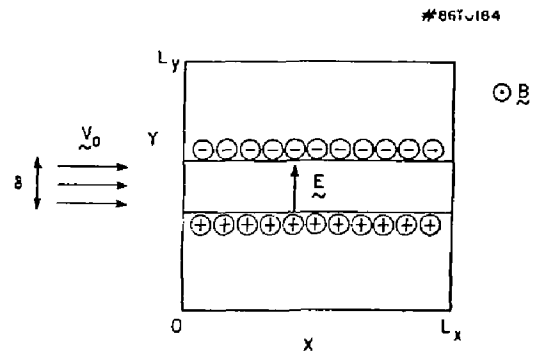

Fig. 11. The equilibrium resulting from the injection of energetic ions across a plasma.

combined effect of the $\tilde{E}\times\tilde{B}$ drift and the magnetic drift appears to mix the edge plasma with the core of a plasma. However, a detailed study is needed to fully understand the rates of these processes.

The bounce-averaged Fokker-Planck transport code FPSTEL previously developed has been upgraded to be applicable to a wider class of stellarator magnetic fields, including those modeling transport-optimized configurations, for which analytic theory only exists in the more collisional $1/\nu$ regime of ripple transport. For the less collisional regimes, the Fokker-Planck results are contrary to some previous heuristic estimates, which had concluded that those configurations which have reduced transport in the $1/\nu$ regime would have enhanced transport at lower ν.

For example (see Fig. 12), in the collisonal $1/\nu$ regime, the configuration $\sigma = 0.4$ has much less transport than the $\sigma = 0$ and $\sigma = -0.4$ configurations. Sigma is a parameter indicating the localization of the ripple to the inside ($\sigma > 0$) or outside ($\sigma < 0$). The new numerical Fokker-Planck results show that the $\sigma = 0.4$ configuration has lower transport for all collisionalities.[20]

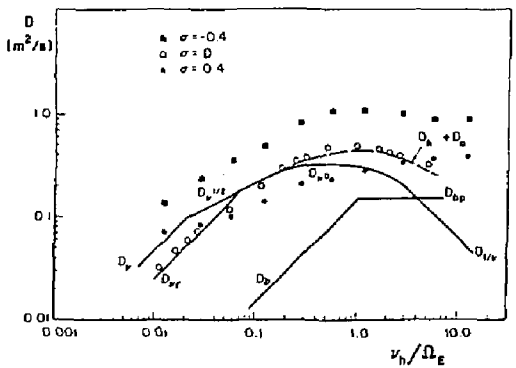

Fig. 12. The diffusion coefficient D versus ν_h/Ω_E for the device parameter σ = -0.4, 0, 0.4. The dashed line is the sum of helical D_h and axisymmetric D_a diffusion as predicted by analytic theory. D_b and D_{bp} are banana and plateau-banana diffusion coefficients. The points are the result of the Fokker-Planck code.

GYROKINETICS, 3-D CODES, AND BASIC THEORY

Gyrokinetic particle simulation techniques have been successful in the investigation of electrostatic low-frequency microinstabilities.[21,22] As reported earlier,[21] a gyrokinetic plasma in the electrostatic limit possesses some very attractive numerical properties. More specifically, in comparison with the usual Vlasov description, which is the basis for the conventional particle simulation, the noise level produced by discrete particle effects is much reduced. This is the result of the gyrophase averaging process which eliminates space-charge waves from the governing equations, and, consequently, removes the necessity to simulate the plasma on ω_{pe} and λ_{DE} scales. This scheme not only enables the use of fewer numbers of particles in the simulation, but also affords the luxury of a much longer time step and a much larger grid spacing, characterized by ω_H and ρ_s, respectively, where $\omega_H \equiv [(k_\parallel/k)\, m_i/m_e]^{1/2}\Omega_i$, $\rho_s \equiv \rho_i(T_e/T_i)^{1/2}$, and ρ_i is the ion gyroradius.

In the past year, the development of a finite-β gyrokinetic particle model was initiated. A preliminary study has shown that magnetic perturbations associated with shear-Alfvén waves can further improve the numerical properties of the gyrokinetic plasma. For example, according to the fluctuation-dissipation theorem, the noise level for electrostatic fluctuations in this case is drastically reduced due to a different dispersion relation (finite-β effects). For $\beta >> m_e/m_i$ and $(k_\perp\rho_s)^2 << 1$, the thermal fluctuation amplitude $|e\Phi(k)/T|$ depends only on the number of simulation particles N within one wavelength of the mode. In addition, even longer time steps can be utilized in the simulation, since the shear-Alfvén frequency ω_A is usually much smaller than ω_H, where $\omega_A = k_\parallel v_A/[1+(ck/\omega_{pe})^2]^{1/2} \equiv \omega_H/[1+(\omega_{pe}/ck)^2]^{1/2}$ and v_A is the Alfvén speed. Furthermore, finite-β effects can also suppress the alias-induced grid instabilities, which enables the use of a much larger plasma volume in the simulation with no restrictions on the grid spacing. The numerical properties for various simulation models are summarized in Table II. Thus, the gyrokinetic particle model indeed gives us the capability to carry out realistic simulations of the tokamak discharge with the present generation of supercomputers. The development of nonlinear gyrokinetic equations including magnetic perturbations is now in progress.

A fully three-dimensional MHD equilibrium code capable of dealing with the islands and stochastic regions is being developed.[23] Initially directed towards stellarator equilibria, the code has been modified to handle islands and stochastic regions that arise from nonaxisymmetric instabilities in tokamaks. The numerics involved are still being optimized. One ultimate goal of this effort is to follow plasma evolution on the resistive and transport time scales. Evolution on these time scales is governed by the three-dimensional MHD equilibrium equation, coupled to the pair of equations determining the evolution of the current and pressure profiles. In describing plasma behavior in the large S limit (resistive time scale much longer than the Alfvén time scale), the code will provide information which complements that coming from inertial codes, which are restricted to values of S much smaller than those encountered experimentally. As a near-term application, the code will be used to look at the combined effects of finite beta, shaping, and finite aspect ratio on tearing-mode stability.

The ultimate goal of a theory of turbulent transport is an accuraie prediction, both in magnitude and scaling, of the flux of some quantity such as energy through the boundary of the turbulent region. No such

Table II. Numerical Properties for Several Simulation Models.

Numerical Properties	Vlasov (unmagnetized)	Gyrokinetic (electrostatic)	Gyrokinetic (finite-β)
$\left\lvert\frac{e\Phi}{T}\right\rvert_{th}$	$\cong 1/N^{1/2}k\lambda_D$	$1/N^{1/2}k_{\rho s}$	$\cong 1/N^{1/2}$
Δt	$\lesssim \omega_{pe}^{-1}$	$\lesssim \omega_H^{-1}$	$\lesssim \omega_A^{-1}$
Δx	$\lesssim \lambda_D$	$\lesssim \rho_s$	no limit

theory yet exists. Instead, as a lesser goal, a formalism has been developed which predicts rigorous upper bounds on fluxes.

Consider for definiteness the transport of energy in a plasma slab filled with steady-state microturbulence. If inhomogeneous boundary conditions are imposed in x—e.g., $T(x=0) = T_0$, $T(x=L) = 0$—a steady-state temperature profile will develop which is nonlinearly self-consistent with the fluctuations. (It is not arbitrarily assumed that the profile gradient is constant.) The gradient of the profile at the edge is proportional to the energy flux. Determining the exact profile, and thus the flux, is very difficult because the problem involves an infinite number of statistical constraints, described by unclosed BBGKY-like hierarchies. However, one can pose the simpler question: What is the maximum self-consistent flux possible subject to just one or two important constraints? The basic method,[24] which has been adapted and extended from applications in fluid dynamics,[25] employs just the steady-state energy balance as a constraint. From that, a (nonlinear) variational problem can be posed from which a rigorous upper bound on the flux emerges. Further constraints can be added to refine the bounds.

It can be argued that these bounds should be reasonably accurate, and this has been verified for one nontrivial, yet exactly solvable, test case.[26] Furthermore, the formalism has been applied to the case of particle transport in given stochastic magnetic fields, and consistency with known results has been demonstrated. For more general situations, the variational equations must be solved numerically; a code has been developed for that purpose. Application to collisional drift-wave turbulence is in progress,[26] and it is planned to study other important fluctuations of interest to confinement in tokamaks.

A project has been initiated to develop a new type of computational tool, a plasma "apprentice" program (PAP), whose purpose is to assist the plasma theorist[27,28] in developing theory. The system's facilities may be divided into a lower and an upper level (measured in terms of intelligent performance). The lower level includes a knowledge base (KB), i.e., a store of useful plasma physics information, and a semi-intelligent plasma formulary, which can access the KB for needed formulae, device parameters, and relevant plasma lore in order to perform straightforward calculations that normally would occupy the time of the human theorist. As an example, the command

numval([nu,nuslow],[per{cit,species=alfa}])

instructs PAP to numerically evaluate the two physical quantities nu (the collision frequency) and nuslow (the slowing-down frequency) for (currently-cited) CIT parameters and for alpha particles. In the current nonoptimized version, the evaluation takes about 20 seconds.

The higher-level facilities are intended to allow PAP to do substantial portions of nontrivial plasma physics calculations, drawing on the KB and on a collection of analytic mathematical techniques for analyzing and solving the equations which PAP finds are relevant. The early implementations of the higher-level routines have recovered some known, but nontrivial, results of ripple-transport theory, following a solution procedure which seems easily extendable to a much wider class of problems.

SPACE AND ASTROPHYSICS

In the last decade, a number of active space experiments have been carried out using rockets and satellites in which an energetic beam is injected into the ionosphere. As the beam energy and density increase, it is important to understand the interaction between the particles and the ambient plasma. Such an interaction is a complex process which includes the effects of enhanced ionization, spacecraft charging, beam-plasma instability, and radiation generation.

A two-dimensional electrostatic model has been developed which can simulate an injection and propagation of a nonrelativistic electron beam from a spacecraft into the space plasma.[29] It has been found that as long as the beam density is much smaller than the ambient plasma density, the space-charge effect due to nonneutrality is not important and that the beam can propagate in space despite the presence of a beam-plasma instability. A beam-

plasma instability causes the spread of the beam in velocity space and generates a tail of high-energy electrons, whose mean-free path for propagation is longer than that of the original beam particles.

As the beam density approaches the ambient plasma density, the radial electric field becomes very important and produces a radial expansion of the beam electrons by anomalous scattering until the beam density is reduced below the ambient density. Beam propagation is not prohibited in this case, but radial divergence of the beam line cannot be neglected.

When the beam density exceeds the ambient plasma density, strong spacecraft charging takes place which prevents the beam electrons from leaving the spacecraft. Injected electrons therefore come back to the spacecraft in this case. These numerical simulation results appear to be supported by the recent Skylab-2 experiment in which an energetic electron beam was injected into the auroral zone ionosphere from a space shuttle in order to trigger an artificial aurora. It is planned to make a more detailed comparison between simulation results and space data. (This work was supported by the National Science Foundation.)

Magnetic fields spontaneously arise in astrophysical bodies such as the sun. Dynamo theory addresses the question of how the presence of plasma flows, which must occur in connection with turbulent heat convection, can cause a small seed magnetic field to amplify itself to the level of the observed fields. If the sun is a representative example, then astrophysical dynamos are inherently phenomena involving several spatial scales: with sufficient resolution, the large-scale magnetic field pattern is observed to be composed of much smaller elements of intense magnetic fields.

To abstract this feature, a simple, but mathematically tractable, example has been formulated which exhibits three spatial scales. A prescribed velocity flow is posited on the intermediate scale as is a large-scale magnetic field. The simplicity of the flow enables one to show that if the plasma is a good conductor, then the magnetic field will exist only in thin sheets which form natural boundaries of the flow circulation pattern. Furthermore, the plasma must, at some points, necessarily flow across the magnetic field, thereby generating an electric field $\vec{E}$ whose spatial average $\langle\vec{E}\rangle$ points antiparallel to the large-scale magnetic field $\langle\vec{E}\rangle = \alpha\langle\vec{B}\rangle$. This relation, called the α-effect, is well-known to cause spontaneous amplification of the large-scale magnetic field $\langle\vec{B}\rangle$. The solution shows, moreover, that the higher the conductivity of the plasma, the thinner the magnetic field sheets and the smaller the value of α. In other words, the magnitude of the α-effect depends on a transport coefficient—the plasma resistivity.

These findings suggest that attempts to simulate the solar dynamo via large-scale computation will be sensitive to the assumed value of the plasma resistivity, which, for numerical reasons, must be taken to be much larger than the true physical value. The most productive approach appears to be to numerically establish how the dynamo scales with the assumed value of conductivity (and also viscosity and heat conductivity) and then to extrapolate to physical values of these transport coefficients.

RADIO-FREQUENCY HEATING, CURRENT DRIVE, AND NUCLEAR SPIN POLARIZATION

The status of the field of radio-frequency (rf) current drive was reported in two major reviews articles: (1) *a review of theoretical and experimental work on rf current drive*[30] and (2) a review of numerical methods for solving the Fokker-Planck equation.[31]

The past two years has seen a unification of the theory of rf current drive. This has largely arisen because of the adoption of the so-called adjoint technique. Now, lower-hybrid and electron-cyclotron current drive are understood as manifestations of the same basic physics. Similarly, the nonrelativistic results are derived as the appropriate limit of the relativistic theory, and the steady-state current drive results are given by the limit of vanishing dc electric field in the more general nonsteady problem.

An approximate analytical solution of the Fokker-Planck equation in the presence of rf was obtained.[32] This is useful in obtaining information about the wave spectrum from the bremsstrahlung emissions.

A detailed understanding of both rf current drive and rf heating requires the consideration of profile effects. This entails coupling the solution of the Fokker-Planck equation to a code which describes the propagation of the waves and the various transport processes. Because the Fokker-Planck equations need to be solved many times in such a simulation, these studies have usually been carried out using "simplified" Fokker-Planck equations.[33] Currently, work is underway to develop a much faster Fokker-Planck solver which will allow realistic simulations to be performed. This will be used to analyze the ion-cyclotron radio-frequency heating experiment on TFTR.

It is known that polarization of the nuclear spins in a plasma wall will increase the nuclear reaction rate by about fifty percent. However, it is important to ascertain whether any magnetic oscillations exist with frequencies near the precession rate of these nuclear spins, because these oscillations can rapidly depolarize the nuclear spins. Because the reaction products of a polarized plasma are anisotropic in velocity, they could interact with various waves and excite them. It has been shown that there is one class of magnetoacoustic waves that are trapped long enough in a plasma to be excited.[34] However, any such waves near the deuteron precession frequency (equal to eight-six percent of the cyclotron frequency) are damped by electron transit time damping at a rate faster than they are excited by alpha particles. On the other hand, waves near the triton frequency can be excited if the gradient of the toroidal field is

sufficiently weak. The estimate shows that these waves are excited if the aspect ratio is greater than about four.

References

[1]S.C. Jardin, N. Pomphrey, and J. DeLucia, "Dynamic Modeling of Transport and Positional Control of Tokamaks," Princeton University Plasma Physics Laboratory Report PPPL-2258 (1985) 47 pp; J. Comp. Phys. 66 (1985) 481.

[2]F.W. Perkins and Y.C. Sun, "On Confinement Scaling and Ignition in Tokamaks," Princeton University Plasma Physics Laboratory Report PPPL-2261 (1985) 10 pp.

[3]F. Romanelli, W.M. Tang, and R.B. White, "Anomalous Thermal Confinement in Ohmically Heated Tokamaks," Princeton University Plasma Physics Laboratory Report PPPL-2310 (1986) 41 pp; Nucl. Fusion 26 (1986) 1515.

[4]W.M. Tang, C.M. Bishop, B. Coppi, *et al.*, "Microinstability-Based Models for Confinement Properties and Ignition Criteria in Tokamaks," in *Plasma Physics and Controlled Nuclear Fusion Research 1986* (Proc. 11th Int. Conf., Kyoto, Japan, 1986), Paper CN-47/A-VI-1-2 (IAEA, Vienna, 1987), to be published.

[5]F.W. Perkins and R.A. Hulse, "On the Murakami Density Limit in Tokamaks and Reversed Field Pinches," Princeton University Plasma Physics Laboratory Report PPPL-2087 (1984) 31 pp; Phys. Fluids 28 (1985) 1937.

[6]B. Coppi and W.M. Tang, "Influence of Anomalous Thermal Losses on Ignition Conditions," Princeton University Plasma Physics Laboratory Report PPPL-2343 (1986) 22 pp.

[7]C.Z. Cheng, H.P. Furth, and A.H. Boozer, "MHD Stable Regime of the Tokamak," Princeton University Plasma Physics Laboratory Report PPPL-2372 (1986) 28 pp.

[8]H. Soltwisch, "Current Distribution Measurement in a Tokamak by FIR Polarimetry," Rev. Sci. Instrum. 57 (1986) 1939.

[9]H. Soltwisch, W. Stodiek, J. Manickam, and J. Schlueter, "Current Density Profiles in Textor Tokamak," in *Plasma Physics and Controlled Nuclear Fusion Research 1986* (Proc. 11th Int. Conf., Kyoto, Japan, 1986), Paper CN-47/A-V-1-2 (IAEA, Vienna, 1987), to be published.

[10]W. Park, D.A. Monticello, and T.K. Chu, "Sawtooth Stabilization through Island Pressure Enhancement," Princeton University Plasma Physics Laboratory Report PPPL-2385 (1986) 12 pp; Phys. Fluids (in press, 1987).

[11]R. Izzo, D.A. Monticello, W. Stodiek, W. Park, "Stochasticity and the m = 1 Mode in Tokamaks," Princeton University Plasma Physics Laboratory Report PPPL-2342 (1986) 16 pp; Phys. Fluids (in press)

[12]J. Manickam, N. Pomphrey, and A.M.M. Todd, "Ideal MHD Stability Properties of Pressure Driven Modes in Low Shear Tokamaks." Princeton University Plasma Physics Laboratory Report PPPL-2420 (1987) 40 pp.; submitted to Nucl. Fusion.

[13]J.M. Greene and M.S. Chance, "The Second Region of Stability Against Ballooning Modes," Nucl. Fusion 21 (1981) 453.

[14]W.A. Cooper, "Kinetic and Fluid Ballooning Instability in Anisotropic Ion Tokamaks," Phys. Fluids 26 (1983) 1830.

[15]E.R. Salberta, R.C. Grimm, J.L. Johnson, J. Manickam, and W.M. Tang, "Anisotropic Pressure Tokamak Equilibrium and Stability Consideration," Princeton University Plasma Physics Laboratory Report PPPL-2413 (1986) 38 pp; submitted to Phys. Fluids.

[16]M.S. Chance, A.M.M. Todd, J. Manickam, and A.E. Miller, "Stabilization of Free Boundary Modes with Open Conductors," in *Tokamak Concept Innovations*, IAEA-TECDOE 373, June 1986, p. 145.

[17]L. Chen, R.B. White, and M.N. Rosenbluth, "Excitation of Internal Kink Modes by Trapped Energetic Beam Ions," Phys. Rev. Lett. 52 (1984) 1122.

[18]H. Biglari and L. Chen, "Theory of Energetic Trapped Particles Induced Resistive Interchange-Ballooning Modes," Princeton University Plasma Physics Laboratory Report PPPL-2302 (1986) 42 pp; Phys. Fluids 29 (1986) 2960.

[19]H. Okuda and S. Hiroe, "Diffusion of a Plasma Subject to Neutral Beam Injection," Princeton University Plasma Physics Laboratory Report PPPL-2388 (1986) 39 pp; submitted to Phys. Fluids.

[20]W.N.G. Hitchon and H.E. Mynick, "Ripple Transport in Optimized Stellarators," Princeton University Plasma Physics Laboratory Report PPPL-2338 (1986) 42 pp; submitted to Nucl. Fusion.

[21]W.W. Lee, "Gyrokinetic Particle Simulation Model," Princeton University Plasma Physics Laboratory Report PPPL-2360 (1986) 36 pp; J. Comput. Phys. (in press).

[22]J.F. Federici, W.W. Lee, and W.M. Tang, "Nonlinear Evolution of Drift Instabilities in the Presence of Collisions," Princeton University Plasma Physics Laboratory Report PPPL-2354 (1986) 44 pp; Phys. Fluids (in press).

[23]A. Reiman and H. Greenside "Calculation of Three-Dimensional MHD Equilibria with Islands and Stochastic Regions," Princeton University Plasma Physics Laboratory Report PPPL-2355 (1986) 38 pp; Comput. Phys. Comm. 43 (1986) 157.

[24]J.A. Krommes and R.A. Smith, "Rigorous Upper Bounds for Transport Due to Passive Advection by Inhomogeneous Turbulence," Princeton University Plasma Physics Laboratory Report PPPL-2422 (in press) 91 pp.

[25]F.H. Busse, "Optimum Theory of Turbulence," Adv. Applied Mech. 18 (1978) 77.

[26]R.A. Smith, "Aspects of Turbulent Transport in a Bounded Plasma," Ph.D. Thesis, Princeton University, 1986.

[27]H.E. Mynick, "Introducing PAP: A Plasma Apprentice Program," Princeton University Plasma Physics Laboratory Report PPPL-2323 (1986) 36 pp; submitted to J. Comput. Phys.

[28]H.E. Mynick, "Alpha Particle Effects as a Test Domain for PAP: A Plasma Apprentice Program" Physica Scripta (in press).

[29]H. Okuda and J. Berchem, "Injection and Propagation of a Nonrelativistic Electron Beam and Spacecraft Charging," Princeton University Plasma Physics Laboratory Report PPPL-2438 (1987) 50 pp.

[30]N.J. Fisch, "Theory of Current Drive in a Plasma," Princeton University Plasma Physics Laboratory Report PPPL-2401 (1986) 153 pp; Rev. Mod. Phys. (in press).

[31]C.F.F. Karney, "Fokker-Planck and Quasilinear Codes," Princeton University Plasma Physics Laboratory Report PPPL-2290 (1985) 9 pp. Computer Phys. Reports *4* (1986) 183.

[32]N.J. Fisch and C.F.F. Karney, "Asymptotic Analysis of Radio Frequency-Heated Collisional Plasma," Princeton University Plasma Physics Laboratory Report PPPL-2205 (1985) 40 pp; Phys. Fluids *28* (1985) 3107.

[33]E.J. Valeo and D.C. Eder, "Numerical Modeling of Lower Hybrid Heating and Current Drive," in *Applications of RF Waves to Tokamak Plasmas*, Vol. *II* (1985) 493-511; Princeton University Plasma Physics Laboratory Report PPPL-2272 (1986) 26 pp.

[34]B. Coppi, S. Cowley, R. Kulsrud, P. Detragiache, and F. Pegararo, "High Energy Components and Collective Modes in Thermonuclear Plasmas," Princeton University Plasma Physics Laboratory Report PPPL-2294 (1986) 57 pp; Phys. Fluids *29* (1986) 4060.

TOKAMAK MODELING

The Tokamak Modeling Group is engaged in developing and applying computer codes which simulate plasma physics experiments conducted at PPPL and elsewhere. These codes are used in the interpretation of experimental results, in the planning of experimental operations, and in the design of new experimental devices such as the Compact Ignition Tokamak (CIT). These predictive codes are distinguished from data analysis codes, such as TRANSP, in that much of the input is fundamental physical data (e.g., atomic data, diffusivities) and the output (e.g., electron temperature) may be compared with experimental data. The plasma transport code BALDUR simulates the widest range of physical processes: diffusive and advective plasma particle and energy transport; plasma current diffusion; MHD equilibrium and stability; heating by ohmic dissipation, neutral-beam injection, ion-cyclotron frequency waves, fusion-produced alpha particles, and magnetic compression; neutral hydrogen particle and energy transport; impurity transport and radiation; and pellet injection.

Since some of these processes are modeled primitively in BALDUR, several codes of reduced scope, but greater detail and sophistication, have been developed to treat the physics of plasma interactions with divertors and limiters. The PLANET code simulates two-dimensional (2-D) transport in the outer layers of the plasma where the magnetic flux surfaces intersect diverters or limiters. DEGAS is used to calculate the transport of atomic and molecular hydrogen through plasmas in complex magnetic geometries bounded by realistic walls.

The multicharge-state impurity transport code MIST models the details of excitation, radiative decay, ionization, recombination, and radial transport of impurity ions in tokamaks, and is used to interpret spectroscopic measurements.

ONE-DIMENSIONAL PLASMA TRANSPORT

The BALDUR code was used to calibrate and test recent theoretically based models for thermal electron and ion energy transport[1,2] against twenty-one TFTR discharges. Most of the discharges were gas fueled and ohmically heated, but some were pellet fueled and others were heated by neutral beams. Empirical models for particle transport were adjusted so that the simulated density resembled the measured density and the simulated temperature was compared to the measured temperature to test the energy transport model. Good agreement was obtained in simulating the steady-state electron-temperature profiles and confinement times for these experiments when the collisional trapped-electron model for χ_e was used together with η_i-driven model for χ_i (Fig. 1). In the simulations, the η_i-driven χ_i produced a mild saturation of τ_E as a function of $\bar{n}_e$; this trend in the large-plasma TFTR experiments could not be well simulated by using a constant times neoclassical χ_i. Shortly, after multiple pellet injection in one of the simulated discharges, τ_i is ≤ 1 and, according to theory, no η_i-driven ion-thermal transport is expected; this expectation is consistent with the experiments in that the absence of the η_i-driven χ_i is required in the simulations in order to match the measured instantaneous energy confinement. Preliminary simulations indicate that the collisionless trapped-electron χ_e may be consistent with supershot experimental data.

Global time-dependent transport simulations of ICRF-heated tokamaks with circular and noncircular plasma cross sections were obtained by interfacing the WHIST 1½-dimensional transport code developed by Oak Ridge National Laboratory (ORNL) with an

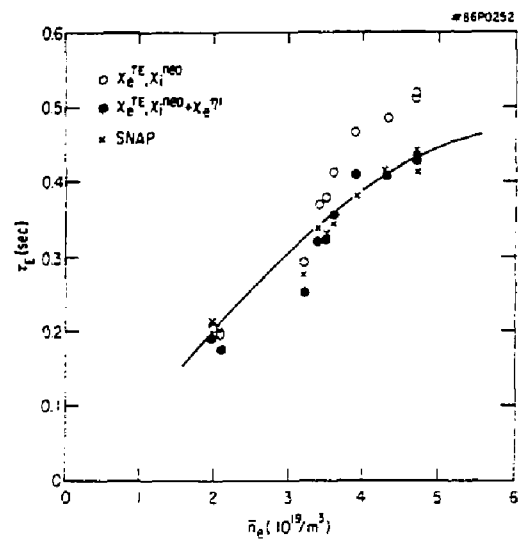

Fig. 1. Density scaling of the total energy confinement time for large plasma (R = 2.6 m, a = 0.82 m, I_p = 2.2 MA, B_T = 4.7 T) experiments in TFTR. Experimental and simulation results are shown.

ion-cyclotron radio-frequency (ICRF) wave propagation and power deposition package, developed previously by Hwang and Karney for use with the BALDUR one-dimensional (1-D) transport code. The ICRF package was generalized to treat ICRF-wave heating in 2-D tokamak equilibria. Princeton Large Torus (PLT) experiments[3] and proposed experiments in TFTR and CIT were simulated using an empirical transport model derived from Kaye-Goldston energy confinement scaling. Comparison of the simulations with the data from ICRF-heating experiments on PLT support the experimental observation that energy confinement scales more favorably with increasing ICRF power than the Kaye-Goldston relation implies. Simulation of a TFTR discharge heated by 8 MW of neutral-beam injection indicates that the ion temperature should increase by about 50% with addition of 6 MW of ICRF heating. Finally, CIT was simulated using the empirical transport model for both L-mode and H-mode scalings. While ignition under L-mode conditions is difficult in CIT, the simulations indicate that ignition is possible in a H-mode regime with the present design parameters.

1½-DIMENSIONAL PLASMA TRANSPORT

The 1½-D BALDUR code solves the flux-surface-averaged transport equations for tokamaks with noncircular cross section.[4] Recently, the capability to study ballooning-mode-enhanced transport was incorporated into the code. It was found that suppressing sawtooth oscillations also suppresses short-wavelength, ideal ballooning modes at higher pressure gradients in the central part of elongated tokamak plasmas.

Simulations of both the TFTR[5] and CIT[6] tokamaks with the BALDUR transport code show that global ignition requirements are substantially relaxed when the density and temperature profiles are centrally peaked. Since the steady-state sawtooth mixing radius in CIT may be quite broad (since the plasma is elongated and run at high current), scenarios were developed that use a combination of pellets, current ramp, and off-axis heating in order to delay the onset of broad sawtooth oscillations and produce centrally peaked profiles.[6,7]

A fast, accurate algorithm was developed[8] to map from rectangular to optimized harmonic representation of magnetic surfaces. This algorithm was implemented in the 1½-D BALDUR code[4] to simulate the transport of free-boundary plasma equilibria.

A direct method for determining Hamada coordinates[9] was developed to facilitate the computation of saturated tearing-mode island widths in toroidal geometry.[10]

CIT Reference Simulation

The 1½-D BALDUR Transport code[4] was used to simulate a reference ignition scenario for the Compact Ignition Tokamak and to study the sensitivity of ignition to variations around the reference parameters.[7] These simulations include the effects of magnetic-field ramp and current ramp during the first six seconds, multiple pellet injection, 20 MW of off-axis auxiliary heating, helium and carbon impurities, experimentally calibrated anomalous thermal transport,[11] sawtooth oscillations, and ballooning-mode-enhanced transport. It is found that ignition depends strongly on the size of the sawtooth mixing region, the peak density that can be sustained, the temperature dependence of the thermal diffusivity, and Z_{eff}. The timing of the current ramp, pellet injection, and auxiliary heating was specifically designed to keep the sawtooth mixing radius small.

It is relatively easy to achieve ignition in transport simulations of the Compact Ignition Tokamak[12,13] if the energy confinement time is better than L-mode (Kaye-Goldston) scaling, if the density equals or exceeds the Murakami limit, and if the plasma beta is close to the Troyon limit without producing disruption. If more pessimistic conditions prevail, ignition is still possible if the density and temperature profiles are centrally peaked.[6] Centrally peaked profiles can be maintained in simulations only if broad sawtooth oscillations are suppressed by current drive or delayed by using pellet injection, current ramp, and off-axis heating in order to hold the central q value above unity.[6,7] These conditions also allow larger pressure gradients to be supported against short wavelength, ideal-MHD ballooning modes in the central part of the plasma. If the current profile is allowed to reach steady state, broad sawtooth oscillations flatten the profiles and maintain low magnetic shear over about 70% of the plasma half-width (about 50% of the plasma volume), making ignition more difficult to achieve. Since this low shear, $q \gtrsim 1$ region is not able to support any substantial pressure gradient against short wavelength, ideal-MHD ballooning modes, the temperature and density remain flattened within the mixing region between sawtooth crashes, limiting fusion power production under these conditions.

PLASMA OPTIMIZATION

A plasma optimization code was developed to find the plasma conditions which maximize the fusion power multiplication Q under a variety of assumed conditions. This 1½-D code is not a transport code because the plasma density and temperature profile shapes are fixed; typically they are taken from experimental data. For a given thermal energy confinement time the code varies the plasma density and the ion and electron temperatures to find the plasma which produces the highest possible Q for the given tokamak configuration (fixed plasma size, profile shapes, beam power, etc.). Although a transport code is not used, the plasma conditions are physically self-consistent in the sense that the neutral-beam deposition is calculated for the optimum plasma, and the ion temperature is limited by an ion power balance

calculation. The optimum Q is an increasing function of τ_E and the peakedness of the plasma density profile, but only a weak function of the peakedness of the temperature profiles.

This code has been used to find the plasma requirements for achieving energy breakeven Q = 1 in TFTR. It was found that the thermal energy confinement time must be at least 0.20 sec (Fig. 2); the optimum temperatures are $T_{eo} \simeq 10$ keV and $T_{io} \simeq 20$ keV. The measured temperatures in TFTR supershots are near these optimum temperatures.

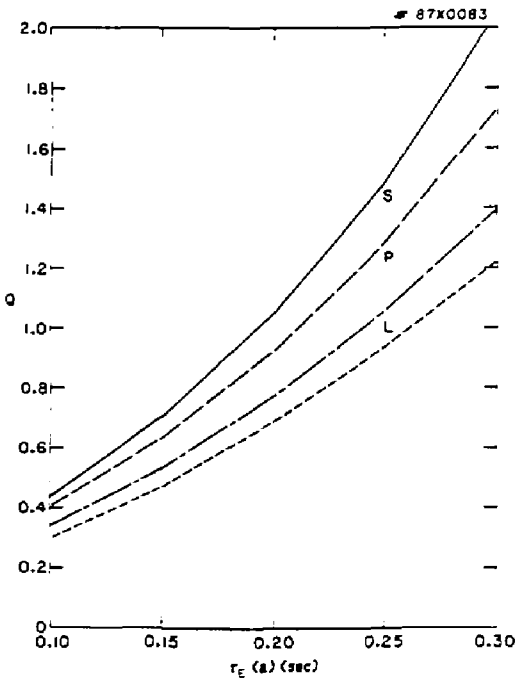

Fig. 2. Fusion power multiplication versus thermal energy confinement time for optimized plasmas based on density and temperature profile shapes measured in a TFTR supershot (S), pellet-fueled shot (P), and two L-mode shots (L).

Maintaining these temperatures while raising the present supershot thermal energy confinement time by 70%, doubling the beam power as planned, and tripling the density will result in break-even plasma conditions. Alternatively, it is noted that more than enough density and energy confinement have been produced in pellet-fueled, ohmically heated low-temperature discharges in TFTR. Raising the temperature of such discharges to the values seen in supershots follows a second route to breakeven.

PLASMA TRANSPORT IN THE SCRAPE-OFF

The emphasis during FY86 was on applications. The PLANET code was used to model divertor designs for the International Tokamak Reactor (INTOR), the Compact Ignition Tokamak (CIT), the Doublet D-III-D, and a limiter for TFTR. Both the (proposed) CIT and the D-III-D experiments have open and rather short divertors which raised the concern of neutral penetration into the main plasma from the high recycling region near the plates. The code predicted a sufficient degree of plugging of neutrals by the plasma despite the fact that, in the case of CIT, the neutral flux from the plates exceeded 10^{24} atoms per sec. Neutral densities above 10^{15} per cm^3 were predicted for the CIT divertor and 10^{14} per cm^2 for the D-III-D divertor. These predictions appear to be borne out by the D-III-D experiment, which so far does not appear to suffer from a degradation of the H-mode confinement due to neutral penetration.

Interesting and potentially very important results were obtained during studies of the INTOR divertor.[14] The present INTOR design employs an outwardfacing, sharply angled, neutralizer plate (plate a in Fig. 3) that causes a rapid radial particle transport along the plate face. This occurs because the neutrals are,

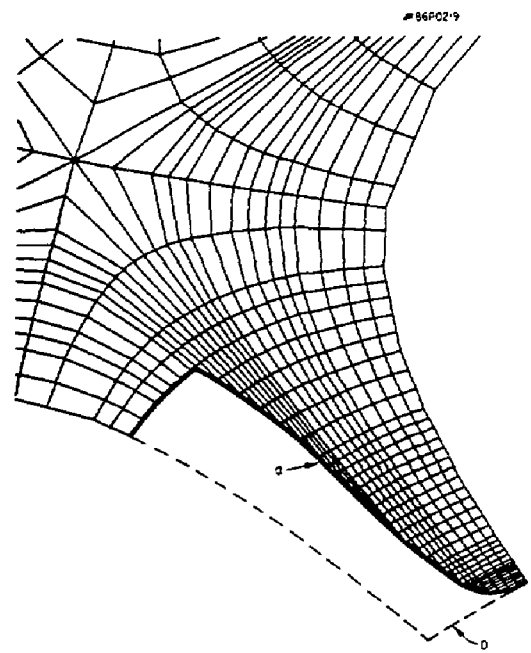

Fig. 3. The neutralizer plate shapes and the plasma-region mesh used in the calculation for the angled plate. (a) is the angled plate and (b) the perpendicular plate.

on the average, emitted normal to the plate, while the ion, produced from the neutrals, travel along the field lines to the right of their point of origin. The result is that a high recycling regime cannot be maintained close to the separatrix, where most of the parallel power flow is concentrated, the plasma temperature remains high all the way to the plate (curve a in Fig. 4). A normal and inward-facing (towards the x-point) plate orientation does not suffer from this effect (b in Figs. 3 and 4). The generality of the above conclusions and their dependence on the plasma-surface interaction models is still being explored.

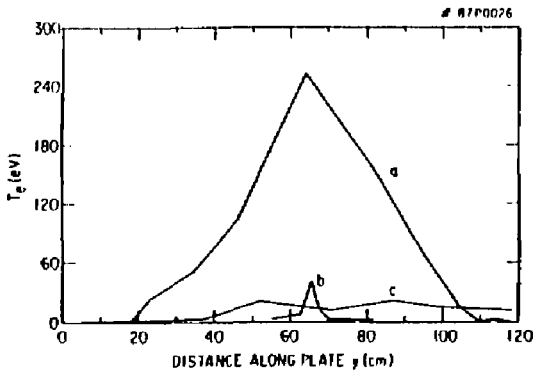

Fig. 4. The plasma temperature distribution along the outward-facing angled plate (a), perpendicular plate (b), and an inward-facing angled plate (c). The origins for the distance y are chosen so that the intersection of the separatrix with the plate has the same y value (62 cm) for all the three plates.

NEUTRAL PARTICLE TRANSPORT

Neutral particles play an important role in plasma experiments by transporting mass, momentum, and energy across magnetic flux surfaces. They also carry a large portion of the plasma's energy to the walls and limters, and sputter impurities into the plasma. A recent review article describes this physics in more detail and surveys the theory of neutral kinetics.[15]

Recycling in PLT

The DEGAS neutral transport code[16] was extensively applied during the last year to the analysis of experimental data. A study of neutral flux measurements at two toroidal positions relative to a pair of limiters in PLT[17] shows close agreement with spectra measured by the low energy neutral system (LENS) detector near the recycling limiter. The computed spectra are sensitive to the assumed ion temperature T_i, so one result of the modeling is a profile of T_i. By finding the neutral flux necessary to match the results for both positions, the ion currents to both the limiter and wall were estimated, along with the corresponding particle confinement times within the limiter and wall minor radii.

Proposed Pumped Limiters for TFTR

A one-dimensional, steady-state edge model was developed to simulate the plasma scrape-off region. The treatment of limiter recycling was calibrated using DEGAS. Langmuir probe data from TFTR, PLT, and ALT-I were modeled. The inferred global particle confinement times appear consistent with other observations. The perpendicular diffusion coefficient appears to be lower than Bohm diffusion for movable limiter discharges on TFTR, and comparable to Bohm diffusion for recent PLT discharges.

In TFTR simulations with a proposed pumped limiter, the scrape-off density is predicted to decrease while the temperature increases. Specific predictions for the TFTR radio-frequency limiters, the Tore Supra pumped limiters, and ALT-II were also made.[18] A study for a TFTR full-power pumped belt limiter system indicated that pumping would reduce the recycling coefficient by 10-25% and that the increased density control might double Q_{fusion}. Pumping with the smaller poloidal radio-frequency limiters for TFTR may reduce the recycling coefficient of low power discharges by 15%.

Particle Confinement in the TMX-U Tandem Mirror

A key term in estimating the magnitude of ion losses in tandem-mirror machines is the measurement of the plasma ionization source current. This current can be estimated from measurements of the closely related H_α emission. The DEGAS code has been used to correctly predict several qualitative features of the ionization data from the TMX-U experiment.[19]

External Collaboration

A number of additional collaborations outside PPPL were begun or maintained during the past year. Dr. F. Sardei's group at IPP-Garching has developed a detailed three-dimensional description of the geometry of the Wendelstein-VII stellarator for use with the DEGAS code. Results from DEGAS for INTOR benchmark problems are being compared with those from other multidimensional transport codes.[20] The DEGAS code is also being used in the TIBER Engineering Test Reactor divertor design.[21]

A first draft of the DEGAS user's manual was written as part of PPPL's user support effort. The on-line manual will include sections on program overview, description of physical processes, creating an input file and running the program, interpreting printed and graphic output, examples, references, and appendices with programming information.

DEGAS Code Development

Carbon and methane are important contaminants in tokamaks with graphite limiters. Earlier calculations[22] showed that carbon can penetrate further into the plasma when it is released from the limiter as part of a methane molecule. The DEGAS code was extended to model this process; results will be compared with the simpler calculations.

A realistic characterization of the interaction of ions and neutral particles with device walls is important in neutral transport calculations. A data set for the distribution of reflected energy and polar and azimuthal angles, as functions of incident polar angle and energy, was developed.[23] The data are represented by three one-dimensional distributions, resulting in fast, realistic reflection models.

Recycling in TFTR

In collaboration with the Sandia National Laboratories, a suite of computer codes were combined that describe hydrogen transport in plasma and solids and that are capable of predicting recycling as well as hydrogen permeation and inventory in vessel components. These codes are used to study hydrogen recycling, limiter conditioning,[24] tritium retention, and isotope exchange.

Figure 5 shows the results from an example calculation applying these codes to a 1.4-MA ohmically heated discharge at the movable limiter.[25] The movable limiter saturated quickly during the discharge, reaching 100% recycling within 0.5 sec. The first wall received a relatively negligible flux and did not saturate. However, after a large number of calculation cycles, the wall retained approximately as many particles as the limiter. A bumper-limited discharge, with a plasma similar to the one described above, was also modeled. The lower particle flux to the larger surface of the bumper limiter leads to delayed saturation and less recycling than with the smaller movable limiter (Fig. 5).

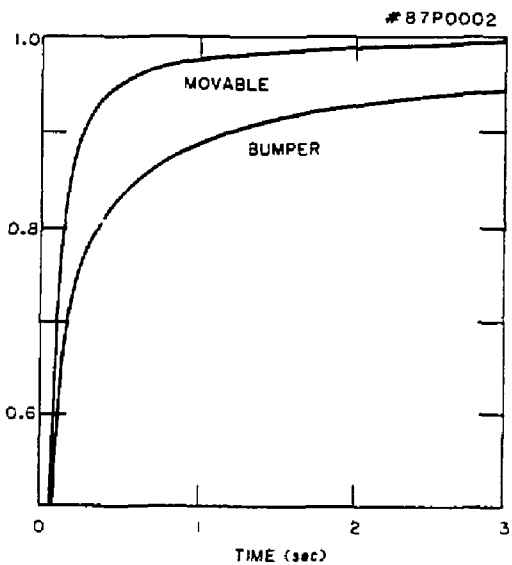

Fig. 5. Ratios of the total particle outflux over the total ion and neutral particle flux onto the movable and inner limiters during the model ohmic-heating discharge. Recycling off the movable limiter reaches approximately 100% in less than 1 sec, while that off the inner limiter peaks at approximately 90%.

IMPURITY TRANSPORT

Continued development of the MIST multispecies impurity transport code proceeded in several directions. First, the basic FORTRAN code generation environment in which MIST was developed has been enhanced by development of the VSOP (variable specification Omni processor) system, a code generation processor that automatically organizes and documents variable names, initialization, common blocks, and other aspects of working with a large FORTRAN code. In addition to aiding code development, the documentation aspects of this system support the growing user group of the MIST code at PPPL and other fusion laboratories. The MIST code was modified to run on the VAX computer as well as on Cray computers. This, together with a new equilibrium solver, allowed the full steady-state impurity transport solutions, together with associated spectral line emission, radiated power, Z_{eff} contributions, etc., to be calculated between shots during TFTR runs. This on-line quantitative impurity analysis capability has greatly aided the timely integration of impurity experimental data into TFTR operations. In another direction, MIST was modified to simulate hydrogen transport where electron, rather than impurity, density is the object of the analysis. As part of this work, a numerically more accurate treatment of plasma recycling was added to the code.

References

[1]W.M. Tang, "Microinstability-Based Model for Anomalous Thermal Confinement in Tokamaks," Princeton University Plasma Physics Laboratory Report PPPL-2311 (1986) 38 pp; Nuclear Fusion (in press).

[2]W.M. Tang, C.M. Bishop, B. Coppi, *et al.*, "Microinstability-Based Models for Confinement Properties and Ignition Criteria in Tokamaks," in *Plasma Physics and Controlled Nuclear Fusion Research 1986* (Proc. 11th Int. Conf., Kyoto, Japan), Paper IAEA-CN-47/A-VI-1-2 (IAEA, Vienna, 1987), to be published; Princeton University Plasma Physics Laboratory Report PPPL-2418 (1987) 13 pp.

[3]D.G. Swanson *et al.*, "Recent Advances in the Theory and Modeling of RF Heating in Inhomogeneous Plasmas," *ibid.*, Paper IAEA-CN-47/F-IV-4.

[4]G. Bateman, "Algorithms for 1½-D Transport," in *Spring College on Plasma Physics* (International Center for Theoretical Physics, Trieste, Italy, 1985), paper SMR/150-45.

[5]S.J. Zweben, M.H. Redi, and G. Bateman,"Central Ignition Scenarios for TFTR," Princeton University Plasma Physics Laboratory Report PPPL-2316 (1986) 73 pp; to appear in Fusion Technol.

[6]G. Bateman, "Delaying Sawtooth Oscillations in the Compact Ignition Tokamak," Princeton University Plasma Physics Laboratory Report PPPL-2373 (1986) 23 pp; to appear in Fusion Technol.

[7]C.E. Singer, L.-P. Ku, and G. Bateman, "Plasma Transport in a Compact Ignition Tokamak," Princeton University Plasma Physics Laboratory Report PPPL-2414 (1987) 34 pp; to appear in Fusion Technol.

[8]W. Schneider and G. Bateman, "Mapping from Rectangular to Harmonic Representation," Princeton University Plasma Physics Laboratory Report PPPL-2361 (1986) 17 pp; to appear in J. Comput. Phys.

[9]G. Bateman and R.G. Storer, "Direct Determination of Axisymmetric Magnetohydrodynamic Equilibria in Hamada Coordinates," J. Comput. Phys. *64* (1986) 161.

[10]G. Bateman and R.N. Morris, "Saturated Tearing Modes in Toroidal Geometry," Phys. Fluids *29* (1986) 753-761.

[11]C.E. Singer, L.-P. Ku, G. Bateman, F. Seidl, and M. Sugihara, "Physics of Compact Ignition Tokamak Designs," in *Fusion Engineering* (Proc. 11th Symp., Austin, 1985), Vol. 1, (IEEE, New York, NY) 41; Princeton University Plasma Physics Laboratory Report PPPL-2317 (1986) 39 pp.

[12]D. Post, G. Bateman, W. Houlberg, *et al.*, "Physics Aspects of the Compact Ignition Tokamak," Princeton University Plasma Physics Laboratory Report PPPL-2389 (1986) 70 pp; to appear in Physica Scripta.

[13]J. Schmidt, G. Bateman, D. Blackfield, *et al.*, "A Compact Ignition Experiment," in *Plasma Physics and Controlled Nuclear Fusion Research 1986* (Proc. 11th Int. Conf., Kyoto, Japan), Paper IAEA-CN-47/H-I-2 (IAEA, Vienna, 1987), to be published.

[14]M. Petravic, D.B. Heifetz, G. Kuo-Petravic, and T. Arzt, "The Effect of the Poloidal Divertor Neutralizer Geometry on the Scrape-Off Plasma Temperature and Density," J. Nucl. Mater. *145-147* (1987) 841.

[15]M. Tendler and D. Heifetz, "Neutral Particle Kinetics in Fusion Devices," Princeton University Plasma Physics Laboratory Report PPPL-2319 (1986) 73 pp; Fusion Tech. *11* (1987) 288.

[16]D. Heifetz *et al.*, "A Monte Carlo Model of Neutral Particle Transport in Diverted Plasmas," J. Comput. Phys. *46* (1982) 309.

[17]D.N. Ruzic, D.B. Heifetz, and S.A. Cohen, "The Density Dependence of Neutral Hydrogen Density and Neutral Hydrogen Emission from PLT," J. Nucl. Mater. *145-147* (1987) 527.

[18]R. Budny, "Scrape-off Profiles and Effects of Limiter Pumping in Tore Supra," Princeton University Plasma Physics Laboratory Report PPPL-2404 (1986) 17 pp.

[19]S.L. Allen *et al.*, "Determination of Ambipolar Radial Transport from the Particle Balance in the TMX-U Tandem Mirror," to appear in Nuclear Fusion.

[20]D. Post *et al.*, U.S. Contribution to INTOR Phase 2A Part 3 (December 1986).

[21]C.D. Henning *et al.*, "TIBER II Tokamak Ignition/Burn Experimental Reactor," Lawrence Livermore National Laboratory Report No. UCID-20863 (October 1986).

[22]W.D. Langer, "Penetration of Molecular Impurities at the Edge of Tokamaks," Nucl. Fusion *22* (1982) 751.

[23]W. Eckstein and D.B. Heifetz, "Data Sets for Hydrogen Reflection and their Use in Neutral Transport Calculations," IPP-Garching Report IPP 9/59 (1986); J. Nucl. Mater. *145-147* (1987) 332.

[24]H.F. Dylla *et al.*, "Conditioning of the Graphite Bumper Limiter for Enhanced Confinement Discharges in TFTR," submitted to Nucl. Fusion.

[25]D.B. Heifetz, H.F. Dylla, and M. Ulrickson, "Calculated Particle Inventories in the TFTR Moveable Limiter and First Wall," Princeton University Plasma Physics Laboratory Report PPPL-2353 (1986) 52 pp; J. Nucl. Mater *145-147* (1987) 326.

SPACECRAFT GLOW EXPERIMENT

During FY86, development of the ground-based experiment to study spacecraft glow and extend research efforts into the closely related topic of spacecraft erosion continued. The nature of the glow and erosion on spacecraft surfaces are of fundamental scientific interest and have important engineering consequences for long-term missions involving sensitive optics and electronic equipment in low earth orbit (LEO).

The Atmospheric Explorer and Space Shuttle orbit at altitudes where the atmospheric gases consist primarily of nitrogen and oxygen at densities ranging from 10^8 to 10^{11} cm^{-3}. The orbital speed of these craft, approximately 8 km sec^{-1}, corresponds to a relative kinetic energy for the gas particles of 4 to 10 eV with respect to the surface. The conversion of this energy into excitation of atoms and molecules, followed by emission, can result in the spacecraft glow. The spacecraft surfaces have adsorbed hydrogen, oxygen and carbon in various molecular forms so that chemical reactions may be occurring on the surface. Theories of the glow are based primarily on the idea that the atmosphere acts as a beam of particles (seen from the reference frame of the spacecraft) of several eV undergoing collisions and reactions at the surface. These chemical reactions also remove molecules from the surface and result in erosion. A review of the subject has recently been published.[1]

The conspicuous lack of neutral atom beam studies in the 1-25 eV range of energies is the result of the difficulty in producing neutral beams of high enough flux to make measurements. In the critical range of energies 2-25 eV, the Princeton Plasma Physics Laboratory has demonstrated the capability of producing such fluxes.[2] In the approach taken, an electrically biased metal plate, called a limiter, inserted into a plasma discharge intercepts, neutralizes, and reflects the ions from the plasma. These neutrals reflected from the surface of the limiter produce a beam. The intensity of the beam is determined by the ion current to the limiter, whereas the energy of the beam can be controlled with the bias voltage.[2]

In the past year, experiments have stressed obtaining optical spectra of beam interactions with Chemglaze Z-306 and Kapton. Parameters such as beam energy and composition were varied to see if there were any threshold or chemical effects that might reveal the underlying chemical and surface reactions producing the glow. Production of the glow should be accompanied by erosion, which is an effect observed for Chemglaze and Kapton on the Shuttle. A number of erosion experiments were performed which were highly successful in simulating the space results.

Spectra due to beam-surface interactions on Chemglaze are shown in Fig. 1. The bias voltage was varied to study the effect of kinetic energy on glow-production mechanisms. As the bias potential on the limiter is increased, the underlying continuum appears to increase to nearly 50% of the total signal. Raising the voltage increases the ratio of the relative intensities tentatively assigned to electronic bands $N_2(B \rightarrow A)$ for vibrational states $\Delta v = 3$ and $\Delta v = 2$, the ratio rising from 1.7 to 2.0. It is possible that the molecular nitrogen comes from either recombination or nitrogen atom abstraction reactions involving beam nitrogen atoms with species adsorbed on the target and thus, the incident beam velocity changes the resulting vibrational distribution. Nitrogen atom recombination can also be responsible for some part of the Shuttle glow.[3]

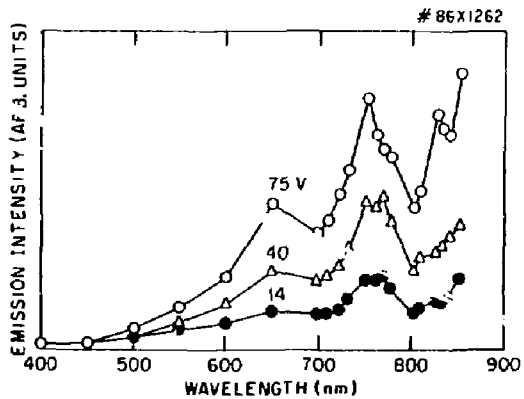

Fig. 1. Spectra of oxygen (5%) plus nitrogen (95%) on a target of Chemglaze Z-306 at different bias voltages. The target is located in the viewing port, out of the field of view of the photomultiplier tube, a few centimeters back of the line of sight. The spectrum appears to have discrete spectral features with [most likely $N_2(B \rightarrow A)$ transitions] on top of an underlying continuum.

To study the oxygen beam-surface interactions, neon was used as a working gas. The spectral features for a Kapton target (Fig. 2) are quite different from those of reflected plasma light. The spectrum

is similar to that observed in nitrogen/oxygen plasmas, showing a "continuum" starting at $\lambda \approx 450$ nm rising sharply into the red part of the spectrum, having broad peaks at $\lambda \approx 650$ and $\lambda \approx 750$ nm.

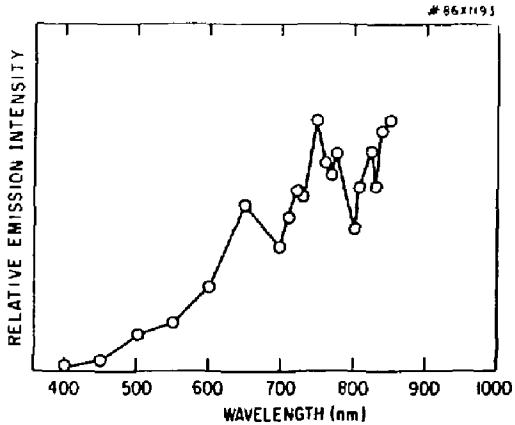

Fig. 2. Spectrum produced by a 10-eV beam of two percent oxygen in neon striking a Kapton target. The spectrum is very different from either the plasma light or a pure neon beam striking the surface. In the latter case the intensity in the far red is enhanced by the presence of oxygen.

The origin of the glow is uncertain. It does not originate from plasma light scattered into the detecting volume. It may originate from long-lived excited molecules created on the target surface by the low energy beam or it may originate from similar molecules created at the limiter, which drift into the glow region and are reflected from the target in emitting states. Much of the data are consistent, however, with collisional excitation of adsorbed surface gases by the incoming beam. A combination of higher resolution spectra and chemical or mass spectrometric determination of the species present near the target will be required in future work to elucidate the mechanisms present in the system.

A series of erosion experiments was also performed to obtain quantitative information on the erosion of carbon and Kapton targets, one of the better studied materials on the Shuttle and one that is observed to glow. The Kapton target (5 cm × 5 cm) was exposed to a 5% oxygen and 95% nitrogen beam with a fluence of 6×10^{19} per cm^2 and a mean beam energy of 10 eV. The erosion was found to be about 1.4 microns, which implies a reaction rate coefficient of 2.0×10^{-24} cm^3 per beam atom, in reasonable agreement with the value 3×10^{-24} cm^3 per atom derived for oxygen alone from Shuttle experiments.[4] If erosion is ascribed solely to the oxygen fluence, the reaction rate coefficient is a factor of 20 higher, suggesting that at these energies nitrogen is nearly as reactive as oxygen. Scanning electron microscopic photographs of our sample as well as those for Kapton samples from Shuttle flights STS-5 and STS-8 were compared. The surface morphology is similar to that obtained in flight, especially during STS-5, where Kapton recession was about 2 microns.

References

[1]B.D. Green and E. Murad, "Surface Reactions and Spacecraft Glow Mechanisms," Space Sci. *34* (1986) 219.

[2]W.D. Langer, S.A. Cohen, D.M. Manos, R.W. Motley, M. Ono, S.F. Paul, D. Roberts, and H. Selberg, "Detection of Surface Glow Related to Spacecraft Glow Phenomena," Geophys. Res. Lett. *13* (1986) 377.

[3]B.D. Green, "Atomic Recombination Into Excited Molecules," Geophys. Res. Lett. *11* (1984) 576.

[4]L.J. Leger, J.T. Visentine, and J.F. Kuminecz, "Shuttle Payload Bay Environment," AIAA *84* (1984) 9548.

COMPACT IGNITION TOKAMAK

Ignition is the major near-term goal of fusion research. Studies have been under way in the United States for some time on the possibility of proceeding to ignition within the resources likely to be available to the national program. The conceptual design work has led to a proposal for a compact (R = 1.2-1.3 m), high-field (B = 10-11 T) tokamak device capable of achieving ignition and equilibrium burn. The name of the device proposed is the "Compact Ignition Tokamak," or CIT. If sited at the Princeton Plasma Physics Laboratory (PPPL), the project could reuse Tokamak Fusion Test Reactor (TFTR) equipment, as well as radio-frequency (rf) power supplies now at other U.S. locations. The estimated cost of CIT is about $300 million, plus operating expenses. At the close of FY86, the federal administration was evaluating the CIT Conceptual Design Report with a view to project authorization in FY88.

In the CIT design, a hydraulic press reacts the vertical separating force on the toroidal-field (TF) coils. The TF and poloidal-field (PF) conductors use explosively bonded laminates of steel and copper to attain the necessary strength and conductivity in the compact configuration. Ion-cyclotron heating in the range 80-110 MHz will resonate with ^{3}He-minority and/or tritium second-harmonic resonances for the full-field pulses, and hydrogen and deuterium resonances during reduced-field trials. The design features a plasma elongation in the range of 2.0 and a double-null poloidal divertor. The plasma current is 9-10 MA and the equilibrium burn time is about 3 sec—roughly $10\tau_E$.

Most of the major U.S. fusion research organizations[1] have specific responsibilities in the CIT project: MIT for the PF system, ORNL for radio-frequency supplies and couplers; GA Technologies, Inc. for the vacuum vessel, its interior hardware and its remote maintenance; LANL for tritium systems and fueling; LLNL for instrumentation and control; PPPL for the toroidal-field system, electrical power, diagnostics, cryogenics, and cooling. FEDC is responsible for design integration and external structure design; and INEL for safety and environmental analysis, as well as conventional facilities.

HISTORICAL BACKGROUND

Until the end of 1983, proposals focused on a facility that cost more than one billion dollars and offered the potential to be nearly prototypical of a fusion reactor. The device would ignite, that is, conditions for the production of fusion power would be maintained by self-heating from the alpha particles of deuterium-tritium fusion. Additionally, experimental times would approximate the resistive time scale in the plasma, several hundred seconds, and operation would test significant engineering features of a reactor, for example, superconducting toroidal-field coils.

Around 1984, the fusion community began to study the option of achieving a burning plasma in a minimum-cost device, while economizing on aspects that will be desirable for the long-term development of fusion power. This led to the consideration of a range of parameters similar to those embodied in the "IGNITOR" (Ignited Torus) concept.[2]

In 1985, four reasonably complete conceptual designs were offered for review in national and international forums. The designs were:

(1) The Ignition Studies Project (ISP) of PPPL,

(2) The Long-Pulse Ignited Tokamak Experiment (LITE) of MIT,

(3) The version of IGNITOR by the FEDC, and

(4) The current version of IGNITOR due to B. Coppi and associates.

By October 1985, the process of selecting a concept for further development was under way. It was followed by the creation of a national organization responsible for developing one concept into a proposal for U.S. Department of Energy (DOE) funding in the federal budget of fiscal year 1988.

BASIC DECISIONS

Technical Concept

The nature of the four conceptual designs can be summarized as follows. All concepts have coils that are cooled to liquid nitrogen temperature prior to operation. No heat is removed from the coils during the experimental time (about ten seconds) during which the temperature of the coil rises to approximately room temperature. While the mechanical stresses in each design exceed the nominal allowable values in common use in the engineering of civil and industrial hardware, the stresses do not exceed values selected by a panel of experts for this particular application. The designs differed in the method used to react the large magnetic forces.

The toroidal-field coils of LITE are self-supporting through use of a high-strength alloy of beryllium and copper. The ISP design incorporates spring-loaded

electrical contacts[3] with the TF coil. This allows the inner leg of the TF coil to experience less of the vertical separating force and hence be smaller in cross section. The vertical separating force of the ISP toroidal-field coils is reacted into a large external C-clamp. Because the TF coil has a slip joint, the TF coil is demountable, and the vacuum vessel can be installed in one piece. This leads to possibilities for a more robust construction of the vacuum vessel than in the other concepts. The IGNITOR design uses a steel clamp aided by a hydraulic press.

In IGNITOR, the TF coils are restrained by the combined action of wedging against one another and bucking on the inner ohmic-heating (OH) transformer. This produces lower stress levels than the wedging-only approach used in LITE and ISP.

The LITE and IGNITOR have an external PF coil set, meaning that the TF and the PF are not linked. For ISP, the poloidal field and toroidal field are linked, but the joint in the TF eliminates assembly problems.

The process of settling on one design approach for further work and for preparation of a proposal involved managers from ISP, LITE, and IGNITOR projects. Guidance was given by the Ignition Technical Oversite Committee (ITOC) and engineering consultants to that committee. Some key points are:

- Combined bucking and wedging in the TF has difficulties with proper fitting and bearing of the surfaces, therefore leading to indeterminate load paths;
- The sliding joint, while workable, would require extensive testing to demonstrate reliability;
- The good plasma behavior commonly associated with a divertor in present-day experiments suggests that a divertor should be incorporated in the next design iteration.

The result of the deliberations was to focus on a design with features of IGNITOR and LITE, but with some additional variants. In particular, a divertor is to be incorporated. Also, the TF and PF coils are to use explosively-bonded laminates of steel and copper, and the hydraulic press is to be added to aid in carrying the vertical separating force on the toroidal field.

Administrative Organization

Concurrently with the process of selecting a design concept for CIT, the Department of Energy and the fusion laboratories agreed on a national organization, shown in Fig. 1, to carry the selected concept to a state of conceptual design suitable for a proposal to DOE. This proposal would be presented to the U.S. Congress for authorization of the CIT in the fiscal year 1988 budget. The Ignition Physics Study Group (IPSG), shown in the organization, represents the community of fusion physicists that gives advice to the CIT project on the suitability of scientific analysis supporting the engineering design.

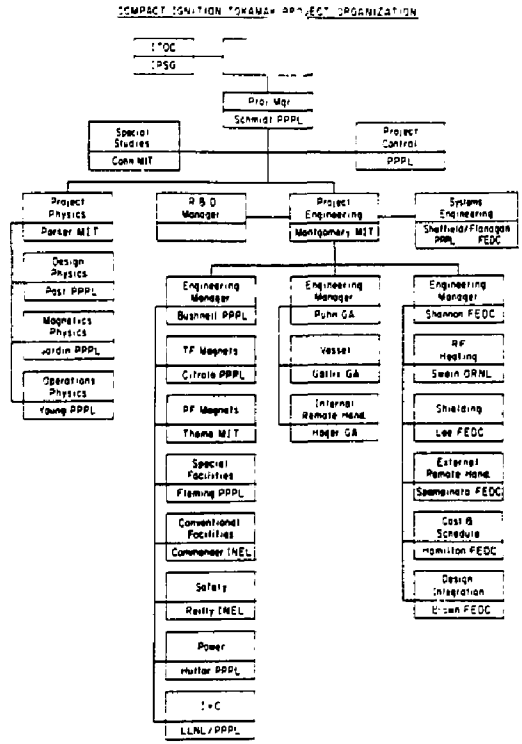

Fig. 1. Organization chart of the Compact Ignition Tokamak. The national nature of the project is indicated by the presence of many widely separated institutions. (86P0245)

From January to June 1986, the participants in the CIT project developed a proposal, including a plan for research development and a plan for diagnostics.[4] The following section summarizes the content of the proposal and associated documents.[5]

Conceptual Design

The mission of the CIT is to achieve ignition at modest cost. This means building a device that has a major radius of 1-1.5 m and a pulse length around 5-10 sec. Criteria were established to make sure that the important parameters of size and time were not reduced without careful consideration. The primary requirements were: that there be an adequate margin to achieve ignition with auxiliary heating for the scaling laws currently under discussion; that the burning last $10\tau_E$ and that the TF be steady for $12\tau_E$; that CIT not exceed certain generally accepted limits on beta (β)[6] and density (n_e)[7]; and, finally, that elongation (κ) and aspect ratio (R/a) be near 2 and 3, respectively. With these requirements, the design summarized in Table I was prepared.

Table I. Important Parameters of the CIT Design.

Parameters (Units)	Value
Major Radius (m)	1.22
Minor Radius (m)	0.45
Elongation (κ)	1.80
Plasma Current, Limiter (MA)	10
Plasma Current, Divertor (MA)	9
Toroidal Field (T)	10.4
Time of Steady Field (sec)	3.7
ICRH Initial Power (MW)	10
ICRH Possible Power (MW)	20
Number of Full-Field Pulses	3,000
Number of Half-Power Pulses	50,000
Fusion Power (MW)	300
Burn Time (sec)	3.1
Divertor Heat Flux (MW/m^2)	9.5

Confinement

Ignition in CIT requires a confinement time of 0.2-0.4 sec, depending on details of the density and temperature profiles. Energy confinement in tokamaks heated with power auxiliary to ohmic heating is commonly discussed in terms of two classes, "L-mode" and "H-mode" — for low and high confinement.[8] However, these two modes have several different parameterizations in the literature. As a result of differences in profiles and differences in confinement models, predictions from computer modeling cover ranges that are quite broad. The range of ignition is compared to the range of predictions in Fig. 2. The top two bars represent predictions of τ_E from H-mode scalings, to be compared with the range of requirements in the bottom (shaded) bar. It can be concluded that, generally, it is possible to gain ignition in CIT, but that there are combinations of models and profiles that will not reach ignition. The remaining unshaded bars show the range of predictions from L-modes. Ignition is possible with L-modes, but somewhat more problematic.

Some results of a time-dependent simulation for an H-mode case with 9 MA of plasma current (appropriate to operation with a divertor) are shown in Fig. 3. The ramp time for both the toroidal field and the current is 3 sec, and 20 MW of ion-cyclotron resonance heating (ICRF) for 1.5 sec is sufficient for ignition. The jagged shape of the behavior of the peak electron temperature [$T_e(0)$] and the peak alpha-particle density [$n_\alpha(0)$] is due to the well-known sawtooth phenomenon in tokamaks. The sawtooth is a relaxation oscillation in the center of a tokamak plasma which causes periodic and rapid expulsion of energy from the center and, as a result, tends to

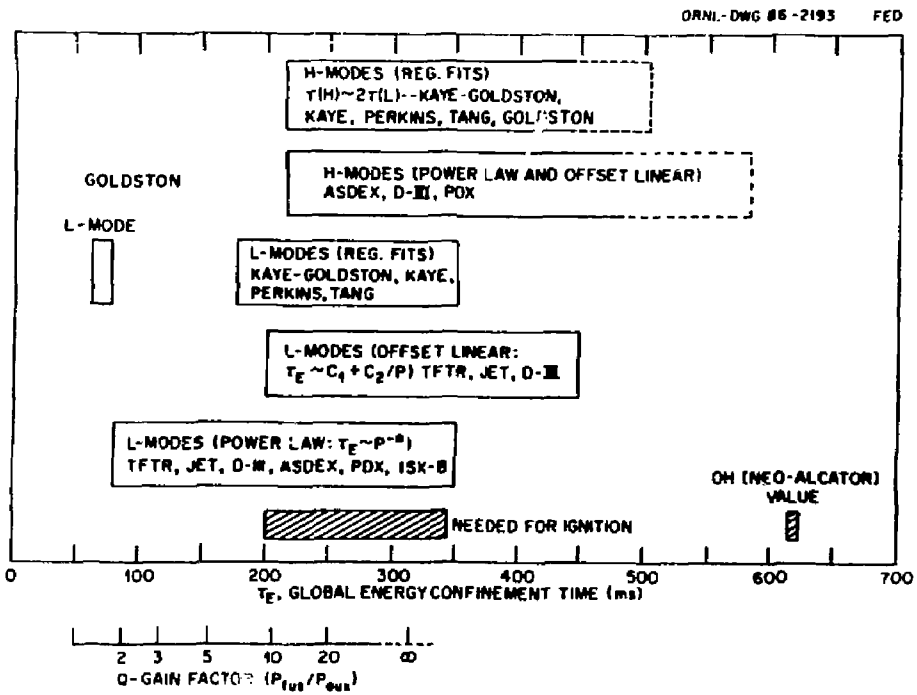

Fig. 2. The range in predicted energy confinement times for CIT using a variety of scalings. The length or each bo: represents the range of predictions using the labeled class of scalings. (86P1072)

resist the temperature and density increases in the center of the plasma required for ignition.

Ignition can be achieved with L-mode confinement if the sawtooth phenomenon can be delayed.[9] The top portion of Fig. 4 shows the result of transport calculations in which two pellets were injected into an initially cold plasma to cause a strong central peak in the density profile; 20 MW of ICRF was then applied to heat the plasma off-axis, at a position halfway between the center and the edge, to delay penetration of the current and the sawtooth relaxation. The lower portion of Fig. 4 shows failure to ignite. The same basic transport calculations were used, but sawtooth activity is present.

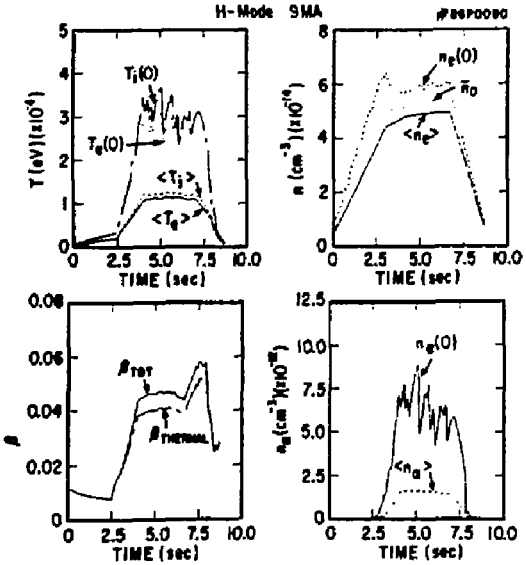

Fig. 3. Time evolutions of the peak and average temperatures, electron and alpha densities, and toroidal beta. These calculations assume H-mode confinement for a 9-MA plasma operating with a divertor.

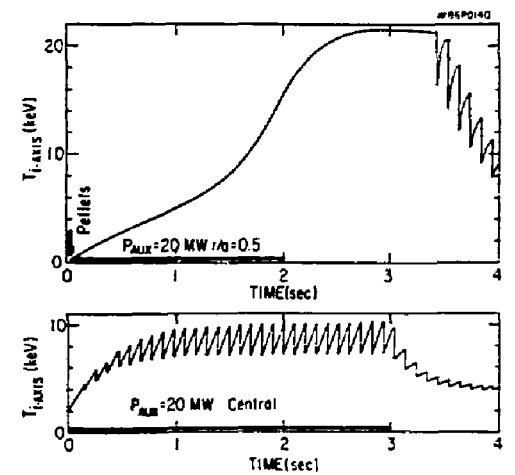

Fig. 4. Time evolution of the central ion temperature for two discharges which are programmed differently, but are assumed to have L-mode confinement. The top curve, which achieves ignition, is created by assuming early large rises in the density and strong off-axis heating to keep the current from penetrating.

Divertor

The CIT has a divertor for two reasons: to aid in improving confinement by making an H mode easier to reach and to help control the density of impurities and fuel particles. Part (a) of Fig. 5 shows a cross-sectional view of the vacuum vessel with divertor plates. The plates are curved on a contour calculated to distribute the heat as evenly as possible after considering the details of the magnetic-field shape and the characteristics of energy flow at the edge of the plasma.

An example of the calculated equilibrium is shown in part (b) of Fig. 5. The Tokamak Simulation Code (TSC) used here[10] also allows study of the active feedback shape control that is necessary because of the high elongation and the close proximity of the vacuum vessel to the plasma. Each of five top/bottom symmetric coil pairs are part of one or more coil groups, which are designed to control the total plasma current, as well as the major radius, ellipticity, and triangularity. As a result, the plasma can initially have a small elongation which is increased in a controlled fashion as the plasma current is increased. Alternatively, with feedback shape control, the elongation can remain high during the entire phase of current ramp. Studies of the stability of the magnetic configuration have shown that cases of ideal-MHD stability exist.[11]

Heat loads in nominal conditions are high, as can be seen in the table of CIT parameters. Of further concern are the heat loads during a disruption, in which both magnetic and kinetic energies appear on the wall of the vessel in a short time. The diagram in Fig. 6 shows one approach to estimating the deposition of energy in a disruption of a plasma at or near an ignited condition. Thermal energy of 36 MJ is added to 42 MJ of the 104 MJ total energy in the poloidal magnetic field, causing 63 MJ to be distributed on a relatively slow time scale to the first wall and the divertor (or the limiter, in case the divertor is not operating), and an additional 15 MJ electron thermal quench lasting 1 msec is distributed to the divertor or limiter. The diagram notes the various power and energy fluxes.

A special arrangement of graphite tiles covers the first wall, as shown in Fig. 7. A somewhat similar construction is envisaged for the divertor plates, but it is not shown.

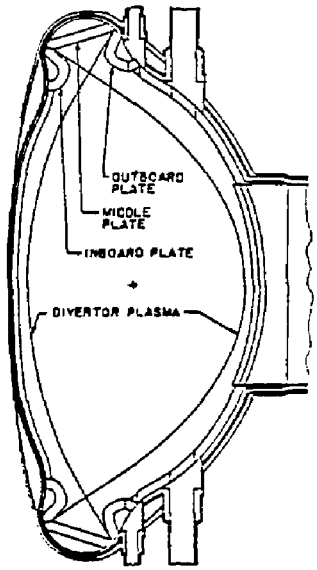

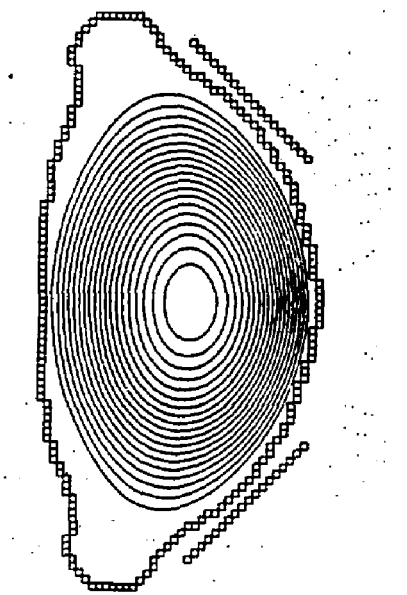

Fig. 5. (a) Cross-sectional view of the vacuum vessel with divertor plates and plasma boundary. (b) Calculated equilibrium in which the vessel and optional aluminum plates for passive stabilization are modeled as square ring conductors. (86P1038 and 86X0713)

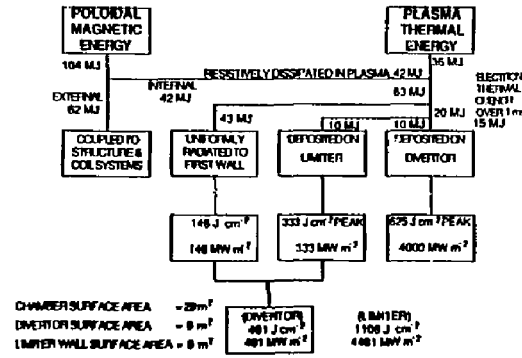

Fig. 6. Estimated energy balance during a CIT disruption with the assumptions given in the text. The maximum power and energy flux loads to the first wall, limiter, and divertor plates are shown. For a limiter, the dotted box applies. (86P1018)

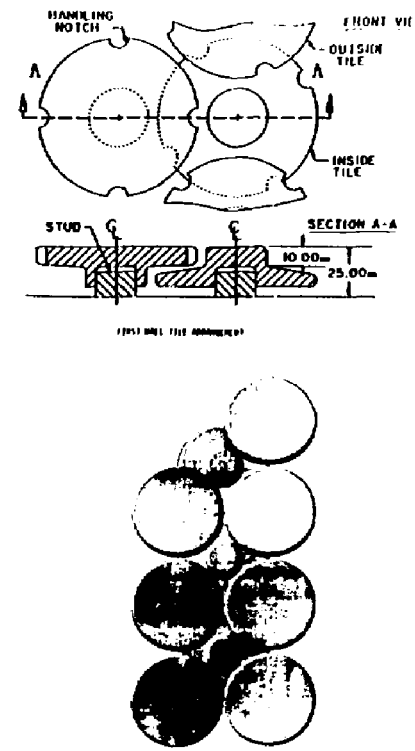

Fig. 7. First wall tile arrangement. Part (a) is a line drawing of the tiling of the vacuum vessel wall. Overlapping disks of graphite, each attached to a central hub, have notches in the side of the disk to facilitate the use of remote-handling equipment for changing tiles. Part (b) is a solid body drawing made by CAD (computer aided design), but without the detail of the notches. (86P1057 and 86P1094)

Heating

Ignition temperatures are achieved through fast-wave ion-cyclotron heating, which has demonstrated efficient ion heating at high power and can be implemented in a high-density tokamak plasma using sources presently available at reasonable cost. The primary heating method has been chosen to be minority ^{3}He and second-harmonic tritium, with a nominal resonant frequency of 90 MHz for full-field operation. To give some flexibility for operating at lower field and with minority ^{1}H and second-harmonic deuterium at considerably reduced field, the power system is specified to cover the range 80-110 MHz, with adjustments requiring a few hours. The alternative choice for heating mode, minority ^{1}H and second-harmonic deuterium, was considered for use in CIT, but has been deemphasized because of the relative difficulties of the higher frequency and because of possible undesired involvement of alpha particles in power absorption.

The single-pass absorptivity of this mode was calculated from a one-dimensional mode-conversion model[12] based on the assumption that wave absorption is dominated by plasma conditions within a small focal spot in the plasma core. Such calculations, illustrated in Fig. 8, are useful in defining the ranges of appropriate minority concentration and parallel wave number. Minority concentrations are measured by the ratio of minority ion density to electron density, and are 5% hydrogen in the top deuterium-tritium (D-T) case, and 5% helium-3 in the lower D-T-^{3}He case. These calculations indicate that absorption is adequately strong over a broad range of parallel wave numbers.

Antenna design requires a trade-off of the conflicting requirements to maximize rf coupling and minimize the damage to the antenna from heat flux from the plasma, which results in significant impurity generation. An antenna array based on presently existing inductive loop technology appears to be workable in the CIT design, provided the loops are adequately protected in recesses in the vacuum wall. The design employs a double resonant loop structure which is protected by a gas-cooled Faraday shield, as shown in a side view in Fig. 9. Estimated loading values of 3-10 Ω are marginally adequate to allow 3.5 MW of rf power per port (6 ports for 20 MW) as necessitated by space requirements on the device. This value of power density (2 kW/cm^2) exceeds slightly that obtained in present experiments and is the most ambitious feature of the launcher.

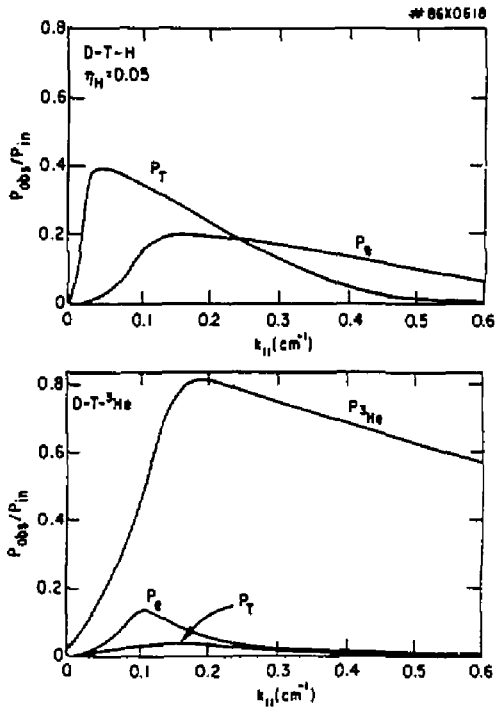

Fig. 8. Single-pass absorption calculations for T = 10 keV, $n_e = 5 \times 10^{20}$ m^{-3} with second-harmonic tritium and a small hydrogen contamination (top) and minority ^{3}He (bottom).

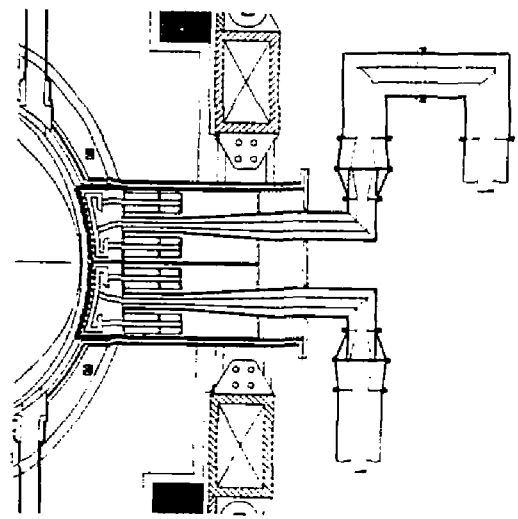

Fig. 9. Side view of the double resonant loop ICRF launcher as mounted in a vessel wall recess. Dual co-axial feed lines enter the vessel through a long and high port, passing between two outboard poloidal-field coils. Power is coupled to the plasma through two resonant double loops, which terminate in capacitors inside the vessel. A Faraday shield prevents improper polarizations from entering the plasma. (86X3278)

Mechanical Design

The toroidal magnetic field is generated by liquid nitrogen precooled coils which undergo adiabatic temperature rise during a pulse. The coils are of modified Bitter coil construction, with the turns cut from plate. The inner leg section of each plate is a composite of copper explosively bonded to Inconel. This permits the turns to withstand the high wedge pressures, while still maintaining relatively high electrical conductivity. The turns are insulated with molded polyimide glass sheets. A partial coil case is provided, supporting the outer and horizontal leg sections for in-plane loading. A tight fit between the conductor and the case is economically obtained by the use of inflatable shims. Stainless steel pillow shims inflated under pressure with silica-epoxy transmit the loads from the turns to the coil case. The coils are edge-cooled with liquid nitrogen between pulses.

A case is required to support the magnet conductors against the out-of-plane loads — overturning moments from the poloidal field interacting with current in the TF coils. The structure supports the vacuum vessel against both gravity and transient loads coming from a disruption of the plasma current. At the interface between sectors of the case, interlocking teeth are used to transmit the high shear forces between coils. The TF coil and case assembly are illustrated in Fig. 10.

The axial separating force in the center legs of the TF coils is reacted by an external preloading system, which also preloads the ohmic-heating solenoid. A total preload of about 250 million newtons (56 million pounds) is applied to the top and bottom of the tokamak by force reacted through the external preload "picture frame" structure shown in Fig. 11. The dynamic pressure is provided by a hydraulic assembly located between the top of the tokamak and the external structure. The hydraulic system is designed to reduce the pressure at the end of the pulse so as to limit the maximum load as the TF coils grow vertically when their temperature rises during the latter portion of the pulse. Consideration is also being given to a fully programmed hydraulic system in which the pressures follow directly the magnetic pressures.

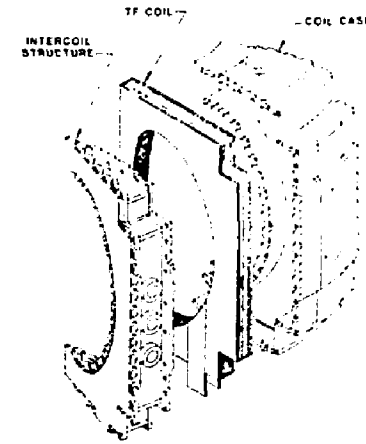

Fig. 10. Toroidal-field coil and case assembly. The square teeth are to transmit overturning forces. (86P1032)

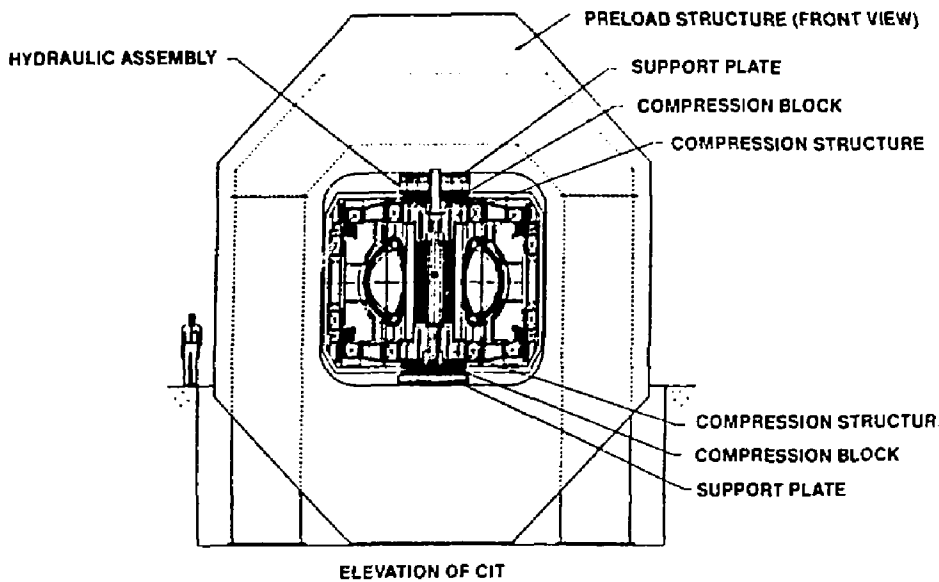

Fig. 11. Diagram of the preload structure which takes the vertical separating force on the toroidal-field coil system. The structure is called a picture frame, and is placed in the building before moving in the preassembled CIT tokamak. (86P1026)

Costs and Schedules

An integrated view of the CIT experiment is shown in elevation in Fig. 12. Figure 13 shows the location of the CIT relative to TFTR and other landmarks, assuming that PPPL is the site eventually chosen. Using that assumption, the cost estimate summarized in the conceptual design report is $285 million in 1986 dollars, including contingency, but not including operating costs of the experiment, research and development (R&D), and plasma diagnostics. The primary milestones of the construction period are: start construction in October 1987, start tokamak assembly in April 1990, and obtain plasma in September 1992. The planned R&D costs about $30 million and focuses on remote maintenance, shielding, magnet design, and the vacuum vessel combined with the first wall. Diagnostics need funding of $24 million through the end of the construction period.

The conceptual design and associated costs were reviewed by DOE groups whose responsibility it is to assure that projects proposed for line-item funding are on a sound basis. Independent cost estimates did validate the CIT project analysis in total, although there were differences from subsystem to subsystem. Reviews of the technical merits of CIT were also positive. As a result, DOE is seeking line-item funding for the project in the federal budget for fiscal year 1988. The response of the administration will not be known until January 1987.

After the Conceptual Design Report was submitted (June 1986), studies continued on the suitability of all design choices. At the end of FY86, changes in parameters of the reference design were being studied. Some of the more basic changes under consideration are a major radius increase to 1.34 m and an increase in the number of large ports from ten to fourteen.

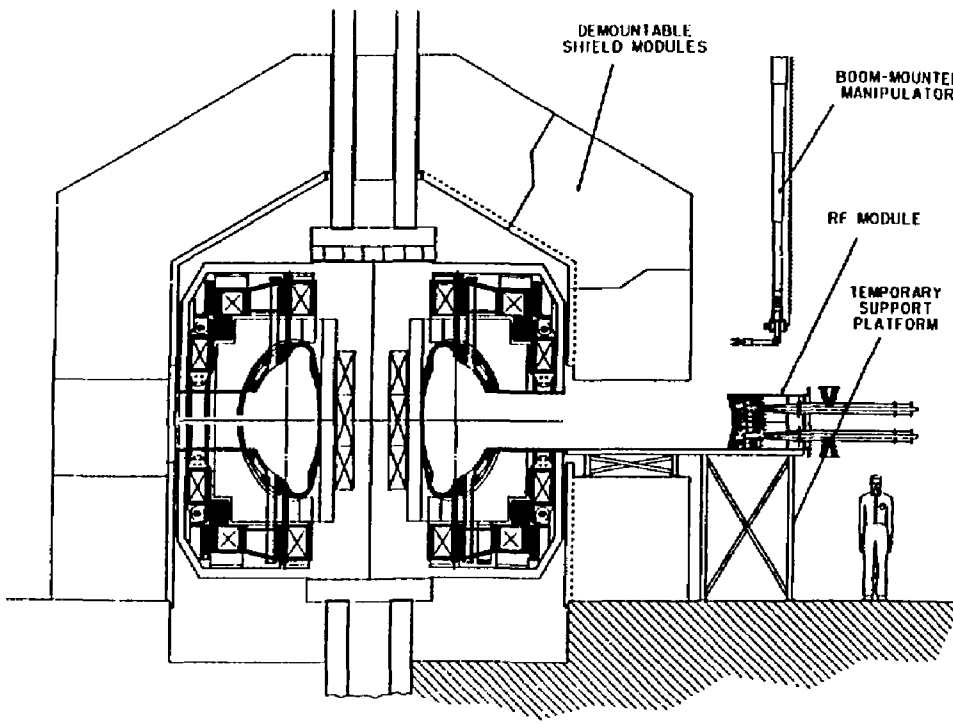

Fig. 12. Elevation view of the assembled CIT, with remote-handling equipment, shield, ICRF lines, picture frame clamp, and diagnostic basement. Note that the plane of the picture frame clamp is out of the figure. The close-in proximity shield is approximately a figure of rotation. (86P1040)

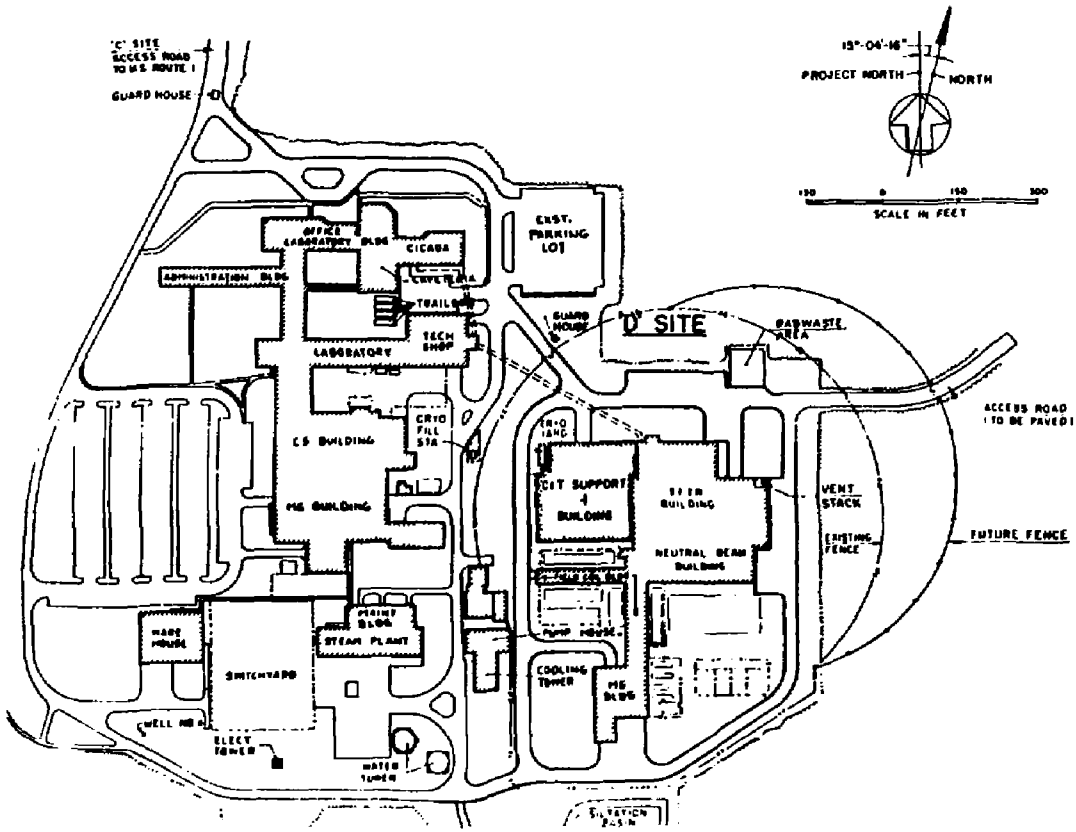

Fig. 13. Plan of the site at the Princeton Plasma Physics Laboratory which might be used for the CIT. The TFTR buildings adjoin the CIT building at D-Site. Other laboratory and administrative areas at C-Site are to the left—west—of CIT. (86P1056)

References

[1]The names of institutions cooperating on the Compact Ignition Tokamak have been abbreviated as follows. MIT is the Massachusetts Institute of Technology in Cambridge, Massachusetts. ORNL is the Oak Ridge National Laboratory in Oak Ridge, Tennessee, operated for the Department of Energy by the Martin Marietta Corporation. LANL is the Los Alamos National Laboratory in Los Alamos, New Mexico, operated for the Department of Energy by the University of California. LLNL is the Lawrence Livermore National Laboratory in Livermore, California, operated for the Department of Energy by the University of California. FEDC is the Fusion Energy Design Center in Oak Ridge, Tennessee. INEL is the Idaho National Engineering Laboratory in Idaho Falls, Idaho, operated for the Department of Energy by the EG&G Idaho, Inc.; GAT is GA Technologies, Inc. (formerly General Atomic), a private company operating a major fusion experiment, the Doublet III-D, with funding from the Department of Energy. GAT is located in San Diego, California.

[2]The most recent document describing IGNITOR is: B. Coppi, A. Airoldi, G. Ambrosino, *et al.*, "Ignitor Project Feasibility Study," ENEA Contract No. 25878, March 1986, 483 pages.

[3]Holt Murray, "High Current Density, Cryogenically Cooled, Sliding Electrical Joint Development," Princeton University Plasma Physics Laboratory Report PPPL-2370 (1986) 42 pp; published in the Proceedings of the Thirty Second Meeting of the IEEE Holm Conference on Electric Contact Phenomena, Boston, Massachusetts, October 27-29, 1986, pp. 109-120.

[4]Conceptual Design Report—Compact Ignition Tokamak, submitted to DOE June 6, 1986; CIT controlled document A-860606-P-01, 317 pages. There are separate volumes for the Research and Development Plan, 63 pages, and for the Diagnostics Plan, 50 pages. The content of the Conceptual Design Report relevant to physics will be published: D. Post, G. Bateman, W. Houlberg, *et al.*, "Physics Aspects of the Compact Ignition Tokamak," to be published in Physica Scripta.

[5]Physics and engineering of the CIT are discussed in the following paper: J. Schmidt, G. Bateman, D. Blackfield, *et*

al., "A Compact Ignition Experiment," in *Plasma Physics and Controlled Nuclear Fusion Research 1986* (Proc. 11th Int. Conf., Kyoto, Japan, 1986), Paper IAEA-CN-47/H-I-2 (IAEA, Vienna, 1987), to be published.

[6]F. Troyon and R. Gruber, "A Semi-Empirical Scaling Law for the Beta Limit in Tokamaks," Physics Letters *110A* (1985) 29-34. The result proposed is that $\beta \geq (2.0 - 2.5)\, \mu_0 I_p/(aB)$.

[7]M. Murakami, J.D. Callen and L.A. Berry, "Some Observations on Maximum Densities in Tokamak Experiments," Nucl. Fusion *16* (1976) 346. It is observed that the average density in units of 10^{13} is numerically equal to (B/R) in units of Tesla and meters for ohmically heated discharges. This equivalence was attributed to current density, or to power density in the general case with auxiliary heating.

[8]S.M. Kaye and R.J. Goldston, "Global Energy Confinement Times for Neutral Beam Heated Tokamaks," Nucl. Fusion *25* (1985) 65-69.

[9]G. Bateman, "Delaying Sawtooth Oscillations in the Compact Ignition Tokamak," Princeton University Plasma Physics Laboratory Report PPPL-2373 (1986) 23 pp; to be published in Fusion Technology.

[10]S.C. Jardin, N. Pomphrey, and J. DeLucia, "Dynamic Modeling of Transport and Positional Control of Tokamaks," Princeton University Plasma Physics Laboratory Report PPPL-2258 (1985) 47 pp; to be published in the Journal of Computational Physics *66* (1986).

[11]A.M.M. Todd, M.W. Phillips, M.S. Chance, J. Manickam, and N. Pomphrey, "Stable Tokamak Access to, and Operation in, the Second Stability Region," in *Plasma Physics and Controlled Nuclear Fusion Research 1986* (Proc. 11th Int. Conf., Kyoto, Japan, 1986), Paper IAEA-CN-47/E-I-2-3 (IAEA, Vienna, 1987), to be published.

[12]P.L. Colestock and R.J. Kashuba, "The Theory of Mode Conversion and Wave Damping Near the Ion Cyclotron Frequency," Nucl. Fusion *23* (1983) 763-780.

ENGINEERING DEPARTMENT

Engineering and Scientific Staff assignments in FY86 involved work in all areas of the experimental program. Of the 143 engineers in the four engineering divisions, 127 worked in multiple and diverse activities, 10 worked on only one job and 6 devoted all of their time to home cost center matters. A decrease in manpower of roughly 7% resulted from personnel transfers to the Tokamak Fusion Test Reactor (TFTR) core group and to other Laboratory projects and from attrition. The multiple activities were spread over all of the experimental projects as well as between subdivisions within projects. Every effort was made to consolidate work into the least number of jobs possible. The average dollar value of an engineering job in FY86 was $101k, up from $94k the previous year.

Two organizational changes were made during FY86. The Engineering Analysis Division merged all of its personnel into two branches: the Thermo-mechanical Branch and the Plasma Engineering Branch. Mechanical Engineering created a Tritium Section in the Vacuum and Cryogenic Branch to respond to the need for greater support of TFTR in its deuterium-tritium (D-T) readiness effort. Personnel were drawn from other activities to staff this section.

Engineering Department efforts in fabrication centered in four major areas. Princeton Beta Experiment Modification (PBX-M) work, as reported last year, involved upgrades in virtually all areas. New coils, both active and passive, were designed and fabricated. New power supplies were designed and procured. Internal vacuum vessel support hardware was substantially modified.

The second fabrication effort was the production of a new flux core for the S-1 Spheromak. This job also began in FY85, as was reported in last year's report. During FY86, the flux core was fabricated, installed, and operated at full specification levels. This work was not completed without some difficulty. In initial electrical testing, there was an insulation system failure that caused roughly a three-month delay in delivery. Because of that delay, work on the S-1 current transformer fabrication was pushed forward. The transformer is to be completed in FY87. Further detail on this work is given in the text.

In-house work was started and contracts were placed by the Engineering Department for a maintenance manipulator for TFTR. This device will provide viewing, leak checking, and some repair capability inside the vacuum vessel without breaking vacuum. Kernforschungszentrum (KfK) of West Germany will provide the operating arm. Centre Energie Atomique (CEA) of France will develop the viewing system and Seiko of Japan the leak detector. The fabrication of a chamber to house this equipment was started at PPPL.

The fourth major project was the upgrade of the PLT ion-cyclotron radio-frequency heating system for use on TFTR. Included was the development of two antenna arrays and associated protective limiters. Antenna design was shared between the Oak Ridge National Laboratory (ORNL) and PPPL. Details of this and the other projects are given in the following division reports.

Support continued for the operation of all experimental devices. At the same time, emphasis continued to be placed on reducing indirect costs. Administrative-type personnel were reduced along with indirect budgets. Safety continued to be stressed by Engineering Department management as a matter of primary concern.

COMPUTER DIVISION

During FY86, the Computer Division concentrated on upgrading and enhancing scientific computing resources in support of the Laboratory projects and programs. A Digital Equipment Corporation (DEC) VAX-8600 computer was installed to replace the obsolete User Services Center (USC) DEC KL-10 computer. New stand-alone minicomputers were installed to support TFTR diagnostic needs. Memory and disk storage were increased on most systems in accordance with an increased demand in computing and storage needs. Software was developed and integrated to support hardware advances and new diagnostics and facility applications. In addition, existing network facilities are being replaced and upgraded with state-of-the-art technology. Requirements were defined for tritium handling, and the Division began to plan for computer support for the Compact Ignition Tokamak (CIT) project.

A listing of publications by Computer Division personnel is given in Refs. 1-6.

Support for the TFTR Central Computing System

The TFTR computer system consists of a network of 13 online Gould/SEL computers, two DEC VAX superminicomputers, and three DEC MicroVAX minicomputers. The system configuration is shown

in Fig. 1. System memory and data characteristics are shown in Fig. 2.

The Gould/SEL Model 32/87 and 32/77 computers comprise the TFTR control and data system. Currently, over 60 distinct systems of diagnostic and engineering applications are in operation. Approximately 16,500 hardware points in a total of 310 CAMAC (Computer Automated Measurement and Control System) crates are monitored every two seconds, and almost 7,000 points are controlled.

The system acquires over 20 megabytes of data for each TFTR shot. From this data, approximately 330 results waveforms are automatically computed and made available for display and for transmission to the TFTR data reduction system (RAX) and TFTR high-level data analysis system (HAX) computers for subsequent reduction, high-level analysis, and archival.

The HAX VAX-8600 computer and the RAX VAX-11/785 computer are part of a clustered configuration. In a cluster, the computers are separate systems but share disk resources, which enables users to move among the central processing units to access information, manipulate data, and, when appropriate, to interact with the large codes available on the supercomputers of the National Magnetic Fusion Energy Computer Center.

During FY86, three DEC MicroVAX minicomputers were integrated into the TFTR computer system. These computers serve as stand-alone control and data acquisition systems, and they are linked to the VAX cluster for transmission of data for data reduction and high-level analysis. The systems currently operating on the MicroVAX computers are: Thomson scattering edge system; charge-exchange recombination spectroscopy (CHERS), which has a special high-speed interface to an image processor; and deuterium pellet injector (DPI), which was developed jointly by PPPL and the Oak Ridge National Laboratory.

Enhancements to the TFTR computer system during FY86 included the following:

- The off-line Program Preparation Gould/SEL 32/87 computer was swapped with the Central Facility ARCHIVE Gould/SEL 32/77 computer, thereby upgrading ARCHIVE. All central facility computers comprising the TFTR control and data system (FACILITY, EXP1, EXP2, and ARCHIVE) were upgraded to six megabytes of memory.
- The main memory for the HAX VAX-8600 computer was increased from 12 megabytes to 36 megabytes. The main memory for the RAX VAX-11/785 computer was increased from 12 megabytes to 16 megabytes. In addition, 3.6 gigabytes of direct access rotating storage were added to the VAX cluster to support TFTR raw data spooling and physics results.

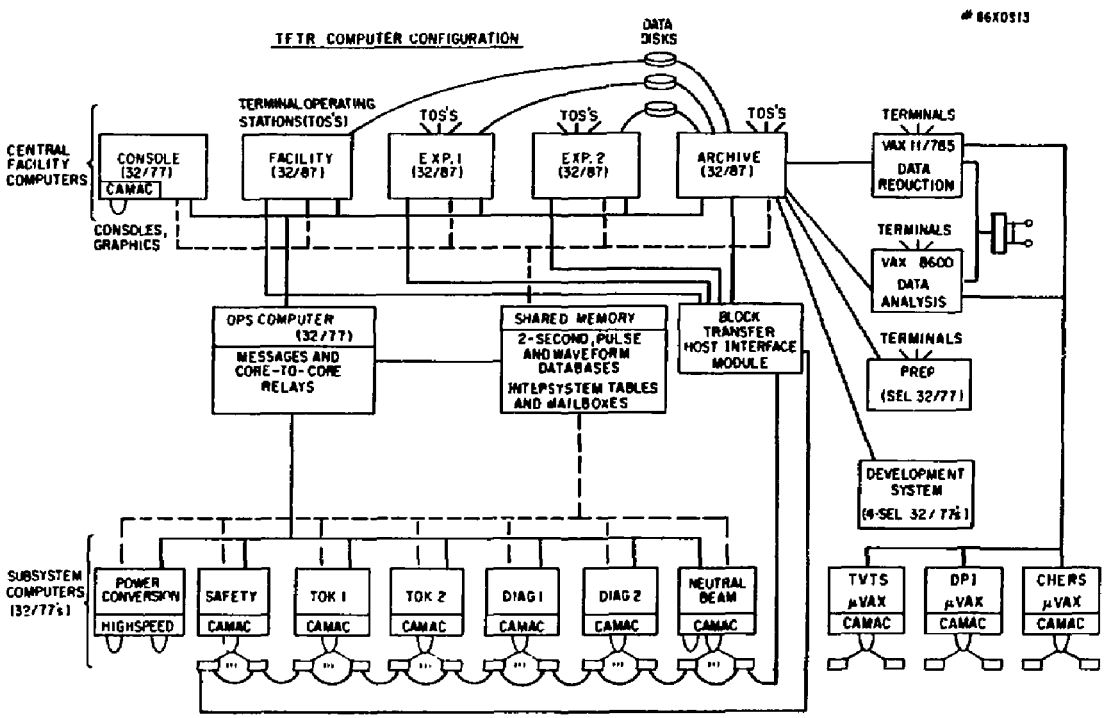

Fig. 1. The TFTR computer system configuration.

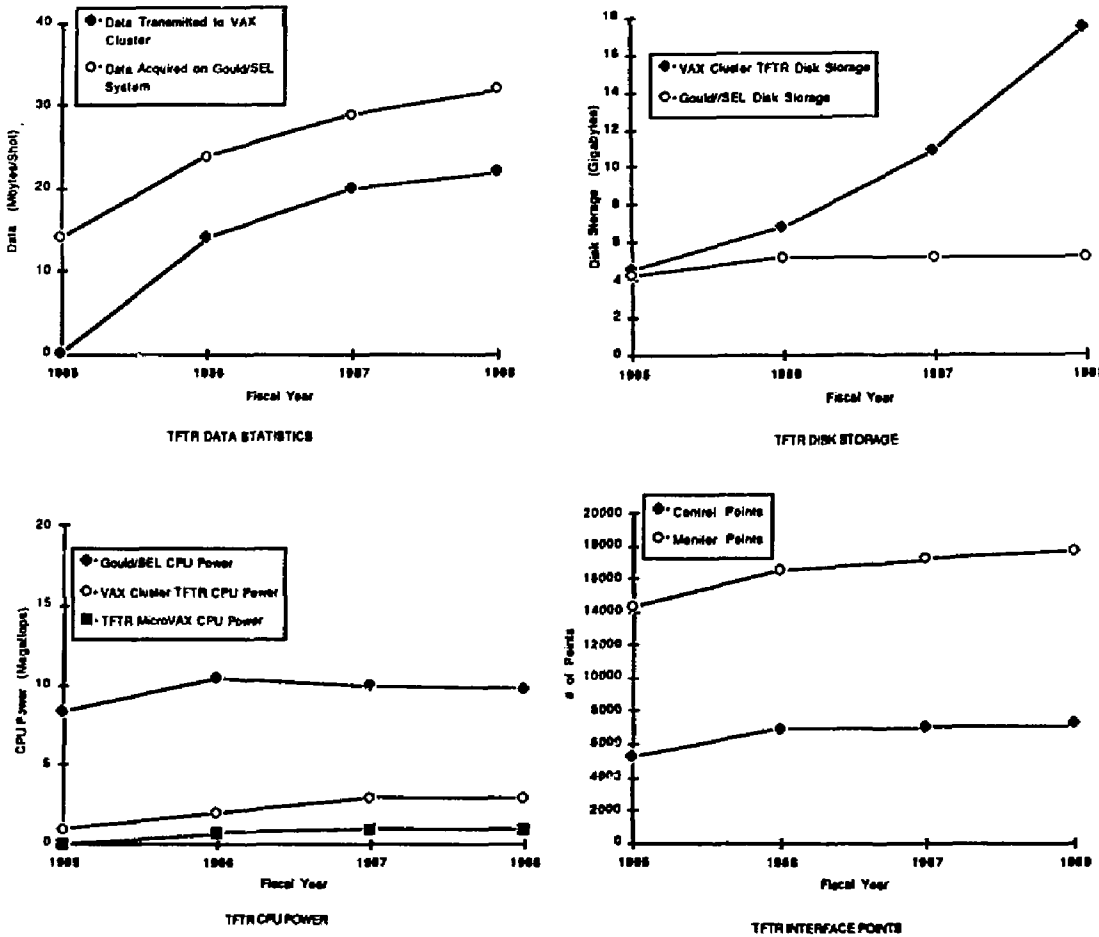

Fig. 2. The TFTR computer system memory and data characteristics.

- The CAMAC interfaces on three of the Gould/SEL subsystem computers were upgraded from nonstandard, custom-built hardware to Kinetics Systems 2070 hardware, which improved reliability and maintainability. Interface software was developed to support this installation. In addition, the old U-port adapter hardware on all CAMAC links were replaced with new, more reliable U-port adapter hardware.
- A status and alarm system was developed. This system displays the values of monitored devices. The system shows abnormal conditions within both hardware and software, so that machine operations personnel may take corrective actions if needed.
- Graphics software was enhanced to increase graphics throughput. As a result, plot production has increased from 40 plots per minute in FY85 to 450 plots per minute in FY86.
- Software was developed to support the transmission of data from the Gould/SEL-based computer system to the VAX-based computer system for archival and subsequent analysis.
- Skimmer software was developed to manage disk space on the VAX-based computer system.
- Terminal operating station (TOS) graphics hardware were developed to increase throughput speeds.

TFTR Neutral Beam, Diagnostics, and Facilities Applications Support

The final two neutral beamlines were integrated and made operational in FY86. A remote control system, which provides for operation of all four beamlines from the TFTR control room, was integrated, tested, and is now operational. The following neutral-beam

systems were installed for all four beamlines: pyrometer system, the general purpose data acquisition system, the water flow calorimetry system, clock system, CAMAC link system, and hardwired interlock system. The neutral-beam optical multichannel analyzer was installed and is operational for two beamlines.

The neutron fluctuation and disruption-thermal-monitor diagnostics were implemented and integrated into the real-time system. Other diagnostic systems were enhanced.

Support of PLT, PBX and PBX-M, S-1

The DEC-based data acquisition system's DEC KL-10 and VAX-11/785 computers continued to support PLT, PBX, and S-1. Memory for the data acquisition system supplemental VAX system (DAX) was increased from 12 megabytes to 16 megabytes, to aid in more efficient machine usage.

A substantial effort was begun to prepare for migrating from the obsolete DEC KL-10 computer to a VAX-8600 computer. Software conversion efforts are underway to prepare for the upgrade.

The PBX control system is being replaced with a new system based on programmable logic controllers (PLC). The system will control all human-machine interface to PBX-M, including the power sources, motor generator sets, and water, vacuum, and safety systems. The PLC's are scheduled to be implemented in early calendar 1987.

Plans were developed to allow PBX-M and S-1 to run concurrently, and to acquire up to seven megabytes of data on a four-minute shot cycle.

New Computer Systems and Network Facilities

The obsolete DEC KL-10 USC computer was replaced with a VAX-8600 computer during FY86. This computer, which was integrated into the VAX cluster configuration, serves both the general and scientific computing needs at the Laboratory.

Networking throughout PPPL was upgraded during FY86. PPPL's Digital Communications Associates terminal network was replaced by a MICOM Micro 600 Port Selector. This allows the network to manage adequately the medium and high-speed (4800-9600 baud) graphics requirements associated with all the host computers supported by PPLNET (i.e., the VAX cluster computers and the Gould/SEL computers).

Work began on an Ethernet-based file transport network that will connect the computers of the VAX cluster and the three TFTR control and data acquisition MicroVAX computers.

Design Activities in Support of TFTR and CIT

During FY85, engineers within the Computer Division began the design effort for a tritium remote control and monitoring system to support TFTR tritium operation. This system, which will interface to approximately 1,600 input/output points throughout the facility, will support automated control, remote control, and monitoring for the tritium handling equipment used to store, deliver, and contain tritium for TFTR. The procurement specification will be prepared and released during FY87.

The Computer Division also began to review the requirements for computer support for the Compact Ignition Tokamak (CIT). A task force of both hardware and software engineers developed a preconceptual design for a computer system that would perform control, monitoring, and data acquisition and analysis for CIT.

ENGINEERING ANALYSIS DIVISION

The role of the Engineering Analysis Division (EAD) is to support the physics programs of the Laboratory and the national fusion effort by providing evaluation and planning of a new and upgraded experiments, conceptual and preliminary engineering design services, and systems engineering services. The EAD also develops and maintains computer programs for design and analysis and performs engineering and scientific analyses in specialized areas of technology such as radiation, solid and fluid mechanics, heat transfer, vacuum and cryogenics, superconductivity, electromagnetics, and field design.

During this fiscal year, the organization of the EAD was streamlined by merging the four technical units into two branches: the Thermomechanical Branch and the Plasma Engineering Branch.

Thermomechanical Branch

The Thermomechanical Branch provides a broad spectrum of capabilities in engineering mechanics, finite element analysis, thermal analysis, and mechanical design. Most of the activity for this year centered on the TFTR project and included a substantial amount of nonlinear finite element analysis (FEA), performed in support of CIT.

TFTR/TFM/OSES

Engineering support of the TFTR project was a primary activity of the Branch. Much of the TFTR work centered around the Operations System Engineering Support (OSES) project which was performed by

Grumman Aerospace Corporation under an EAD-directed subcontract. One objective of the OSES project is to determine the stress levels in the poloidal-field coils on TFTR. In addition to monitoring and verifying the work of the subcontractors, the Thermomechanical Branch performed the FEA for five of the nine poloidal-field coil stacks on TFTR.

The models that were developed for the OSES project were run with separate radial, vertical, and thermal loads. The output from these runs were analyzed, and the stress coefficients were extracted for use in the TFTR systems code. These coefficients enable the calculation of critical stresses in the TFTR poloidal-field coil system for any operating scenario. A review of the allowable interlaminar shear stress in the insulation was performed in support of this task. This review included an extensive literature search which obtained all available test data. The results of the search were combined with the existing data base from the TFTR Research and Development Activity (RDAC) program to provide a sound basis for determining allowables.

The Branch also supported other areas of the TFTR project. A preliminary analysis of the Mode-D coil configuration on TFTR was conducted. This configuration, if implemented, would increase the volt-second capacity of the poloidal-field coil system. The results of this analysis were encouraging.

A code that calculates scrape-off layer heating and/or disruption heating of a generic limiter in TFTR was developed and used in the design of a carbon/carbon radio-frequency (rf) limiter.

The feasibility of cutting a hole in the center plug of TFTR was investigated. The purpose of the hole is to gain access to the machine floor beneath the internal support structure (ISS) and thus enable replacement of the shim blocks between the toroidal-field coils and the ISS. A detailed finite element analysis of the plug was initiated.

Additional thermal and mechanical analyses of the toroidal-field coils were performed in order to study the behavior of the coils under upgraded loading conditions.

PBX Modification

A complete dynamic analysis of the PBX-M vacuum vessel was performed. This analysis used NASTRAN substructuring techniques and image superelements.

During fabrication of the passive coils, some delamination of the explosion-bonded plates occurred. A nonlinear analysis of the forming process was performed in order to determine the requirements for fasteners which would prevent delamination.

A finite element analysis of the toroidal-field coils was performed.

Compact Ignition Tokamak

The Branch lent considerable support to the ongoing effort to design the Compact Ignition Tokamak (CIT). A complete structural analysis of one toroidal-field coil configuration was performed. Figures 3 and 4 show the response of the toroidal-field structure to the out-of-plane loading produced by the interaction of the current in the toroidal-field coils and the magnetic field produced by the poloidal-field coils. This structural model simulates the presence of all of the other toroidal-field coils in the machine by the use of appropriate boundary conditions, and it provided the opportunity to study in detail the structural performance of the proposed design. Figure 3 shows the full model (coil and case) while Fig. 4 shows the case alone. Using loads calculated by the Massachusetts Institute of Technology (MIT), the CIT design was analyzed for preload, toroidal-field loads, divertor loads, and limiter loadings.

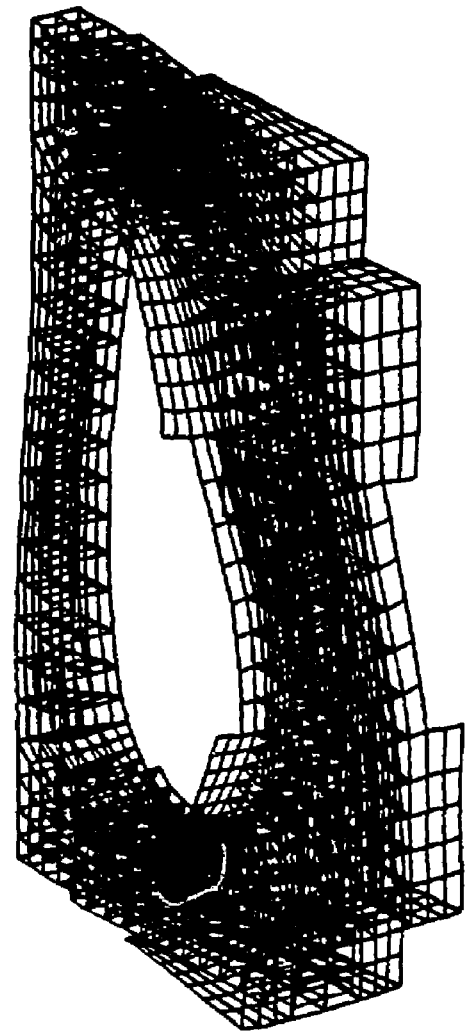

Fig. 3. Deformed shape of CIT toroidal-field coil model showing coil and case. (87E0447)

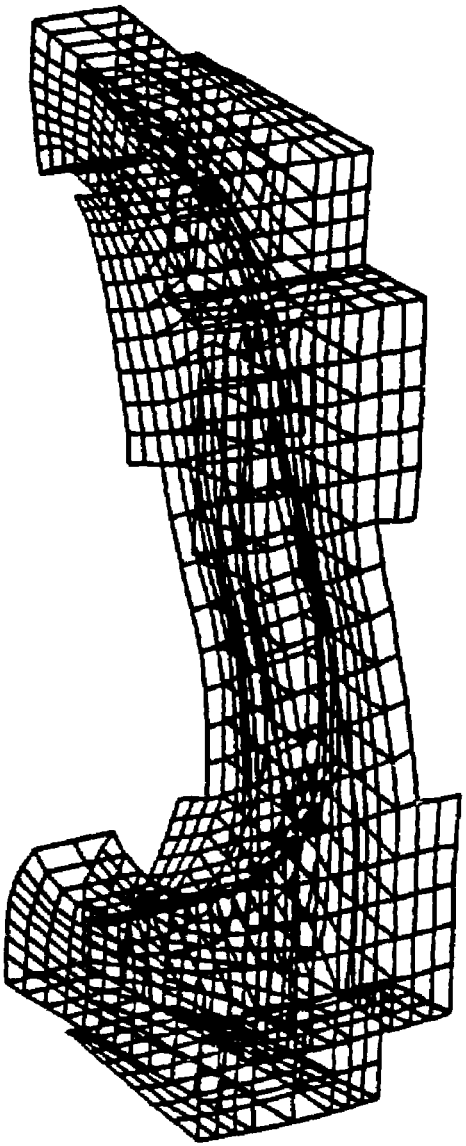

Fig. 4. Deformed shape of CIT toroidal-field coil model showing coil case only. (87E0446)

Nonlinear stress analysis was necessary for some parts of the CIT design. The Branch performed some nonlinear finite element analyses in order to assess the feasibility of the present CIT design. Much of this work was aimed at verifying and understanding the preliminary structural tests of the copper-Inconel laminate proposed for use on CIT. Figure 5 shows a comparison of test data with calculations.

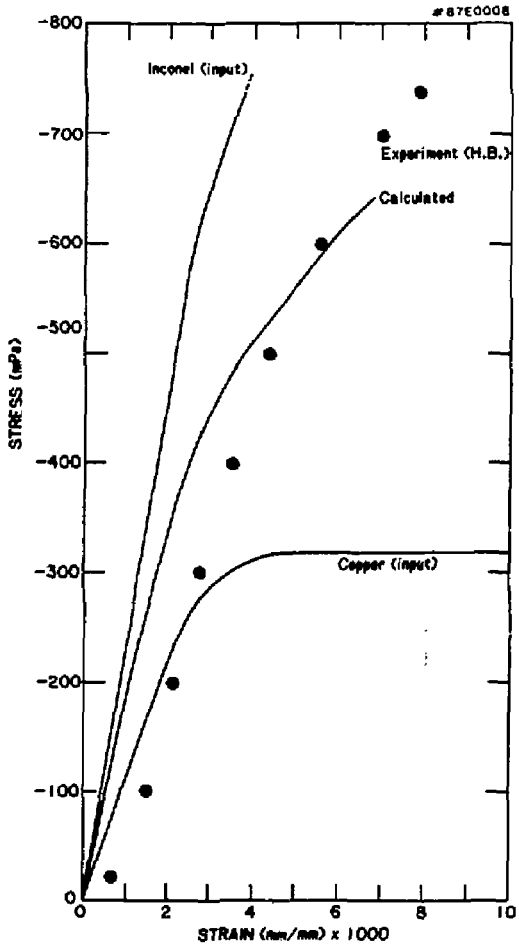

Fig. 5. Comparison of experimental data from compression test of laminated conductor with results of nonlinear finite element analysis.

S-1 Spheromak

A nonlinear finite element analysis of the toroidal-field coil was performed.

Plasma Engineering Branch

The Plasma Engineering Branch combines the functions of the technical units that were previously known as the Systems Group, Radiation Analysis Group, and the Electromagnetics Branch. This reorganization combines the functions that are necessary for the conceptual design of fusion devices into a single operating unit. The branch provides overall systems support for large experiments, from the preconceptual design stage to the start of

operation. Design and analysis of magnetic field systems and their interaction with the associated electrical and mechanical systems are performed. In addition, the Branch performs radiological and radiation-related analyses, evaluation and assessments for the design, operation, and instrumentation of experimental devices at PPPL.

Compact Ignition Tokamak

Systems studies were performed to size CIT and to understand the sensitivity of the physics performance to variations in the design parameters. The device requirements were tailored to stay within the performance envelope of some TFTR resources, in particular the motor generator (MG) sets and power supplies. As a result of these studies, a boundary was found within which a set of device parameters can be chosen that satisfy the physics objectives, cost constraints, and engineering requirements.

The sliding-joint development program was concluded in February 1986. After 400,000 power cycles, the majority of which were run at liquid nitrogen temperatures, a single concept was found to have superior performance. This concept was based on a contact system developed over five years ago by Westinghouse. More than four million such systems have been installed in various applications.

In early summer, a program was initiated to demonstrate the feasibility of a composite conductor through manufacture, testing, and analysis. The materials used were C10700, a silver bearing copper, and age-hardened Inconel 718. All raw materials were manufactured, processed, characterized, and delivered to two fabricators of explosion-bonded metals. An extensive test program has been developed at PPPL which complements the work of each vendor.

Field penetration studies were performed on the toroidal-field coil system. These studies included the dependence of resistivity on temperature and the toroidal-field ripple at various field penetrations. A circuit analysis for the poloidal-field system was initiated.

Radiation analysis was carried out for generic device shield penetrations in order to assess the impact of these penetrations on diagnostic systems.

Plasma Transport Modeling

In cooperation with the Applied Physics Division, the Plasma Engineering Branch participated in plasma transport modeling. Efforts were made in three areas: edge neutral transport, development of 1½-dimensional transport simulation, and the simulation of CIT physics performance. Specific activities included the documentation of the user's guide for the DEGAS code, implementation of methane physics into DEGAS, development of a semiempirical calculation of electron thermal diffusivity, and the development of a zero-dimensional plasma performance contour generator (POPCON). This code was used extensively to compare the ignition potential and auxiliary heating requirements for various CIT options, using different confinement scalings.

TFTR Systems Code

The TFTR systems code is used to determine safe operating limits for the machine and to improve its operation. This year, the code was refined by drawing on the experience and data obtained from the OSES project to develop a set of algorithms that predict the thermal and mechanical behavior of the coil systems. Peak stress levels in any coil can be calculated for any machine operation scenario by using the systems code in conjunction with the TFTR electrical simulation code, POCOES. The accuracy and efficiency of the algorithms was substantially increased, and extensive graphic display capabilities were added to the code. These algorithms are directly applicable to the implementation of the real-time coil protection calculator.

Radiation Transport Analysis for TFTR

Detailed three-dimensional calculations of the radiation fluences in the TFTR diagnostic basement were completed and the results were summarized and reported.[7,8] The methods and models used were found to be reliable and useful for predicting the radiation levels of future TFTR configurations. Shielding design analyses for the diagnostic systems in the TFTR basement were also rendered more reliable with these results.

Neutronics Analysis for TFTR Diagnostics

Higher radiation levels in the diagnostic basement are anticipated as a result of the decision to leave five large floor penetrations open through the deuterium-deuterium Q = 1 phase. New shielding requirements were determined for the vertical pulse-height analyzer (PHA), vertical charge-exchange neutral analyzer (CENA), and the X-ray crystal spectrometer (XCS). A shield-optimization study of the horizontal CENA was performed. Detailed three-dimensional calculations were performed in order to evaluate the final shield design for the vertical X-ray imaging system (XIS).[9] In investigating the feasibility of deuterium-tritium-fusion gamma-ray diagnostics, radiation transport calculations were performed to determine the relative attenuation of neutron and gamma ray fluences through a diagnostic penetration with a borated polyethylene plug.

Lithium Blanket Module

Neutronics analysis was performed for the experimental lithium blanket module program.[10] In addition, the Lithium Comparison Code (LCC)[11] was written to compare the computational results with experimental data.

Meteorological and Radiological Analysis

Meteorological data for TFTR were processed and summarized for the period from January 1984 to December 1985.[12] These data were used to evaluate the expected TFTR off-site dose due to any release of tritium, to ensure compliance with the guidelines set by the Department of Energy.[13]

TFTR Ohmic-Heating Electrical Upgrade

The increased volt-second requirements of the TFTR ohmic-heating system will require an upgrade of the electrical supply. Various options were studied and one, the reduction of the impedance of the ohmic-heating feeders, was selected for implementation.

Thermal Analysis of TFTR Electrical Components

The thermal properties of critical components such as thyristors, power diodes, and rectifier transformers were investigated. The study showed that the rectifier transformers were adequate for service beyond the design limits.

TFTR Motor Generator Power Upgrade

A variety of techniques were investigated for augmenting the energy that can be extracted from the MG sets, and the most promising alternatives were selected for further development.

Plasma Circuit Analysis

A computer code that treats the plasma as a circuit element was developed to simulate the bouncing plasma experiment. This simulation, which includes the field coils on TFTR, is able to model vertical plasma movement and was benchmarked against experimental data. The importance of modeling the toroidal-field coils in field penetration calculations was revealed as a result of this work.

This analysis was also used for modeling of vertical disruptions and for the TFTR magnetic reconfiguration.

S-1 Spheromak

Extensive magnetics work was required to design the current transformer for the S-1 upgrade. This work included additional circuitry, a new poloidal-field coil pair for the pulsed equilibrium field, and eddy current analysis for the Inconel liner of the current transformer.

ELECTRONIC AND ELECTRICAL ENGINEERING DIVISION

The Electronic and Electrical Engineering Division was involved in a majority of the ongoing Laboratory research programs in FY86. This involvement was in the areas of design, development, installation, maintenance, operation, and specification of electronic and electrical equipments. In addition, the Division contributed significantly to three of the Laboratory's newer programs: for the Compact Ignition Tokamak (CIT), substantial electronic and electrical engineering contributions were made in several areas, with special emphasis in the power and diagnostic disciplines; for the PBX Modification (PBX-M) program, the Division provided guidance in the power and program management activities; for the TFTR Ion-Cyclotron Radio-Frequency (ICRF) program, the Division made major contributions to all phases of the operation. This program is an example of excellent project and engineering coordination and cooperation.

In FY86, the Electronic and Electrical Engineering Division maintained a high standard of engineering design and performance and continued to expand its technical capabilities. Some of the more significant examples are: use of 68000 microprocessors in several newly designed systems; adoption of the VME bus standard; widespread application of Programmable Array Logic devices; continued use and expansion of the Eurocard packaging standard; Division-wide personnel training in and use of personal computer circuit-design analysis programs; studies in the use of gate turn-off thyristor technology for fusion-related power conversion systems; and computation and automatic setting of matching stub settings for ICRF. The TFTR ICRF program also included a design application for the Eimac X-2159 vacuum tube at elevated power levels that use it to its maximum capacity.

Radio-Frequency Branch

RF Operations Section

The PLT 30-MHz ICRF sources were used extensively throughout the year. These systems will be upgraded and used on the TFTR ICRF Project, an $11 million program authorized in March, to provide 6 MW of ICRF heating on TFTR by June 1987 with an additional 4 MW by April 1988. The four high-power radio-frequency (rf) sources used on PLT will be modified in place, with the output power fed via nine-inch coaxial transmission lines from C-Site to D-Site.

Two 30-MHz sources will be modified to provide 5 MW each of output power at 47 MHz; as part of the redesign, a new interstage amplifier will be used

to improve stability. Similarly, the two 80-MHz Fusion Materials Irradiation Test (FMIT) facility transmitters will remain in place at C-Site and be upgraded to provide 2 MW each at frequencies between 40 MHz and 80 MHz.

Two antenna arrays in the TFTR Test Cell will couple the ICRF power to the plasma. These antennas will have tuning components near TFTR that will keep the voltage standing wave ratio (VSWR) on the transmission lines leading out of the Test Cell to less than 4:1. Fine tuning for these lines is done in the rf enclosure (RFE) in the TFTR mock-up area to minimize the power losses in the coaxial transmission lines spanning the distance from C-Site to D-Site. A μVAX II processor will be used in conjunction with the main TFTR computer in the TFTR ICRF control subsystem. The conceptual designs and some final designs for all subsystems of the TFTR ICRF equipment were completed in FY86.

The RF Operations Section continued to support the TFTR diagnostic neutral-beam (DNB) system. The rf break-down oscillator was operated successfully at twice its original power output and will be modified in FY87 to improve its long-pulse capability.

The Section did the restoration and repair of some of the TFTR Field Coil Power Conversion (FCPC) rectifier and bypass modules that had experienced catastrophic failures and extensive damage. These modules were completely dismantled, decarbonized, and reassembled with new (or 100% tested) reclaimed components.

RF Projects Section

The RF Projects Section continued to support the microwave diagnostics on PLT, TFTR, and the Lower-Hybrid (LH) Electron-Cyclotron Resonance Heating (ECRH) and fast-wave experiments on PLT. In addition, the Section undertook project management of the ICRF system for TFTR in March.

The 2.45-GHz lower-hybrid system was modified for operation with a new, sixteen-waveguide antenna to side-launch 1 MW of power in addition to the 500 kW of power that is top-launched (see Figs. 6 and 7). After assembly in the Matterhorn Vacuum Shop and installation on PLT, the new antenna was easily commissioned and attained full-power operation. The results of subsequent plasma heating experiments with the new antenna have been very successful. After the PLT shutdown, it is planned that the three 2.45-GHz 500-kW klystrons from this system will be shipped to the Max-Planck Institut für Plasmaphysik, Garching, West Germany to be used for about two years in a 3-MW experiment on Axially Symmetric Divertor Experiment (ASDEX).

Work on the 60-GHz ECRH system concentrated on minimizing losses in the bends of the corrugated waveguide system. Although the single gyrotron was operated at its maximum rating of 200 kW into a dummy load, only 60-70 kW was achieved at the antenna. Efforts were made to correct the dent-sensitive waveguide bends, but other priorities

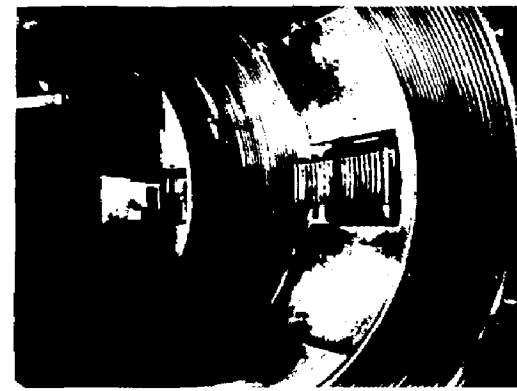

Fig. 6. Sixteen-waveguide 2.45-GHz antenna for PLT.

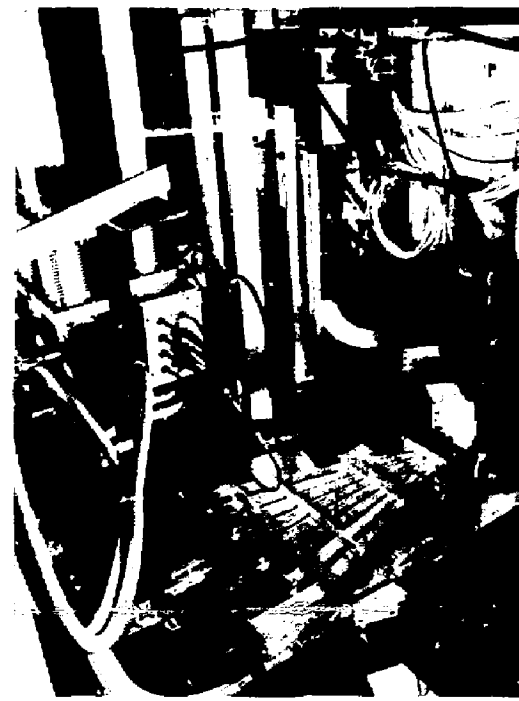

Fig. 7. Transmission line system for sixteen-waveguide antenna. (86E0959)

appeared and the electron-cyclotron heating work was not continued beyond February 1986. This work is documented in three referenced publications.[14-16] It is planned that this equipment will be lent to the University of Texas for experiments on the TEXT machine.

Modifications to the 800-MHz system to adapt it to the new fast-wave Grumman coupler were

completed this year. Experiments with this coupler will be completed early in FY87.

The PLT 2-mm interferometer was modified and improved by increasing the power of its millimeter-wave source. Other work in millimeter-wave diagnostics included: development of a new rectangular waveguide with corrugated wall for transmission of overmoded 300-GHz power and design of a 60-GHz scattering system for TFTR, to be built during FY87.

The Section provided engineering support to the neutral-beam program throughout the year.

Power Branch

AC Power Section

The AC Power Section continued to provide installation and operational support to TFTR. This support was a significant factor in improving overall reliability and availability of the motor generator (MG) sets and the ac power system for high-power pulsing (HPP) operations. Design was completed for the power system modifications necessary to upgrade the TFTR ohmic heating (OH) volt-second system, and procurement of materials and equipment was initiated. An investigation on the feasibility of operating the TFTR motor generators in the super-pulse region was also completed; modifications to the control system are in progress. Finally, power system modifications were completed for the repeating pneumatic injector (RPI) system as part of the changeover to the deuterium pellet injector (DPI) system.

In FY86, the Section's broad range of Laboratory-support tasks included the continued planning, coordination, and implementation of the Laboratory-wide, subcontractor-conducted, ac transmission/distribution/generating system preventive maintenance program. This program identifies inoperative/fault-prone components, resulting in early identification and repair. As a next phase to this electrical preventive maintenance subcontract, an expanded specification was authored, bid, and evaluated; award is imminent.

Designs were completed for three major General Plant Projects, including replacement of two PCB transformers, upgrade of TFTR ring bus emergency power system, and replacement of two 138-kV disconnect switches with SF6 circuit interrupters. Installation was completed for trip and alarm provisions to all remaining indoor PCB transformers. Procurement, installation, and start-up were successfully completed for a new 5-kV feeder to the CICADA substation, providing immediate access to TFTR's emergency generator.

Design was completed, and procurement initiated for the major power system equipments associated with the modification of the PBX-M power supplies.

Additional tasks performed by the Section included: successful installation and start-up of the tritium motor control center; addition of back-up battery chargers to the TFTR MG and FCPC battery banks; procurement and receipt of necessary TFTR power system spare parts; identification, removal, and repair of a gassing pulse-power transformer (Fig. 8); support implementation of a PSE&G-PPPL interruptible power contract; and conceptual design support for CIT power system equipment.

As in FY85, the Section continued its review, inspection, and supervision of construction-related activities. Included in this task were the upgrading of site drawings to accurately reflect the status of various electrical equipment and the design completion and procurement of energy metering components.

Fig. 8. Personnel from the AC Power Section coordinating rigger removal of the faulted PLT/PBX transformer QT2. (8650807)

Motor Generator Section

In FY86 the C-Site Motor Generator (MG) Section accomplished the following:

Three high-speed dc circuit breakers were remanufactured and returned to the Laboratory. They were power tested to 25,000 amperes dc by MG technicians and were found to be acceptable with only one unit requiring minor correction.

The phase-connecting boots for the liquid rheostats of the 7,000-horsepower motors were replaced. The boot design was the result of cooperative efforts by the Electronic and Electrical Engineering and Mechanical Engineering Divisions.

A peak-current-reading digital ammeter was designed, built, and installed by the MG Section. This ammeter is used on the 30-kW multiamp-dc breaker tester and is accurate to three quarters of one percent. The unit responds correctly to high-speed breaker tripping currents of 21 kA, despite tripping times as short as 51 msec.

The project to install eight new Leeds and Northrup microprocessor-based temperature recorders in the C-Site MG control room was completed. A project to design and construct a powered test stand for performing break-down maintenance on the dc resistor breakers was also finished.

Rotating blue beacon lights were installed in the MG basement to warn if the carbon dioxide used for fire extinguishing in the motors and generators is released by the fire detection system.

Motor generator technicians became proficient in the use of the new digital rotational balance and alignment tools, especially in support of the TFTR pump room water systems' pumps and motors. Motorized safety disconnects were installed to provide PBX discharge cleaning and coil alignment for the PBX modification.

Preventive maintenance subcontracts were renewed as a time and material subcontract to allow the Laboratory optimum flexibility for preventive maintenance work orders.

Power Conversion Section

Installation of TFTR neutral-beam heating system electrical apparatus continued. Work was completed on design, fabrication, and start-up of CICADA interface equipment, as well as on control elements for neutral beamline vacuum and cooling subsystems. TFTR neutral beams are now operated from CICADA controls, as opposed to the semiannual operation previously required. One-half of the Section personnel were placed on extended temporary assignments as TFTR neutral-beam operators; the others continued to work on tasks such as the long-pulse modification for the TFTR neutral-beam power supplies.

The Section contributed substantially to the design, fabrication, installation, and start-up testing of the TFTR diagnostic neutral-beam system. In addition, maintenance services were supplied for the system. The Section also participated in the characterization (determining limitations) of the TFTR field coil power conversion (FCPC) control system supplies; the supplies were carefully tested and evaluated to determine adequacy of performance. Substantial contributions were made to the FCPC/CICADA interface specifications.

Since its installation in FY85, the bidirectional horizontal-field (HF) power supply has been used for vertical plasma position control on TFTR. This supply uses an inverse parallel connection of two independently controllable six-pulse bridge rectifiers to achieve bidirectional voltage and current capabilities. In FY86, advanced digital design techniques were used to implement a new, extremely accurate and reliable rectifier firing generator for this system. Included in the new firing generator is the control function required as a "special case" by the standard FCPC Transrex rectifiers which can be used as the firing control for any of the existing FCPC rectifier power supplies. Two upgrades were also made to this system in FY86: (1) hardware modifications to eliminate the previously observed horizontal-field supply current spikes and (2) control programs to add a test mode and a linear voltage control mode.

Additional activities completed include the commissioning of the final two TFTR equilibrium field rectifiers and commissioning of the poloidal-field and toroidal-field power supply upgrades for the S-1 Spheromak (adding an additional 192 kJ of energy capability for the poloidal field and 96 kJ for the toroidal field).

Engineering specifications based on results of a Conceptual Design Review (CDR) were prepared for six new shaping-field power supplies for PBX-M. (Engineering services required for the CDR were also provided, based on initial functional requirements received from the Experimental Division.) A bid package was prepared for the power supplies and circulated to industrial sources. After Subcontract Proposal Evaluation Board (SPEB) deliberation and Department of Energy review, a subcontract for the supplies was awarded to Robicon, Inc. By the end of the fiscal year, this subcontract had proceeded through preliminary and final design review stages, and fabrication was well under way. Delivery of the supplies is scheduled for November and December 1986. Preparations at C-Site, including cabling, provision of disconnect switches, and instrumentation, were approximately 60% complete.

Electronics Branch

Analog Engineering Section

A vacuum vessel illumination system was designed for TFTR to replace the present manually operated lamp probes. This new system, which can be operated manually or remotely, will provide monitoring of probe position and intensity. The probe position is interlocked to machine operation to prevent plasma formation if the probes are in the "in" position.

To control the arc operating point on the TFTR long-pulse ion sources, an arc/filament closed-loop system was designed. This system controls the filament and arc power supplies and allows the arc current to be set from 0 to 2 kA and the arc voltage to be set in the range of 0 to 200 V. The controller will maintain these values to better than 1%.

A feedback control system, installed on PLT, enables the relative phase of the three 30-MHz ICRF sources to be preset. One source acts as a reference, and the other two can be independently adjusted ±180 degrees. This system, initially developed for antenna phasing experiments, also corrects for phase drift in the sources due to effects of heating and nonlinearities during the rf pulse.

A system was designed to allow parallel operation of the rectifiers feeding the equilibrium-field coil systems at TFTR. The firing generators were redesigned to operate in a master-slave configuration. The modified design provided for a minimal configuration slave unit directly driven by the master firing generator. Test results show excellent tracking of rectifier pairs and excellent current sharing. This will allow the equilibrium-field coils to be operated in parallel with high-current (approximately 30 kA) drive. The equilibrium-field master-slave pairs are in-phase rectifiers, which made the implementation straightforward. Design work is under way to apply the same master-slave principle to the out-of-phase toroidal-field rectifiers. The same results are expected with regard to current sharing and tracking.

A new zero-current detector was designed for use with the reversing switches at the FCPC facility. The new design provides an adjustable current threshold with greater range for generating a permissive signal. Associated control circuitry was also redesigned to provide improved fiber-optic links and high-speed, reliable relay interfaces.

A system was designed to provide real-time monitoring of thermal stress in each of the power diode arrays on TFTR. An algorithm for transient thermal characteristics of the diode array was developed with the Engineering Analysis Division and substantiated by tests performed on one section of the array. The real-time analysis is being handled by a single-board, 68000, microprocessor unit. One such unit will accommodate ten power diode arrays. A Rogowski coil with an integrator was designed to provide a cost-effective means for monitoring the diode current, which is used as the input for the thermal monitor.

A contract was entered into between PPPL and the Oak Ridge National Laboratory (ORNL) for construction of a complete charge-exchange neutral analyzer. The Electronic and Electrical Engineering Division was responsible for design and construction of the signal acquisition equipment and the system control and monitoring equipment. Delivery will take place in early FY87.

Another set of front-end electronic equipment was built and tested for use in the vertical charge-exchange diagnostic on TFTR. Installation is under way and will be completed during FY87.

A neutral-beam water-instrumentation system was installed on TFTR, with full operation expected in FY87. The system will permit calculation of injected beam power by accurately measuring the neutral-beam water calorimeter temperatures. The vertical X-ray imaging system (providing a second view needed to image the plasma properly) was installed on TFTR, and is presently under test.

Electro-Optics Section

A motion control system was built and installed on the horizontal charge-exchange diagnostic on TFTR. This system allows both azimuthal and vertical positioning of the charge-exchange analyzers from the TFTR control room.

A control system was developed and implemented to allow high-speed positioning of a probe to be used to measure plasma surface effects in TFTR. An eight-channel, ground-fault monitor system was delivered to the Institut de Recherche d'Hydro-Quebec in Varennes, Quebec, Canada for Canadian fusion research. An upgraded ground-fault monitor system for TFTR was also designed, fabricated, and tested. The unit will be installed during the December 1986 opening. This upgraded system uses a GE programmable logic controller to provide added features in addition to simplifying future revisions. A remote display is provided in the Test Cell.

The following items were also accomplished:

- Design, fabrication, and installation of fiducial timing generators for TFTR.
- Fabrication and testing of a high-voltage control chassis for the Thomson scattering edge system.
- Delivery of the Thomson scattering edge system ratio positioning electronics.
- Completion of installation on TFTR and the testing of a fifteen-channel, two-color temperature measuring system for the thermal disruption monitor.
- Installation of the neutron activation diagnostic on TFTR. This system uses a pneumatic transport system to send capsules of selected elements out to TFTR for neutron bombardment and then back to the LOB basement for gamma ray analysis. A microcomputer controls system operation.

Forty-eight dual-input differential integrator modules were constructed for PBX poloidal-field measurements. The features included a switchable integration time constant with a gain accuracy of ±0.5% and an auto-zero loop which holds the integrator drift to ±100 mV per 10 sec (time constant 0.1 msec) when the integrator was enabled. Integrator gate timing of 0.1 sec to 99 sec was provided by four timing modules.

Four portable systems were completed to measure neutrons and gamma rays in the Test Cell, upper and lower darm, and Test Cell Basement. Each system may be positioned up to 35 feet from one of 13 remote patch panels from which the data is sent, by way of the safety check area, to CICADA for processing.

Instrumentation Section

The repeating pneumatic injector system, installed last year, continued operation through April 1986. It injected frozen pellets of hydrogen into TFTR to rapidly increase plasma density during a discharge. During this same period, a control system was designed for the deuterium pellet injector system which was being developed by ORNL. The DPI provides three different pellet sizes in an eight-barrel,

single-shot-per-barrel injector, allowing the barrels to fire pellets closer together in time than was possible with the RPI.

The DPI replaced the RPI during the summer opening. The expanded control electronics (see Fig. 9) were relocated away from the Test Cell to remove them from the TFTR radiation area. The DPI is now operational and is being operated by the Instrumentation Section.

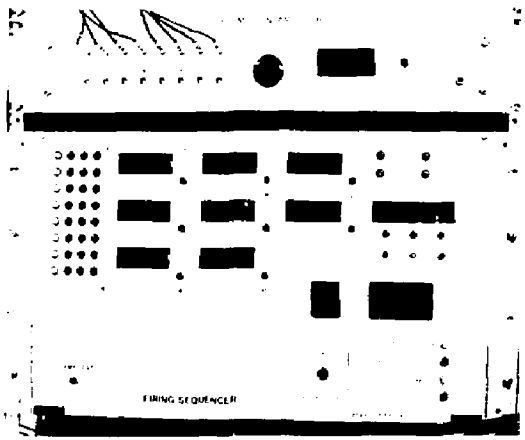

Fig. 9. Firing sequencer and pellet motion amplifier on the deuterium pellet injector. (86E1016)

The multichannel infrared interferometer (MIRI) ten-channel electron line density electronics were upgraded to include an additional ten Faraday channels to measure the poloidal field generated by the plasma current. After successful tests, four channels were further upgraded to provide signed-value Faraday amplitudes. Faraday calibration electronics were also provided. They include a calibration carriage controller and simulated Faraday signals. Additional electronics were made to enhance operation and monitoring, to provide remote control of the high-voltage power supply, chiller, and laser gas supply, and to reduce susceptibility to TFTR's magnetic field.

Numerous improvements were made to the neutral-beam system electronics. These included design and installation of an expanded fault disruption isolation system with additional sensors and controls, five uninterruptible power supplies, a data link monitor, a resistive thermal detector (RTD) signal conditioning system, and interfaces with the torus interface valve (TIV) controller. The telemetry fault detector (TFD) distribution boards were modified to improve noise immunity, and 14 neutral-beam timer chassis were upgraded to improve reliability.

The TFTR's torus vacuum pumping system (TVPS) electronics were upgraded to include first-fault alarms and an alarm in guard headquarters that alerts vacuum personnel of a problem in the TFTR main vacuum system during off-hours.

The TFTR diagnostic vacuum system was also upgraded. New or revised diagnostics commissioned during this year included probe systems: WE1, WE2, WE3, and NL; charge-exchange EV0, EV4, EH4; and impurity injector WI. Numerous problems caused by TFTR's magnetic field were identified. The diagnostic vacuum controller (DVC) firmware was modified to compensate for the magnetic susceptibility of the vacuum system hardware. A plenum interface valve (PIV) control was added to both the horizontal and vertical charge-exchange diagnostics. This control was added within the versatile DVC. The CICADA ion gauge controller interface was standardized; this improvement was implemented on all diagnostics. Ready for commissioning are a TIV control air alarm and a fiber-optic interface to monitor the neutral-beam TIV status.

Controls were added to the TFTR gas delivery system to allow both local and CICADA computer control. In addition, an interlock with the TIV system was also designed.

A prototype Rogowski loop was designed and built to improve the 17 energy conversion system power diode current monitor systems.

Two interlocks were designed for the TFTR surface pumping system: a watchdog timer interlock on the TFTR vessel thermocouple computer and an interlock with the vessel vacuum pressure. These are ready for commissioning.

MECHANICAL ENGINEERING DIVISION

The Mechanical Engineering Division (MED) provides engineering and technical services to the many projects and programs at the Laboratory. The Division consists of three branches: the Mechanical Technology Branch, the Vacuum and Cryogenics Branch, and the Coil Systems Branch. In addition to the branches, there is an independent Engineering Services Group. The Division's major efforts and activities during FY86 were for TFTR, however significant resources were applied to the PBX-M and S-1 projects. The needs of the remaining research programs were met as required.

The Engineering Services Group provides skilled technicians to perform maintenance, fabrication, and installation work for the various MED branches and for any other groups within the Laboratory. This group is organized into several shops according to skill. The electrical shop pulls heavy cable and performs electrical work up to 480 V, both for the major experimental devices and the smaller individual laboratories at PPPL. The electrical shop also installs control wiring, interconnecting computer cabling, and some instrumentation wiring. The metal shop and weld shop fabricate various mechanical structures. The plumbing shop maintains water systems for the experimental devices as well as fabricating new systems. The carpenter shop builds wooden structures, platforms, and enclosures. It also fabricates

special molds and forms for coil winding and models for developmental studies.

Mechanical Technology Branch

The Mechanical Technology Branch consists of two engineering sections: the Diagnostics and General Fabrication Section and the Materials Test and Machine Design Section. In addition, the Branch includes the Mechanical Drafting Group and the Machine Shop Services Group.

Diagnostics and General Fabrication Section

The deuterium pellet injector (DPI) is used to inject solid pellets of deuterium to fuel the plasma in TFTR. Figure 10 shows the DPI installed on TFTR. During FY86, the Diagnostics and General Fabrication Section (D&GF) provided engineering support to install this device and its support equipment on TFTR.

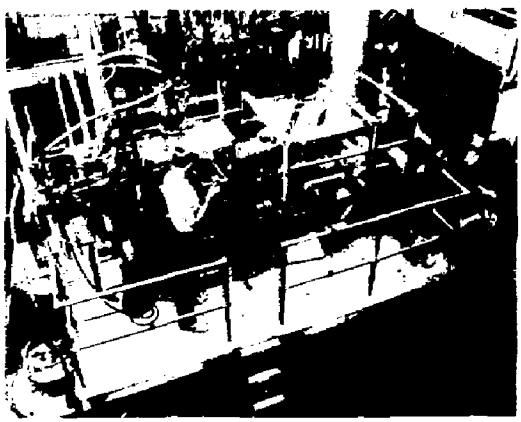

Fig. 10. Deuterium pellet injector installed on TFTR. (86X3228)

Design was started on a new plasma limiter for the TFTR during FY86. This stationary limiter is made of carbon-carbon composite material to withstand the high heat loads inside the tokamak. It will replace the movable limiter which is presently being used on TFTR. Fabrication is scheduled to start November 1986, with installation planned for June 1987.

Radiation shielding for the horizontal charge-exchange analyzer on TFTR was designed, fabricated, and installed (see Fig. 11). A unique feature was the use of a low-cost, water-extended, polyester/polyethylene-bead/boron frit combination as a neutron moderator. As installed, it reduced the background radiation levels at the analyzer by a factor of 125, almost 50% better than originally calculated.

The horizontal calorimeter for the TFTR diagnostic neutral beam was completed and installed during the winter of 1985-1986. It was redesigned from the original vertical design to incorporate the use of linear

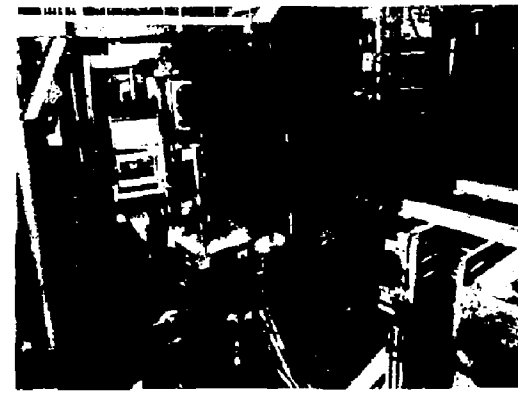

Fig. 11. Radiation shielding for the horizontal charge-exchange analyzer on TFTR. (86E0936)

bearings running in air to reduce the tendency to bind or drag.

Two new types of probes were designed for TFTR during FY86. First, a midplane probe positioner was completed and installed during the summer. The midplane probe positioner is unique in that it is designed to quickly run itself into the edge of the plasma during flattop, to take data, and then back out again before the end of the pulse. This new feature will help prevent probe head damage due to overheating from plasma disruptions. Second, four new vacuum vessel illumination probes were designed and fabricated. They are scheduled to be installed during the spring opening of 1987.

A heating and cooling system for the S-1 Spheromak vacuum vessel was designed, built, and installed during FY86. It is capable of baking out the vessel to 150°C, using a hot air system similar to the one on TFTR. The Section also worked on a design for a new current transformer for the S-1 Spheromak. The resulting coil was unique in that it minimized the error fields and simplified existing designs. A patent disclosure for this design was filed.

Conceptual designs for the Compact Ignition Tokamak diagnostics were also started by the Diagnostics and General Fabrication Section during FY86. Approximately 30 diagnostic devices are presently being considered for the CIT.

Materials Test and Machine Design Section

In FY86, the Materials Test Laboratory performed a total of 118 tasks, approximately 70% were for TFTR and 12% for CIT. As in previous years, these tasks involved a wide range of PPPL activities, including component testing, transducer installations on TFTR, thermal and pressure instrumentation calibration, MG instrumentation, neutral beam thermocouples, and CIT materials studies. In preparation for a move to a new laboratory site during FY86, the Materials Test

Laboratory reduced its equipment and supplies inventory by approximately 50%.

Machine design activities by the Section included the design and fabrication of new active and passive coil supports, as well as coil vacuum cans for the PBX-M. Figure 12 shows the mechanical supports for the IF coil and the DF1 upper and lower coils in place in the PBX-M vacuum vessel. Installation of these items is scheduled to be completed by the end of December 1986. Other tasks in this category included the design study of the PBX-M cooling system alterations and the assembly and test of a winding mechanism for winding the new active coils inside the vacuum vessel.

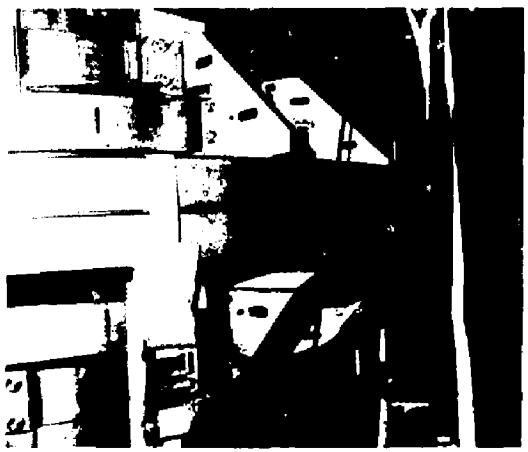

Fig. 12. Mechanical supports for the IF coil and the DF1 coils during installation on PBX-M. (86E0975)

TFTR activities included the preliminary designs for additional supports for coil stack No. 5. These designs were developed and analyzed for Modes A, B, and D. Analyses were also performed of the TFTR center plug, which supports the center column. The analyses showed that loads on the plug must be limited to a value not exceeding 1.5 million pounds.

The Mechanical Technology Branch was also active in the scheduling and coordination of all tasks performed by the Mechanical Engineering Division relative to the PBX modification.

Vacuum, Cryogenics, and Tritium Branch

Vacuum Section

During FY86, the Vacuum Section provided major support to the PBX-M program, the S-1 Upgrade program, and the TFTR long-pulse neutral-beam program.

The Vacuum Section fabricated the supports for the new poloidal-field arrangement located inside the PBX vacuum vessel, installed stainless steel vacuum liners onto coils wound in place inside the vacuum vessel, and fabricated the new passive coil system from purchased, explosively-clad stainless steel/aluminum composite plates. Figure 13 is a view of the PBX-M vessel interior during fabrication.

The S-1 Upgrade flux core fabrication program was successfully concluded this fiscal year. The Vacuum Section performed final machining of the G-10 coil form; installed and tested the fabrication and installation of the vacuum feed-thru assemblies, Fig. 14; and installed and aligned the core in the vacuum chamber. The new core was tested to full operational levels and is now in routine service.

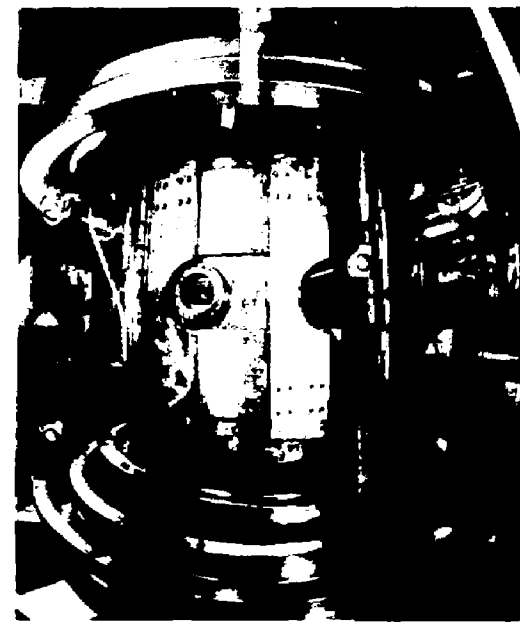

Fig. 13. PBX-M vacuum vessel interior during internal fabrication. (86E0731)

Fig. 14. Typical vacuum penetration for current feed-thru assembles on S-1. (86X3211)

In FY86, the Vacuum Section fabricated 75% of the required stainless steel vacuum bellows assemblies (15 will be required in total) and copper "scraper" assemblies (43 will be required in total) for the TFTR long-pulse neutral-beam program. These components will be ready for installation in November, 1986. These fabrication tasks involved high-precision machining, welding, and furnace brazing. Figure 15 shows one of the bellows assemblies.

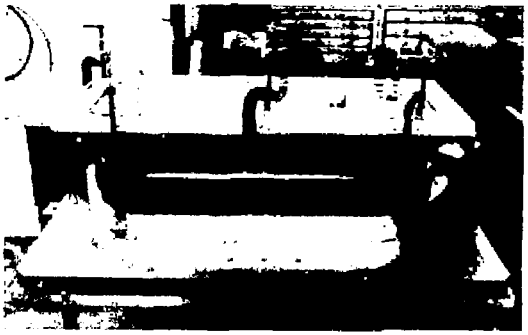

Fig. 15. Bellows assembly for the TFTR long-pulse neutral-beam program during leak check. (86E0795)

The Vacuum Section continued to provide general vacuum fabrication, testing, and repair support to the operational PPPL devices, especially in the area of diagnostic devices.

The Branch assumed responsibility for the maintenance manipulator program early in FY86. The maintenance manipulator is an extendable boom, which will be housed in a vacuum antechamber connected to the TFTR vacuum vessel torus. The manipulator is capable of accessing all points within the vessel and can be controlled automatically or manually. Its primary tasks will be to provide internal viewing of the vessel while under vacuum, perform in-vacuum leak detection, and, with an existing master-slave manipulator attached, perform repair and maintenance operations in a radioactive environment. A cost-sharing agreement was finalized with Kernforschungszentrum Karlsruhe (KfK), a nuclear research organization in West Germany with extensive remote handling experience. Under this Agreement, KfK is providing the required engineering, including all supporting personnel, and PPPL is providing funds for fabrication of the boom and associated controls. The visual inspection system is being provided by Centre Energie Atomique (CEA) under a separate cost-sharing agreement. The format of this agreement is quite similar to that negotiated with KfK, with CEA providing the personnel for the design and PPPL providing funds for the hardware. A successful final design review for the boom was held in July, 1986, and KfK has placed a subcontract with a German industrial firm for the fabrication. The vision system design has been established and a final design review of this system will be held early in 1987. The Vacuum Section designed the vacuum antechamber and has started fabrication. Following discussions with JT-60 engineers, an order was placed with Seiko in Japan for the in-vessel leak detector. A test stand is being prepared and the unit will be tested early next year.

Cryogenics Section

The TFTR 1070-watt helium refrigerator supplies liquid helium at 4.5°K to cool the helium cryogenic pumping panels in the TFTR neutral beams, both in the Test Cell and test stand. During FY86, the refrigerator was operated for a total of 5,621 hours, no machine down time was attributable to refrigerator operations. The operating time per month versus total hours available is shown in Fig. 16. The cryogenic control panel is shown in Fig. 17. The 1070-watt helium refrigerator was operated and maintained by CVI, Inc. of Columbus, Ohio under a PPPL subcontract. The CVI, Inc. operating crew was supplemented with PPPL personnel.

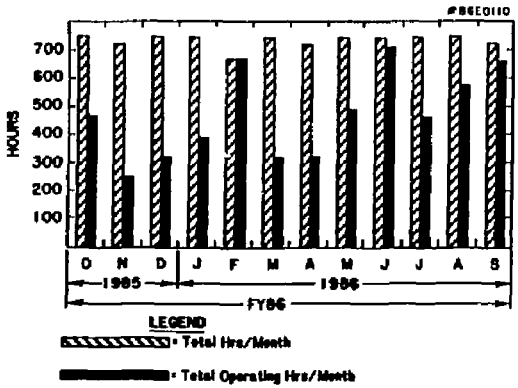

Fig. 16. The TFTR 1070-watt helium refrigerator operating hours versus total hours available per month during FY86.

Fig. 17. Cryogenic control panel for the 1070-watt helium refrigerator TFTR neutral-beam system. (86E0948)

Tritium Section

The Tritium Section was formed during the last quarter of FY86. The purpose of this Section is to provide engineering and technical support for the commissioning of the TFTR tritium system. The tasks undertaken include the design and construction of the Igloo shield around the TFTR device and providing support in a variety of technical areas, such as environmental monitoring, the heating ventilation, and air conditioning (HVAC) system, and HVAC system modifications.

Coil Systems Branch

During FY86, the Coil Branch participated in work for PBX, TFTR, S-1 and CIT. The largest participation was for the redesign and modification of PBX to PBX-M. In this project, a "first of a kind" was achieved by winding and fabricating the vacuum impregnated active coils inside the PBX vacuum vessel. This procedure was chosen over the conventional method of fabrication at another location, because of the constraints dictated by a tight time schedule. Using the conventional approach would have necessitated a major dismantling of the PBX machine to install the coils.

A total of five coils were fabricated inside the confined area of the vacuum vessel, with many new winding techniques adopted to maintain the high levels of mechanical and electrical integrity dictated by Coil Branch Engineering. Furthermore, fabrication was achieved on schedule and within budget. Figures 18 and 19, respectively, show the equipment outside the vessel used for brazing, straightening, and taping the conductor before it enters the vessel for winding and a coil being wound on the mandrel inside the vacuum vessel.

In addition to the active coil fabrication for PBX-M, extensive work was done with the passive coil system, the internal active coil leads, and the external bus system. Coil Branch engineers designed the passive coil system and directed the many aspects of its fabrication, from the explosion bonding of the stainless steel to aluminum through cutting and forming and, eventually, trial fitting of the eighty-segment system. A major part of the passive coil system, the complex bus system which interconnects all segments, was designed and directed through fabrication by the Branch. The external bus system and connection panels were also designed and fabricated by Branch.

The original S-1 flux core failed its electrical tests due to a design concept requiring perfect vacuum impregnation during the epoxy/fiberglass insulation. An evaluation of the failure mechanism indicated that the vacuum impregnation was near perfect, but less than the 100% required by the design concept. A major project was undertaken by the Coil Branch to redesign and fabricate a new S-1 flux core. The design modifications resulted in a significantly higher mechanical and electrical integrity of the windings

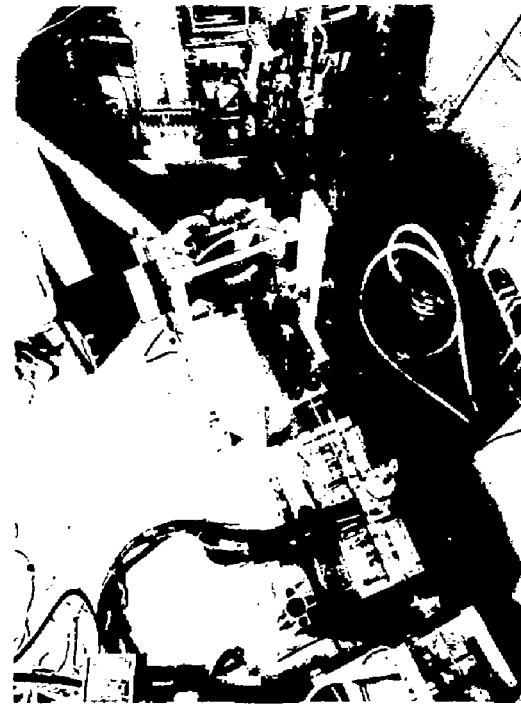

Fig. 18. Coil winding equipment located outside of the PBX-M vacuum vessel used for active coil fabrication. (86E0458)

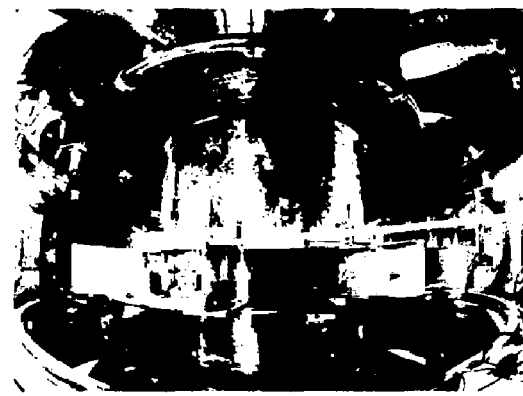

Fig. 19. Winding a DF1 coil inside the PBX-M vacuum vessel. (86E0485)

inside the core and the associated leads and bus work. These modifications adequately accommodate all of the mechanical and electrical stresses that will develop during the planned higher magnetic-field operating scenarios.

Considerable work was accomplished on TFTR during FY86. Two significant tasks were the color coding of every bus work connection on the machine and the measurement and recording of the mechanical and electrical condition of every bus joint. This will provide a system to accommodate high reliability and simplified maintenance of the coil bus systems. The Coil Branch continued to support the CIT project design effort.

References

[1]N. Sauthoff *et al.*, "Current Configuration and Performance of the TFTR Computer System," in *Fusion Engineering 1985* (Proc. 11th Symp., Austin, Texas, 1985) Vol. *I* (IEEE, New York, NY) 590.

[2]W. Rauch, "TFTR CAMAC Data Acquisition System," Rev. Sci. Instrum. *57* (1986) 1698.

[3]L. Randerson, J. Chu, C. Ludescher, *et al.*, "TFTR Data Management System," Rev. Sci. Instrum. *57* (1986) 1892.

[4]L. Lagin, U. Schneider, N. Arnold, *et al.*, "CHERS Software System - A MicroVAX-based Diagnostic," Rev. Sci. Instrum. *57* (1986) 1889.

[5]J. McEnerney *et al.*, "TFTR Neutral Beam Computer Control System," in *Fusion Engineering 1985* (Proc. 11th Symp., Austin, Texas, 1985) Vol. *I* (IEEE, New York, NY) 301.

[6]J.A. Murphy and T.R. Gibney, "PLT Data Acquisition and Analysis System," Rev. Sci. Instrum. *57* (1986) 1886.

[7]S.L. Liew, L.P. Ku, and J.G. Kolibal, "Three-Dimensional Monte Carlo Calculations of the Neutron and Gamma-ray Fluences in the TFTR Diagnostic Basement and Comparisons with Measurements," Princeton University Plasma Physics Laboratory Report PPPL-2275 (1985) 39 pp.

[8]S.L. Liew, L.P. Ku, and J.G. Kolibal, "TFTR Basement Radiation Fluence Calculations and Comparisons with Measurements," Fusion Technol. *10* (1986) 591-596.

[9]L.C. Johnson, M. Bitter, R. Chouinard, *et al.* "TFTR Vertical X-Ray Imaging System," Rev. Sci. Instrum. *57* (1986) 2133.

[10]J. Kolibal, L.P. Ku, and S.L. Liew, "The Neutronic Analysis for the LBM/LOTUS Experiment," Fusion Technol. *10* (1986) 956-961.

[11]J. Kolibal, L.P. Ku, and S.L. Liew, "LCC - A Program to Compare the Experimental Data from the LBM with Computational Results from MCNP, A User's Guide," Princeton University Plasma Laboratory Report PPPL-EPRI-12 (1986) 36 pp.

[12]J. Kolibal, L.P. Ku, and S.L. Liew, "Meteorological Data Summaries for the TFTR from January 1984 to December 1985," Princeton University Plasma Physics Laboratory Report PPPL-2369 (1986) 73 pp.

[13]J. Kolibal, L.P. Ku, and S.L. Liew, "TFTR Offsite Dose Levels from Fusion Radiation and Effluent Releases," Fusion Technol. *10* (1986) 1234-1239.

[14]J.L. Doane, "Propagation and Mode Coupling in Corrugated and Smooth-Wall Circular Waveguides," Chapter 5, *Infrared and Millimeter Waves*, K.J. Button editor, Vol. *13*, Academic Press (1985).

[15]J.L. Doane, "Polarization Converters in Overmoded Circular Waveguide of Electron Cyclotron Heating (ECH) at 60 GHz," Conference Digest, *Tenth International Conference on Infrared and Millimeter Waves*, Orlando, Florida (1985) 166.

[16]J.L. Doane, "Waveguide Elliptic Polarizers for ECH at Downshifted Frequencies on PLT," Princeton University Plasma Physics Laboratory Report PPPL-2297 (1986) 20 pp; also published in *Proceedings Fifth International Workshop on Electron Cyclotron Emission and Electron Cyclotron Heating* (San Diego, 1985) 345.

PROJECT PLANNING AND SAFETY OFFICE

PLANNING OFFICE

In FY86, the Project Planning Office continued the functions of a Technology Transfer Office for PPPL, including the submission of the FY85 Annual Report on Technology Transfer. In addition, the Office continued to serve as the single point of contact for PPPL with the Department of Energy (DOE) on matters regarding Automated Data Processing Equipment (ADPE).

The Office also played a key role in PPPL's safety program. In addition to the Project and Operational Safety Office (P&OS) functions described below, the Head of the Project Planning and Safety Office serves as the Departmental Safety Officer for technical operations. The Departmental Safety Officer is directly responsible for safety policies and programs within the Department.

PROJECT AND OPERATIONAL SAFETY OFFICE

The Office continued to work closely with TFTR and other PPPL projects in the areas of operational safety and environmental concerns. Heavy emphasis was placed on day-to-day interactions and on close support of project personnel. Input was supplied for future projects, especially in the area of environmental concerns for the Compact Ignition Tokamak. In May, PPPL published its fourth Annual Environmental Report.[1] This document reported on PPPL's environmental monitoring program and reviewed PPPL's compliance with government regulations. The retention basin was completed. An oil-separator and alarm system were added to the basin. Permits for groundwater discharge and for the treatment works were applied for, as requested by the New Jersey Department of Environmental Protection (NJDEP).

An Environmental Protection Agency (EPA) certification process started in FY85 was brought to a successful conclusion in FY86. After an inspection by EPA/Las Vegas and the NJDEP, the P&OS Radiation Environmental Monitoring Laboratory (REML) was certified for tritium analysis. A high-efficiency germanium detector was procured in order to initiate similar certification procedures for gamma spectroscopy. An REML Handbook was completed by the Health Physics Group. This project began in FY85 as a joint effort between the PPPL Health Physics Group and the Idaho National Engineering Laboratory. Tritium enrichment processes, which were perfected as a part of this undertaking, were used to analyze baseline samples of soils, waters, and biota. A prototype station for tritium gas/oxide (HT/HTO) particulate sampling was assembled and tested (see Fig. 1). A patent is pending on the tritium instrument. A presentation was made on its unique features at the National Bureau of Standards in October 1986.

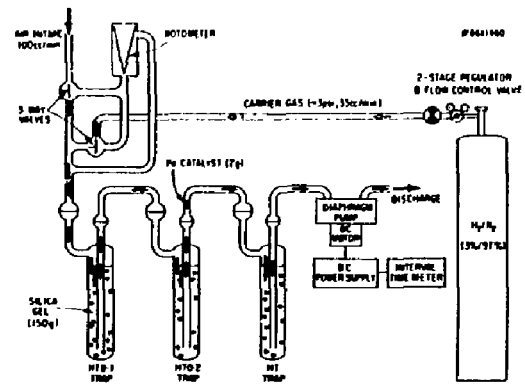

Fig. 1. Differential atmospheric tritium sampler (DATS) shown in "sampling mode," rotometer bypassed.

A program to revise and update PPPL's Health and Safety Directives (HSDs) was initiated. The HSD on Radiation Protection[2] was updated to reflect current DOE Orders. The HSD on electrical safety[3] was updated and combined with a supplement; it was submitted to DOE for approval. When so determined by the PPPL Safety Officer, written Safe Operating Procedures (SOPs) are required to document the safety of Class IV lasers and other lasers.

Health physics surveys, electrical inspections, interlock testing, and overall safety reviews continued for all PPPL projects. The P&OS Office participated in a DOE intercomparison study on health physics instrumentation calibration in addition to its usual personnel dosimetry intercomparison. A charter was established for a standing committee to control electrical responses to site emergencies involving electricity. Capacitor banks and their accessors are now under an annual recertification program.

The Laboratory emphasis on early safety reviews has been effective. Projects are now requesting and receiving safety input much earlier in their development. This will be especially important to the Compact

Ignition Tokamak in which P&OS is taking an active role at an early stage. PPPL participates in the DOE program which provides accident hazard information to DOE facilities to help prevent accidents.[4]

References

[1]J.R. Stencel, "Environmental Monitoring Report for *Calendar Year 1985," Princeton University Plasma Physics* Laboratory Report PPPL-2345 (1986) 85 pp.

[2]*Princeton University Plasma Physics Laboratory* Health and Safety Manual, Health and Safety Directive (HSD) 5008, Section 10.

[3]Princeton University Plasma Physics Laboratory Health and Safety Manual, Health and Safety Directive (HSD) 5008, Section 2.

[4]DOE/EH-0019, Serious Accident Bulletin, "Hydrofluoric Acid Burn: Misleading Latent Period was Key Factor," Issue 12, October 1986.

QUALITY ASSURANCE AND RELIABILITY

The need to decrease cost while simultaneously complying with project demand for increased support made FY86 an interesting year. Both objectives were achieved by judicious staff reduction, a reassessment of priorities, staff co-location, and paper systems automation. PPPL Quality Assurance and Reliability (QA&R) had more than a few significant achievements during this past year. Some are reported below:

DOE ASSESSMENT

The DOE Chicago Operations Office conducted a formal assessment of the Quality Assurance and Reliability Program in July. This was the first in-depth evaluation of the Program since the planning phase of early 1984. The result was "Highly Satisfactory," an indication that the Program is on the right track. However, much of the credit for achieving this important group milestone goes to the articulate PPPL user community that provides immediate feedback and course correction.

IMPROVED QUALITY IN PURCHASED MATERIALS

One early objective of the QA Program was to improve the quality of purchased products. Data for FY86 indicate that this objective was partially achieved. Figure 1 quantifies the percentage of improvement for selected, high-volume, high-risk products since 1983. The data is conservative because during the measurement period standards of acceptability were tightened. This was a total Laboratory accomplishment. Quality Assurance, working with projects, procurement, and engineering, took action to:

- improve specification content and format,
- develop performance standards,
- tighten subcontractor selection criteria,
- assure early subcontractor awareness,
- strengthen PPPL field quality systems,
- selectively utilize DCAS inspection services,
- equip and staff a receiving inspection facility, and
- improve the defect reporting system.

In the beginning, some suppliers had difficulty adapting to the changed environment. The Procurement Quality Assurance Group worked with each vendor to assure an understanding of PPPL requirements and to improve their internal processes. Several early "problem suppliers" are now at the top of today's list of "superior performers."

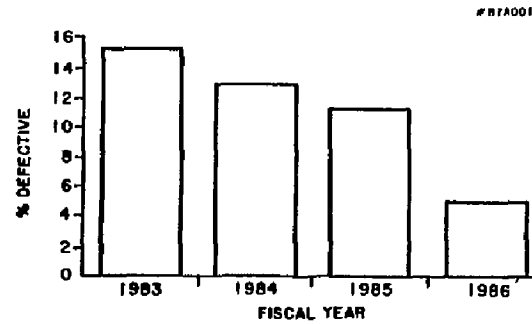

Fig. 1. The performance of PPPL subcontractors and suppliers has improved markedly since 1983. This chart is based upon data collected by receiving inspection and involves critical components (lots).

JET SUBCONTRACT

The Joint European Tokamak (JET) subcontracted with PPPL to provide QA services in support of procurement of beryllium tiles from the Brush-Wellman, Inc., in Ohio. The assignment included planning a verification scenario and providing expert on-site quality control services that immediately addressed occasional problems and assured the delivery of acceptable tiles within JET's schedule window.

PAPER SYSTEMS AUTOMATION

Automation of the QA paper systems was driven by a need to expand successful activities in the face of reduced staffing. MacIntosh computers were available and were already being used for a variety of clerical, administrative, and data analysis tasks. It was decided to use the MacIntosh, with commercially available software, to develop systems that would reduce administrative labor and improve performance. Several were commissioned during FY86. They achieved the initial objective, and they provided access to previously invisible management data.

A few applications are described as follows:

Quality Control Risk Assessment

Quality Control (QC) manages and prioritizes its resources via a review of jobs, involving fabrication, integration, and construction. Annually this runs in excess of 500 individually tracked activities. Quality Control's involvement in each job is determined and documented via a Risk Assessment Plan. Subsequent actions involve inspections, nonconformance control, and job closure. The manual system was labor intensive and error prone.

The automated system, developed by Assurance Engineering, provides a relational data base that supports all records, reports, and correspondence. Planning is simplified, jobs are readily tracked, and open items clearly flagged. The concerns of other activities, such as Project and Operational Safety, have, at their request, been incorporated.

Purchased-Materials Planning

Procurement Quality Assurance (PQA) maintains a data base of critical procurements based upon early information from a variety of sources. This data base contains PQA's assessment of risk and describes actions required to assure the delivery of a conforming product. The plan baselines QA staffing and budget control and is coordinated with the cognizant engineer. The data base also receives and tracks actions resulting from nonconformances encountered and provides a variety of useful reports.

TFTR Operations Data Base

Assurance Engineering maintains a spreadsheet data base using TFTR Operations' Logs, Trouble Reports, and other data. This, integrated with graphics software, permits charting of availability by system and subsystem. These data are used to assess progress towards subsystem performance goals and provide the TFTR Trouble Report Working Group with an objective measure of its ability to identify and eliminate repetitive problems.

Audit Control

Full automation of the quality audit/assessment program was implemented by Assurance Engineering. The data base includes scheduling, checklists, results, action items, and correspondence information, and it provides special reports.

PROJECT SUPPORT

Quality Assurance's main concern as an organization is to find solutions to existing quality and reliability problems, but it must also be an active participant in seeking out and characterizing events which may inhibit the achievement of quality. Accordingly, Assurance Engineering now assigns an engineer to a new project as early as possible. That engineer is considered a working member of the project manager's staff and provides support to the project team in matters relating to quality achievement. This program was initiated (as a trial) with PBX-M. Benefits were immediately evident, and the practice was extended to include the ICRF Project, CIT, and TFTR tritium commissioning. Quality Assurance as an up-front working member of the project team appears to be worth a thousand after-the-fact audits and inspections.

PROJECTION

Quality Assurance and Reliability ended the year with many initiatives underway and a few issues remaining to be addressed. However, the sparsity of resources dictates that the coming year be devoted to refining and simplifying rather than addressing new and innovative approaches.

Maintaining staff enthusiasm requires the establishment of realistic internal goals. Yet, as project managers learn to effectively use quality assurance, the demand for services will continue to grow. The future should prove to be even more challenging.

ADMINISTRATIVE OPERATIONS

In FY86, management emphasis continued to be on maintaining levels of administrative services in the face of declining laboratory budgets. This was accomplished by improvements in efficiency and stringent cost reduction efforts, as the Laboratory continued to match reductions in controllable general and administrative (G&A) expenses to overall reductions in program funding.

During FY86, the number of Princeton Plasma Physics Laboratory (PPPL) staff was reduced from 1121 on September 30, 1985 to 1040 on the same date in 1986. This decrease of 7.2% was effected through managed attrition, the completion of a Voluntary Separation Program begun in FY85, and a second reduction-in-force (RIF) of 30 people in February 1986. The RIF was related to the across-the-board Gramm-Rudman-Hollings reduction in Federal outlays, which decreased PPPL's FY86 funds by $3.8M in February 1986. Overall, the PPPL staff by the end of FY86 was 19.6% below the peak employment in October 1984. The resulting composition of PPPL by staff component on September 30, 1986 is shown on Table I.

Turning to G&A-supported staff, which includes Administrative Operations and the Director's Office, the reduction in manpower over the two years FY85 and FY86 is a reasonable measure of PPPL's overhead cost reduction efforts, as shown in Table II.

An important development for the Laboratory in FY86 was completion of negotiations for most of the provisions of a new contract between Princeton University and the Department of Energy (DOE) under which the University will continue to operate PPPL for a five-year period (FY87-91). Although the final contract was not executed until early FY87, a Memorandum of Understanding was signed in August 1986, and, by letter, the parties had begun to operate under the terms of the new agreement.

One of the important understandings reached in August required the closing of PPPL operations at the Forrestal Campus A- and B-Sites by the end of fiscal year 1987, and moving most of the operations to C- and D-Sites (where the PPPL experimental devices are located) and some to off-site leased space. This effort will involve a major relocation of engineering and shop activities, as well as laboratory and office space. In all, about 50% of the Laboratory personnel will be moved in FY87, as well as about 75% of the engineering shops and laboratories. The planning and implementation of this consolidation falls mainly on the Laboratory's move coordinator,

Table I. Fiscal Year 1986 Staff Composition.

Faculty	2
Physicists	111
Engineers	207
Technicians	499
Administrative	110
Office and Clerical Support	111
TOTAL	1040

Table II. G&A Supported Manpower.

	PPPL Employees	Percentage Reduction over Sept 84	Subcontract Employees	Percentage Reduction over Sept 84
September 30, 1984	360	---	51	---
September 30, 1985	310	11	21	59
September 30, 1986	278	23	15	71

Jack Joyce, Head of the Engineering Department, and on the Administration Department; it adds substantial managerial burdens and unplanned costs to an already tight FY87 Laboratory budget. However, there will be long-term benefits to the Laboratory, if all or most personnel and activities can be consolidated in one area.

Other administrative activities of note in FY86 are the following:

- Discretionary expenses in the G&A area were reduced from $18.3M in FY85 to $15.8M in FY86, or a reduction of 13.7%.
- An Institutional Plan was developed for review by the University and the DOE. The Plan integrates the schedules and programs for TFTR, the proposed Compact Ignition Tokamak, and other Laboratory projects.
- An employee attitude survey was conducted for Laboratory management by the Opinion Research Corporation.
- Administrative support was provided for the Director's reorganization plans for the TFTR Project and the Program and Research Area.
- A new administrative computing strategy was developed, proposed to Laboratory management, and discussed with the University and the DOE.
- Major improvements in the automated data processing systems supporting budget, accounting, procurement, and personnel functions were put in place, permitting significant efficiencies and cost reductions in these activities.
- Planning for the upgraded integration of PPPL financial systems with those of DOE's Financial Information System (FIS) was initiated.
- The Laboratory's improved system for property management and control was approved by the DOE.
- Environmental analysis, looking to siting the Compact Ignition Tokamak at PPPL, was initiated with the Idaho National Engineering Laboratory (INEL) as subcontractor.

ADMINISTRATION DEPARTMENT

Plant Maintenance and Engineering

The Plant Maintenance and Engineering (PM&E) Division is a technical and administrative support organization. Its function and purpose is to support the Laboratory's research programs by operating, repairing, constructing, and modifying physical facilities, systems, and equipment at A-, B-, C-, and D-Sites. Table III shows the gross square feet (GSF) maintained by PPPL at each site during FY86.

Table III. Princeton Plasma Physics Laboratory FY86 Square Foot Occupancy.

Location	GSF
A-Site	209,811
B-Site	140,088
C-Site	467,136
D-Site	219,856
Trailers (C- and D-Sites)	16,128
TOTAL	1,053,019

Project Engineering

The Project Engineering Branch is responsible for the planning, engineering, and coordination of General Plant Projects (GPP), as well as for energy studies and conservation projects. Table IV summarizes the number and value of active projects at year-end.

Energy Conservation

In FY86, emphasis was primarily directed toward implementation of energy conservation projects and addressing energy conservation refinements in the physical plant preventive maintenance operation. As part of this intensified effort, the Energy Monitoring and Control System and the Power Line Carrier System were clearly PPPL's FY86 leading edge of energy conservation management and control.

The results of these intensified activities produced an energy consumption reduction of 5.1% in the FY86 Laboratory's Buildings Energy Utilization Index (Btu/ft^2) versus the *new*, DOE-mandated, FY85 Base Year. Considering that experimental device activity increased by 34.2%, the 5.1% reduction in building energy usage (FY86 versus FY85) was most rewarding. Reflected within these impressive conservation statistics are a 4.8% reduction in building electrical usage and a 6.8% reduction in building fuel oil usage. These reductions, when normalized, resulted in a savings of $105k in electric and $16.2k in fuel oil costs (FY86 versus FY85 Base Year).

These significant reductions were chiefly attributed to two distinctly different types of energy management systems which were in operation during FY86: the Energy Monitoring and Control System (EMCS) and the Power Line Carrier System (PLCS). These systems established conservation control of energy consuming loads and produced both reductions in energy consumption and cost of energy for the Laboratory.

Table IV. Fiscal Year 1986 Project Engineering Summary.

	No. of Projects	Value ($K)
Energy Conservation		
Conservation		
Previous Fiscal Year	5	$1,438
Current FY86	2	645
Studies		
Previous Fiscal Year	0	0
Current FY86	1	77
SUBTOTAL	8	$2,160
General Plant Projects (GPP)		
Authorized		
Previous Fiscal Year	3	132
Current FY86	16	985
Proposed FY87/88		
New Research Equipment, Storage, and Assembly Bldg.	1	1,200
Conceptual Design Studies	8	80
SUBTOTAL	28	$2,397
Other Engineering Support*	24	720
TOTAL ALL CATEGORIES	60	$5,277

*Includes engineering support for relocating A- and B-Site facilities to C- and D-Sites.

The EMCS is a "hard-wired" system that is designed for comprehensive and complex operational conservation tasks. The EMCS installation includes microprocessors, data gathering network, field sensors, recording devices, and the control of heating, ventilating, and air conditioning (HVAC) units, valves, motors, fans, and other operating equipment. Even though during FY86 this initial EMCS phase addressed applications at A- and C-Sites, the installed EMCS system is expandable to accommodate all sites through the existing Central Processing Unit.

The PLCS, a less sophisticated system than EMCS, communicates and controls applications via a frequency signal superimposed on the existing facility electrical distribution system. The PLCS installation includes a controlling microprocessor, transponders, transceivers, receivers, a data gathering network, and field sensors. This is an initial phase which presently addresses applications only at C-Site.

Some of the larger energy retrofit profits completed in FY86 were: PLCS Phase II, Energy-Efficient Motors, Variable Frequency Drives for Large Motors, C-Site Central Plant Chiller Optimization Control, and D-Site "A" Chiller Crossover Conversion. Completed energy studies in FY86 were: EMCS and PLCS Expansion, D-Site Lighting Survey, Water Treatment and Phase II Thermostatic Study.

To keep maintenance personnel up-to-date in energy conservation, equipment operations, and procedures, periodic training sessions were conducted. Also, in order to enhance and implement energy management and conservation measures, special in-depth energy conservation seminars were attended by PPPL engineers.

Public relations interface with Laboratory staff was maintained through the PPPL *HOTLINE* Newsletter. Energy Awareness month, using the DOE theme, "Energy Security For Peace and Prosperity," was conducted at the Laboratory in October, 1985. Posters encouraging energy conservation were displayed on bulletin boards throughout the Laboratory. Overall, employee cooperation and energy conservation awareness is high. All of this contributed to an effective Laboratory-wide Energy Management and Conservation Program that produced outstanding results.

Additionally PPPL, in an effort to preserve Laboratory funds, went into contract in May with PSE&G for interruptible electric service. This three-year

contract will be adjusted annually (kilowatt and dollar credit) on the basis of the previous summer's kilowatt demand peak average. In FY86, a $420k saving in electricity costs were realized because of this contract.

Plant Maintenance

The Plant Maintenance and Engineering (PM&E) Division's work force was reduced for the second consecutive year. Full-time equivalent (FTE) employees within PM&E dropped from 150 in FY84 to 127 in FY85 to 108 in FY86 (a 28% reduction over the two years). This was done at a time when the Laboratory was in full operation and great demands were made to provide smooth, uninterrupted operating time for TFTR. Curtailment of nonessential services, reductions in preventive maintenance, careful selection of work projects, and work procedural changes aimed at greater efficiency were initiated in order to keep the level of operations safe and acceptable.

Cost savings and greater efficiency were made possible by expanded use of the computerized maintenance work order program and the now totally in-house computerized preventive maintenance system. The computerized minor work order system (under 4 hours of labor to complete), with efficient controls, established 100% time reportability. Consolidation of some work forces made the Plant Maintenance Branch more versatile and productive. Fiscal year 86 saw 4,425 service calls, 3,008 major work orders (requiring four or more hours of labor to complete), and 1,100 preventive maintenance work orders, for a total of approximately 70,000 scheduled man-hours.

Physical plant upgrading projects that were accomplished during FY86 included the reroofing of the east wing of the Lab Office Building, installation of an energy-efficient hot water system for the cafeteria, and the addition of bathroom facilities in a remote area of the TFTR complex. Also, in order to meet the fire code, a new emergency diesel engine was installed on a canal water pump. Another project that will reduce our utility costs was the installation of a canal water filter that enables the cooling tower to use low-cost canal water instead of the municipality-supplied potable water. An interconnection of chilled water plants allows the operating plants to be more versatile, to have back-up capabilities, and saved a large capital outlay for new equipment.

Safety improvements in FY86 included the installation of sprinkler systems and fire protection alarms. A 48-inch storm sewer that serves most of C-Site was redirected through an upgraded D-Site detention basin where oil-detection equipment was added. Several other oil spill containment projects were also completed.

Many of the above projects were completed by a labor-hour force supplied by outside contractors but administered by Plant Maintenance. This is the second year that contracts for all trades were awarded to outside contractors to supply manpower on demand on a cost-per-hour basis. Sixteen projects were completed within budget and a total of $137,000 was expended in FY86 using the labor-hour system. This was managed despite a reduction in PM&E manpower.

In spite of the adverse affects of funding and manpower cutbacks, the Plant Maintenance Division received an "excellent" rating in FY86 as the result of an audit by the Department of Energy. This was the first time in the history of PPPL that Plant Maintenance received such a rating.

Maintenance Training

In-house training in maintenance procedures continued to receive strong support in FY86. Nine PM&E employees attended in-house classes for two hours, twice weekly for an eight month period. This was the ninth year that these vendor-designed (Technical Publishing Company) courses were given. With the reduction of manpower in Maintenance, this program is more important than ever, because it enables the staff to work more efficiently. Safety training also continued to receive strong emphasis, with all PM&E mechanics attending monthly training sessions on various safety-related subjects. Additionally, the need for special instruction on specific equipment was recognized, with training provided for pyrotronics and radiation safety.

Maintenance Safety Support

The Administration Department Area Safety Coordinator Program provided adequate safety support in FY86 through monthly safety meetings and inspections which enabled prompt response to safety-related problems and situations as they occurred. Safety inspections generated a total of 352 safety-related work orders with an expenditure of 1,800 man-hours of effort in FY86.

The computerized work order system enables the accurate tracking and timely response to safety-related items, thereby contributing to the overall Laboratory safety program, which is presently recording 1.5 million man-hours without a lost-time accident. The PM&E Division alone continues to add to a Laboratory record of 971 consecutive days by a major Division without a lost-time accident.

Library

Library operations and activities continued apace in FY86 as 2,741 books, 1,331 journal articles and 437 technical reports were circulated to PPPL staff. A total of 1,396 or 31% of these materials were borrowed from other libraries, most from within the Princeton University system. During FY86, a total of 1,332 fusion-related journal articles and 1,110 technical reports were catalogued by the Assistant Librarian. A PPLTEST file using SPIRES data base software on the IBM 3081 was designed for inputting bibliographic information and is currently being used to produce catalog cards and a monthly acquisitions

list of the fusion-related materials received by the Library. The next objective is to provide Laboratory-wide access to this file.

Computerized Information Retrieval Systems

By using terminal emulation software and/or dial-up access privileges, the Library uses its IBM PC/XT microcomputer to access the Princeton University Library's acquisitions and circulation system (Geac) and online catalog (Carlyle). It is also used to access the Research Libraries Information Network (RLIN), the Physics Information Network (PINET), the DOE Energy Data Base, NASA/RECON, the National Library of Medicine's MEDLINE, Chemical Abstracts Service's CAS ONLINE, and a wide variety of data bases available through DIALOG's information retrieval system.

Computerized Information Dissemination Systems

Using the electronic mail facilities on the Laboratory's PPLNET, the Library staff can send messages to Library patrons (recalls, notices that a requested book has arrived, etc.) and patrons are encouraged to transmit their information requests electronically. A Library News "bulletin board" was established (a daily list of new journals received) which the patrons can access from their home and/or office terminals.

The results of bibliographic searches have been downloaded on the IBM PC/XT and delivered to patrons in a variety of formats, including floppy disks, or transferred directly to the user's computer account. Library staff has also used MFENET to communicate with MIT's Plasma Fusion Center Library, TigerNET, to communicate with librarians and computer staff on main campus, and BITNET to communicate with patrons and colleagues around the world. The microcomputer and modem have not changed what the Library does—it is still involved in information storage, retrieval and dissemination—but they have certainly influenced how the Library accomplishes those tasks.

Information and Administrative Services

The Information and Administrative Services Branch includes all Laboratory services supporting the preparation and dissemination of information pertaining to PPPL's program. Included are photography, graphic arts and technical illustration, word processing, printing, duplicating, technical information, and public and employee information. Various administrative services—specifically, telecommunications, mail, and travel services—are also provided.

Public and Employee Information

The Public and Employee Information Section of the Information and Administrative Services Branch is responsible for providing up-to-date information on PPPL's program for members of the general public, the news media, representatives of government and industry, and employees of the Laboratory. The section maintains an information kit consisting of brochures and information bulletins that are written for the layman. An employee newsletter, PPPL *HOTLINE*, is published monthly. The staff coordinates an active speakers bureau, Laboratory tour program, as well as media relations and community outreach activities.

During FY86 several of PPPL's public information publications were updated to incorporate new experimental results. Updated editions of the TFTR and S-1 Information Bulletins were produced and the first edition of a PBX-M Information Bulletin issued. Review and updating PPPL's lobby displays was also undertaken, which resulted in the modification of the Tokamak Plasma Conditions wall mural in the TFTR Visitor's Gallery to reflect the major advances achieved by TFTR. The large wall display opposite the cafeteria entrance was completely replaced with new panels summarizing PPPL's current program as well as plans for the future.

A substantial portion of July and early August was spent in preparation for a news conference to announce the achievement of 200 million degree Celsius temperatures on TFTR. The conference, held Thursday, August 7, was well attended by the news media and resulted in substantial national and international coverage. Articles appeared in the *New York Times*, *The Washington Post*, *The Wall Street Journal*, and the *Boston Globe*. Television coverage included a broadcast on NBC network's evening news as well as coverage by local and Philadelphia stations. The resulting upsurge in media interest in TFTR and PPPL's plans for the Compact Ignition Tokamak continued into the early months of FY87.

PPPL's Community Outreach Program was initiated in 1982 with the goals of fostering a broad base of local public understanding of the Laboratory's program and forging closer communication links to local government, industry, and educational institutions.

In January 1986, as part of Community Outreach, PPPL repeated the Science-on-Saturday Seminar Program. The program was expanded from 35 to over 150 local high school students who attended an eight-week series of lectures, demonstrations, and tours arranged by PPPL, covering a variety of scientific subjects.

PPPL's Summer Work Grant Program was also expanded in FY86. Eight outstanding high school students were hired for eight weeks by PPPL's and

assigned to assist the Laboratory's scientists and engineers. As in previous years, both students and PPPL participants found the experience rewarding.

Graphic and Photographic Services

In FY84, a voice recording capability was added to PPPL's photographic arsenal with the purchase of a 3/4-inch video camera and recorder. To the extent possible, and within manpower limitations, this capability has been used to create stock footage of TFTR and to support the TFTR technical training effort. During FY86, video editing equipment and a second camera were purchased, thereby giving PPPL the ability to create edited video productions.

Word Processing Services

In mid FY86, as a result of a reduction-in-force, centralized word processing production service could no longer be provided by the Word Processing Center. The group continued to provide NBI network management, training, and operations services.

During FY86, NBI users enjoyed favorable uptime as evidenced by records for the three NBI central units: MUTT, 97%; JEFF, 99%; and A-Site, 99%. In-house word processor training was provided for seven clerical staff. A mid-range volume laser printer was acquired early in the year.

Printing and Duplication Services

The PPPL Duplicating Facility was reconfigured in FY86; this included its relocation to a smaller area at A-Site and the replacement of the Xerox 9200 with a Xerox 1090. There was a 6% decrease in production from FY85 to 4.5 million impressions; however, the Duplicating Facility's share of lab-wide copying increased from 35% in FY85 to 42% in FY86.

The number of individual printing procurements through the U.S. Government Printing Office in FY86 totaled 37 with a total dollar outlay of $66.5k.

Telecommunication Services

The Telecommunications Services Section of the Information and Administrative Services Branch is responsible for the provision of cost-effective voice communication services. The section recommends hardware and supervises and coordinates repairs, installations, and the billing process. During FY86, the staff handled 3,300 requests for moves, installations, and changes in telephone service.

Several major projects were underway during FY86 including:

- Conversion of PPPL's radio communication system from VHF to UHF. The fixed radio equipment was installed during FY86 with replacement of VHF mobile equipment to occur in early 1987.
- Procurement of a digital telephone switch to replace PPPL's current Centrex System. The schedule calls for a contract to be awarded in June of FY87 and installation in early FY88.
- Selection of an equal-access carrier for PPPL's toll calls. The contract will be awarded in early FY88.
- Design and implementation of a computer program that identifies telecommunication facilities and equipment throughout the Laboratory.

Personnel

The Personnel Division was responsible for several major activities during FY86. Summaries for each are given below.

Work Force

The two-year voluntary separation program implemented in FY85 did not generate sufficient staff reductions to meet the budget reductions under the Gramm-Rudman-Hollings legislation. Thus, a second, involuntary reduction-in-force was required and was implemented in February 1986. This action, plus the continuing termination of employees through the Voluntary Separation Plan, attrition, and other separations, enable the Laboratory to meet its targeted FY86 year-end staffing objectives.

Small Group Meetings with Employees

The Laboratory initiated a major program to improve communications between managers and their staff. Eighty meetings with employee groups called "Dialogue Sessions," were conducted by the Employee Relations Branch. These sessions were designed to respond to employee concerns or complaints and to provide a vehicle for upward communication. Following the initial Dialogue Session, the Employee Relations representative met with managers several levels above the employee group and, protecting the anonymity of the individuals, reviewed the items discussed. Responses prepared jointly with line managers were discussed in a subsequent second meeting of each employee group with a manager at least one level above the supervisor of the group present. Following these discussions, each issue was responded to by the line manager.

Communication to Supervisors

A program of quarterly information meetings with all supervisory personnel was implemented during FY86. The purpose of the meetings was to provide an update on Laboratory programs and objectives, to advise supervisors of anticipated changes, and to give supervisors the opportunity to raise questions and concerns they might have for top management (to address).

Position Descriptions

The Compensation Section began the process of updating all Administrative position descriptions by various job families. The project requires the reevaluation of all such positions by a Laboratory Evaluation Committee utilizing the Hay System. It is designed to audit internal equity among jobs and their relative value to the Laboratory.

The Compensation Section conducted and completed a study of all computer-related positions within the Administrative, Office Support, Laboratory and Shop, and Engineering and Scientific Staffs. The study addressed questions regarding the ranking, classification, and compensation of all computer-related positions at PPPL. A task force was formed consisting of representatives from the Information Resource Management Division, PMS Section, CICADA, and the Personnel Division. Based upon task force recommendations, career paths and specific job families were created for Computer Operators, Scientific Applications Programming, Business Applications Programming, and Data Processing Assistants.

Opinion Survey

The Laboratory contracted with Opinion Research Corporation of Princeton to conduct an Employee Attitude Survey. Eighty percent of the employees completed the survey questionnaire which was designed to measure employee attitudes and to compare them to other organizations in such areas as job satisfaction and commitment, working conditions, pay and benefits, career development opportunities, management and supervision, and operating procedures. The results will be disseminated during the first quarter of FY87.

Occupational Medicine and Safety Office

The Occupational Medicine and Safety (OM&S) Office provides services to Laboratory personnel and organizations in occupational medicine, health counseling, alcoholism rehabilitation, worker's compensation administration, industrial hygiene, hazardous safety, safety training, fire prevention, emergency planning, safety management auditing, and safety policy administration. It also provides consultation and guidance to Laboratory management in health matters and assists the Personnel Division in administration of disability absence and the employee-assistance program.

Computerized data bases have been created and are being expanded for accident analysis; safety training needs, safety courses given, and the training status of individual employees; hazardous materials inventory; hazardous materials labels; scheduling medical surveillance procedures; and tracking employee's medical qualifications for specific jobs and tasks.

Safety Branch

The OM&S Safety Branch provided leadership in the revision of several sections of the Health and Safety Manual. The Manual provides guidance to Laboratory personnel in the safe performance of their work.

Radiation monitoring was improved from a system of monitoring personnel on a monthly basis for some employees and a quarterly basis for others to a uniform monthly program. This was done in response to the need for more careful monitoring due to the increase in the activation of the TFTR during pulses and for brief periods following them. Analysis of the film badges continued to demonstrate a level of radiation exposure well within the limits prescribed by the DOE.

The Laboratory's accident experience continued to show improvement. On August 6, the Laboratory accumulated one million person-hours of work time without a lost-time injury—the second time in the past two years it achieved this record. Consequently, the Laboratory received the DOE Award of Excellence for continued safety performance. Further, its improved safety record for research laboratories nationwide continued during 1985, earning the National Safety Council's highest recognition, the Award of Honor. In addition, the State of New Jersey presented the Laboratory with its Industry Recognition Award for the Laboratory's low number of lost-time accidents and lost workdays as compared to the records of industries and companies within Mercer and surrounding counties.

The Safety Branch initiated a program of safety audits of Laboratory organizations. Six groups were audited and a Laboratory-wide audit of lifting and hoisting procedures was done. This program will continue with each segment of the Laboratory being audited every three years.

The Area Safety Coordinator (ASC) program was improved by strengthening management support and by conducting periodic meetings with safety professionals. The success of the efforts by the ASCs has been reflected in the steady decrease in unsafe conditions noted on the periodic safety inspections and by the decrease in the Laboratory's injury rate.

Industrial Hygiene Section

The Industrial Section continued its activities in control of potentially hazardous exposures to chemical and physical agents and in bringing the Laboratory into compliance with the New Jersey Worker and Community Right-to-Know Act and with the federal Occupational Safety and Health Administration's (OSHA) Hazard Communication Standard. Training sessions were held for employees on several topics of hazard control.

Medical Branch

The Medical Branch continued to provide diagnostic and therapeutic services to Laboratory personnel.

A computerized electrocardiograph analysis program was installed to enhance its capabilities in this area.

Department of Public Safety

In October 1984, the Emergency Services Unit and the Security Department on Forrestal Campus were merged to help reduce public safety expenditures. In July 1985, the Princeton University Security Department was renamed the Department of Public Safety, and the unit on the Forrestal Campus was designated as the Forrestal Division of the Department of Public Safety. A Managing Director was hired to administer the Forrestal Division.

The impact of the "Gramm-Rudman-Hollings Act" required the reduction-in-force of four Emergency Service Officers. This reduction complicated the normal and predictable difficulties of merging a fire-fighting force with security operations. Notwithstanding, personnel at all levels cooperated to maintain a high level of service which merited a DOE exemplary rating.

A number of appraisal and functional audits were conducted during the fiscal year. The agencies involved were:

- DOE/Chicago Office and Princeton Area Office
- Factory Mutual Life Insurance Company
- Inspector General's Office of DOE
- Princeton University-Office of the Controller
- PPPL Occupational Medicine and Safety

In FY86, the Department of Public Safety provided PPPL senior management with a comprehensive "Bomb Threat" procedures manual to assist senior managers in dealing with potential and actual incidents.

During FY86, the Security Unit initiated new procedures at the C-Site entrance booth to enhance security at both C- and D-Sites, new visitor's badges were designed and introduced, and the Emergency Services Unit moved into new facilities adjacent to the Office of Occupational Health and Safety at C-Site. These facilities provide quarters for the Duty Fire Captains and Driver Operators.

Procurement

Fiscal Year 1986 was a time of transition for the Procurement Division, as the emphasis in the Laboratory budget for external purchases shifted decisively toward maintenance and operation of existing facilities. The Division entered the year with an authorized staff level of 24 and completed it with 22. To maintain and improve the productivity of its staff, the Division completed the first phase of a four-year plan to automate its operations through the use of a personal computer-based local area network which will eventually link all managerial, professional, and clerical personnel through shared data bases.

Continuing in the tradition established over the past three years, the Procurement Division successfully sought out new methods to achieve its commitment to increase the amount of goods and services procured from small businesses and small businesses owned and operated by socially disadvantaged individuals (see Fig. 1). In 1986, the Laboratory's goal was to place 46% of its procurement dollars with small businesses and 4% with small disadvantaged businesses. The actual results were 59.8% with small businesses and 7.5% with small disadvantaged businesses—once again exceeding the agreed-upon goals. Three buyers in the Purchasing Branch—Dorothy Quinn, Skip Schoen and Arlene White—were honored for their work with the minority business community by the New York/New Jersey Minority Purchasing Council at its annual awards banquet in April, 1986.

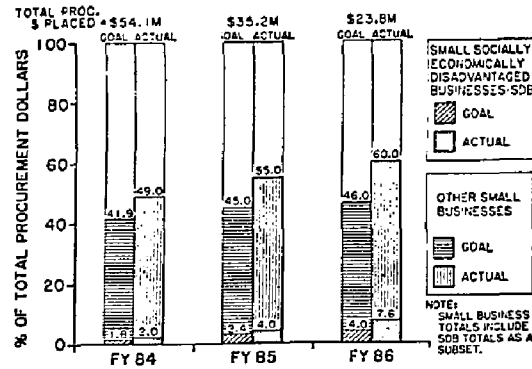

Fig. 1. Small Business (SB) and Small Disadvantaged Business (SDB) sales to PPPL. Goals versus actuals by fiscal year. Note increased participation in a period of reduced funding. (87A0011)

During November 1985, DOE conducted a contractor procurement system surveillance which again found the Procurement Division to be performing in a manner judged "...responsive to contract requirements...with more than adequate results...," and requiring correction of only a few minor deficiencies. As a result, Procurement's authorization levels were increased to $250,000 for cost-type actions and $1,000,000 for fixed-price actions awarded competitively.

Reduced budgets once again curtailed staff education, but specific training was provided to individuals rotating to new job assignments within the Division. In all, a total of three people attended procurement-related courses during the year.

Materiel Control Office

The focus of Materiel Control's efforts during the past year was directed toward increasing the efficiency and effectiveness of internal operations. Reductions in staff and budget, coupled with a relatively stable workload, required improvements in productivity and space utilization. A number of

projects were undertaken to achieve these objectives. Storage facilities were consolidated and storage racks installed to provide better utilization of space and personnel. As a result of the consolidation, there was a 10,000 square foot reduction in Laboratory storage requirements. Receiving #3 and #4 functions were combined and a conveyor system was installed to increase productivity, reduce material backlogs, and provide an orderly flow of material from receipt to delivery. Hardware acquisition and software development for the Automated Receipts Processing System were completed. This system, which will be fully implemented during the coming months, will eliminate redundant tasks, streamline receipts processing, and provide automatic update of procurement files. Maintenance spares were cataloged to provide visibility of assets for review and redistribution. Bar coding of capital and sensitive equipment was concluded, resulting in faster and more accurate physical inventories.

A major project was undertaken this year in the Stockroom Operations Branch to obtain a vendor to supply all Laboratory office supplies. When implemented, the process will improve supply support to the Laboratory, reduce our inventory investment, increase available storage space, and result in a substantial workload savings in the stockroom. The planned implementation date is March 1987. In other stockroom activities, there were 85,000 withdrawals processed, resulting in sales of $1.5 million. The Spares Parts Section processed $311k in withdrawals and had receipts of $1.2 million.

In the Warehouse Operations Branch, a comprehensive review was conducted of material left over from the construction phase of the TFTR project. A substantial number of assets were applied against Laboratory requirements, while others were held for future use. Walk-thrus of storage areas were conducted, which resulted in disposing of unneeded material and equipment and reduced rented storage space. In Property Administration, the inventory of 13,000 equipment items continued; 85% of the project was completed. An equipment-custodian training program was developed, and property-awareness training will be provided during the coming year.

The Excess Property Section obtained 31 equipment items valued at $230k for use by Laboratory activities. Retirements and transfers accounted for a reduction of 491 items valued at $1.0 million. Monies returned to PPPL, as a result of recycling scrap, were $91k. The Shipping and Receiving area processed over 20,000 deliveries and made 3,000 outgoing shipments.

Hazardous material disposal continued to be an important function of the Materiel Control Office in FY86. Additional manpower was assigned to expedite pick-up and disposal of hazardous material generated by the Laboratory. Forty-four shipments of hazardous material were made, including over 1,200 PCB capacitors which were taken out of service. Total expenditures for hazardous material disposal for FY86 was $75k. Additional actions to reduce hazardous material at the source were emphasized as disposal costs continued to rise and regulations governing disposal became more restrictive.

CONTROLLER'S OFFICE

The Controller's Office has responsibility for Laboratory Planning and Budgeting, Accounting and Financial Control, and Information Resource Management. During FY86, the Performance Measurement System (PMS) Office was combined with the Budget Office to increase efficiency and to improve the integration of the Laboratory planning activity with the financial management systems.

Funding reductions were a dominant factor in FY86. The Controller's Office continued to conduct its operations at the Laboratory with a reduced staff by increasing efficiency without markedly changing the essential services provided by the various units. Significant benefits resulted from improvements in data management and in the software that operates the Laboratory management information systems. These include the implementation of a new microcomputer-based Receiver System and the complete restructuring of the PMS information management to make better use of more modern technology and to better fit within the overall Laboratory management information systems.

A management information system design review held over a two-day period in July was attended by major users of PPPL administrative systems as well as three outside reviewers. Over 100 comments were received and are in the process of being acted upon. It is clear that additional reviews should be planned, since substantial benefits were derived by both the reviewers and the system managers responsible for the operation, maintenance, upgrade, and development of the management information systems at the Laboratory. Most importantly, the review provided an opportunity for Laboratory staff to understand the scope and interrelationships of the management systems in place at PPPL, thereby improving communications in this area.

Table V summarizes the financial activities of the Laboratory for the last five years.

Budget Office

The usefulness of the Budget System to Laboratory management for budget status and control continued to improve during FY86. The preparation of the Field Task Proposals utilized for the first time information from PMS to help in the formulation of the proposals. The proposals were submitted to DOE ahead of schedule.

The projects continue to enter spending plans into the Accounting System through the PMS Office and maintain these independent of the institutional budgets entered by the Budget Office. This enables the individual project to optimize plans around funding needs, staffing, and other factors without the

Table V. PPPL Financial Summary
(Thousands of Dollars)

	FY82	FY83	FY84	FY85	FY86
OPERATING (Actual Costs)					
Department of Energy					
TFTR Res and Develop Operations	$ 2,945	--	--	--	--
TFTR Facility Operations	10,424	$ 18,029	$ 16,725	$ 18,988	$20,035
TFTR Tokamak Flexibility Mod	13,033	17,725	19,358	13,658	--
TFTR CICADA	4,044	8,588	10,327	9,578	6,817
TFTR Neutral Beams	6,253	24,410	22,166	23,475	16,091
TFTR Experimental Research	2,835	5,682	5,422	4,776	6,179
TFTR Diagnostics	8,973	14,143	13,146	10,124	11,343
TFTR Remote Handling	--	65	813	807	--
TFTR Tritium Systems	--	301	2,628	1,501	3,688
TFTR Pellet Injector System	--	--	129	1,049	(1,049)
PLT/PDX/PBX	18,893	17,846	18,501	14,425	13,785
RF Development	--	742	617	361	185
ACT-I	443	458	408	408	269
S-1	3,254	3,703	3,561	3,270	3,047
Ignition Studies Project	--	--	2,744	1,205	2,094
Theory	2,488	2,808	3,061	3,162	2,629
Applied Physics	1,280	1,352	655	833	519
Other Operating	495	418	457	1,379	190
Fusion Engineering Device	412	--	--	--	--
Change in Inventories	(237)	(3,169)	(599)	(721)	(173)
X-Ray Laser Development	266	313	16	743	1,543
Energy Management Studies	197	47	125	146	67
Department of Defense	297	77	278	228	343
Other Contracts	565	893	1,880	2,837	903
Total Operating	$76,860	$114,431	$122,418	$112,232	$88,505
EQUIPMENT (Budget Authorization)					
Capital Equipment not Related to Construction	$ 9,272	$ 10,285	$ 8,896	$ 5,920	$ 6,350
CONSTRUCTION (Budget Authorization)					
TFTR	$31,600	$ 1,800	$ 255	--	--
General Plant Projects	1,400	1,000	1,000	1,532	874
Energy Management Projects	--	499	1,049	847	192
Total Construction	$33,000	$ 3,299	$ 2,304	$ 2,379	$ 1,066

customary institutional constraints that are present when considering the Laboratory as a whole. The individual project spending plans are reviewed by the Program Committee and, in conjunction with the Budget Office, an overall program is developed within institutional boundaries. Throughout the year, this results in more management attention being drawn to the real or perceived needs of the projects and helps address conflicts with the institution as a whole. Towards the end of the fiscal year, institutional reality and project plans become focused at the funding level.

The Budget Office, working with the Laboratory's Budget and Manpower Committee, continues to play a major role in manpower planning. This was important in FY86, since the PPPL staffing was reduced from 1,121 to 1,040. This cutback was achieved by a reduction-in-force and the continuation of the incentivised voluntary separation program. The indirect expenses at the Laboratory continued to attract management attention during the FY86 period. Careful review and analysis of the real needs in the indirect area continued, and quarterly Indirect Cost

Reviews organized and administered by the Budget Office are the forum for this.

Performance Measurement System

Efforts continued during the year toward maintaining and enhancing PPPL's Performance Measurement System (PMS) as a management tool used by both project and engineering departments for cost and schedule control. Despite a reduction-in-force of 16% in the PMS Office during the year, improvements in systems operations lead to the continued accomplishment of PMS objectives.

Ongoing efforts during FY86 included:

- Formal work planning, estimating, and authorization processes, including processing and controlling approximately 840 job plans in FY86.
- Formal monthly progress statusing and variance analysis.
- Utilization of PMS data in monthly management meetings as well as in the PPPL budgetary process. The PMS was most useful in anticipating potential cost and schedule impacts, including estimating project at completion costs.

In addition to ongoing system maintenance, significant accomplishments were made in the following areas:

- Summary schedules were produced for major PPPL programs including TFTR, PBX-Modification, and CIT. These plans highlight critical tasks and milestones necessary to achieve project goals and objectives.
- Easy on-line access to PMS data via PUBSYS was implemented in midyear resulting in enhanced user report capabilities and improved turnaround in monthly report processing.
- General Plant Project (GPP) and Energy Conservation projects were added to the PMS system data base, providing increased cost and schedule visibility into these areas.
- Production of monthly management summary graphs was automated, resulting in reduced processing time as well as simplified maintenance (Fig. 2).

Information Resource Management

In FY86, Information Resource Management (IRM) continued developments initiated in FY84 through FY85 with emphasis on three major areas: the enhancement of the Performance Management System (PMS); the development of an automated receiving system; and increased utilization of the PPPL IBM 4361.

The Performance Management System interface to other systems (Accounting, Budget, etc.) was

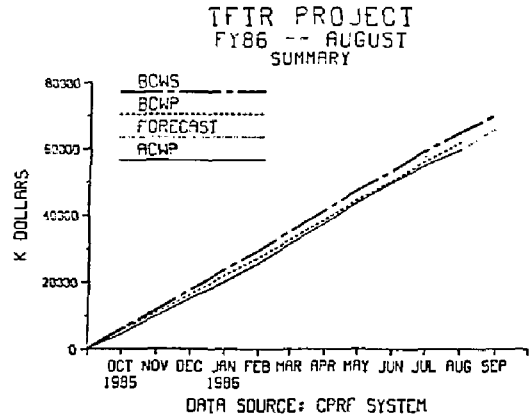

Fig. 2. Cumulative cost performance graph for TFTR. (87A0253)

completely rewritten and revised to accomplish the following goals:

- Complete integration of projected job cost estimates into the accounting system operational files on a timely basis.
- Availability of reasonable reporting files and report routines for PMS data.
- Straightforward and clearly defined means of updating PMS data.

All of the above goals were met, and development will continue into FY87 with emphasis on improving the end user interfaces in managing the PMS source data.

The Automated Receipts Processing (ARPS) was written and accepted by the users as a functioning system (Fig. 3). The system is based primarily on personal computers (AT/370) and utilizes mainframe files and processing code. This system, while important in itself as a useful tool for the Materiel Control Office, has even greater importance as a successful pilot project in demonstrating the potential for utilizing personal computers in applications to replace or enhance mainframe processors.

The IBM 4361 was pressed into even heavier usage as the computer programming staff moved development and testing from the PUCC 3081 to the 4361. This resulted in substantial cost savings. It also resulted in a study and subsequent proposal to increase the processor capacity of the 4361 to a 4381 in FY87. Projections indicate that costs associated with usage of the PUCC 3081 would be substantially reduced, while local costs would increase only slightly.

Accounting and Financial Control Division

During FY86, the Accounting and Financial Control Division staff was reduced by three. Productivity was maintained, and efficiency and effectiveness were

```
                        PPL Receiving System - Receiver Entry
P.O.  P973260          Buyer  : 10                  Attention: STOCKROOM
Vendor: PROFTECH CORP.
Internal-
Notes
A  LN   Ordered   Recvd  EQ QA Deliv UM      D  E  S  C  R  I  P  T  I  O  N
X  01      1.00    0.00      860926 E  IPCO PLAIN PAPER, 8 1/2 X 11 GOLDEN ROD
?  02    200.00    0.00      860926 E  #2 SEMI-HEX PENCILS PPL STK #180446


 F3-QUIT(NOUPD) F5-SELECT F7-PAGEBWD F8-PAGEFWD F12-PRINT
L4^                                    2                  1 Local 3270 Session
```

Fig. 3. Sample input screen for Automated Receipts Processing System. (87A0255)

increased by cross training the current staff so that each staff member can perform a number of functions. Accounts Payable personnel were also retrained to access the many files that were upgraded and transferred to the Public Information System (PUBSYS). PUBSYS has significantly decreased the time spent in researching and retrieving information and in responding to vendor inquiries.

During the year, the activities and personnel of the Data Base Administration Branch were transferred from the IRM Division to the Payroll Branch. Consolidation of these activities has improved efficiency and speeded payroll processing. The payroll timesheet was redesigned and the nonproductive time report reformatted. Both changes were implemented October 1, 1986.

A new system for recording and processing travel advances and expense reports was designed, tested, and installed. This provides detailed information by traveler for each trip and a more accurate aging schedule for outstanding advances (Fig. 4).

To comply with a DOE Directive, staff from the General Accounting Branch received training in the DOE electronic reporting system for automated data processing equipment in order to transmit PPPL data directly to DOE records. The Laboratory records and procedures were also revised to meet the new DOE definitions and recording requirements for all types of capital equipment.

All branches of the Division provided extensive assistance to the auditors of the DOE Inspector General and to the Internal Audit staff of the University in connection with a number of surveys and audits of PPPL records and procedures. In those cases where the Division procedures were involved, the audits found no material weaknesses. In addition, the Division procedures and performance were evaluated "good" by the DOE area office.

The Division is participating in a Cooperative Education Program of the West Windsor-Plainsboro High School. This program provides the students with work experience and skills which will be useful to them after graduation, and it enables the Laboratory to meet peak work loads and job coverage for employees' unscheduled absences.

During the year, PPPL was elected to full membership in the DOE Laboratories Finance and Accounting Group.

```
          PRINCETON UNIVERSITY - PLASMA PHYSICS LABORATORY
                ACCOUNTING DIVISION - TRIP SYSTEM

     TRIP NUMBER                          T001423
     DEPARTURE DATE (MMDDYY)              021087
     RETURN DATE (MMDDYY)                 031087
     DESTINATION                          SAN DIEGO_____________
     EMPLOYEE ID                          090718
     LAST NAME                            GANTIOSA F
     PARTIAL ACCT NUM (CC,WF,JN)          6341****NUL
     ------------------------------------------------------------
     TYPE    TRANSACTION   EXP   VENDOR        AMOUNT        PAYSTUB
     CODE    DATE (MMDDY) CLASS   NO                         DESCRIP
X    A         022?7       3901  090718    1500.00_____     CALIF A
_    _         _____       ____  ______    ___________      _____ _
_    _         _____       ____  ______    ___________      _____ _
_    _         _____       ____  ______    ___________      _____ _
_    _         _____       ____  ______    ___________      _____ _

 PF2-SUBMIT CHANGE  PF3-QUIT
```

Fig. 4. Sample input screen for travel advance system. (87A0254)

PPPL Invention Disclosures for Fiscal Year 1986.

Title	Inventor(s)
Improved "OSM Connector" Assembly Tool for Semi-Rigid Coax Cable	H. Dymowski
Generating Current by Inverting the Energy Distribution of Alpha Particles	N. Fisch
Alfvén Wave Heating in Toroidal Plasmas by the Low-n Toroidicity-Induced Shear Alfvén Eigenmodes	C. Cheng
Feedback Control of Sawtooth Mode in Tokamaks	R. White
Relativistic Electron Beam Driven X-Ray Laser	E. Valeo S. Suckewer
Energetic Particle Stabilization of m=1 Kink Modes in Tokamaks	I Chen Hastie
Interdigital Fast Wave Antenna	P. Colestock
Beam-Ion Profile Diagnostic Using Pellets and Neutron Flux Measurements	W. Heidbrink
Zero to 360° Phase Detector	L. Meixler
Apprentice System for Plasma Physics Theory	H. Mynick
MHD Current Drive in a Tokamak by Oscillating Loop Voltage and the Horizontal or Vertical Field	A. Boozer
Hydrogen Isotope Separation Utilizing Bulk Getters	R. Knize J. Cecchi
A Novel Modification of Toroidal Plasma Device to Produce Low Energy Neutral Beams	W. Langer S. Cohen D. Manos R. Motley
Neutral Beam Facility	R. Motley S. Cohen W. Langer D. Manos
Gyro-Electron Ghost Images Due to Microchannel Plate Operation in Transverse Magnetic Fields	A. Roquemore S. Medley
Collisional Plasma Phase Conjugator	J. Federici D. Mansfield
Neutral Beam Interlock System on TFTR Using Infrared Pyrometry	S. Medley H. Kugel T. Kozub J. Lowrance V. Mastrocola G. Renda K. Young

PPPL Invention Disclosures for Fiscal Year 1986. (Continued)

Title	Inventor(s)
Large Angle Optical Scanning by a Curved, Static, Steering Mirror	A. Ramsey
Tokamak Device Configurations for Laser Pumping	D. Jassby
A Software Package for Controlling Stellarator Equilibrium	A. Reiman H. Greenside
Method for Breaking Up Chemical Wastes by Bombardment of Plasma Ions on Metallic Walls	R. Motley W. Langer
High Current Density, Cryogenically Cooled Sliding Electrical Joint	H. Murray
Coil for Production of Optimum Magnetic Fields	J. Faunce
Differential Atmospheric Tritium Sampler	O. Griesbach J. Stencel
Coil Protection Calculator	R. Woolley
Pico-Second Delay Timer	L. Meixler K. Ilcisin J. Robinson W. Tighe L. Guttadora
Right Angle High-Voltage Connector	S. Kilpatrick M. Dereka
Personal Computer Equipment Antitheft Device	T. Kozub H. Kugel
Perforated Toroidal-Field Coils for Maximizing Neutron Transmission	D. Jassby
Woodruff Key Extractor	R. Pope

GRADUATE EDUCATION: PLASMA PHYSICS

The Plasma Physics Program was first offered at Princeton University in 1959 and two years later was incorporated into the Department of Astrophysical Sciences. The constant aim of the Program has been to provide pertinent graduate education in an environment that, over the past three decades, has seen enormous changes in the fields of plasma physics and controlled fusion. In this period, the Program has established its own traditions of education—centered on fundamentals in physics and applied mathematics and training—based on intense exposure to the cutting edge of research in plasma physics.

Graduate students entering the Plasma Physics Program at Princeton spend the first two years in classroom study, acquiring a firm foundation in the many disciplines that make up plasma physics: classical and quantum mechanics, electricity and magnetism, fluid dynamics, hydrodynamics, atomic physics, applied mathematics, statistical mechanics, and kinetic theory. Table I lists the departmental courses offered this past academic year. Many of these courses are taught by the members of PPPL's research staff who also comprise the seventeen-member plasma physics faculty (see Table II). The curriculum is supplemented by courses offered in other departments of the University and by a student-run seminar series in which PPPL physicists share their expertise with the graduate students.

Most students hold Assistantships in Research at PPPL through which they participate in the continuing experimental and theoretical research programs. In addition to formal class work, first- and second-year graduate students work side by side with the research staff, have full access to laboratory facilities, and learn firsthand the job of a research physicist. First-year students assist in experimental research areas, including TFTR diagnostics development, PBX, PLT,

Table I. Plasma Physics Courses Offered and Instructors.

Course Number	Course Title	Instructor
	Fall 1985	
AS 551	General Plasma Physics I	S.A. Cohen and S.E. von Goeler
AS 553	Plasma Waves and Instabilities	T.H. Stix
AS 558	Seminar in Plasma Physics	C.R. Oberman
AS 561	Special Topics in Magnetic Confinement	R.B. White
	Spring 1986	
AS 552	General Plasma Physics II	R.M. Kulsrud and W.M. Tang
AS 554	Irreversible Processes in Plasma	J.A. Krommes
AS 556	Advanced Plasma Dynamics	C.F.F. Karney and H. Okuda
AS 557	Advanced Mathematical Methods	M.D. Kruskal

Table II. Astrophysical Sciences/Plasma Physics Faculty.

Faculty Members	Title
Thomas H. Stix	Associate Chairman, Department of Astrophysical Sciences, and Associate Director for Academic Affairs, PPPL
Liu Chen	Principal Research Physicist and Lecturer with rank of Professor
Samuel A. Cohen	Principal Research Physicist and Lecturer with rank of Professor
Harold P. Furth	Professor of Astrophysical Sciences
Stephen C. Jardin	Research Physicist and Lecturer with rank of Associate Professor
Charles F.F. Karney	Research Physicist and Lecturer with rank of Associate Professor
John A. Krommes	Research Physicist and Lecturer with rank of Associate Professor
Martin D. Kruskal	Professor of Mathematics and Astrophysical Sciences
Russell M. Kulsrud	Principal Research Physicist and Lecturer with rank of Professor
Carl R. Oberman	Principal Research Physicist and Lecturer with rank of Professor
Hideo Okuda	Principal Research Physicist and Lecturer with rank of Professor
Francis W. Perkins, Jr.	Principal Research Physicist and Lecturer with rank of Professor
Paul H. Rutherford	Principal Research Physicist and Lecturer with rank of Professor
William M. Tang	Principal Research Physicist and Lecturer with rank of Professor
Schweickhard von Goeler	Principal Research Physicist and Lecturer with rank of Professor
Roscoe B. White	Principal Research Physicist and Lecturer with rank of Professor
Shoichi Yoshikawa	Principal Research Physicist and Lecturer with rank of Professor

S-1, CDX, and the X-Ray Laser Project. In a similar fashion, second-year students assist in theoretical research. Following the two years of class work, students concentrate on the research and writing of a Ph.D. thesis, under the guidance of a member of the PPPL staff. Of the thirty-five graduate students in residence this past year, nineteen were engaged in thesis projects—eight on theoretical topics and eleven on experimental topics. Table III lists the doctoral thesis projects completed this fiscal year under the Plasma Physics Program.

Outside support for the graduate program came, in part, from the Westinghouse Educational Foundation. Three students currently in residence hold Magnetic Fusion Science Fellowships and one student holds a Magnetic Fusion Energy Technology Fellowship. In addition, other students hold awards from the National Science Foundation, the Fannie and John Hertz Foundation, the State of New Jersey Department of Higher Education, and from the National Science and Engineering Research Council of Canada. Some of these fellowships are supplemented by partial research assistantships.

Overall, the plasma physics graduate studies program in Princeton University's Department of Astrophysical Sciences has had a significant impact on the field of plasma physics. One hundred and twenty-three physicists have received doctoral degrees from Princeton. Many have become leaders in plasma research and technology in academic, industrial, and government institutions. And this process continues as the Laboratory trains the next generation of scientists, preparing them to take on the challenging and diversified problems of the future.

Table III. Recipients of Ph.D. Degrees.

Carl Richard DeVore	
Thesis:	Theory and Simulation of the Evolution of the Large Scale Solar Magnetic Field, May 1986
Advisor:	R. Kulsrud
Employment:	Naval Research Laboratory
Gregory W. Hammett	
Thesis:	Fast Ion Studies of Ion Cyclotron Heating in the PLT Tokamak, April 1986
Advisor:	R. Kaita
Employment:	Princeton Plasma Physics Laboratory
Yuan Hu	
Thesis:	Trapped-Electron Transport via Microinstabilities, July 1986
Advisor:	F.W. Perkins, Jr.
Employment:	Department of Nuclear Engineering, National Tsing Hua University, Taiwan
Christopher J. Keane	
Thesis:	Studies of Population Inversions in the Soft X-ray Spectral Region in CO_2 Laser Produced Plasmas, May 1986
Advisor:	S. Suckewer
Employment:	Lawrence Livermore National Laboratory
Kyoung W. Min	
Thesis:	Numerical Study on the Earth's Magnetotail Formation and Magnetospherica Substorm, September 1985
Advisor:	H. Okuda
Employment:	Department of Space Physics and Astronomy, Rice University
Eric R. Salberta	
Thesis:	A Numerical Study of the Effects of Anisotropic Pressure on Ideal MHD Equilibrium and Stability in Tokamaks, May 1986
Advisor:	J.L. Jonnson
Employment:	S. Cubed, Division of Maxwell Labs
Ralph A. Smith	
Thesis:	Aspects of Turbulent Transport in Bounded Plasma, June 1986
Advisor:	J.A. Krommes
Employment:	Department of Physics, University of California, San Diego
Frederick J. Wysocki	
Thesis:	Experimental Investigation of Line Tying Effects on the Spheromak Tilt Mode, December 1985
Advisor:	M. Yamada
Employment:	AT&T Bell Labs

GRADUATE EDUCATION: PLASMA SCIENCE AND FUSION TECHNOLOGY

The new Interdepartmental Program Plasma Science and Fusion Technology completed its first academic year during FY86. Graduate student enrollment decreased by one, from 11 to 10, in response to increasingly stringent budget pressures. At the present time, there are more students expressing an interest in entering the program than the number of positions available for which there is funding. Additional sources of funding must be found if the momentum generated over the last two years is to be maintained.

PROGRAMS

Princeton University has participated in the U.S. Department of Energy's Magnetic Fusion Energy Technology Fellowship (MFETF) Program for six years. There are two recipients of this grant in residence. One presently works in the Chemical Engineering Laboratory and the other has worked in the Spacecraft Glow Plasma Experimental Laboratory.

Attracted by the Laboratory's strong radio-frequency program, PPPL was host this past summer to two MFETF graduate students—one from the Massachusetts Institute of Technology and the other from the University of Michigan. Both elected to do their practicum work at PPPL. A Princeton student chose the Argonne National Laboratory as the site for his second summer practicum, as well as a winter session. This practical work, combined with independent research, is a requirement for all MFETF fellows.

The Cooperative Industrial Program in Plasma Science and Fusion Technology granted two certificates during the past fiscal year (Fig. 1). Mr. Ramakrishnan, on assignment from Ebasco Services, Inc., participated in the design, test, and commissioning of the hardwired controls for the high-powered rectifier for TFTR. Dr. Singh, on assignment from RCA Laboratories, brought with him some specialized radio-frequency plasma equipment for solid-state materials production. He worked with Dr. J.L. Cecchi in this activity, an example of how fusion-power-oriented plasma activities can be broadened to include various "spin-offs" stimulated by fusion research.

Fig. 1. Dr. Bawa Singh and Mr. Subrahmanya Ramakrishnan receive their certificates at a luncheon held at Prospect House following successful participation in the Cooperative Industrial Program in Plasma Science and Fusion Technology (86A0297)

ACTIVITIES

At the end of FY86, ten of the eleven students who were enrolled in the Interdepartmental Program in FY85 returned to continue their studies; one had received the M.S. degree and departed. A shortage of available funds prevented the admission of other students into the program, despite the unsolicited expressed interest of four Princeton students already in residence. It appears that with adequate resources the program could be expanded readily to include 15 graduate students. Seven of the ten students participating in the program are receiving support from PPPL. The remaining three students have fellowships. Their activities are detailed in Table I.

Table I. Graduate Students Participating in Interdepartmental Program in Plasma Science and Fusion Technology.

P. Pang[b]	
Thesis Topic:	Polymers
Advisor:	J.K. Gillham
Department:	Chemical Engineering
K.W. Goossen[a]	
Thesis Topic:	Fast Response Detectors
Advisor:	S.A. Lyon
Department:	Electrical Engineering
J.S. Lee[b]	
Thesis Topic:	Coupled Mechanical/Electrodynamic Analysis
Advisor:	J.H. Prevost/P.C.Y. Lee
Department:	Civil Engineering
G.D.C. Dhondt[b]	
Thesis Topic:	Radiation Damage
Advisor:	A.C. Eringen
Department:	Civil Engineering
R. Myers[b]	
Thesis Topic:	Plasma Propulsion
Advisor:	R.G. Jahn/A.J. Kelly
Department:	Mechanical and Aerospace Engineering
J.F. Quanci[a]	
Thesis Topic:	Tritium Recovery Experiments
Advisor:	R.G. Mills/D.L. Jassby
Department:	Chemical Engineering
D.-S. Shen[b]	
Thesis Topic:	High Speed Detectors
Advisor:	S. Wagner
Department:	Electrical Engineering
S. Chaturvedi[b]	
Thesis Topic:	Fusion Reactors
Advisor:	R.G. Mills
Department:	Chemical Engineering
Y.-G. Kim[b]	
Thesis Topic:	Coupled Mechanical/Electrodynamic Analysis
Advisor:	P.C.Y. Lee/J.H. Prevost
Department:	Civil Engineering
D.W. Roberts[a]	
Thesis Topic:	Undecided
Advisor:	W.D. Langer
Department:	Astrophysical Sciences

[a]Supported by Fellowship.
[b]Supported by the Princeton Plasma Physics Laboratory.

DEPARTMENT CURRICULUM

The Chemical Engineering Department at Princeton University offers a strong undergraduate curriculum to stimulate interest in fusion research (see Table II). In keeping with Princeton's tradition of undergraduate thesis work, Junior and Senior independent work in this field is also sponsored. The undergraduate course, Introduction to Fusion Power (Ch.E. 417), is suitable for both undergraduate and graduate students, and it has been elected by graduate students in four different departments.

Each year Chemical Engineering 417 welcomes as auditors several members of the professional engineering staff of the Laboratory. These people are specialists seeking a broader understanding of aspects of the Laboratory work that differ from their professional specialty. Since FY87, this arrangement has provided a unique opportunity for students to associate with working professionals in the topic of the course. To reinforce this opportunity, a key feature of the course is a machine design project. The class is divided into two teams for a competition. The professional staff members are divided into three groups, two sets of consultants for the teams and a selection board to evaluate the final design and "award the contract." Oral presentations before the board are a fairly realistic preview of the "real world's" contractor selection procedures.

With the addition of the remaining School of Engineering and Applied Science (SEAS) departments to the Program, other pertinent courses, both on the graduate and undergraduate level, are available to the students. These are listed in Table III, together with three courses of interest in Astrophysical Sciences.

Chemical Engineering 417, Introduction to Fusion Power, was founded by Dr. R.G. Mills fourteen years ago. He taught it for the last time this past year. At the end of FY86, the beginning of academic year 1986-1987, the teaching of this course was undertaken by Dr. J.L. Cecchi. Dr. Cecchi intends to broaden the coverage of the course to include other plasma applications, in keeping with other activities of the program.

Table II. Chemical Engineering Courses Relating to the Plasma Science and Fusion Technology Program and Instructors.

Course Number	Course Title	Instructor
CHE 351,352	Junior Independent Work	Staff
CHE 451,452	Senior Independent Work	Staff
CHE 417	Introduction to Fusion Power	R.G. Mills
CHE 418	Nuclear Engineering	R.C. Axtmann
CHE 550	Fusion Reactor Technology	R.C. Axtmann R.G. Mills

Table III. Pertinent Courses in Allied Departments.

Graduate Courses of Interest

Chemical Engineering

544	Chemical Reactor Engineering
545	Mathematical Methods of Engineering Analysis II (also CE 502)
550	Fusion Reactor Technology

Civil Engineering

501	Mathematical Methods of Engineering Analysis I
502	Mathematical Methods of Engineering Analysis II (also CHE 545)
553	Advanced Structural Mechanics
576	Electromagnetic Interactions with Continua

Electrical Engineering

541	Electronic Materials
542	Surface Properties of Electronically Active Solids
543	Transport Processes in Solids

Mechanical and Aerospace Engineering

511	Experimental Methods
513	Dynamic Data Analysis
547	Optics and Lasers
583	Electric Propulsion

Astrophysical Sciences

551	General Plasma Physics I
552	General Plasma Physics II
553	Plasma Waves and Instabilities

Undergraduate Courses of Interest

Chemical Engineering

417	Introduction to Fusion Power
418	Nuclear Engineering
441	Chemical Reactor Engineering
445	Process Control

Civil Engineering

310	Computer Methods for Engineering Problems
463	Finite Element Methods in Structures and Mechanics

Electrical Engineering

471	Solid State Electronics I
483	Microwave Electronics

Mechanical and Aerospace Engineering

433	Automatic Control Systems

SECTION EDITORS

Tokamak Fusion Test Reactor
S. Duritt, Jr.
D. Jassby

Princeton Large Torus
S. Bernabei

Princeton Beta Experiment
K. Bol
M. Okabayashi

S-1 Spheromak
A. Janos

Current-Drive Experiment
M. Ono

X-Ray Laser Studies
C. Skinner

Theoretical Division
R. Kulsrud

Tokamak Modeling
D. Mikkelsen

Spacecraft Glow
W. Langer

Compact Ignition Tokamak
D. Ignat
M. Machalek

Engineering Department

Engineering Analysis Division
R. Ellis, III

Electronic and Electrical Engineering Division
P. Murray

Mechanical Engineering Division
D. Knutson

Computer Division
S. Connell

Project Planning and Safety Office
E. Simon

Quality Assurance and Reliability
H. Howard

Administrative Operations
O. Bernett
A. Ammons

Graduate Education: Plasma Physics
T. Stix

Graduate Education: Plasma Science and Fusion Reactor Technology
R. Mills

GLOSSARY OF ABBREVIATIONS, ACRONYMS, SYMBOLS

A	Ampere
Å	Angstrom unit; 10^{-8} cm
ac	Alternating Current
ACT-I	Advanced Concepts Torus-I
ACWP	Actual Cost of Work Performed
A/D	Analog-To-Digital
ADP	Automated Data Processing
ADPE	Automated Data Processing Equipment
Alcator	A family of tokamak devices being developed and built at the Massachusetts Institute of Technology (from the Italian for high-field torus)
ALT-I	Advanced Limiter Test on TEXTOR (Jülich, West Germany); Version I
ALT-II	Version II of ALT
amu	Atomic Mass Unit
ANL	Argonne National Laboratory
ASC	Area Safety Coordinator
ASDEX	Axially Symmetric Divertor Experiment (Max-Planck-Institut für Plasmaphysik, Garching, West Germany)
ATC	Adiabatic Toroidal Compressor (Princeton Plasma Physics Laboratory, 1970's)
ATF	Advanced Toroidal Facility (a stellarator at Oak Ridge National Laboratory)
ATF-1	Advanced Toroidal Facility-1
AWAFT	Automatic Work Approval Form Transfer (System)
BALDUR	A Princeton Plasma Physics Laboratory one-dimensional tokamak transport code
BBGKY	Bogoliubov Born Green Kirkwood Yvon
BCWP	Budgeted Cost of Work Performed
BCWS	Budgeted Cost of Work Scheduled
CAD	Computer-Aided Design
CADD	Computer-Aided Design and Drafting (Facility)
CAE	Canadian Aviation Electronics (known as CAE Electronics Ltd.)
CAMAC	Computer-Automated Measurement and Control (System)
CAR	Computer-Assisted Retrieval
CAR	Cost Analysis Report
CCD	Capacitor Charge/Discharge
CCD	Charge-Coupled Device
CDR	Conceptual Design Review
CDX	Current-Drive Experiment (at the Princeton Plasma Physics Laboratory)
CEA	Commisariat A L'Energie Atomique
CENA	Charge-Exchange Neutral Analyzer
CHERS	Charge-Exchange Recombination Spectrometer
CICADA	Central Instrumentation, Control, and Data Acquisition (System)
CICS	Customer Information Control System
CIPREC	Conversational and Interactive Project Evaluation and Control System
CIT	Compact Ignition Tokamak
cm	Centimeter
COO	Chicago Operations Office
COS	Console Operating Station
CPSR	Contractor Procurement System Review
CPU	Central Processing Unit
CRAY	A brand of computer made by Cray Research, founded by S. Cray
CSR	Cost and Schedule Review
CTR	Controlled Thermonuclear Research
CY	Calendar Year
°	Degrees

°C	Degrees Centigrade
°K	Degrees Kelvin
D/A	Digital-To-Analog
DARM	Data Acquisition Room
DAS	Data Acquisition System (on PLT, PBX, S-1)
DAX	DAS supplemental system (uses a VAX computer)
dc	Direct Current
D-D	Deuterium-Deuterium
DDC	Disruptive Discharge Cleaning
DEC	Digital Equipment Corporation
DECAT	Drivers Energy Conservation Awareness Training
DEGAS	A PPPL computer code for studying the behavior of neutrals in plasma
DEMO	Demostration Power Reactor
D&GF	Design and General Fabrication (Section)
DIALOG	An interactive on-line information retrieval system used by the PPPL Library
DIFFUSE	A computer code use to calculate the one-dimensional diffusion and trapping of atoms in a wall
D-III	Doublet-III—A tokamak located at GA Technologies, Incorporated
D-III-D	Doublet III-D (recent upgrade of D-III, with D-shaped plasma)
DITE	Divertor and Injection Tokamak Experiment (Culham Laboratory, United Kingdom)
DNB	Diagnostic Neutral Beam
DOE	Department of Energy
DOE/RECON	An interactive on-line information retrieval system used by the PPPL Library
DPI	Deuterium Pellet Injector
D-T	Deuterium-Tritium
DVC	Diagnostic Vacuum Controller
EAD	Engineering Analysis Division
ECE	Electron Cyclotron Emission
ECH	Electron Cyclotron Heating
ECRF	Electron Cyclotron Range of Frequencies
ECRH	Electron Cyclotron Resonance Heating
ECS	Energy Conversion System
EF	Equilibrium Field
ELM	Edge Localized Mode
EMCS	Energy Monitoring and Control System
EPA	Environmental Protection Agency
EPFL	École Polytechnique Fédérale de Lausanne
EPRI	Electric Power Research Institute
ERB	Engineering Review Board
ERP	Edge Relaxation Phenomena
ESO	Emergency Services Officer(s)
ESU	Emergency Services Unit
ETACS	Equipment Tracking and Control System
ETR	Engineering Test Reactor
ETS	Engineering Test Station
eV	Electron Volt
EZB	Exclusion Zone Boundary
FAST	Fast Automatic Transfer System
FCPC	Field Coil Power Conversion
FEA	Finite Element Analysis
FED	Fusion Engineering Device
FEDC	Fusion Engineering Design Center (Oak Ridge National Laboratory)
FELIX	An experimental test facility under construction at the Argonne National Laboratory
FEM	Finite Element Modeling or Finite Element Method
FER	Fusion Engineering Reactor
FIDE	Fast Ion Diagnostic Experiment
FIR	Far-Infrared
FIS	(Department of Energy) Financial Information System
FLOPSY	Flexible Optical Path System
FMIT	Fusion Materials Irradiation Test
FPSTEL	Computer code used to solve the ripple-bounce-averaged Fokker-Planck equation numerically

FSAR	Final Safety Analysis Report
FTE	Full-Time Equivalent
FTS	Federal Telecommunications System
FWCD	Fast-Wave Current Drive
FWHM	Full Width at Half Maximum
FY	Fiscal Year (October 1 to September 30)
G	Gauss
G&A	General and Administrative (cost or expense)
GAO	General Accounting Office
GAT	GA Technologies, Incorporated
GDC	Glow Discharge Cleaning
GHz	Gigahertz; 10^9 cycles per second
GJ	Gigajoule, a unit of energy; 10^9 joules
gpm	Gallons Per Minute
GPP	General Plant Projects
GSA	General Services Administration
GSF	Gross Square Feet
HAIFA	Hydrogen Alpha Interference Filter Array
HAX	High-Level Data Analysis (System); uses a VAX computer
HEDL	Hanford Engineering Development Laboratory
HELIAC	A computer code used to calculate vacuum magnetic surfaces in nonaxisymmetric three-dimensional toroidal geometries
HERA	Helically invariant code
HF	Horizontal Field
HFIX	High-Field Ignition Experiment
HLDAS	High-Level Data Analysis System; equivalent to HAX
H-mode	High-Confinement Mode
HPA	High Power Amplifier
HPP	High Power Pulsing (Operations)
HSD	Health and Safety Directive
HTA	Hard Tube Amplifier
HV	High Voltage
HVAC	Heating, Ventilating, and Air Conditioning
HVE	High-Voltage Enclosure(s)
IBW	Ion-Bernstein Wave
IBWH	Ion-Bernstein-Wave Heating
ICH	Ion Cyclotron Heating
ICRF	Ion Cyclotron Range of Frequencies
ICRH	Ion Cyclotron Resonance Heating
IGNITOR	Ignited Torus
IMAPS	Interstellar Medium Absorption Profile Spectrograph
INEL	Idaho National Engineering Laboratory
INTOR	International Tokamak Reactor
I/O	Input/Output
IPP	Initial Protective Plates
IPP	Institut für Plasmaphysik at Garching, West Germany
IPSG	Ignition Physics Study Group
IR	Infrared
IRM	Information Resources Management
ISP	Ignition Studies Project
ISS	Internal Support Structure
ISX	Impurity Study Experiment (at Oak Ridge National Laboratory)
ITOC	Ignition Technical Oversight Committee
ITR	Ignition Test Reactor
JAERI	Japan Atomic Energy Research Institute
JET	Joint European Torus
JT-60	JT stands for JAERI Tokamak and 60 means plasma volume in m^3. An energy breakeven plasma testing device in Japan
kA	Kiloamperes
keV	Kilo-Electron-Volts
KFA	Kernforschungsanlage Jülich, W. Germany
KIK	Kernforschungszentrum Karlsruhe, W. Germany

kG	Kilogauss
kHz	Kilohertz
kJ	Kilojoule
ksi	Kilopounds Per Square Inch (Pressure, Stress)
kV	Kilovolt
kV A	Kilovolt Ampere
kW	Kilowatt
kW h	Kilowatt Hour
LANL	Los Alamos National Laboratory
LBL	Lawrence Berkeley Laboratory
LBM	Lithium Blanket Module
LC	Inductance Capacitance
LCC	Lithium Comparison Code
LCCs	Local Control Centers
LCFS	Last Closed Flux Surface
LCP	Large Coil Program
LED	Light Emitting Diode
LENS	Low Energy Neutral System
LEO	Low Earth Orbit
LH	Lower Hybrid
LHCD	Lower Hybrid Current Drive
LHe	Liquid Helium
LHRF	Lower Hybrid Range of Frequencies
LHRH	Lower Hybrid Resonance Heating
LITE	Laser Injected Trace Element (System)
LITE	Long-Pulse Ignited Test Experiment (at the Massachusetts Institute of Technology)
LLNL	Lawrence Livermore National Laboratory
L-mode	Low-Confinement Mode
LO	Local Oscillator
LOB	Laboratory Office Building
LOTUS	Nuclear testing facility at École Polytechnique Fédérale de Lausanne in Switzerland
LPIS	Long-Pulse Ion Source
μm	Micrometer; equivalent to micron
μsec	Microsecond
m	*Meter*
MA	Megamperes
MARFE(s)	Region(s) of enhanced edge radiation localized poloidally on the inner-major-radius side of a plasma
MARS	Mirror Advanced Reactor Study (Lawrence Livermore National Laboratory)
Mb	Megabyte
MCNP	Monte-Carlo Neutron and Proton Code
MED	Mechanical Engineering Division
MeV	Mega-Electron-Volt
MFAC	Magnetic Fusion Advisory Committee
MFE	Magnetic Fusion Energy
MFETF	Magnetic Fusion Energy Technology Fellowship (Program)
MFTF-B	Mirror Fusion Test Facility at Lawrence Livermore National Laboratory
MG	Motor Generator
MHD	Magnetohydrodynamics
MHz	Megahertz
mil	*A unit of length equal to 0.001 inch*
MIRI	Multichannel Infrared Interferometer
MIST	A computer code which follows impurity species through various stages of ionization, charge-exchange, radiation, and transport within the plasma
MIT	Massachusetts Institute of Technology
MJ	Megajoules
mm	Millimeter
MPa	Mega-Pascal (Pressure, Stress)
MSDA	Material Safety Data Sheet
msec	Millisecond
MTL	Material Test Laboratory
MVA	Megavolt Ampere

mW	Milliwatt
MW	Megawatt
NASA	National Aeronautics and Space Administration
NASA/RECON	An interactive on-line information retrieval system used by the PPPL Library
NASTRAN	A structural analysis code
NB	Neutral Beam
NBETF	Neutral Beam Engineering Test Facility
NBI	Neutral Beam Injection
NBI	NBI, Incorporated (word-processing equipment and service company)
NBLs	Neutral Beamlines
NBPS	Neutral Beam Power Supply
NBTC	Neutral Beam Test Cell
NCR	Nonconformance Report
NET	Next European Torus
NJDEP	New Jersey Department of Environmental Protection
nm	Nanometer
NMFECC	National Magnetic Fusion Energy Computer Center
NRC	Nuclear Regulatory Commission
nsec	Nanosecond
NTGD	Nontritium Gas Delivery
NTIS	National Technical Information Service
OFE	Office of Fusion Energy
OH	Ohmic Heating
OMA	Optical Multichannel Analyzer
OM&S	Occupational Medicine and Safety
ORC	Operations Review Committee
ORNL	Oak Ridge National Laboratory
ORR	Operational Readiness Review
OSES	Operations System Engineering Support
OSHA	Occupational Safety and Health Administration
OSR	Operational Safety Requirements
PADS	Procurement Automated Data Processing System
PAP	Plasma "Apprentice" Program
PBX	Princeton Beta Experiment
PBX-M	Princeton Beta Experiment Modification
pC	Pico Coulomb
PC	Personal Computer
PDC	Pulse Discharge Cleaning
PDR	Preliminary Design Review
PDX	Poloidal Divertor Experiment
PEST	Princeton Equilibrium, Stability, and Transport Code
PF	Poloidal Field
PFC	Plasma Fusion Center (at the Massachusetts Institute of Technology)
PHA	Pulse-Height Analysis
PIV	Plenum Interface Valve
PLANET	A two-dimensional transport code used to study the scrape-off region created by divertors and limiters
PLC	Programmable Logic Controller
PLCS	Power Line Carrier System
PLT	Princeton Large Torus
PM	Preventive Maintenance
PM&E	Plant Maintenance and Engineering
PMS	Performance Measurement System
PMS	Performance Management System
P&OS	Project and Operational Safety
PP-Lasers	Power, Picosecond Lasers
PPPL	Princeton Plasma Physics Laboratory
psec	Picosecond
PSE&G Co.	Public Service Electric and Gas Company
psi	Pounds Per Square Inch
PUBSYS	PPL Public Information System (installed on the Princeton University IBM 3081 computer)
PUCC	Princeton University Computer Center

QA	Quality Assurance
QA/R	Quality Assurance and Reliability
QMS	Quadpole Mass Spectrometer
RAX	TFTR off-line data reduction system (uses a VAX computer)
R&D	Research and Development
RDAC	Research and Development Activity
REML	Radiation Environmental Monitoring Laboratory
rf	Radio Frequency
RFBA	Request for Baseline Adjustment
RFP	Request for Proposal
RFP	Reversed-Field Pinch
RFTF	Radio-Frequency Test Facility
RGA	Residual Gas Analyzer
RIF	Reduction-in-Force
RIV	Rapid Intervention Vehicle
RLIN	Research Libraries Information Network
rms	Root Mean Square
RPI	Repeating Pellet Injector also Repeating Pneumatic Injector
rpm	Revolutions Per Minute
RTD	Resistive Thermal Detector
S-1 Spheromak	A compact toroid device (at the Princeton Plasma Physics Laboratory)
S-1 Upgrade	
SCR	Silicon Controlled Rectifier
S/DB	Small and Disadvantaged Businesses
SDS	Safety Disconnect Switch(es)
SEAS	School of Engineering and Applied Science
sec	Second
SEM	Scanning Electron Microscope
SF	Shaping Field, equivalent to EF
SHEILA	Australian Heliac
SIMS	Secondary-Ion Mass Spectroscopy
SNAP	Time-independent power equilibrium code
SNL	Sandia National Laboratories
SOP	Safe Operating Procedure
SOXMOS	Soft X-Ray Monochromator Spectrometer
SPARK	A general geometry computer code that calculates transient eddy currents and the resulting fields
SPEB	Subcontract Proposal Evaluation Panel
SPICE	A general purpose circuit simulation code
SPRED	Survey, Power Resolution, Extended Domain Code
SPS	Surface Pumping System
Sr	Steradian
SR	Safety Requirements
STARTUP	A computer code which evaluates free boundary axisymmetric equilibria and transport
STEP	Stellerator expansion equilibrium and stability code
Supershots	Low-current, high-density plasma discharges combined with intensive neutral-beam heating that are fired in a machine where the walls have been scrupulously condition via high-power discharges to remove adsorbed deuterium.
SURFAS	A fast between-shot moments code
TAC	Technical Advisory Committee
TCV	Tokamak Condition Variable—a tokamak under construction at École Polytechnique Fédérale de Lausanne in Switzerland
TDC	Taylor-Discharge Cleaning
TEXTOR	Tokamak Experiment for Technologically Oriented Research (Jülich, West Germany)
TF	Toroidal Field
TFCD	Tokamak Fusion Core Device
TFCX	Tokamak Fusion Core Experiment
TFD	Telemetry Fault Detector
TFM	TFTR Flexibility Modification
TFTR	Tokamak Fusion Test Reactor
TiC	Titanium Carbide
TIV	Torus Interface Valve

TLD	Thermoluminescent Dosimeters
TMPs	Turbo-Molecular Pumps
TMX	Tandom Mirror Experiment at Lawrence Livermore National Laboratory
Torr	A unit of pressure equal to 1/760 of an atmosphere
TOS	Terminal Operating Station
TPI	Tritium Pellet Injector
TRANSP	Time-dependent transport analysis code
TRECAMS	Tritium Remote Control and Monitoring System
TSC	Tokamak Simulation Code
TSCALE	A computer code that scales plasma equilibrium parameters over a wide range of major radius and aspect ratio
TSDS	*Tritium Storage and Delivery System*
TSTA	Tritium Systems Test Assembly
TVPS	Torus Vacuum Pumping System
TVTS	TV Thomson Scattering
UCLA	University of California at Los Angeles
UHF	Ultrahigh Frequency
USC	User Service Center; implemented on a Digital Equipment Corporation (DEC) PDP-10 computer
USGS	United States Geological Survey
USNRC	United States Regulatory Commission
UV	Ultraviolet
V	Volt
VAX	Digital Equipment Corporation computer; "Virtual Address Extention"
VC	Variable Curvature
VCD	Viscous Current Drive
VF	Vertical Field
VHF	Very High Frequency
VIPS	Visible Impurity Photometric Spectrometer
VSOP	Variable Specification Omni Processor
VSWR	Variable Standing Wave Ratio
VUV	Vacuum Ultraviolet
VXCS	Vertical X-Ray Crystal Spectrometer
W	Watt
WAF	Work Approval Form (System)
WBS	Work Breakdown Structure
WHIST	A 1½-dimensional transport code developed by the Oak Ridge National Laboratory
WKB	Wentzel-Kramers-Brillouin (A method for analyzing wave behavior if propagation characteristics depend on position.)
XCS	X-Ray Crystal Spectrometer
XIS	(Horizontal) X-Ray Imaging System
XUV	Extreme Ultraviolet
ZrAl	Zirconium-Aluminum